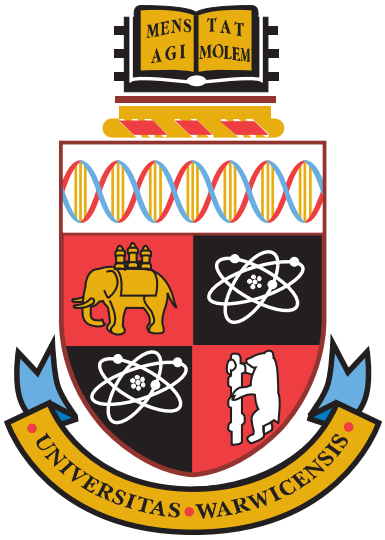

Multi-segment foot modelling to enable an understanding of altered gait in diabetes

by

Abigail Denise Jaitman

Thesis

Submitted to the University of Warwick

for the degree of

Doctor of Philosophy

School of Engineering

September 2016

Contents

List of Tables

List of Figures

Acknowledgments

I would like to thank my supervisors Dr. Neil Evans and Dr. Michael Chappell for giving me the opportunity to pursue this PhD and for their continuous support, guidance and motivation. It has been a rewarding and enriching experience to work together. I would also like to acknowledge Prof. Charles Hutchinson and Prof. Adrian Wilson for their advice on imaging and soft tissue modelling.

Special thanks go to Dr. Roberto Rojas who has been fundamental for my academic development, encouraging me to continue studying and always giving me thoughtful advice with his wise words. I would also like to thank his team in the Medical Diagnosis and Breast Research Center 'Diagnostico Rojas', whose expertise was invaluable and who were always eager to help me.

I thank my friends and colleagues at the University of Warwick for their company and support during the PhD. I would also like to thank the administrative staff in the School of Engineering. Thanks to my friends in Argentina for whom distance does not matter whenever I need them.

I would like to thank my partner Ignacio, for always believing in me and being by my side.

Finally, I would like to thank my parents Iosi and Andrea, and my sister Laura for their unconditional love and support during every stage of my life. Words cannot express how much you mean to me.

Declaration and published work

I, Abigail D. Jaitman, declare that the work presented in this thesis is my own except where stated otherwise, and was carried out entirely at the University of Warwick, during the period of October 2012 to October 2016, under the supervision of Dr. Michael J. Chappell and Dr. Neil D. Evans. Where information has been derived from other sources, I confirm that this has been indicated in the thesis.

I declare that the research reported here has not been presented nor submitted in any previous application for any degree at another university.

Experimental analysis was carried out in the Gait Laboratory within the School of Engineering at the University of Warwick and surroundings, complying with all data protection requirements as stated in the University of Warwick's BSREC ethical approval process: BSREC full approval REGO-2013-582 Foot Modelling.

Some parts of the work reported in this thesis have been published, as listed below. Further parts of this work will be submitted for publication in due course.

Published papers

1. Jaitman, A.D., Evans, N.D. and Chappell, M.J. (2015). Barefoot and shod conditions: how to reconcile them for plantar pressure analysis in the Oxford Foot Model, *Journal of Mechanics in Medicine and Biology*, 15:1–6.

Conference presentations

1. Jaitman, A.D., Evans, N.D. and Chappell, M.J. Multi-segment musculoskeletal foot model, *International Conference and Expo on Biomechanics and Implant Design*, Florida, July 2015.
2. Jaitman, A.D., Evans, N.D. and Chappell, M.J. Reconciling barefoot and shod conditions in the Oxford foot model for plantar pressure measurement, *XIX International Conference on Mechanics in Medicine and Biology*,

Bologna, September 2014.

3. Jaitman, A.D., Evans, N.D. and Chappell, M.J. Reconciling barefoot and shod conditions in the Oxford foot model for plantar pressure measurement, *8th IEEE EMBS UK & Republic of Ireland Postgraduate Conference on Biomedical Engineering and Medical Physics/IEEE EMBS International Student Conference (ISC)*, University of Warwick, July 2014.

Abstract

Diabetes is a multisystemic disease that affects the whole human body, in particular, the musculoskeletal system. Muscles, tendons, ligaments and bone marrow are its main victims, the foot being the most common target. Changes in its anatomy can occur rapidly, and therefore an early diagnosis is imperative in order to provide the appropriate medical care, thus avoiding amputation which is a high factor of morbidity. In order to understand the biomechanical implications of the disease, it is necessary to develop new and improved models that allow the study of the foot during gait. The difficulties arising in foot modelling are inherent in its complex composition, thus most models simplify the foot geometry, structure, materials and kinetic analysis.

This thesis presents a new approach towards foot modelling, combining readily available non-invasive methodologies to develop multi-segment foot models. This research helps in the in-depth understanding of the effects of changes in structure and shape of the foot brought about by diabetes and in the evaluation of the effects of interventions and long-term rehabilitation.

Intermediate results are presented in order to establish the reliability of the proposed methods, developing first a new method for simultaneous plantar pressure and gait study. New approaches to muscle-tendon length and moment arm measurement are tested and validated, following an analysis of different pennation angle assumptions for force production assessment. Both extrinsic and intrinsic muscles are included in the model using the Hill muscle model. Stiffness and damping parameters are estimated on a per-subject basis. In order to model the soft tissue, which is of particular interest in diabetic patients, a model consisting of a system of parallel spring and damper, is proposed. Parameters are presented for 15 subjects with the purpose of characterising the properties of the soft tissue under the calcaneus (heel pad), metatarsal heads and hallux. A further analysis is provided by simulating different diabetic foot injuries and comparing their effect in joint range of movement and moment and soft tissue. Combined, these studies produce a complete subject-specific musculoskeletal and soft tissue model that enhances our understanding of both normal and altered gait.

Abbreviations

ADM	Abductor Digiti Minimi
AIC	Akaike information criterion
AH	Abductor Hallucis or Abductor Hallux
CT	Computarised Tomography
EDL	Extensor Digitorum Longus
EHL	Extensor Hallucis Longus or Extensor Hallux Longus
EMG	Electromyography
FDB	Flexor Digitorum Brevis
FDL	Flexor Digitorum Longus
FHB	Flexor Hallucis Brevis or Flexor Hallux Brevis
FHL	Flexor Hallucis Longus or Flexor Hallux Longus
GAS L	Lateral Gastrocnemius
GAS M	Medial Gastrocnemius
GRF	Ground Reaction Force
MRI	Magnetic Resonance Imaging
MTU	Muscle-tendon Unit
OFM	Oxford Foot Model
PIL	Participant Information Leaflet
PL	Peroneus Brevis
RMSE	Root mean square error

R^2	R-Squared
TA	Tibialis Anterior
TP	Tibialis Posterior

1

Introduction

1.1 Motivation

In the field of biomechanics, there is a growing interest in motion analysis, kinematics and kinetics. In this context, the foot plays an important role, providing support to the body and also distributing loads. Although many foot models have been developed during recent years, most of them simplify the foot geometry, structure and material [Qiu et al., 2011]. Authors agree that an evaluation of the approach to foot modelling is extremely difficult due to its complex nature [Cheung and Nigg, 2008]. In fact, it is usually modelled as a single rigid body, which is perhaps somewhat misleading for this type of research. Thanks to evolutions in technology, the development of biomechanical models of body motion - and specifically of the foot - has improved. A combination of different techniques such as gait analysis, plantar pressure measurements and image processing, together with biomechanical principles, can contribute to the development of multi-segment models that can be validated using subject data. It is therefore possible to gain insight into the forces applied to the musculoskeletal system including the joints, and both movement and deformation of soft tissue. However, there is yet no model that combines all the available methodologies to provide a complete foot model.

A well validated foot model can also provide an insight on different alterations in

the manner of walking (gait) produced by diverse injuries. In this context, diabetes is a progressive disease which still represents a challenge for medical experts and has a particularly harmful effect on the foot, ankle and soft tissue, producing changes in its function and structure [Frykberg et al., 2006]. A clear understanding of the changes brought about by the disease in the foot biomechanics is essential. As seen in the reviewed articles (see, for example, Cavanagh and Ulbretch [2008] and Ledoux [2007]), the injuries that occur to the feet of diabetic patients are caused by neuropathy, namely ulcers caused during walking due to forces that are generated because of movement. To the best of my knowledge, there are few studies performed on the diabetic foot that analyse the foot during movement. Biomechanics research in this field is a very important avenue for future research.

1.2 Aims and objectives

The aim of this work is to develop a musculoskeletal scaled model of the human foot that can be validated using patient data: a general model to study the healthy foot that can be adapted to characterise altered gait in diabetes. This can provide an in-depth understanding of the effects of changes in the structure and shape of the foot brought about by the disease. The ultimate goal of this research is to contribute to a better mechanistic understanding aimed at improving quality of life and allowing a cost-benefit assessment of the treatment alternatives that diabetic patients have at different stages of the illness. It will also offer valuable input to promote innovations in the orthopaedic industry, and to improve and develop novel widely accepted and validated foot models.

1.3 Thesis outline

Throughout its chapters, this dissertation provides a comprehensive analysis of foot biomechanics as follows:

- **Chapter 2**: This chapter provides a thorough literature review and necessary background to understand foot biomechanics. This chapter presents

not only anatomical basis but also foot models and available technological methodologies and clinical data necessary to develop a multi-segment foot model, including both empirical and theoretical approaches to the topic.

- **Chapter 3**: This chapter describes the methodologies used, in particular, for the development of an innovative foot model combining motion capture, electromyography, plantar pressure measurement and imaging techniques, which are used in the following chapters.

- **Chapter 4**: This chapter provides intermediate results for this research. In order to develop a multi-segment musculoskeletal foot model it was necessary to assess reliability and repeatability of the proposed methods. First, a new method for simultaneous plantar pressure and gait study with the development of a specially design shoe that can reconcile barefoot and shod conditions for plantar pressure measurement is described. An extensive analysis of the muscle-tendon unit parameters needed for model parameterisation is undertaken, such as length, moment arm, pennation angle and muscle activation, and how these can be obtained from the non-invasive techniques used in this thesis. Length is analysed using a via-point model to represent the muscle-tendon unit as an arrangement of straight lines connected by virtual markers. In order to assess the reliability of the method, results from motion capture and magnetic resonance imaging are compared for ten lower limb muscles. The moment arm is calculated using the principle of virtual work, which relates change in length with the change in angle of the joint of interest, and validated against magnetic resonance imaging. An analysis was also performed on pennation angle (angle between muscle fibres and aponeurosis of the tendon) using ultrasound to obtain information on fibre length and angle for six lower limb muscles which present the largest angles. Results were then compared with different pennation angle scenarios. Muscles were also studied from activation perspective, for experimental design purposes.

- **Chapter 5**: The main objective of this chapter is to develop a mechanical model that can describe both passive and active behaviour of skeletal

muscle. There are several models describing muscle function, of particular interest is the Hill muscle model which is analysed from a numerical and structural point of view in this chapter. The validated methodologies designed in chapter 4 are used to obtain muscle tendon length and moment arm. Thirteen muscles are analysed for the proposed multi-segment foot model, and parameters for tendon and muscle damping and stiffness are obtained for fifteen subjects through fitting techniques. These values are validated towards measured moments.

- **Chapter 6**: This chapter refers to plantar soft tissue modelling. The plantar soft tissue protects the structure of the foot, providing cushioning to the underlying bones and shock attenuation [Cavanagh, 1999]. It is the only interface of the body with the ground during any type of motion activity. In this chapter, first a brief introduction on plantar soft tissue, its architecture and different viscoelastic models is given. Models are fitted to subject data and compared in order to find the model that can best describe soft tissue behaviour. A new method is proposed to obtain loaded plantar tissue thickness during gait, by assessing the displacement of markers placed at medial and lateral side of calcaneus, metatarsals and hallux. Once plantar thickness is obtained, it is possible to reconstruct the stress-strain curves. Parameters for a non-Newtonian Kelvin-Voigt model are presented for fifteen subjects with the purpose of characterising the properties of the soft tissue under the calcaneus (heel pad), metatarsal heads and hallux (great toe).

- **Chapter 7**: In chapters 5 and 6 normal gait was described by parameterising both muscle-tendon units and soft tissue. Knowledge of a normal gait is necessary in order to understand a pathological one. In this study normal gait is defined as the gait of a healthy subject and pathological the one corresponding to a diabetic patient. According to many authors (Boffeli et al. [2002], Edmonds and Watkins [1999] and Frykberg et al. [2006], for example), diabetic patients have an altered gait in terms of kinetics and kinematics thus affecting plantar pressure. In this chapter different types of injuries are simulated and results are obtained in terms of ankle moments

and joint angles, among others. Different scenarios are also presented for soft tissue alteration, increasing peak pressure and decreasing tissue thickness.

- **Chapter 8**: This chapter compiles the conclusions inferred from the presented work, demonstrating how the proposed aims and objective were met. It also provides avenues for future research.

All experimental analysis was carried out in the Gait Laboratory within the School of Engineering at the University of Warwick and surroundings, complying with all data protection requirements as stated in the University of Warwick BSREC ethical approval (BSREC full approval REGO-2013-582 Foot Modelling) and written informed consent was obtained for the participating subjects. The proposed methods in chapters 5, 6 and 7 are either newly developed or, for pre-existing methods, they were tested and validated against other methodologies (i.e. MRI and ultrasound). For each of the experiments, a repeatability analysis was first assessed to understand the sensitivity to consider and prove the reliability of the proposed method.

2

Background

In the field of biomechanics, there is a growing interest in motor analysis, kinematics and kinetics. In order to predict how a subject can move under certain circumstances, it is essential to start from the base, i.e. the foot which is the main contact that humans have with the ground. Foot models have evolved with technology breakthroughs, from one single rigid segment to multi-segment models. This chapter reviews the literature on Foot Modelling, its anatomy and function, the available technologies, methodologies and clinical data necessary to develop a multi-segment foot model, including both empirical and theoretical approaches to the topic.

2.1 Sources of References and Inclusion Criteria

New approaches in theoretical and experimental papers have been revised and consulted. The electronic databases that were used are: ISI Web of Science, ScienceDirect, BioMed Central, IEEE Xplore, Scopus and Elsevier, accessed through the Library of the University of Warwick. According to the inclusion criteria, all the papers considered were published between 1981- 2016. Most of them are case studies and experimental papers that focus on foot modelling, gait analysis and the diabetic foot.

2.2 Gait

Gait is defined as the manner of walking [Whittle, 2007b], and its study allows us to measure and analyse movement patterns, kinematics and kinetics, as well as the forces that are produced by movements and reactions [Switaj and O'Connor, 2008].

Walking requires one foot to be always in contact with the ground. A gait cycle (figure 2-1) is the period that occurs from the initial contact of the foot with the ground (heel strike), to the next initial contact of the same foot [Richards, 2008]. When both feet are in contact with the ground there is "double support", and when only one foot is in contact with the floor, we have "single support" (and the free leg is in "swing phase"). Therefore, the right and the left leg will alternately be in the support and swing phase. The gait cycle can then be divided into two phases: Stance phase (60% of the cycle, when the foot is in contact with the ground) and Swing phase (40% of the cycle, when the foot is not in contact with the ground).

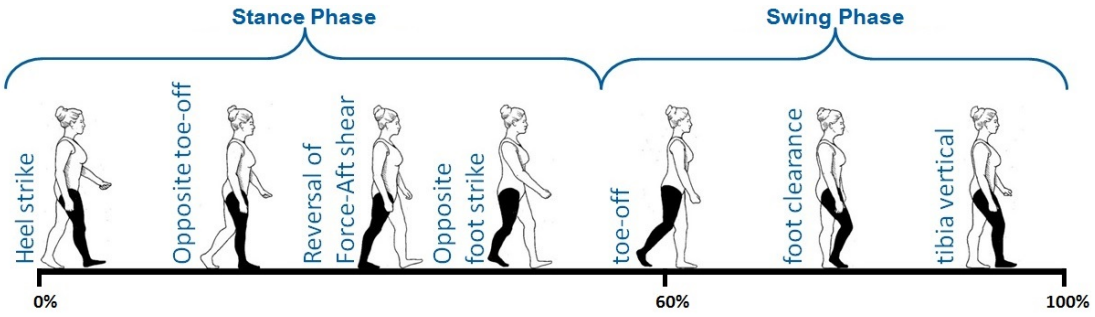

Figure 2-1 Gait cycle events, adapted from Hrones and Nelson [1983].

Different methodologies are used to study gait and will be described in section 2.5, as it is necessary to describe the foot structure first.

2.3 Foot Structure

As the main object of analysis of this research is the foot, a clear understanding of its complexities and specificities is crucial.

The foot is not only a structural support for the body, but it also has to cope with different types of surfaces and speeds [Nordin and Frankel, 2001]. It has the capability of acting both as a flexible or rigid structure, depending on the situation. The foot is comprised of 26 bones, 33 joints, 19 muscles and 107 ligaments (see figure 2-2); which represent 25% of the bones of the human body [France, 2009]. The foot can be divided into three parts [Whittle, 2007a]:

- Hindfoot: Composed of the talus and calcaneus bones.
- Midfoot: Composed of the cuboid, navicular and cuneiforms (lateral, intermediate and medial) bones.
- Forefoot: Composed of the 5 metatarsals and 5 phalanges.

Figure 2-2 The foot, its bones and joints. Adapted from Whittle [2007a].

2.3.1 Movements of the foot

In order to define foot movements, it is necessary to understand the planes over which these movements occur [Jenkins, 2005]; these are described in figure 2-3 and listed below.

(a) Sagittal plane: This divides the foot (between 2nd and 3rd metatarsals) into medial and lateral regions. The movements that occur in this plane are dorsiflexion (dorsum, or upper surface of the foot, moves towards the leg)

and plantarflexion (dorsum of the foot moves away from the leg). See figure 2-3(a).

(b) Horizontal or transverse plane: This divides the foot into superior and inferior regions. The movements that occur in this plane are abduction (the foot and leg are rotated away from the mid-line of the body) and adduction (the foot and leg are rotated towards the mid-line of the body). See figure 2-3(b).

(c) Frontal or coronal plane: This divides the foot in anterior and posterior regions. The movements that occur in this plane are inversion (the plantar surface of the foot rotates towards the mid-line of the body) and eversion (the plantar surface of the foot rotates away from the mid-line of the body). See figure 2-3(c).

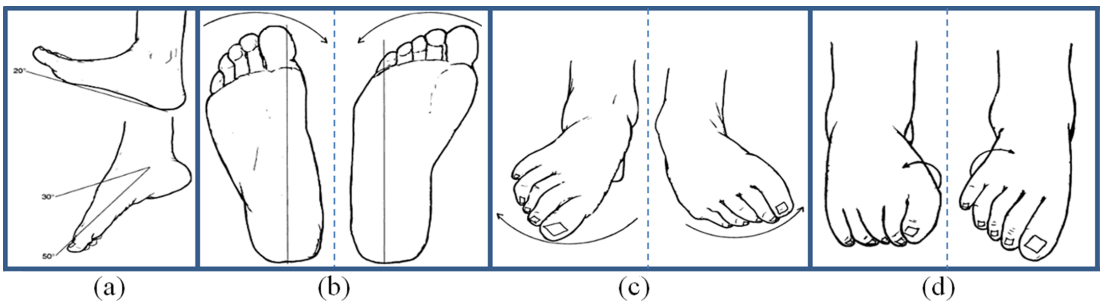

Figure 2-3 Movements of the foot: (a) Dorsiflexion (top) and plantarflexion (bottom). (b) Abduction (left) and Adduction (right). (c) Inversion (left) and Eversion (right). (d) Pronation (left) and Supination (right). Adapted from Logan and Rowe [1995].

When describing gait, two other terms should be considered: Pronation and Supination (see figure 2-3(d)). These include movements in all of the three planes. Pronation consists of abduction, eversion and dorsiflexion; supination consists of adduction, inversion and plantarflexion.

2.3.2 Arches

The foot hast two arches [Logan and Rowe, 1995]:

- Transverse arch: This is composed of the tarsal bones (cuneiforms and cuboid) and the five metatarsal bases.

- Longitudinal arch: This is divided into medial and lateral regions. The medial longitudinal arch is composed of the inner part of the calcaneus, talus, navicular, cuneiforms and the first three metatarsals; and is responsible for moving the foot forwards during locomotion. The lateral longitudinal arch is formed by the calcaneus, cuboid and fourth and fifth metatarsals; it provides a proper weight distribution over the foot.

The arches do not only depend on the bones, but also on the support and stability provided by the surrounding ligaments and muscles.

2.3.3 Muscles

There are two types of muscles that control the foot during any motor task: intrinsic and extrinsic muscles. The first type originates and inserts into the foot, while the latter originates in the anterior, posterior and lateral part of the leg and inserts into the foot. In total there are twelve extrinsic muscles and nineteen intrinsic muscles that control the foot. The extrinsic muscles can be anterior, lateral or posterior according to their position. Intrinsic muscles can be dorsal (if they are in the superior half of the foot) or plantar (when they are in the inferior part). The latter are divided into four anatomic layers by depth, the first layer being the most superficial one and the fourth layer being the deepest one.

According to Nordin and Frankel [2001], the extrinsic muscles are the strongest and most important during motion analysis. These authors performed an electromyographic study of the musculature of the foot in order to identify the intervention of the muscles during the gait cycle (see figure 2-4). These muscles were reviewed [Snell, 2004; Nordin and Frankel, 2001] in order to understand their origin, insertion, and function and are summarised in table 2-1.

Muscle	E/I	Origin	Insertion	Function
TIBIALIS ANTERIOR	E	Proximal half of tibia	Medial cuneiform and 1st metatarsal bone of foot	Brings leg towards the back of the foot while weight bearing and flexes foot dorsally in non-weight bearing
EXT. DIGITORUM LONGUS	E	Along fibula	2nd to 5th phalanges	Dorsiflexes the digits
EXT. HALLUX LONGUS	E	Medially on fibula	1st phalanx	Dorsiflexes the big toe and acts on the ankle in the unstressed leg
GASTROCNEMIUS	E	Knee	Calcaneus	Primary active muscle when standing still
TIBIALIS POSTERIOR	E	Back to interosseus membrane	Tarsus & navicular (4th layer)	Supports medial longitudinal arch, inverts the foot and plantarflexes at the ankle
FLEX. DIGITORUM LONGUS	E	Shaft of tibia	2nd to 5th phalanges	Supports longitudinal arches, flexes the lateral four toes and plantarflexes foot
FLEX. HALLUX LONGUS	E	Back of fibula	1st phalanx (2nd layer, plantar surface of hallux)	Supports medial longitudinal arch, plantarflexes the foot and flexes the great toe
PERONEUS LONGUS	E	Shaft of tibia	Between medial cuneiform and 1st metatarsal (4th layer)	Supports longitudinal and transverse arches, everts the foot and plantarflexes at the ankle
PERONEUS BREVIS	E	Calcaneus	Base of 5th metatarsal	Assists plantarflexion and eversion of the foot
ABD. HALLUX	I	Calcaneus (medially)	Base of 1st phalanx (1st layer)	Supports medial longitudinal arch and abducts and flexes big toe
FLEX. HALLUX BREVIS	I	Cuboid and lateral cuneiforms	Phalanx of big toe (medially and laterally) (3rd layer)	Supports medial longitudinal arch and flexes metatarsophalangeal joint of big toe
FLEX. DIGITORUM BREVIS	I	Calcaneus (medially)	Medial phalanges (2nd–4th) (1st layer)	Supports lateral longitudinal arch and flexes lateral toes (2nd–4th)
ABD. DIGITI MINIMI	I	Calcaneus (laterally and medially)	5th phalanx (1st layer)	Supports lateral longitudinal arch and flexes and abducts 5th toe
INTEROSSEI	I	Between metatarsals	Phalanges (4th layer)	Adduction of phalanges 3rd–5th
EXT. DIGITORUM BREVIS	I	Calcaneus	2nd, 3rd and 4th metatarsals	Extends digits 2nd to 4th

Table 2-1 Extrinsic and intrinsic muscles involved in gait cycle, where FLEX. is Flexor, EXT. is Extensor and ABD. is Abductor. Table summarised from Snell [2004] and Nordin and Frankel [2001].

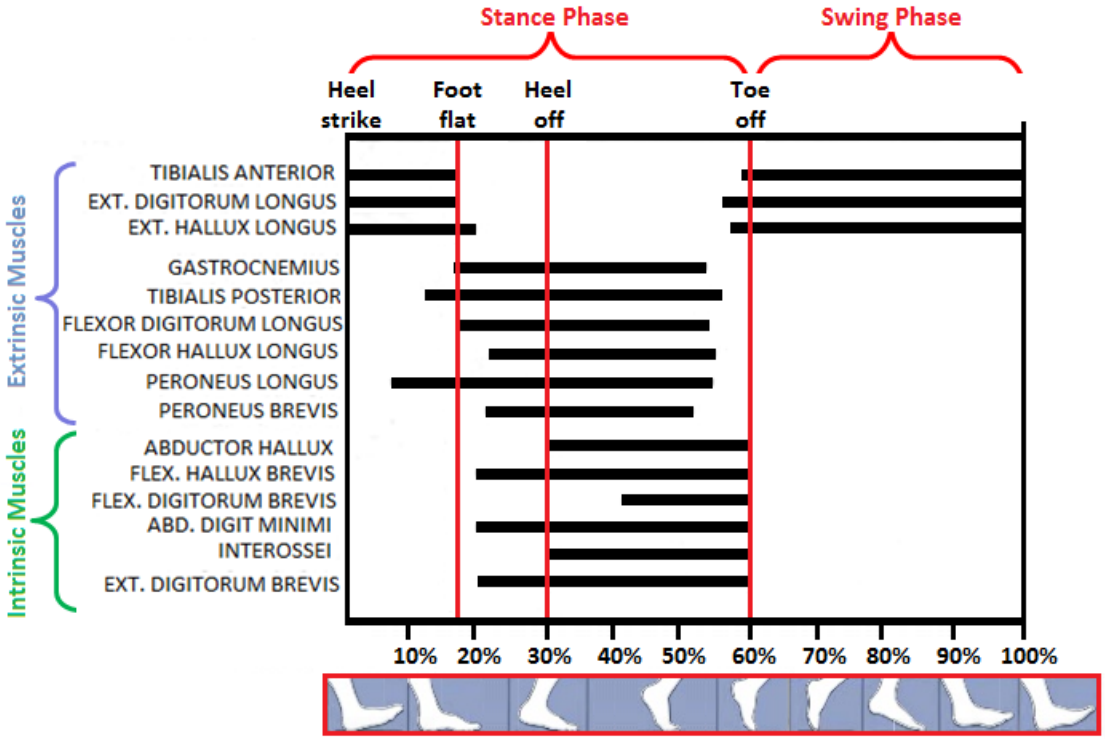

Figure 2-4 Electromyographic activity of foot muscles. Adapted from Nordin and Frankel [2001].

The final aim of this group of muscles is to provide an efficient transfer of the forces generated during any motor task to the ground and adequately shift the weight of the body along the progression axis. A deeper knowledge of muscle architecture is necessary for understanding human movement as it is the elementary basis for muscle function and will be reviewed in the following section.

2.3.4 Joints

The joints allow the movement of two connecting bones. According to the structure, the foot contains two types of joints [Thordarson, 2004]:

- Fibrous: This type of joint connects the bones through fibrous connective tissue.
- Synovial: This type of joint contains synovial fluid that allows smooth movement of the connecting bones. This joint allows a large range of motion.

Synovial joints present in the foot are shown in figure 2-5:

(a) Saddle: one concave bone and one convex bone, with angular movements (see figure 2-5(a)).

(b) Clondyloid: oval shaped, allowing movement in two axes (see figure 2-5(b)).

(c) Hinge: one bone is slightly rounded and the other one slightly curved, one moves and the other remains fixed (see figure 2-5(c)).

(d) Ball and Socket:one ball-like bone and one socket (see figure 2-5(d)).

(e) Plane: connecting bones are almost flat, allowing gliding (see figure 2-5(e)).

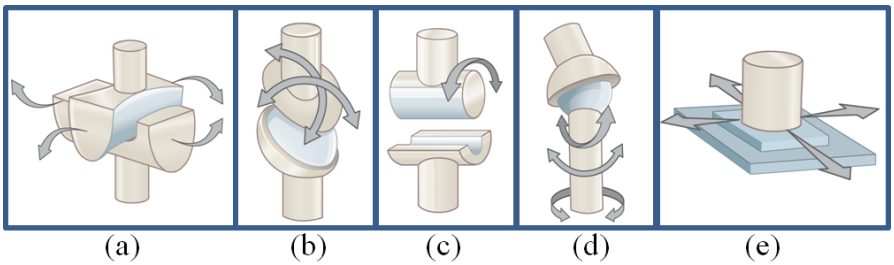

Figure 2-5 Types of joints: (a) Saddle. (b) Clondyloid. (c) Hinge. (d) Ball and Socket. (e) Plane. Modified from Boundless Biology [BB, 2013].

Joints are grouped according to the division made at the beginning of this section: hindfoot, midfoot and forefoot. Table 2-2 summarises the foot joints.

Joint	Position	Function	Type
Taloclural (ankle)	Hindfoot	Provides stability during dorsiflexion and mobility in plantarflexion	Synovial, Hinge
Subtalar (Talocalcaneal)	Hindfoot	Produces motion of supination and pronation	Synovial
Talocalcaneonavicular	Midfoot	Gliding and rotation	Synovial, Ball & Socket
Cuneonavicular	Midfoot	Gliding and rotation	Synovial, Plane
Cuboideonavicular	Midfoot	Gliding and rotation	Fibrous
Intercuneiform	Midfoot	Gliding and rotation	Synovial, Plane
Cuneocuboid	Midfoot	Gliding and rotation	Synovial, Plane
Calcaneocuboid	Midfoot	Gliding with rotation	Synovial, Saddle
Tarsometatarsal	Forefoot	Gliding (Lisfranc joint)	Synovial, Plane
Intermetatarsal	Forefoot	Gliding	Synovial, Plane
Metatarsophalangeal	Forefoot	Flexion, extension, abduction and adduction	Synovial, Clondyloid
Interphalangeal	Forefoot	Flexion and extension	Synovial, Hinge

Table 2-2 Foot joints

2.3.5 Soft tissue

The aim of soft tissue is to protect the structure of the foot and provide cushioning. The plantar fascia or plantar aponeurosis supports the foot arches and absorbs shock during heel strike. It is a ligament-like tissue that goes from the calcaneus to the base of the digits, that surrounds the muscles of the first layer in the plantar surface of the foot [Bartold, 2004]. This tissue elongates during the gait cycle [Voloshin and Kim, 1995].

The heel pad absorbs the shock in weight-bearing activities, attenuating the impact when in contact with the ground and protecting the foot structure. It is a specialised structure consisting of fat-filled columns, reinforced with transverse fibres [Holst et al., 2013].

2.4 Muscle Architecture

Muscles produce both force and heat, and their production depends on many properties, such as pennation angle, amount of fibres and cross-sectional area, which will be explained in this section. In essence, muscles have the capacity of producing mechanical work by moving the bones via the tendons [Zajac, 1989]. Due to their excitability, elasticity, contractability, plasticity and extensibility, muscles are able to generate force and movement, but they need the nervous system in order to function. Each muscle is capable of contracting and shortening, moving bones to which they are connected via tendons (mainly made up of a fibrous and elastic tissue). A muscle-tendon unit (MTU) is the ensemble of muscle and tendon. Muscle origin is defined as the proximal attachment, and insertion is the distal attachment. A second, and opposing, set of muscles is needed to return the limb to its initial state. Antagonist is the muscle which opposes motion and agonist the one that resists motion [Freivalds, 2004]. Therefore, movement is not produced by one muscle, but as a collaboration among many muscles.

Muscles are made up of long cells that are bundles of fibres, arranged on the axis of force generation [Zatsiorsky and Prilutsky, 2012]. As shown in figure 2-

6(a), they are comprised of multiple layers of connective tissue, the endomysium surrounds each of the muscle fibres, which are grouped by the perimysium, and these are covered by the epimysium. Muscle fibres are supplied by blood vessels and intramuscular nerves that transmit an activation signal.

As mentioned earlier in this section, motion tasks are neuro-musculoskeletal tasks. In order for a muscle to work, it needs to be electrically activated by a motor neuron axon. Figure 2-6(b) shows this process, which starts in the central nervous system, the brain and the spinal cord. The latter, among many functions, includes the motor neuron and connects to muscle fibres through nerves. Once it leaves the spinal cord, this neuron and an axon (that goes through a peripheral nerve), innervate the muscle's fibres, thus creating a motor unit. The strength of the muscle, is directly related to the number of fibres contracting in synchrony [Trigo and Navarro, 2005].

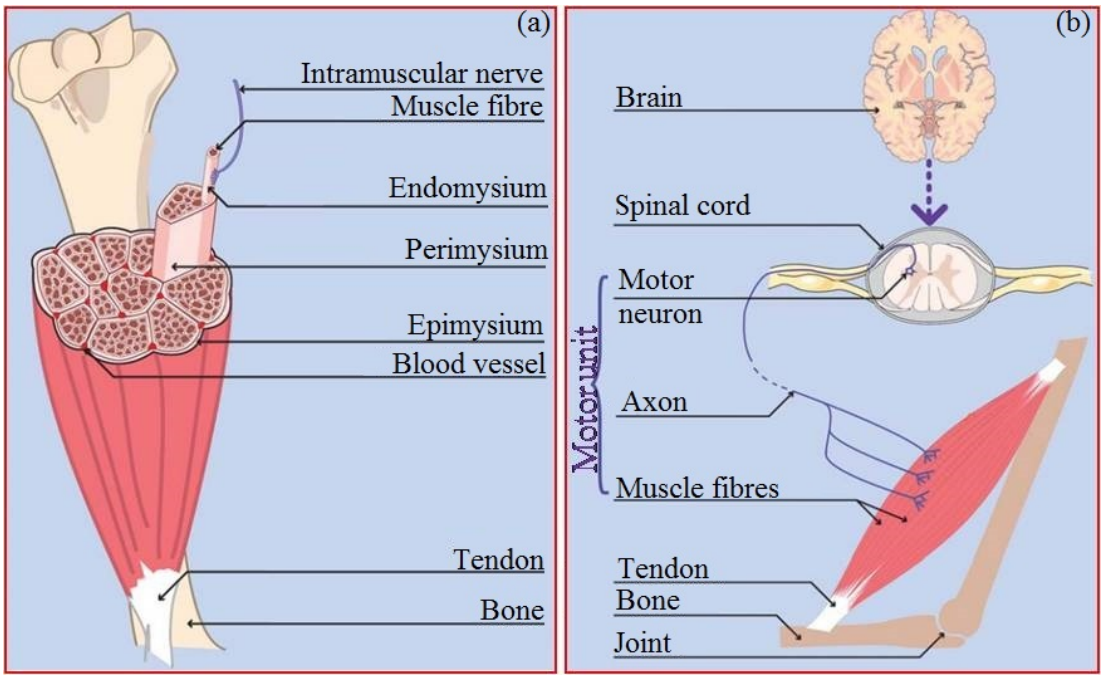

Figure 2-6 Muscle architecture. Adapted from Trigo and Navarro [2005].

Each muscle fibre is covered by a membrane called Sarcolema and contains an arrangement of myofibrils, which are the contractile elements of the muscle (figure 2-7). The myofibrils are made of bundles of thin and thick myofilaments (actin and myosin respectively). The most basic unit is the sacromere, which is the space

in between two Z-discs. Sacromeres are connected in series, and contractions occur when there is a gliding of actin and myosin. When the muscle is activated, the sacromere shortens producing an overlap of the filaments, thus creating more bonding points and therefore force.

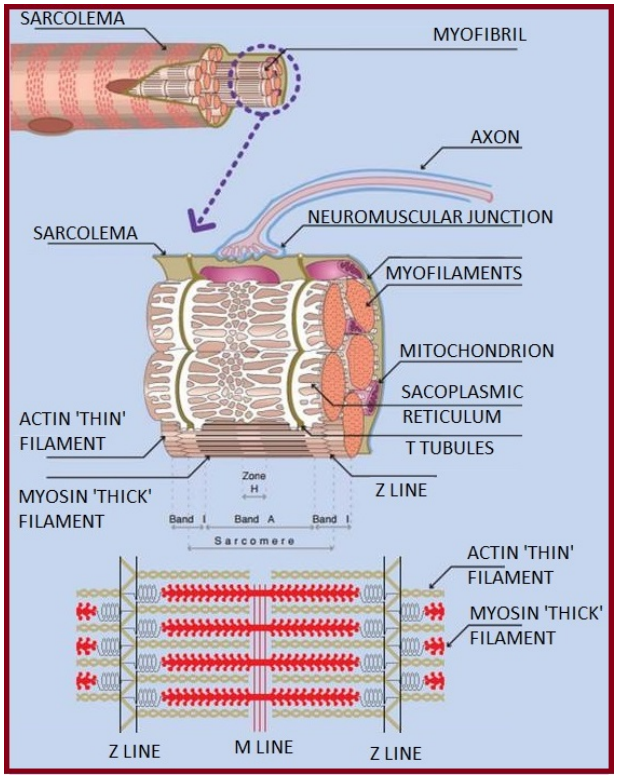

Figure 2-7 Muscle fibre architecture. Adapted from Trigo and Navarro [2005].

Muscles can be classified depending on the arrangement of their fibres as parallel-fibred, when the fibres extend parallel to the tendon, or pennated, when fibres are attached to the tendon at a certain angle. This means that for pennated muscles the force produced by the muscle will be the force produced by the fibres multiplied by the cosine of the pennation angle. This topic will be further covered and analysed in section 4.4.4.

Muscles can contract in three different ways: isometric contraction (muscle tension changes, but muscle-tendon length remains the same), isotonic contraction (muscle-tendon length changes, but muscle tension remains the same) or isokinetic contraction (linear or angular velocity remains constant).

Due to their nature, muscles can produce two types of forces: active and passive.

Active force occurs when the muscle is neurally activated as explained earlier, while passive force is due to the connective tissues. Therefore, muscle force can be expressed as:

$$F^M(t) = F_a^M(t) + F_p^M(t) \tag{2-1}$$

where $F_a^M(t)$ is the active component and $F_p^M(t)$ the passive component. There are two relationships that characterise muscle function: Force/length and Force/velocity.

2.4.1 Force/length relationship

Figure 2-8(a) depicts the process of force production through the overlapping of filaments. The filaments in the sacromere are overlapped and therefore cannot glide properly when the muscle length is short, producing low active tension. As the muscle starts to lengthen, the overlap portion of the filaments decreases resulting in a higher amount of active tension. When muscle length is ideal (optimal length or resting length), actin-myosin interaction is optimal and produces the maximum possible active force. When the muscle is extended beyond this point, the myofilaments start to separate, resulting in a reduction of the active force.

Figure 2-8(b) shows the tensile active and passive force produced by the muscle fibres at different lengths and describes the dependence of muscle force as a function of muscle length when fibres are recruited simultaneously. Beyond the resting or optimal length, the only type of force the muscle can produce is passive, which will restore it back to its resting length. The passive forces are negligible when muscle fibres are shorter than the optimal length (L_0^M) and rise exponentially. The force-length relationship is expressed as a percentage of the optimal length (L_0^M) and the percentage of maximum isometric force (F_0^M). It is assumed that muscles only produce force in the range of $0.5L_0^M - 1.5L_0^M$ [Buchanan et al., 2004].

2.4.2 Force/velocity relationship

This relationship describes the phenomenon that the (maximal) force that muscles can deliver depends on the speed at which they contract. If the muscle shortens

(concentric contraction), the maximal force decreases and if the muscle lengthens (eccentric contraction) the maximal force increases (figure 2-8(c)).

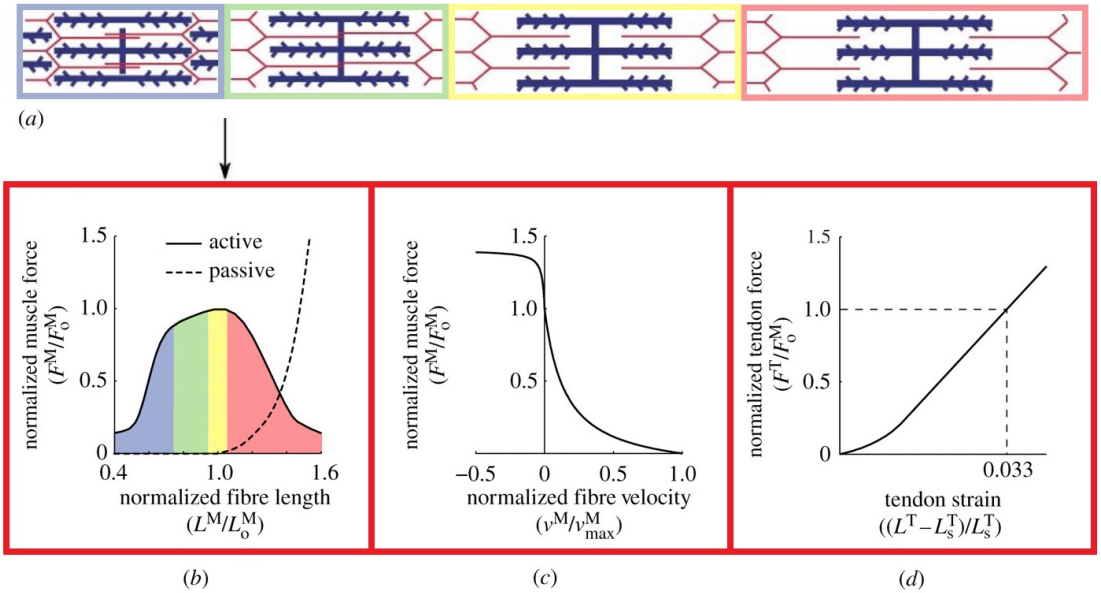

Figure 2-8 Muscle Force/length and Force/velocity relationships: (a) Actin-myosin bridges. (b) Muscle Force/length relationship. (c) Muscle Force/velocity relationship. (d) Tendon Force/length relationship. Adapted from Arnold and Delp [2011].

2.5 Methodologies

2.5.1 Gait Analysis

In this kind of analysis, many cameras are located in a way that at least three can see the reflective markers that are attached to the body of the subject under study [Kirtley, 2006]. The resulting 3D trajectories can be reconstructed from these data points, thus tracking the movement of the body in motion. A technique commonly used in gait laboratories is to separate the foot into three different segments according to their function: hind, mid and forefoot [Wu et al., 2002].

A forceplate is commonly used for these kinds of experiments. According to Newton's third law, *"for every action there is an equal and opposite reaction"*. Such a platform yields the ground reaction force (GRF) which is the total force applied by the foot to the ground during the gait cycle as a resultant force under the foot.

Experiments related to this research project were carried out in the University of Warwick's Gait Laboratory, and will be described in chapter 3.

2.5.2 Plantar Pressure Measurement

The forceplate used in gait analysis can measure and record the ground reaction force and centre of pressure, but it does not extrapolate the forces acting on specific foot areas. Plantar pressure, on the other hand, provides the distribution of that force over the foot. Given that the foot experiences loads of around 120% of bodyweight during walking (and up to 275% during running) [Nordin and Frankel, 2001], plantar pressure is a crucial factor since when in excess it can damage foot tissue. With this type of assessment, areas of high pressure and potential ulceration can be found before any damage occurs, thus allowing early treatment and preventing further damage.

There are different types of methods for measuring plantar pressure, designed for different purposes, but which can be divided into pressure-sensitive mats and in-shoe pressure systems. These all have the same working principle, an array of sensing elements in the shape of a matrix, which can be either capacitive or resistive. In the first case, it consists of two electrically charged plates, which approach as a result of pressure and this action is translated as a variation of its capacitance in order to calculate the pressure applied. In the case of a resistive sensor, these measure the resistance of conductive foam between two electrodes when pressure is applied, resulting in an increase in current [Razak et al., 2012]. Unlike a forceplate, they can only measure the vertical component of the ground reaction force with the advantage of measuring the distribution of the foot contact area [Richards, 2008]. For this research, a Tekscan in-shoe system is used as will be described in chapter 3.

2.5.3 Electromyography

Electromyography (EMG) is the study of the electrical potentials (called motor unit action potentials, MUAPs) generated by the muscle during contraction in

any motor task, and these recordings can provide an insight into muscle activation. This contraction generates an electric field that can be detected using EMG electrodes, which can be surface or indwelling [De Luca, 1997]. Many factors can introduce noise, such as cross-talk from other muscles or the state of the surface where the electrodes are placed. In principle, the EMG signal will increase with the amount of muscle fibres recruited (stronger muscle contraction) [Heintz, 2006]. The raw data obtained in these types of studies has to be filtered, smoothed and processed in order to produce valuable data. Signal processing will be further explained in chapter 4 when analysing EMG data for lower limb muscles during stance and swing phase.

2.5.4 Imaging

In the assessment and diagnosis process of foot disorders, the feet should be examined both in weight bearing and non-weight bearing positions, as well as during the gait cycle of the patient [Balint et al., 2003].

Physical examination, including palpation, sensation assessments, measurements of strength and motion and history check, and the appropriate imaging set, can give certain diagnosis [Rao et al., 2007]. Imaging of the foot is in continuous development and the chosen modality depends on the accuracy, cost, invasiveness and clinical indication [Ritchie, 1997].

Despite the continuous development of new technologies in foot imaging, the primary and most common imaging technique is plain radiography [Broder, 2010]. This technique gives a good overview of the region of interest and is useful for detecting fractures, erosions, deformities and dislocations. However, its main disadvantage is the possibility of misinterpretation of shadows that are anatomically normal [Christman, 2003]. Computerised tomography (CT) has proven to be good for complex fracture analysis, but it is not convenient for musculoskeletal abnormalities [Broder, 2010]. Ultrasound is the best tool for assessing tendinopathies and masses in the soft tissue and does not expose the patient to ionising radiation [Rankine, 2009]. Due to this advantage, it is sometimes used in the same physical

examination. Magnetic Resonance Imaging (MRI) provides anatomical details of the bone and the adjacent soft tissue without exposing the patient to ionising radiation [Palestro et al., 2006].

All of the imaging techniques mentioned above can provide information about the internal foot structure.

2.6 Foot Modelling

The difficulties arising in foot modelling are inherent in the complex composition of the foot. In fact, it is usually modelled as a single rigid body, which is perhaps somewhat misleading for this type of research. There are three main reasons that make foot modelling so challenging [Kirtley, 2006]:

1. The foot contains too many bones (26), which make it difficult to place all the necessary markers required for gait analysis.
2. Markers cannot reflect the bone and tissue movement completely.
3. The joints of the foot are complex.

Although many foot models have been developed during recent years, most of them simplify the foot geometry, structure and material [Qiu et al., 2011]. Authors agree that an evaluation of the approach to foot modelling is extremely difficult due to its nature [Cheung and Nigg, 2008].

In 3D foot modelling some problems appear, as they depend on the hard and soft tissue involved, with musculoskeletal forces transferred between them. Kinetic analysis has been restricted to models that describe the foot as one rigid segment, but this could be improved with a multi-segment approach [Dixon et al., 2012].

3D Foot Modelling that has been performed has tried to overcome the constraints of earlier 2D modelling. One of the first theoretical models was a 2D finite element model, which idealised the planar section of the foot [Nakamura et al., 1981]. Its purpose was to predict the stress in soft tissues. The foot was represented only by a single elastic body. One year later a 3D model was developed on the basis of

a matrix structural analysis [Simkin, 1982]. This model was innovative, but could not be validated due to some geometrical misrepresentations. Patil et al. [1996] again used 2D finite element analysis, which proved to be useful in predicting stress distribution, but failed in the geometry as it was reconstructed with X-ray images. Therefore, this kind of modelling was not adequate enough to study foot kinematics in both clinical and biomechanical research.

Following this, many other authors developed multi-segment models [Carson et al. [2001], Cornwall and McPoil [1999], Kidder et al. [1996], Leardini et al. [1999], MacWilliams and Nicholson [2003], Nawoczenski et al. [1998], Stebbins et al. [2006]]. Different approaches have been presented regarding foot segmentation. Gilchrist and Winter [1996] introduced a two-part model of the foot which consists of nine spring- damper systems, dividing the foot into two segments, with one joint representing all the metatarsophalangeal joints together. Morlock and Nigg [1991] developed a six-segment model in order to estimate the joint kinematics and kinetics during stance phase of the gait cycle. Scott and Winter [1993] developed an eight-segment model, dividing the tissue under the foot into seven independent sites and modelled as non-linear spring-damper systems. Hunt et al. [2001] designed a foot model consisting of three segments (Tibia, Hindfoot and Forefoot), which was completed some years later by Wang et al. [2010] adding the Hallux as a vector. Leardini et al. [1999, 2007b] divided the foot into four segments: Tibia, Calcaneus, Midfoot and Metatarsal. In his work, not only did the authors study the motion within the foot, but they also associated foot motion with movement of the leg.

Deschamps et al. [2011] made evident that there was a problem regarding reliability. Their conclusion was that further research was needed in order to validate the models. According to their review, fifteen different models have been derived to represent the foot and the leg, which use four to nine rigid segments. Many marker sets and models are available for foot modelling, though there is currently no gold standard [Bishop et al., 2012]. A summary of the available models is presented on figure 2-9.

According to Kirtley [2006], the most widely accepted foot models for gait anal-

ysis are the Helen Hayes and the Cleveland Clinic models. In contrast, Bishop et al. [2012] conclude that the two foot models that are reliable and have literature support are the Milwaukee foot model and the Oxford foot model. The latter was developed by the Nuffield Orthopaedic Centre (NOC) at Oxford University (UK) and implemented by Vicon. This last model underlines the importance of the midfoot as the mechanism involved for motion transmission between the Hindfoot and the Forefoot and is employed throughout this research for gait analysis purposes.

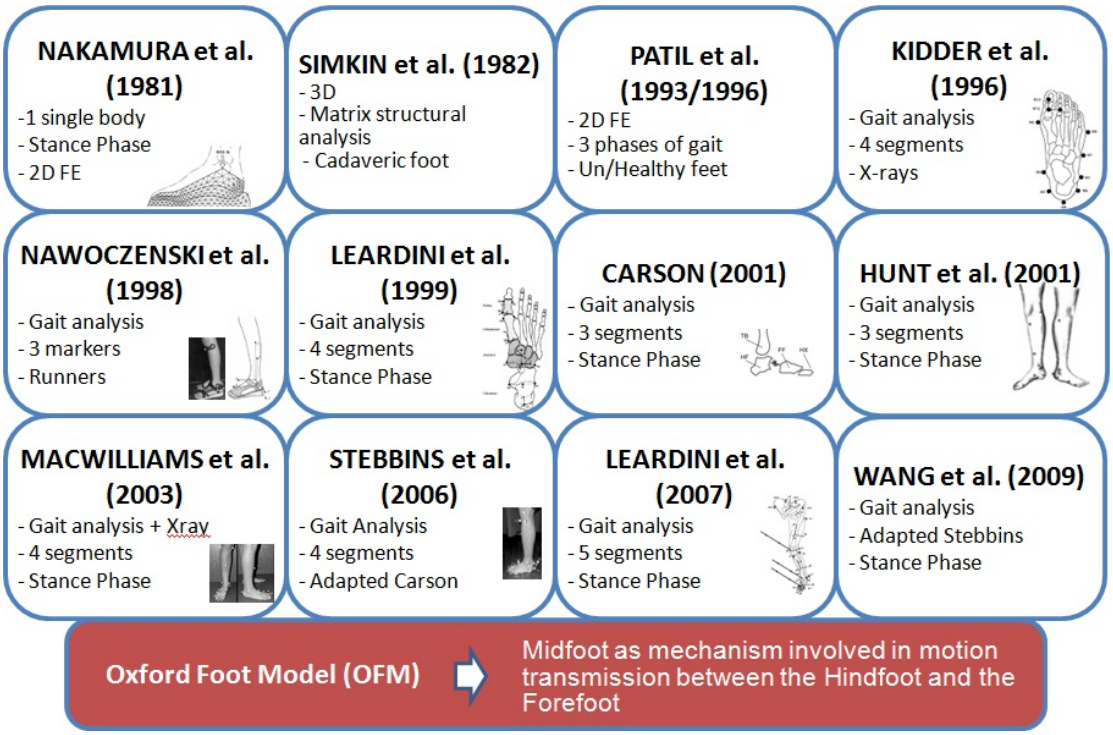

Figure 2-9 Summary of the available foot models

2.7 Diabetic Foot

Diabetes is a continuous challenge for all kinds of medical experts as it is a very complex disease. According to the World Health Organization, the current worldwide population with diabetes (both type 1 and 2) is estimated at 442 million worldwide and is projected to be the 7th most prevalent cause of death by 2030 [WHO, 1998].

Diabetes affects the whole human body, but it particularly affects the musculoskeletal system. Muscles, tendons, ligaments and bone marrow are the most

affected parts. The foot is the most common target and as the changes in its anatomy can occur rapidly, an early diagnosis is imperative in order to provide appropriate medical care, thus avoiding amputation which is a high factor of morbidity [Frykberg et al., 2006]. According to the World Health Organization, "The foot of a diabetic patient has the potential risk of pathologic consequences, including infection, ulceration, and/or destruction of deep tissues associated with neurologic abnormalities, various degrees of peripheral vascular disease, and/or metabolic complication of diabetes in the lower limb" [WHO, 1998].

Most of the injuries diabetic patients suffer in their feet are the result of a mechanical trauma that cannot be perceived due to neuropathy [Cavanagh, 1999]. These injuries occur equally in the forefoot, dorsal and plantar surfaces [Cavanagh et al., 2005]. Neuropathy reduces and can even inhibit the sensation of protection, causing changes in the foot structure and its functions [Sawacha et al., 2012]. Given these conditions, there is predisposition to high foot plantar pressure which is a key factor in the development of diabetic foot ulceration [Giacomozzi and Martelli, 2006]. Such pressure can damage the diabetic foot in different ways depending on its frequency. It can cause direct trauma if there is only one episode of high trauma; but it can cause inflammation, callus formation and more tissue damage if it is intermittent, and causes ischaemic damage if the pressure is continuous [Foster, 2006]. Skin ulcerations are most likely to appear at the points of high pressure [Tan and Teh, 2007]. Moreover, previous studies [Edmonds and Watkins, 1999; Eils et al., 2004] showed diabetes can modify the mechanical properties of the plantar soft tissue, making it stiffer, harder and thinner; it can also absorb more energy and recover more slowly than healthy tissue [Gooding et al., 1986]. Plantar Fascia is also affected by diabetes, making it thicker and resulting in a "stiffer" foot as a consequence of the onset of the windlass mechanism thus making the foot act as a rigid segment [Marks et al., 2007]. Therefore, it is essential to study the properties of the plantar soft tissue in order to understand the ulcer formation mechanisms and their treatment [Pai and Ledoux, 2010].

In the Ledoux [2007] review of the biomechanical changes in the diabetic foot, it was stated that data proved the gait pattern of diabetic patients who suffer

neuropathy was modified to be more cautious, less efficient and variable. Diabetic patients also showed altered lower limb joint mechanics, with limited mobility at the ankle, subtalar and first metatarsal joints. Consequently, biomechanics are of high importance in neuropathic injuries [Simon, 2004]. In many cases, the consequences can be prevented if the disease is identified at an early stage and patients are given appropriate information and education on how to avoid injuring their feet [De Berardis et al., 2005].

Of major interest are the three injuries with the highest incidence (see figure 2-10): Lisfranc joint injuries, Charcot Foot and Hallux Limitus.

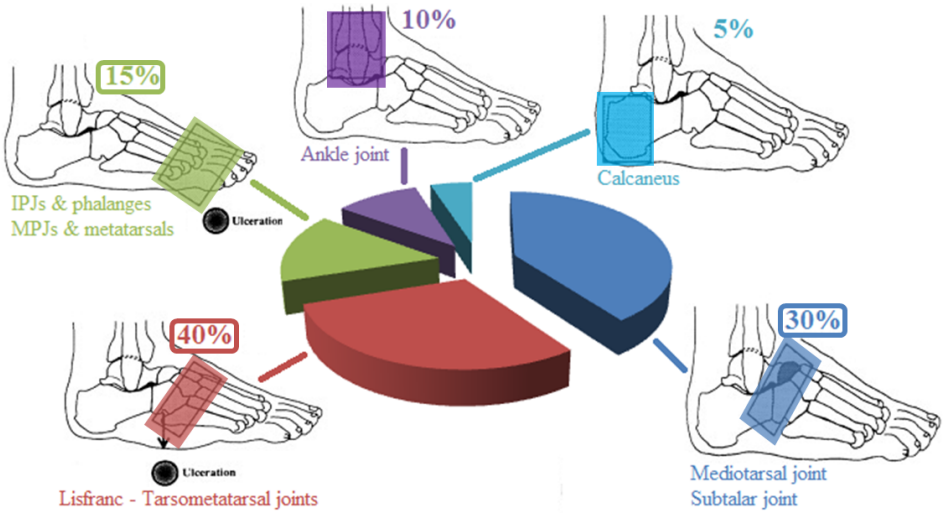

Figure 2-10 Diabetic injuries incidence. Modified from Frykberg et al. [2006].

Figure 2-11 depicts the aforementioned injuries: (a) Hallux Limitus, (b) Lisfranc joint injuries and (c) Charcot Foot.

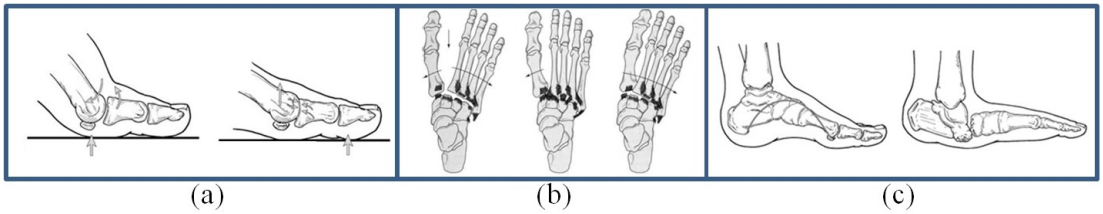

Figure 2-11 Diabetic injuries: (a) Normal foot (left) and Hallux Limitus (right). (b) Lisfranc joint injuries (divergent, isolated and homolateral). (c) Normal foot(left) and Charcot foot (right). Modified from American College of Foot and Ankle Surgeons [ACFAS, 2009].

2.7.1 Hallux Limitus

First metatarsal head or great toe ulceration is one of the most common injuries in the diabetic foot [Boffeli et al., 2002]. The Hallux Limitus (figure 2-11(a)) progressively degenerates the metatarsophalangeal joint of the hallux (great toe) causing pain, joint swelling and decreasing its mobility [Marquez and Oliva, 2010]. It is a consequence of a soft tissue imbalance that modifies the biomechanics of the joint [Flavin et al., 2008]. Although the diagnosis is primarily clinical, an MRI is useful to see how the joint is compromised and decide upon the appropriate treatment.

2.7.2 Lisfranc joint injuries

A joint appears when one bone is in contact with another bone. The Lisfranc (or tarsometatarsal) joint is the articulation between the metatarsals, the three cuneiforms and cuboid and contributes to the midfoot flexibility [Hockenbury, 2006]. The first symptoms are joint swelling and ligamentous laxity [Barlas et al., 2009]. Most of this type of injury are due to an excesive rotation and pronation of the foot. It is classified as divergent (metatarsals displayed in different directions), isolated (one or more metatarsals are separated from the joint) and homolateral (when the metatarsals are displaced in the same direction). See figure 2-11(b) for the injury illustration.

2.7.3 Charcot Foot

Charcot foot (figure 2-11(c)) is a process of joint deterioration which is chronic and almost painless. Its development is due to the loss of protective sensation and continuous (or cascade of) mechanical or minor trauma. Neural function is diminished causing an abnormality in the joint and underlying bone [Mayer and Kabbani, 2003]. As a result of this process, the midfoot is highly affected and patients increase their predisposition of plantar ulceration [Hockenbury, 2006], as well as foot deformity and can lead to amputation [Sanders and Frykberg, 2008].

Its first symptoms are swelling of the foot and a warm sensation. It affects both bones and tissues [Barlas et al., 2009]. Due to its symptoms, it is often confused with osteomyelitis, which is a bone infection [Tan and Teh, 2007]. According to many authors [Frykberg et al., 2006; Roug and Pierre-Jerome, 2012], MRI is a helpful tool for the diagnosis of Charcot foot, but they all agree that the distinction between these two pathologies is very difficult. The difference in the MRI is based mainly on the distribution of the disease [Roach, 2011].

3

Methodology

Thanks to evolutions in technology, the development of biomechanical models of body motion - and specifically of the foot - have improved. A combination of different techniques such as gait analysis, plantar pressure measurements and image processing, together with biomechanical principles, can contribute to the development of multi-segment models that can be validated using subject data. It is therefore possible to gain insight into the forces applied to the musculoskeletal system including the joints. Throughout this chapter, the methodologies applied to study foot biomechanics are explained.

3.1 Motion Capture

Experimental analysis was carried out in the Gait Laboratory within the School of Engineering at the University of Warwick (figure 3-1(b)) and surroundings, complying with all data protection requirements as stated in the University of Warwick's BSREC ethical[1] approval process.

[1]BSREC full approval REGO-2013-582 Foot Modelling. See appendix A for more information.

3.1.1 Capture room

The laboratory's Vicon MX motion capture system consists of a cluster of 12 IR cameras (MX-T20 NIR series 8.5mm & 12.5mm lens, figure 3-1(c)), that are able to capture the movement of reflective markers attached to a subject (figure 3-1(a)). These cameras have four infra-red LED concentric rings that flash at 200 times a second (200Hz), allowing for all types of movements to be recorded, with a resolution of 0.02mm (see appendix B for further information on resolution analysis). As shown in figure 3-1(b), these cameras are attached to a metal frame, aimed at the centre of the capture volume. If a marker is captured by three or more cameras, then the position in 3D space can be identified, and therefore the trajectory of the marker can be tracked. These markers can either be attached to a velcro suit or directly onto the skin by means of double sided tape (approved to be used in healthcare and medical devices) as seen in figure 3-1(a). The markers are spheres covered by reflective tape that are screwed onto a plastic base that permits attachment to any surface (either skin, velcro suit or any object). They come in different sizes, according to different marker placement requirements; in this thesis 9.5mm and 14mm diameter markers were used. There are also two digital video cameras (DV cameras) which can record the trial, being triggered at the same time as the rest of the components of the Gait Laboratory.

The laboratory also has a forceplate (AMTI, model OR6-7) in the centre of the capture volume, which permits calculation of the total force applied by the foot of a subject to the ground (figure 3-1(e)). The forceplate operates at 1000Hz and is made up of four sensing elements (strain gauge bridges), which outputs are F_x, F_y, F_z, M_x, M_y and M_z (forces F and moments M, in the forceplate's axis system, respectively) [AMTI, 2001].

The global coordinate system used in the gait laboratory is represented on figure 3-2, where the vertical direction is denoted by "Z", the direction of progression is "X" and the transverse direction "Y".

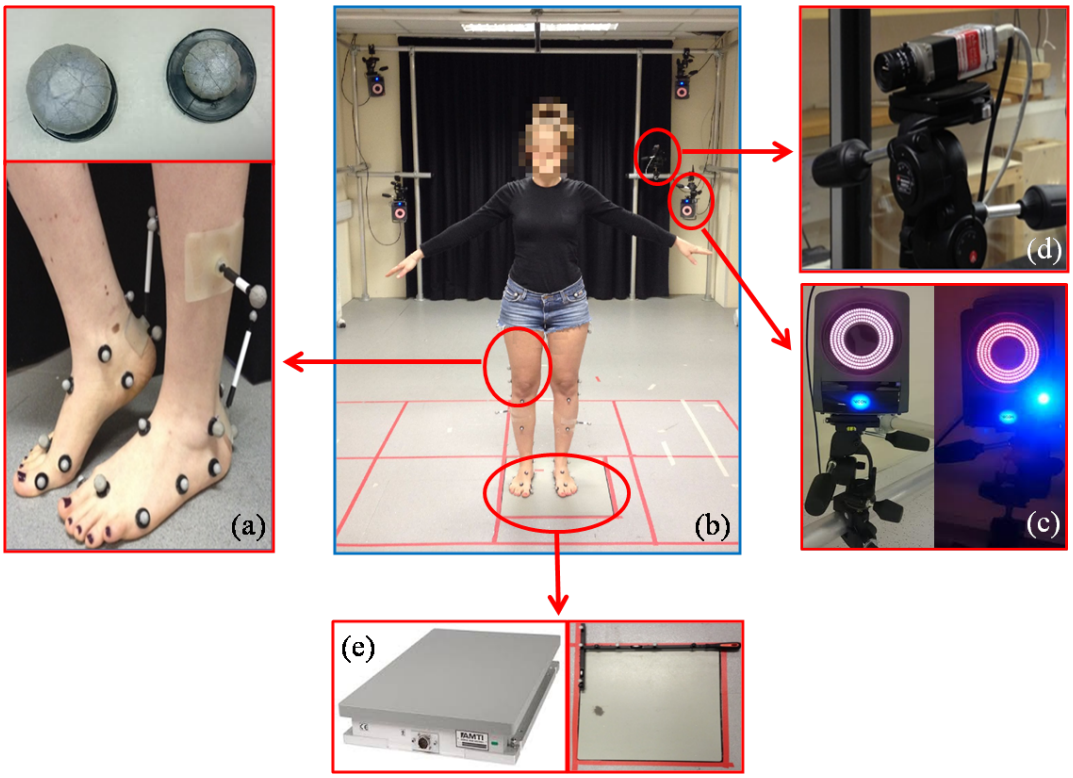

Figure 3-1 Gait Laboratory within the School of Engineering at the University of Warwick - Capture room: (a) Oxford Foot Model marker placement. (b) Gait Laboratory. (c) Vicon Camera. (d) DV Camera. (e) Forceplate.

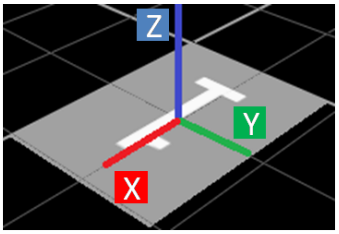

Figure 3-2 Global coordinate system used in Gait Laboratory, where "Z" is vertical direction, "Y" transverse direction and "X" is direction of progression.

3.1.2 Control room

The MX cameras are connected through gigabit ethernet to two Vicon control boxes placed in the control room (figure 3-3), which are linked to a PC containing Vicon related software. The forceplate is connected through an amplifier and a digital converter (as the output of the forceplate is an analogue signal) to the Vicon control box.

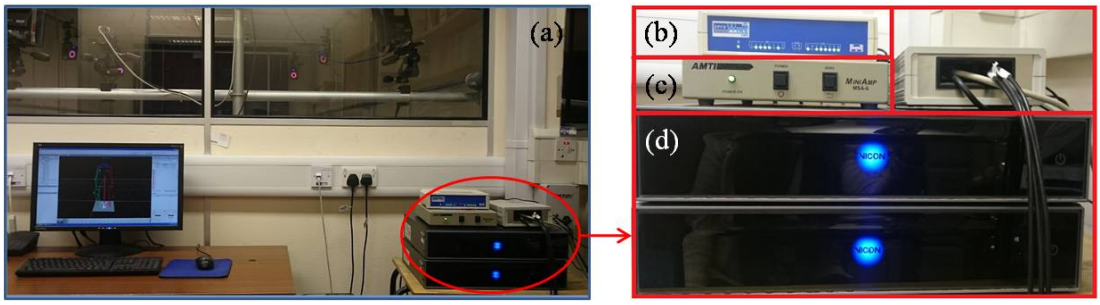

Figure 3-3 Gait Laboratory within the School of Engineering at the University of Warwick - Control room: (a) Control room. (b) EMG main unit box. (c) Forceplate amplifier. (d) Vicon Giganet box (control box)

3.1.3 Data Collection

After masking any reflections present in the laboratory and calibrating the equipment (figure 3-4), a subject's calibration can begin.

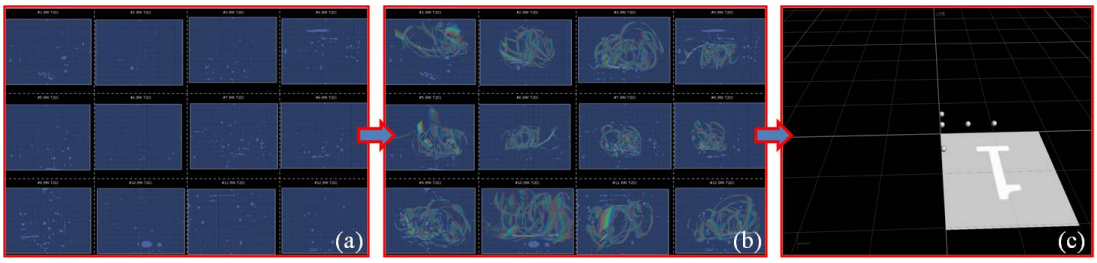

Figure 3-4 Gait Laboratory system calibration.

System calibration consists of three steps: (a) Create MX camera masks, consists of checking for (and blocking) any extra reflections that might be present in the room and cause problem as the system might see them as markers. (b) Calibrate cameras, when the cameras will collect data as a person moves an L shaped wand in the capture room; this step is to prove all the cameras are aimed such that at least three of them can see every marker. (c) Set the volume origin, which means defining the origin of the volume capture.

The system requires specific information about the subject in order to scale the model for the participant and reconstruct foot motion. The physical parameters that are needed are: body mass, height, leg length, knee width and ankle width (the last three, for both legs). Following input of these parameters, a total of 43 markers are placed by palpation on each of the subject's lower limbs in line with the Oxford Foot Model guidelines.

The Oxford Foot Model works in tandem with the Plug-in-Gait model to provide

a complete lower limb analysis [Vicon, 2012]. Figure 3-5 depicts the markers' position for the Oxford Foot Model and table 3-1 lists the anatomic position of each marker for Plug-in-Gait (red) and Oxford Foot Model (red, black and blue). The Plug-in-Gait model uses sixteen markers to define seven segments: pelvis, femur, tibia and foot (the last three for right and left leg). The Oxford Foot Model adds 27 markers in order to provide a detailed analysis of the foot kinematics. Therefore, each foot is instead defined by three segments [Vicon, 2012]:

1. Hindfoot: Defined by markers placed on the posterior end of calcaneus, lateral calcaneus, Sustanticulum Tali, and heel.

2. Midfoot: Defined by markers placed on the distal lateral side of of 5th metatarsal, proximal dorsal side of 1st metatarsal, proximal lateral side of 5th metatarsal and over the second metatarsal head.

3. Hallux: Defined by markers placed on the proximal end of the 1st distal phalanx and the distal medial side of 1st metatarsal.

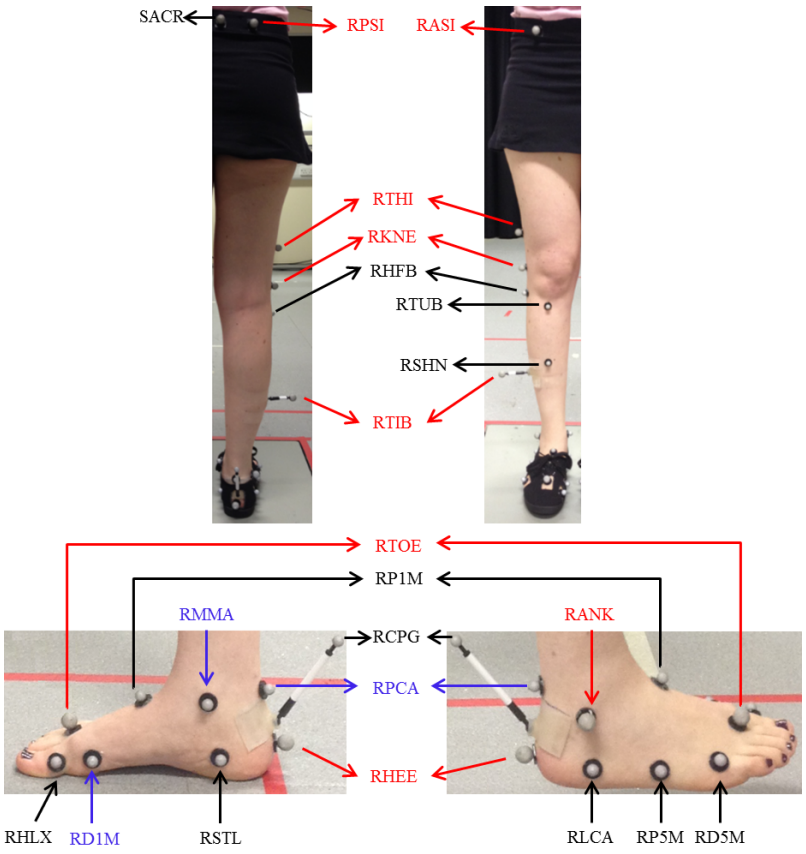

Figure 3-5 Oxford Foot Model and Plug-in-Gait marker placement.

Marker Name	Position
LASI/RASI	Anterior Superior Iliac Spine
LPSI/RPSI	Posterior Superior Iliac Spine
SACR	Sacral marker (midway between LPSI and RPSI)
LTHI/RTHI	Over the lower lateral 1/3 surface of the thigh, just below the swing of the hand, although the height is not critical
LKNE/RKNE	Lateral epicondyle of the left knee
LTIB/RTIB	Over the lower 1/3 of the shank to determine the alignment of the ankle flexion axis
LHFB/RHFB	Lateral head of fibula
LTUB/RTUB	Tibial Tuberosity
LSHN/RSHN	Anterioraspect of the shin
LANK/RANK	Lateral malleolus along an imaginary line that passes through the transmalleolar axis
LMMA/RMMA	Medial Malleoli
LCPG/RCPG	Posterior end of the calcaneus
LHEE/RHEE	On the calcaneous at the same height above the plantar surface of the foot as the toe marker
LPCA/RPCA	Posterior calcaneus proximal
LLCA/RLCA	Lateral calcaneus
LSTL/RSTL	Sustaniculum Tali
LP1M/RP1M	1st metatarsal, proximal dorsal
LD1M/RD1M	1st metatarsal, distal medial
LP5M/RP5M	5th metatarsal, proximal lateral
LD5M/RD5M	5th metatarsal, distal lateral
LTOE/RTOE	Over the second metatarsal head, on the mid-foot side of the equinus break between fore-foot and mid-foot
LHLX/RHLX	Hallux, proximal end of 1st Distal phalanx

Table 3-1 Oxford Foot Model and Plug-in-Gait marker placement. Markers corresponding to Plug-in-Gait are identified in red. Markers in black and blue, combined with the red ones, define the Oxford Foot Model. Markers denoted in blue are used only for static trial when using Oxford Foot Model and subsequently removed for dynamic trials. Prefix **L** indicates Left side and **R** indicates Right side. Table summarised from Vicon [2012] and Vicon [2010].

The markers are placed on anatomically relevant positions in order to model different joints and segments; usually aligned with the modelled segment and aligned to the axes of rotation in case of a joint. The markers are located in specific areas where there is minimal soft tissue between bone, joint and skin, and they are labelled with names referring to their position. These markers have to be carefully positioned in order to be able to replicate the same experiment in all subjects allowing a meaningful comparison between them. Once this task is completed, motion analysis trials can begin. The first step is to perform a static trial, used to scale the model for the participating subject. The participant has to stand on the forceplate and remain still for a few seconds (figure 3-6(a)). The rest of the trials that are carried out are dynamic (figure 3-6(b)), such as walking in different pace, stretching and other types of exercises which will be explained in chapter 4.

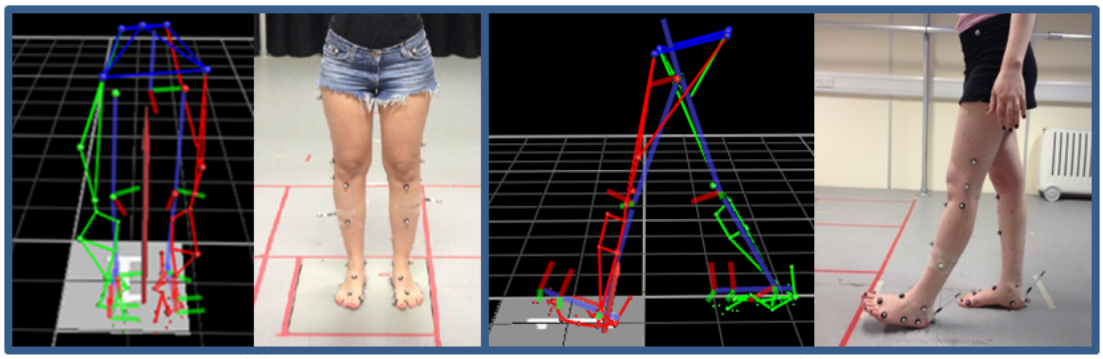

(a) (b)

Figure 3-6 Gait analysis - static and dynamic trials: (a) Marker placement and Vicon Nexus reconstruction for static trial and (b) Marker placement and Vicon Nexus reconstruction for dynamic trial.

As it can be seen in figure 3-6, local coordinate systems are placed throughout the lower limb [Vicon, 2010]. The model outputs provided by Vicon Nexus and Polygon are defined in these local coordinate systems, Table 3-2 displays Plug-in-Gait and Oxford Foot Model output specification for the ankle joint.

Ankle axis	Force Component	Model Component
X	Compression/Tension	Dorsi/Plantarflexion
Y	Medial/Lateral	Abduction/Adduction
Z	Anterior/Posterior	Rotation

Table 3-2 Plug-in-Gait and Oxford Foot Model output specification for the ankle joint

3.1.4 Data Processing

All the acquired information was processed by the Vicon Nexus 1.8.5 software in order to gain deeper knowledge about joint angles, torques, powers and moments. This software has a filtering function embedded and provides different pipelines for exporting the data. The output from the trials were filtered and exported on an ASCII file for further analyses using Matlab 2015b. Data were normalised to a complete gait cycle in all of the cases in order to allow comparison among trials.

3.2 Electromyography

A Aurion Zero-wire electromyography system is also available in the Gait Laboratory (figure 3-7). It is a 16 channel surface electromyography (SEMG) wireless system that uses electrodes placed on the skin above the studied muscle in order to analyse its activation pattern. Each of the probes operates at 1000Hz and connects wirelessly to the main unit, that sends the acquired data to a Vicon Giganet box. As the probes are very small, light (10g) and wireless, the subject under study can move freely, allowing a better understanding of natural gait.

In this thesis, EMG recordings of the lower limb muscles are used to analyse muscle activation during different activities (walking, passive stretching and maximum voluntary contractions). As explained in the previous chapter, the data obtained from these types of studies need to be processed in order to produce meaningful data. This process is depicted in figure 3-8.

As described in Winter [2005], the first step in the process is to high-pass filter the raw EMG. Then the signal is rectified using a full-wave rectifier, which will provide absolute values. The last process consists of creating a linear envelope, by filtering the rectified signal with a low pass filter. A 4th order zero-lag butterworth filter with a cut off frequency of 4Hz is used for this purpose. The Matlab code used for analysing these signals can be found in appendix C.

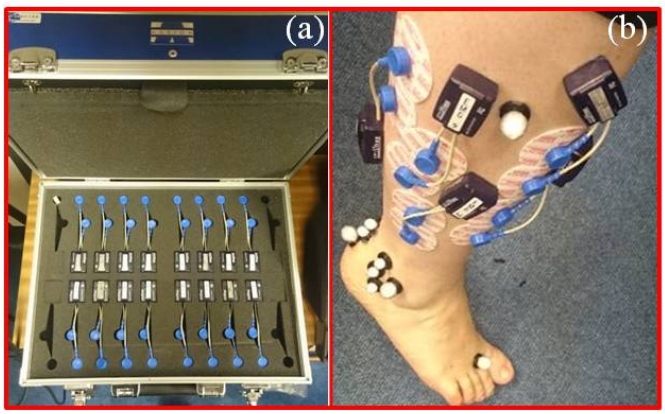

Figure 3-7 Aurion Zero-wire electromyography system: (a) EMG probes. (b) EMG probes connected to surface electrodes and mounted on the skin surface on the lower limb muscles of the lateral compartment.

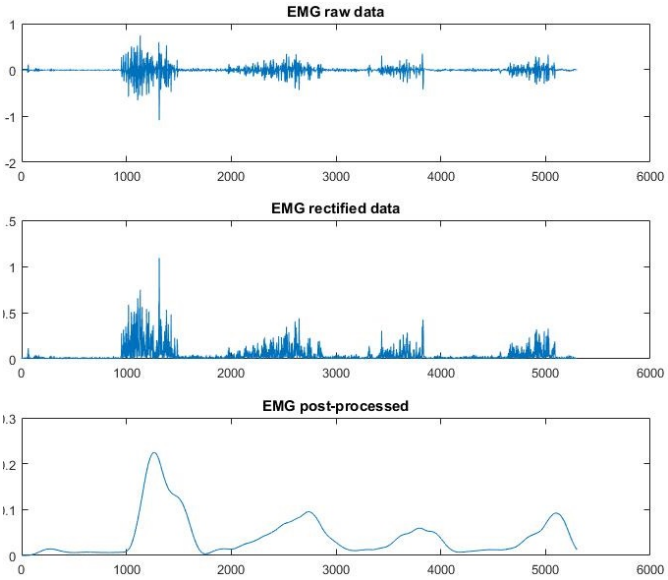

Figure 3-8 EMG processing (Tibialis anterior): The image depicts the raw signal, the high-pass filtered signal and the full-wave rectified and finally the envelope (low pass filtered at 4Hz).

3.3 Plantar Pressure

Interest is focused in measurement of the force distribution under the subject's foot, mapped plantar pressure to show distribution of ground reaction force. A Tekscan F-Scan plantar pressure system was used with in-shoe 3000E sensors (insoles), see figure 3-9. These insoles are made of a thin film with pressure/force sensors that can detect, display and record real time in-shoe pressure information in 2D and 3D.

In order to perform the experiments, insoles were first trimmed to standard shoe sizes and placed in the shoes (figure 3-9(b)). The cuffs connected to the thin sensors are responsible for gathering and processing the data that are sent to the datalogger via an ethernet cable (figure 3-9(c)). This information is then sent wirelessly to the computer (figure 3-9(d)). The system only needs a step calibration in which the subject is asked to stand on the right foot first and then the left one, and viceversa. The only necessary parameter is the subject's body mass. Collected data are then exported to an CSV file and analysed using Matlab 2015b.

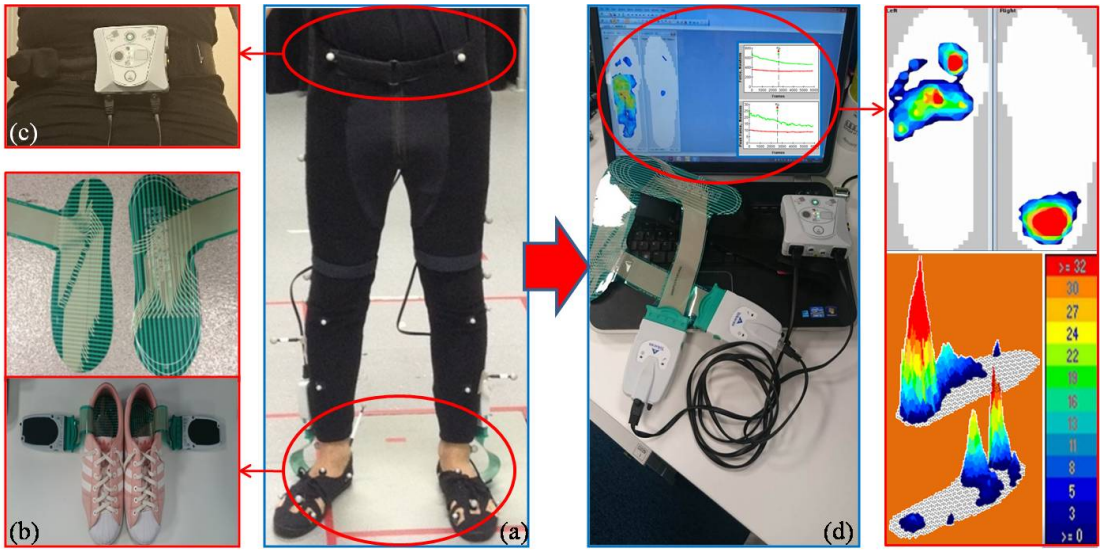

Figure 3-9 Tekscan pressure system setting: (a) Tekscan setting. (b) Insole trimming and placement inside footwear. (c) Datalogger. (d) F-scan software.

4

Intermediate Results

Intermediate results are presented and compared to establish the reliability of the proposed methods. This chapter describes this exploratory analysis, proposing first a new method for simultaneous plantar pressure and gait study. It also explores foot anthropometry and validates new approaches to muscle-tendon length and moment arm measurement, following an analysis of different pennation angle assumptions. Finally, muscle activation is examined.

4.1 Introduction

When embarking in the study of the altered gait, I first noticed that there are still important gaps in the literature of foot modelling in general (for normal/healthy gait). This is the case both for theoretical and empirical literature of the field. In my understanding, even though there is a plethora of foot models, frontier research does not profit from the recent technological developments that would allow for the analysis and development of more complex foot models. If a foot model combines the available technological tools with biomechanical principles, it can provide insights on the healthy gait and the pathological gait. However, combining different methodologies is not an easy task. The first problem encountered, was that they do not permit simultaneous experimentation: while gait analysis requires barefoot experimentation, plantar pressure assessment requires subjects to

be shod. Therefore this chapter provides intermediate results to show the validity of alternative methods to examine gait and plantar pressure simultaneously.

The chapter is structured as follows: In the first section (section 4.2), a method is proposed to reconcile barefoot and shod conditions, necessary for gait and plantar pressure analysis respectively.

The second section of this chapter (section 4.3) provides an insight into foot anthropometry, as it is the object of study of this thesis. An analysis is performed over foot segments, arch height, ground reaction force distribution and mass.

After a clear understanding of the available methodologies and how to make them work in tandem, and of the foot structure, it was necessary to analyse muscle-tendon architecture. The main objective of the studies presented in the third section (section 4.4) was twofold:

1. Understand which parameters should be included in the model
2. Develop new techniques to examine the selected parameters or, for pre-existing methods, validate them against other methodologies (i.e. MRI and Ultrasound)

Four main characteristics of the muscle-tendon unit had to be analysed prior to any model application: length (subsection 4.4.2), moment arm (subsection 4.4.3), pennation angle (subsection 4.4.4) and muscle activation (subsection 4.4.5). An analysis of these four topics is performed, comparing and validating different types of non-invasive methodologies.

4.2 How to reconcile Barefoot and Shod conditions for Plantar Pressure Analysis in the Oxford Foot Model

The two main techniques commonly used to study the lower limb in biomechanics are gait analysis and plantar pressure measurements. However, these techniques require different settings: one requires barefoot experimentation and the other

one requires the subject to be shod. A new experimental technique was developed in this study [Jaitman et al., 2015] that can mimic the placement of markers when analysing and comparing barefoot and shod analysis on the same subject. This design allows the analysis of both approaches simultaneously and therefore provides valuable inputs to support a well validated model of the foot.

This study reports results on the reliability of the Oxford Foot Model under barefoot and shod conditions, as well as repeatability intra-person and inter-session. The method proposed introduces the use of specially designed shoes to enable simultaneous gait and plantar pressure analysis.

4.2.1 Methods

The difficulties arising in foot modelling are inherent in the complex composition of the foot. Most foot models developed during recent years simplify the foot geometry, structure and materials [Qiu et al., 2011]. Two well validated techniques for analysing foot biomechanics are gait analysis and plantar pressure measurement. Many previous experiments linked to foot modelling could not be truly validated due to their lack of precision in terms of marker placement during gait analysis and their inability to replicate the experiment under the exact same conditions [Deschamps et al., 2011; Bishop et al., 2012]. All of the studies referred to the motion within the foot and its kinematics, but none of them are conclusive regarding the dynamics. These problems are mainly due to the fact that not all of the available methodologies can be used simultaneously. Given that the two studied methodologies require different conditions, it is fundamental to find a way to perform both experiments at the same time in order to obtain accurate and reliable outputs.

The analysis was performed over two gait cycle events: Heel Strike and Toe Off (the first and fifth events in figure 4-1). The evaluated angles were:

- FF/HFA: Forefoot with respect to hindfoot.
- FF/TBA: Forefoot with respect to tibia.

- HX/FF: Hallux with respect to forefoot.

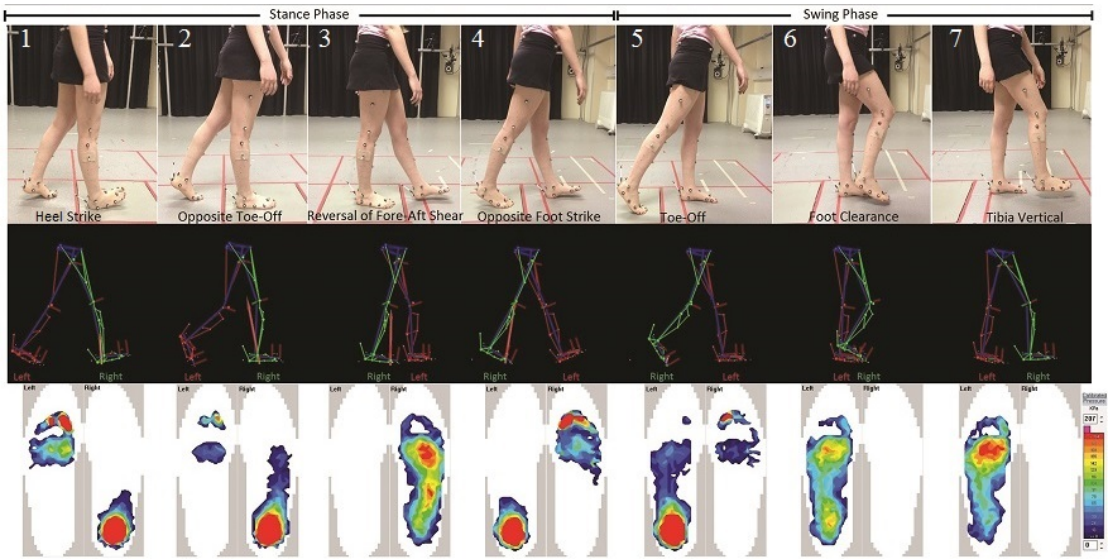

Figure 4-1 Complete Gait Cycle analysed simultaneously with Motion Capture System (Vicon Nexus) and Plantar Pressure Insoles (Tekscan)

Table 4-1 describes each angle in terms of planes, motion and axis using the local coordinate systems.

Angle	Plane	Motion	Axis
FF/HF	Sagittal	Dorsiflexion	Forefoot Y
	Frontal	Adduction	Forefoot X'
	Transverse	Supination	Forefoot Z"
FF/TB	Sagittal	Dorsiflexion	Forefoot Y
	Frontal	Adduction	Forefoot X'
	Transverse	Supination	Forefoot Z"
HF/FF	Sagittal	Dorsiflexion	Forefoot X
	Frontal	Adduction	Forefoot Y'
	Transverse	Supination	Forefoot Z"

Table 4-1 Motion description for the studied inter-segmental angles. Note: According to Vicon [2012], due to the fact that Euler angles are calculated, each rotation causes the axis for the subsequent rotation to be shifted. This means that X' shifted by one previous rotation and Z" shifted by two previous rotations.

4.2.1.1 Subjects

The total number of subjects participating was 15, as this number should yield statistically significant results [Gage, 1997], lying within the upper bound of previous studies which typically included 7-15 participants. The age of the participants was between 22 and 34. The only eligibility requirement for the participants was that they did not have any foot or leg injury and were capable of walking around the Gait Laboratory for up to 15 minutes unaided. Males and females were asked to participate, though no analysis was performed by gender due to the small sample size.

4.2.1.2 Repeatability Analysis

A repeatability analysis was first performed in order to understand which sensitivities to consider for the rest of the experiments. The same subject was markered across four successive days and performed a dynamic trial on each day. Results of the assessments were compared to observe the median and the median absolute deviation (MAD) for the intersegmental angles (see figure 4-2).

The median for each angle was calculated considering 10 trials for each subject and table 4-2 shows these values.

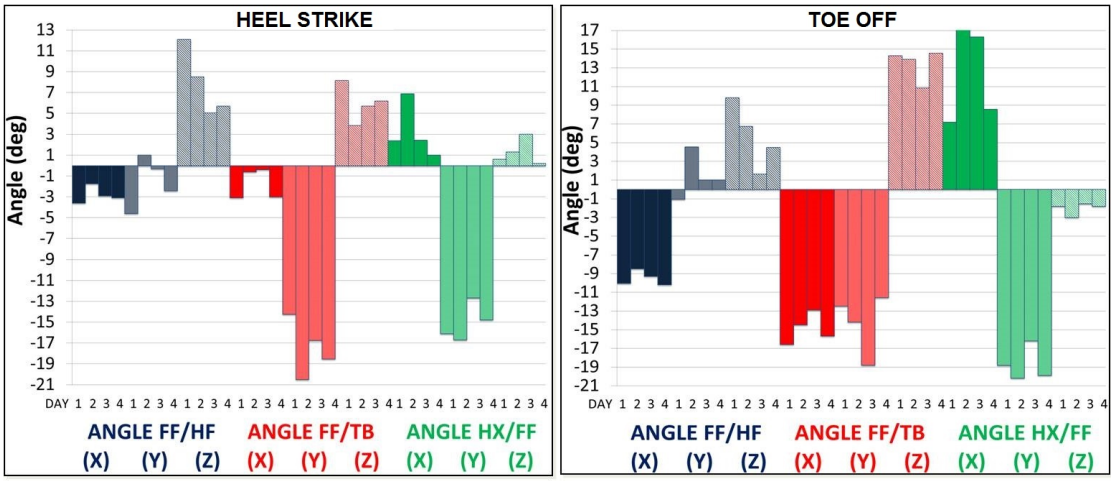

	ANGLE FF/HF (X)	ANGLE FF/HF (Y)	ANGLE FF/HF (Z)	ANGLE FF/TB (X)	ANGLE FF/TB (Y)	ANGLE FF/TB (Z)	ANGLE HX/FF (X)	ANGLE HX/FF (Y)	ANGLE HX/FF (Z)
MAD	0.7	1.9	2.5	1.3	2	1.2	1.9	1.3	1.2

	ANGLE FF/HF (X)	ANGLE FF/HF (Y)	ANGLE FF/HF (Z)	ANGLE FF/TB (X)	ANGLE FF/TB (Y)	ANGLE FF/TB (Z)	ANGLE HX/FF (X)	ANGLE HX/FF (Y)	ANGLE HX/FF (Z)
MAD	0.6	1.5	2.6	1.2	2.2	1.1	4.5	1.3	0.4

Figure 4-2 Repeatability analysis for Oxford Foot Model. Each of the bars represents the angle median for each testing session (10 trails) over a four-day period. The analysis is performed over heel strike (left) and toe off (right) events. Numeric results are presented on table 4-2.

	RFF/HFA			Heel Strike Median RFF/TBA			RHX/FFA	
X	Y	Z	X	Y	Z	X	Y	Z
-2.6°	-1.4°	6.15°	-1.8°	-17.7°	6.05°	1.7°	-15.4°	-0.3°
	RFF/HFA			Toe Off Median RFF/TBA			RHX/FFA	
X	Y	Z	X	Y	Z	X	Y	Z
-9.55°	1.25°	6.25°	-14.45°	-14.05°	13.8°	10.75°	-18.95°	-1.7°

Table 4-2 Median (in degrees) for angles studied in gait cycle events for Oxford Foot Model repeatability

The difference in terms of the joint angles over the four days was found to lie within: 2.6° for FF/HFA, 2.2° for FF/TBA and 4.5° for HX/FF (see table 4-3). These results match previous studies, where repeatability was assessed for successive measurements for one subject [Carson et al., 2001]. In their study, the deviation was slightly higher: 4.3° for FF/HFA, 3.0° for FF/TBA and 6.5° for HX/FF.

Heel Strike									
	RFFHFA			RFFTBA			RHXFFA		
	X	Y	Z	X	Y	Z	X	Y	Z
Day I	-3.6°	-4.6°	12.1°	-3.1°	-14.3°	8.2°	2.4°	-16.1°	0.6°
Day II	-1.8°	1.0°	8.5°	-0.6°	-20.5°	3.9°	6.0°	-16.7°	-1.3°
Day III	-2.9°	-0.3°	5.1°	-0.4°	-16.8°	5.7°	2.5°	-12.7°	-3.0°
Day IV	-3.1°	-2.4°	5.7°	-3.0°	-18.6°	6.2°	1.0°	-14.8°	-0.2°
MAD	**0.7°**	**1.9°**	**2.5°**	**1.3°**	**2.0°**	**1.2°**	**1.9°**	**1.3°**	**1.2°**
Toe Off									
	RFFHFA			RFFTBA			RHXFFA		
	X	Y	Z	X	Y	Z	X	Y	Z
Day I	-10.1°	-1.1°	9.8°	-16.6°	-12.5°	14.3°	7.2°	-18.8°	-1.8°
Day II	-8.5°	4.6°	6.8°	-14.5°	-14.2°	13.9°	17.4°	-20.2°	-3.0°
Day III	-9.3°	1.0°	1.7°	-12.9°	-18.8°	10.9°	16.3°	-16.2°	-1.6°
Day IV	-10.2°	1.0°	4.5°	-15.7°	-11.6°	14.6°	8.6°	-19.9°	-1.8°
MAD	**0.6°**	**1.5°**	**2.6°**	**1.2°**	**2.2°**	**1.1°**	**4.5°**	**1.3°**	**0.4°**

Table 4-3 Median for each of the four days and the corresponding median absolute deviation for each joint angle

4.2.1.3 Designed shoes

The designed shoes consist of basic canvas, that was trimmed around the position of each marker. The shoes had minimum heel height (5mm) and no cushioning as the inner sole was removed. These shoes allow as free as possible movement of the foot segments with replication of marker placement. It should be noted, however,

that the lacing section, does restrict midfoot movement while keeping the shoes in place. Nevertheless, it has been widely reported that the midfoot joint has a small range of movement (see for example Leardini et al. [2007a] and Sanchis-Salesa et al. [2016]), which is negligible when compared with other foot joints. When evaluating this joint, it could be observed that this small range of movement can be found in all of the three planes: from $-2°$ plantarflexion to $5°$ dorsiflexion, from $-5°$ inversion to $3°$ eversion and from $-5°$ adduction to $1°$ abduction.

Figure 4-3 OFM marker placement: barefoot, designed shoes and shoes.

4.2.1.4 Data collection and processing

The experiment consisted of three sessions of 30 trials for each subject. One third of these were in a barefoot condition, another third in a shod condition and the last 30 trials wearing the designed shoes. The last two sets of trials included analysis of the plantar pressure using Tekscan insoles. A static trial was first performed in order to scale the Oxford Foot Model for the participating subject. The subjects were then asked to walk at their own pace, stepping first with the right foot on the forceplate, and then with the left foot. Each session consisted of a total of 15 trials for each leg. Although walking speed was not controlled, only trials with similar velocity were used. Average walking speed for the trials was $0.834 \pm 0.093 m/s$. Once each batch of trials was concluded, the system was calibrated again and markers were removed from the subject. The position of each marker was marked to facilitate the replacement. Afterwards, the markers were replaced and the following sessions were completed. Markers replacement was done with an accuracy of 1mm.

All the acquired information was processed using multiple software tools including Vicon Nexus 1.8.5, Polygon 3.5.2, Matlab 2014a and Excel. As described in Wright

et al. [2011], Heel Strike was considered as being when the ground force reaction was greater than 10N and Toe Off when this force was less than 10N. Data sets were processed/smoothed by applying a fourth order Butterworth filter at a cut-off frequency of 8Hz [Winter, 2005].

4.2.2 Results

4.2.2.1 Plantar Pressure and Gait Analysis

The final aim of this study was to be able to simultaneously analyse both approaches (gait analysis and plantar pressure measurements).

The reliability of the designed shoes was assessed by placing the insole in both kinds of footwear used for all of the trials. Results were similar, proving the reliability of the method: the total force was similar during the gait cycle for both conditions. Figure 4-4 presents results for one of the subjects. Results for the rest of the subjects can be found in appendix D.

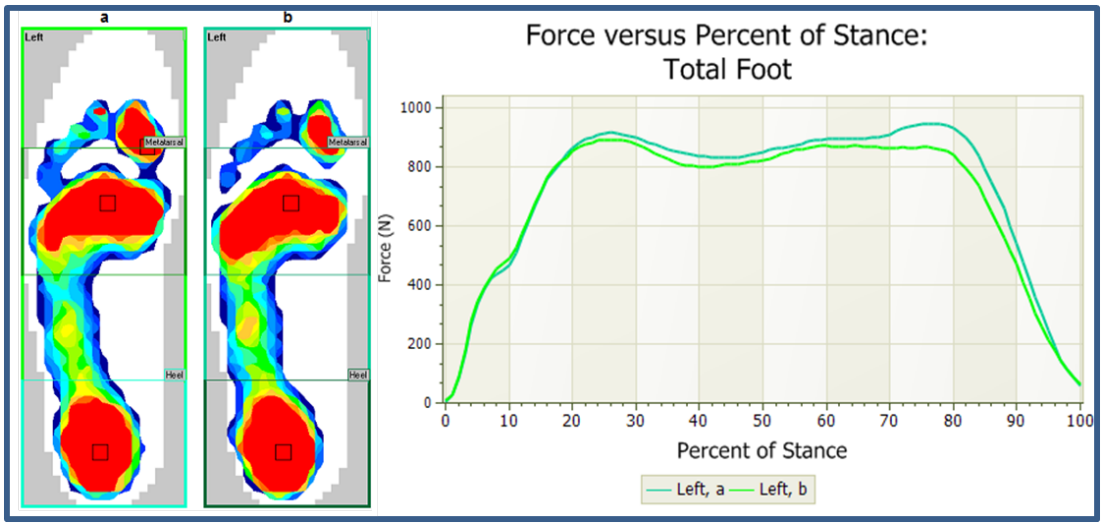

Figure 4-4 Results on plantar pressure for subject 15. Plantar pressure map and corresponding total foot force vs. Percent of Stance graph, for the left foot: (a) plain and (b) designed shoes.

Two stances were averaged, over approximately 50 seconds. A stance is a group of frames in which there is a minimum amount of pressure on the sensor. According to the Tekscan system, it groups all of the frames of pressure data from the heel strike to the toe off into only one "stance". The first and last stances were

excluded because they are usually incomplete. At any time, the total vertical force is calculated as the sum of all of the small vertical "local" forces exerted over each activated sensor. Given that the foot should not be considered as a rigid body, but as a multi-segment structure, it is relevant to observe the resulting force for each segment. A geometrical masking was applied, analysing the force for the heel and metatarsal. The results were also consistent for both sets of measurements (see figure 4-5). Results for the rest of the subjects can be found in appendix D.

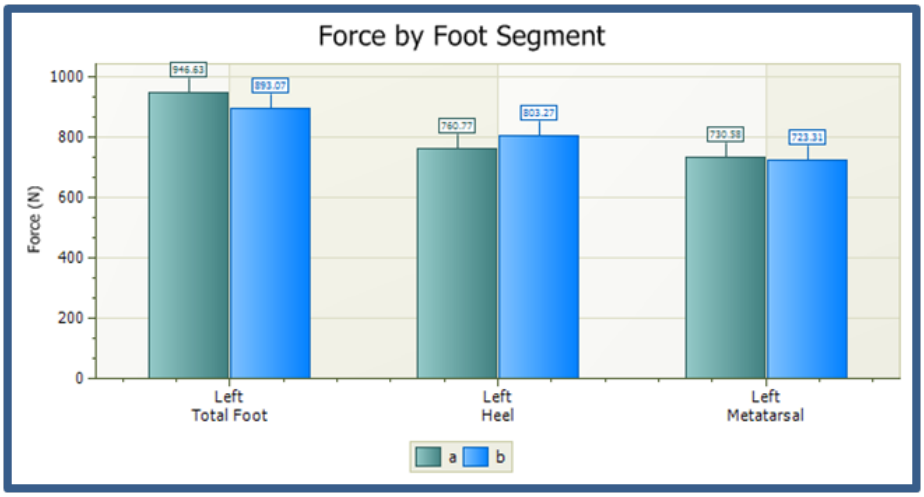

Figure 4-5 Results on plantar pressure for subject 15. Force by foot segment (subject 15): (a) Shod Condition (b) Wearing the designed shoes.

A further analysis was performed, comparing each set of data for each subject. Measurements were grouped in sets of 10 trials (the first two trials out of the fifteen were taken as practice, the following ten were used for analysis); 10 trials when wearing normal shoes and 10 when wearing the designed shoes. These two groups were compared for each subject, all yielding similar results (see table 4-4).

	Group A	Group B	Group B - Group A Diff	Group B - Group A % Diff
Minimum force of PS/A (N)	966.04	987.41	21.37	2.2
Force Average of PS/A (N)	1005.90	1050.80	44.90	4.5
Force Maximum force of PS/A (N)	1029.24	1187.12	157.88	15.3

Note: PS/A means Peak Stance Average and refers to a single movie frame, created by averaging the peak frames.

Table 4-4 Minimum, maximum and average forces for each group and their differences.

Figure 4-6 displays joint angles versus percentage of gait for one subject for the three studied conditions: Barefoot (in blue), Shod (in green) and Designed shoes

(in red). As expected, the results for the same person, under barefoot and shod conditions, showed a significant difference. These differences have been widely studied and reported (see for example Kung et al. [2015], Franklin et al. [2015] and Zhang et al. [2013]). The bespoke gait analysis designed shoes, on the other hand, proved to be reliable as the error introduced was smaller than that for the repeatability analysis performed on (figure 4-6).

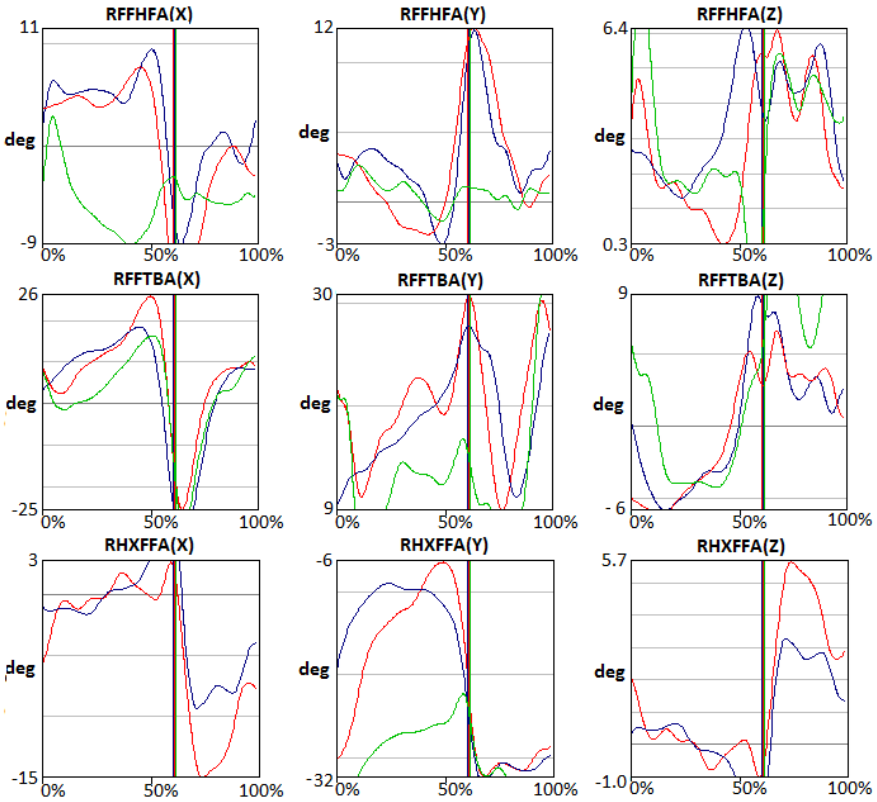

Figure 4-6 Joint angles versus percentage of gait cycle for a subject in three conditions (barefoot, shod and designed shoes). Barefoot (blue), Shod (green) and Designed shoes (red). Heel Strike at 0% and Toe Off approximately at 60% (the vertical line).

4.2.2.2 Statistical Analysis

As a first approach, a mean and standard deviation (SD) analysis was performed over the data collected from one subject (figures 4-7 and 4-8). 10 trials were analysed from each session, providing the mean and the SD for each session.

While showing good reliability for the proposed method, this approach was dismissed as the mean is not a representative measurement for these trials. The median is the most appropriate approach for gait analysis, as it uses the value

of the trial that lies in the middle of all of the values generated. Therefore, the largest and smallest values do not have a significant weight in the overall analysis [Gage, 1997].

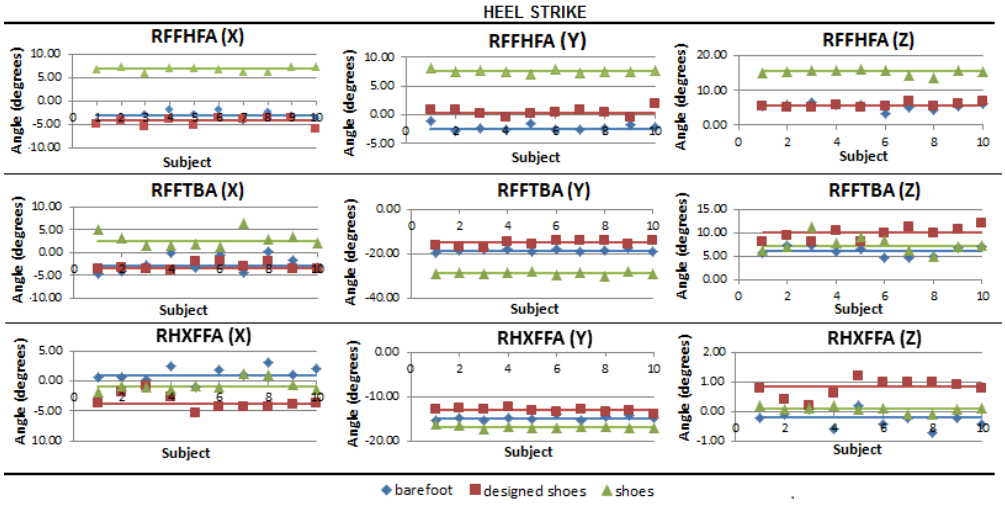

Figure 4-7 Mean joint angles for one person during heel strike for the three conditions.

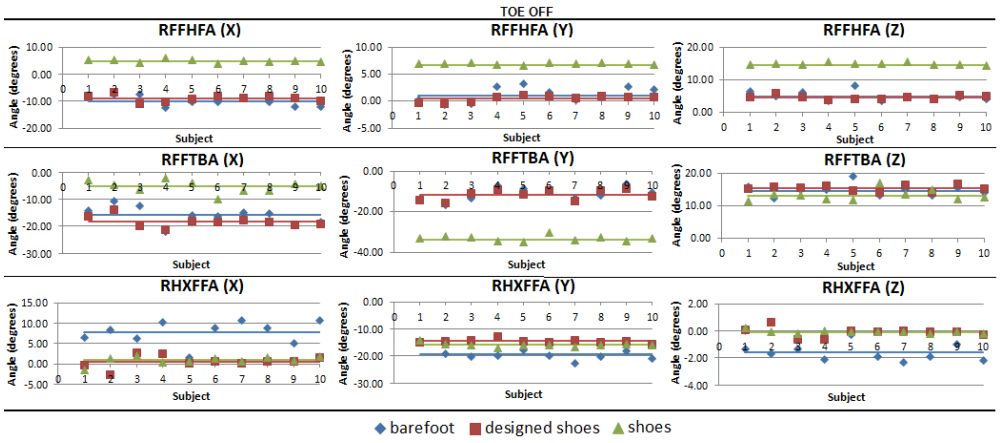

Figure 4-8 Mean joint angles for one person during toe off for the three conditions.

A strong correlation was found (see figure 4-9), and the median absolute deviation showed consistency for both conditions. The correlation coefficient quantifies the strength of the linear association between the two variables. The expression for this coefficient is given by:

$$r = \frac{\sum_{i=1}^{n}(X_i - \overline{X})(Y_i - \overline{Y})}{\sqrt{\sum_{i=1}^{n}(X_i - \overline{X})^2 \sum_{i=1}^{n}(Y_i - \overline{Y})^2}} \tag{4-1}$$

where X and Y are two data sets and $\overline{X}$ and $\overline{Y}$ the averages. It has a value between -1 and 1 and there is perfect correlation when it is exactly 1 or -1. In this

case, we have a positive correlation coefficient, which means that increasing values for one of the variables will mean an increase in the values of the other variable.

In the case of the Heel Strike, the calculated correlation coefficient varies between 0.78 and 0.98 for FF/HF, and between 0.9 and 0.97 for FF/TB. During Toe Off, the values lay between 0.84 and 0.89 and between 0.78 and 0.85 respectively. However, a lower coefficient can be seen in the case of the hallux segment, especially in the sagittal plane. These values are consistent with the repeatability analysis described in section 4.2.1.2.

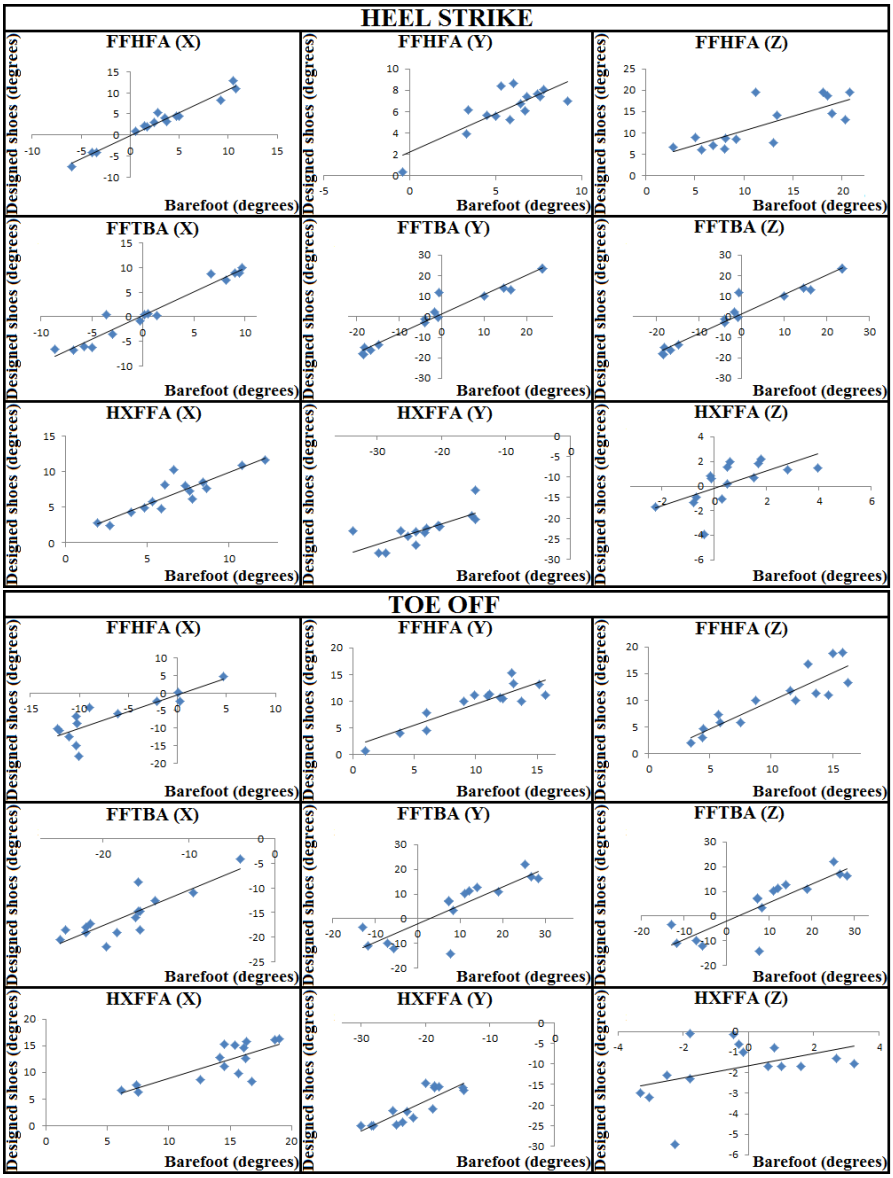

Figure 4-9 Scatter plot, correlation between joint angles for both conditions for the 15 subjects, corresponding to a Heel Strike event (top) and a Toe Off event (bottom).

4.2.3 Discussion and Conclusions

In the Oxford Foot Model, the foot is referenced according to room coordinated positions. Therefore, the local coordinate system of each segment is oriented to the laboratory coordinate system (the static position is 0 degrees). The reference segment is the shank, and the foot is divided into three rigid body segments: Hindfoot, Forefoot and Hallux; where the midfoot is the mechanism responsible for transmitting motion between the Hindfoot and the Forefoot.

The Oxford Foot Model has proven to be repeatable as the kinematics calculated lie within the same range of values for all of the trials in the repeatability analysis. However, particular care should be taken when the static trial is performed as the model scales to the participating subject, thus locating the local coordinates systems in relation to the global coordinate system. An error introduced in the static trial will therefore affect the whole set of subsequent trials. It is also noticeable that the variability among subjects is large, despite keeping a pattern of motion which is consistent throughout all the trials, the values in the different planes do vary (figure 4-10).

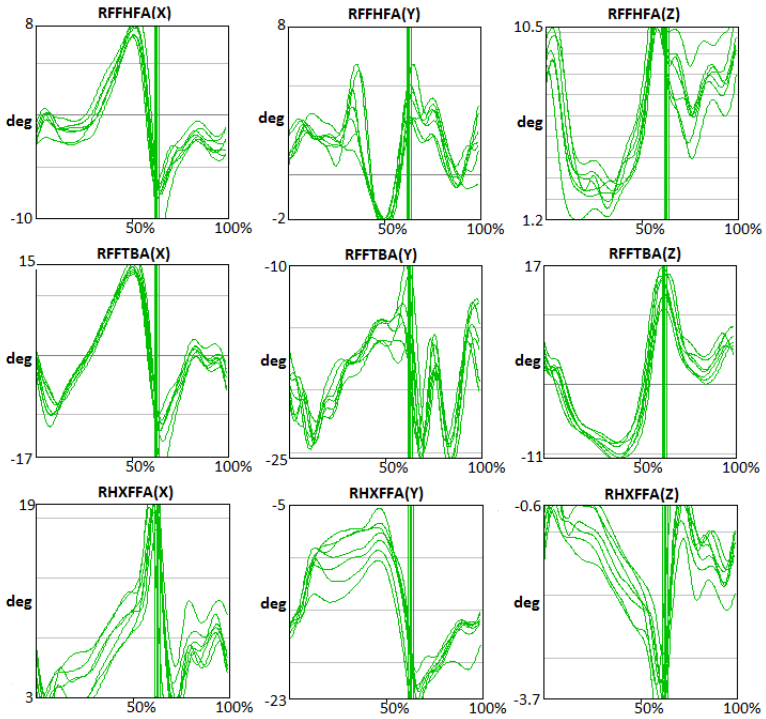

Figure 4-10 Comparison of 2 subjects' gait cycle (shoe size 4). Three trials per subject chosen randomly.

We can define patterns of movements for each plane which will be characteristic of each event in the gait cycle. These movements are: eversion and inversion (for the coronal plane), dorsiflexion and plantarflexion (for the sagittal plane), abduction and adduction (for the transverse plane). It should be taken into consideration that different multi-segment foot models will produce different sets of joint angle data. Therefore, while having a similar waveform, joint angle information for the gait cycle cannot be compared without performing previous mathematical manipulation.

The designed shoes (figure 4-3) proved to be reliable in terms of marker placement and plantar pressure measurements obtained. The proposed method, which introduces the use of specially designed shoes, can be used to reconcile barefoot and shod conditions in the Oxford Foot Model as it can mimic both conditions to study gait and plantar pressure at the same time. This offers a promising method for conducting further research on foot modelling in order to obtain valuable information at the same time from both approaches. Using a system that combines gait analysis and plantar pressure can enhance our understanding of normal gait and therefore a pathological one and its patterns.

4.3 Anthropometric measurements of the foot

4.3.1 Foot segments

Images have been provided by consultants from University Hospitals Coventry and Warwickshire (UHCW) in order to support the models in terms of geometry and parameterisation. A total of 10 series of healthy feet images (involving X-rays, CT scans and MRI) were analysed using Matlab and ImageJ software to obtain information regarding the dimensions for each of the proposed segments as shown in table 4-5.

Segment	% of total horizontal length	Width (mm)	Height(mm)
Phalanges	17.25	81.8	19
Metatarsals	29.72	81.7	28
Midfoot	16.2	69.4	37.7
Talus	28.48	46.9	35.4
Calcaneus	35.69	50.50	48

Table 4-5 Anthropometric measurements of the foot

4.3.2 Arch height

A total of 10 trials from the study introduced in the previous section (4.2) were analysed in order to find the median for the arch height. These trials correspond to 10 subjects (5 female and 5 male, age range: 22-34 years) who performed static trials in the Gait Laboratory within the School of Engineering at the University of Warwick [Jaitman et al., 2015]. A total of 250 frames were analysed and processed using Vicon Nexus 1.8.5 for each subject, yielding a median of 23.28mm for the arch height with a standard deviation of 1.98mm (figure 4-11). The arch height is one of the outputs of the Oxford Foot Model.

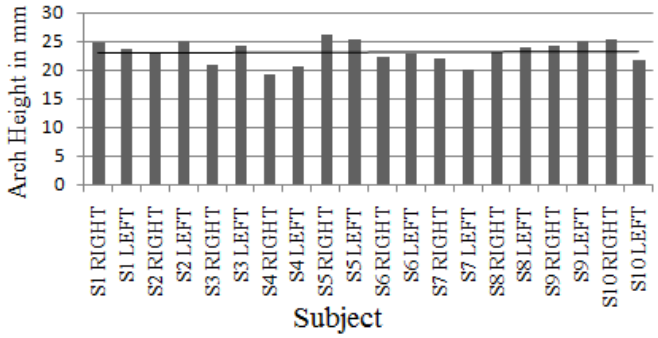

Figure 4-11 Arch height for 10 subjects (S1-S10)

4.3.3 Mass

The mass of the total foot, as defined by Winter [2005], is $0.0145M$ (where M is the total body mass). This mass is distributed throughout the hindfoot,midfoot and midtarsals and forefoot. The rest of the body has a mass of $0.9855M$, assuming that the body mass is equally distributed in the frontal plane.

4.3.4 Ground Reaction Force (GRF)

A forceplate in the Gait Laboratory permits calculation of the total force applied by the foot to the ground, assuming it is located at a single point which is the Centre of Pressure (CoP). However, when examining the foot, the distribution of this force over the foot is a critical issue. The foot plantar pressure is then the pressure acting between the foot and the support surface during motion activities.

While the Morlock and Nigg [1991] model represents the ground reaction force as a vertical component applied at the phalanges, it is more accurate to distribute this force along the plantar surface of the foot.

A Tekscan F-Scan plantar pressure system was used with in-shoe 3000E sensors (insoles). 14 subjects were asked to stand on the insoles for 1 minute[1]. After processing and analysing 750 frames for each trial, the ground reaction force was found to be distributed as described in table 4-6 and figure 4-12. These results match previous studies (e.g. Salathe Jr et al. [1986]).

Subject	% Left Phalanges	% Left Midtarsal & Midfoot	% Left Rearfoot	% Right Phalanges	% Right Midtarsal & Midfoot	% Right Rearfoot	Shoe-size	Body-mass (kg)
S1	2.88	12.53	33.90	2.29	11.86	27.35	8	80
S2	0.93	16.49	35.40	0.00	14.61	26.66	9	79
S3	0.68	15.21	26.70	0.89	15.49	27.59	6	65
S4	1.10	16.14	35.77	0.07	14.98	22.31	6	60
S5	0.59	18.56	20.72	2.32	10.13	44.18	8	80
S6	0.58	18.83	26.85	0.46	29.88	21.65	9	79
S7	0.35	15.71	46.16	0.75	6.90	27.98	4	60
S8	0.00	10.97	41.34	0.01	7.77	38.45	4	46
S9	2.35	19.16	20.87	1.61	24.91	27.92	5	63
S10	1.13	19.31	14.70	0.70	26.93	21.90	8	73
S11	0.00	12.81	39.22	0.08	8.54	32.34	8	77
S12	0.00	11.92	41.12	0.69	9.05	37.69	9	65
S13	0.00	13.73	29.74	0.06	5.80	42.01	6	61
S14	1.67	20.14	21.83	3.66	23.07	20.18	7	80
Median	0.63	15.92	31.82	0.70	13.24	27.75	8	69

Table 4-6 Ground reaction force distribution

[1]The experiments comply with all data protection requirements as stated in the University of Warwick BSREC ethical approval: BSREC full approval REGO-2013-582 Foot Modelling

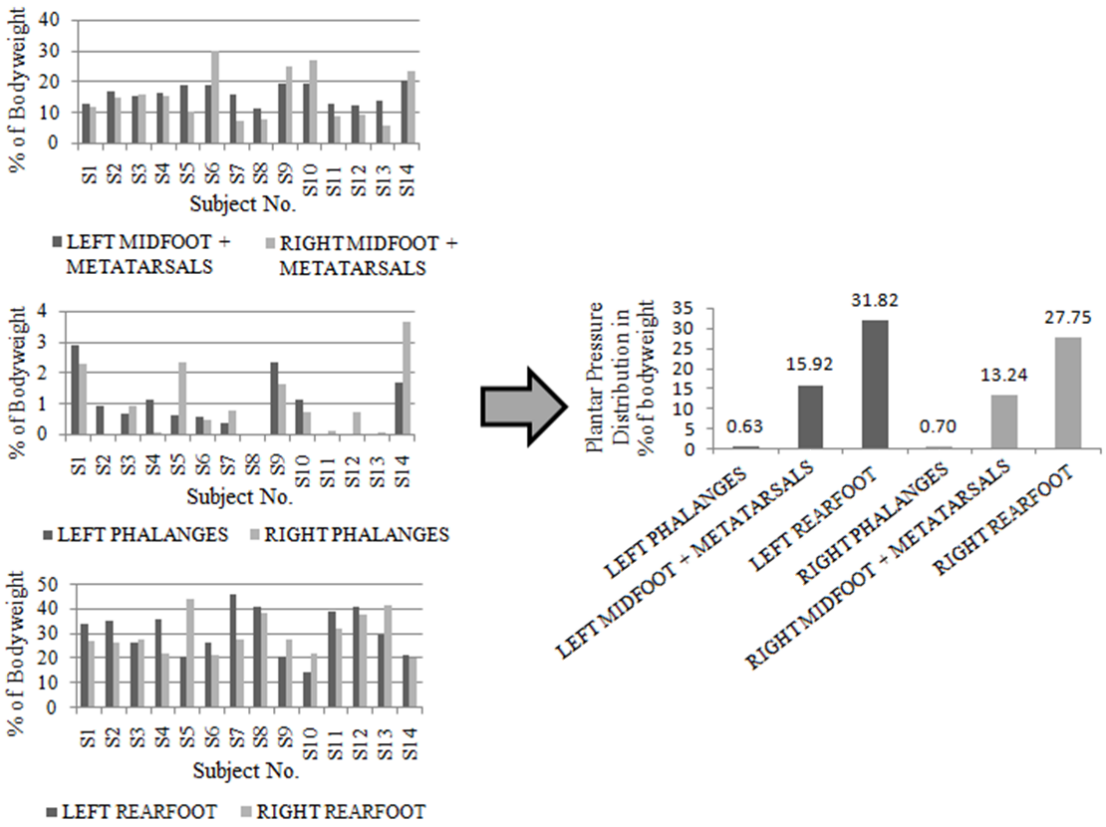

Figure 4-12 Ground reaction force distribution. Plantar pressure analysis for 14 subjects (S1-S14), and the distribution of the ground reaction force (GRF) throughout the foot.

4.4 Muscle-tendon Modelling

It is necessary to analyse muscle mechanics in order to understand motion. Movement is possible due to the force produced by muscles which is transferred to joints via tendons inserted at a certain distance from the joints [Zajac, 1989]. Therefore, there are four main characteristics of the muscle-tendon unit that need to be analysed prior to any model application: length, moment arm, pennation angle and muscle activation. An analysis of these four topics is performed in the following subsections, comparing and validating different types of methodologies.

4.4.1 Data Collection

One subject (male, 34 years old, 186.5cm height and 115kg bodymass) participated in these studies. The studies comprised of different sessions where diverse

methodologies were used in order to assess fibre length, pennation angle, muscle-tendon length and muscle activation of the following muscles: Tibialis Anterior (TA), Extensor Digitorum Longus (EDL), Extensor Hallucis Longus (EHL), Lateral Gastrocnemius (GAS L), Medial Gastrocemius (GAS M), Tibialis Posterior (TP), Flexor Digitorum Longus (FDL), Flexor Hallucis Longus (FHL), Peroneus Longus (PL), Peroneus Brevis (PB). The selection of the analysed muscles was based on previous electromyographic studies [Nordin and Frankel, 2001], identifying muscle activation during the gait cycle. The used methodologies were the following:

1. Ultrasound: ultrasound images were obtained for lower limb muscles in order to study actual fibre length and pennation angles in different ankle angles (resting, plantarflexion and dorsiflexion).

2. MRI: magnetic resonance was used to study muscle-tendon length and moment arm. Three MRIs were obtained: resting, plantarflexion and dorsiflexion.

3. Motion capture: following the input of parameters (body mass, height, leg length, knee width and ankle width) in the Vicon Nexus 1.8.5 system, the subject was markered up with 43 markers according to the Oxford Foot Model marker set, and then a static trial was perfomed (process described in 3.1.3).

4. Electromyography: was used for activation studies; electrodes were placed on the skin, above the studied muscles on the right leg, recording muscle activity sampled at 1000Hz with an Aurion Zero-wire system. Electrodes were placed following SENIAM recommendations [SENIAM, 2003] and studies performed by Hermens et al. [2000].

Motion capture experiments were carried out at the University of Warwick Gait Laboratory, complying with all data protection requirements as stated in the University of Warwick BSREC ethical approval (BSREC full approval REGO-2013-582 Foot Modelling) and written informed consent was obtained for the participating subjects. Images were obtained by the author in Medical Diagnosis and Breast

Research Center, Buenos Aires, Argentina under its ethical approval and informed consent was obtained for the subject (see appendix A for further information on ethical approval).

4.4.2 Muscle-tendon length

Until recently, the only information that could be gathered regarding muscles was obtained through cadaveric studies. A muscle's characteristics such as fibre length and pennation angle were studied individually so no further analysis was performed on synergistic or antagonistic pairs of muscles. With the introduction of imaging techniques, such as MRI and ultrasound, it is now possible to analyse muscle structure in vivo. In order to study muscle-tendon length it is essential to understand the origin, insertion and muscle path. The first two have already been studied in the literature and summarised in table 2-1 (chapter 2). The muscle path will determine the line of action of the force, and establish muscle tendon length. As described in Zatsiorsky and Prilutsky [2012], muscles can have either a straight line path or curved path (wrapped around bones and tissues) and these paths can be determined using different approaches. As lower limb muscles wrap around diverse structures and cross many joints, a straight line approach (where the muscle is modelled as one straight line linking origin and insertion) is not feasible. The selected approach for lower limb muscles is the via-point model, thus representing muscles as an arrangement of straight lines. In order to assess the reliability of the method, results from motion capture and MRI were compared.

In order to assess muscle-tendon length using motion capture, subject was asked to lie on a bed in the Gait Laboratory, where a passive stretching was performed. The subject was asked not to perform any voluntary movement. The ankle was passively dorsiflexed and plantarflexed manually. The reconstructed views from the motion capture system can be seen in figure 4-13.

Due to their complex pathways, initially additional markers were placed along the muscle-tendon unit in order to represent the via points that permit calculation of total length (figure 4-14).

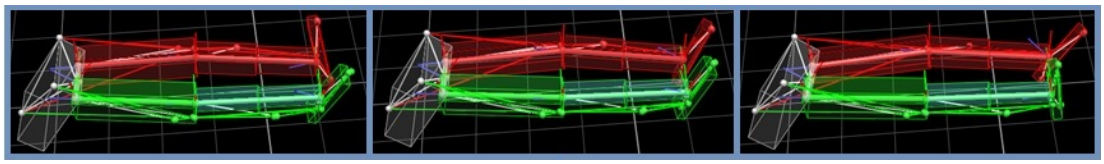

Figure 4-13 Passive ankle dorsiflexion and plantarflexion, reconstruction from Gait Laboratory experiments.

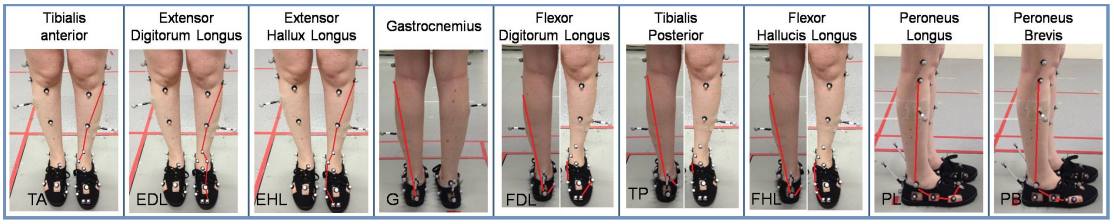

Figure 4-14 Muscle-tendon length (with extra markers) in Gait Laboratory

Although this provides an estimation of muscle-tendon unit (MTU) length, this method overestimates length as it requires the placement of 40 extra markers in order to assess all of the muscles, which cannot be fixed to origin and insertion points. Moreover, it is impossible to assess intrinsic muscles in the sole of the foot. The code developed and presented in Baker [2011] has in this work been extended to include the possibility of adding virtual markers to the skeletal model. Therefore, a combination of extra markers and an adapted dynamic bodylanguage model was used to define muscle pathways. This model provides origin and insertion points that are directly attached to the bone and defines the via points in between. Muscle resting length, tendon slack and their ranges of motion were measured before the experiments, by palpation.

A repeatability analysis was performed in order to understand what sensitivity should be allowed for musculotendon length measurements and also validate the proposed methodology. The same subject was markered upon two consecutive days and was asked to perform five passive trials each day (figures 4-15 to 4-19) which were sampled every 0.005 seconds. Good correlation was found in between days, ranging from 0.965 to 0.9982 (see table 4-7).

In order to validate the method, these measurements were compared to MRIs obtained for the same subject for 3 different ankle angles: plantarflexion, resting and dorsiflexion (figure 4-20). These images were analysed using ImageJ in order

to obtain muscle-tendon lengths for the three ankle angles, each series consisted of 32 T2 weighted MRIs. Another correlation analysis was performed comparing motion capture and MRI, results can be found in table 4-7.

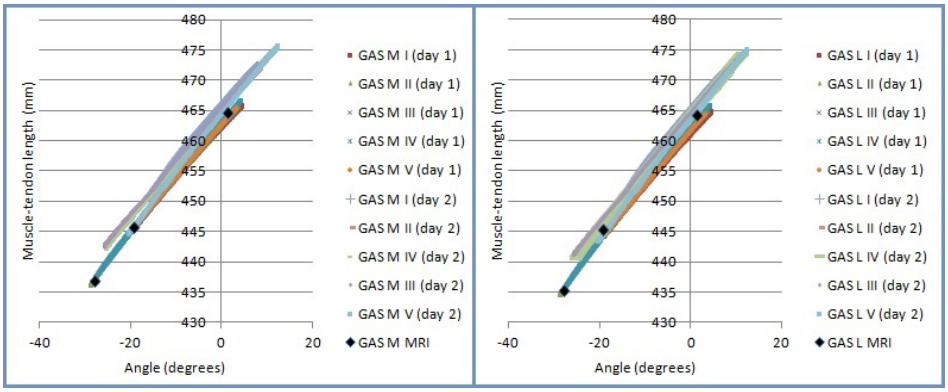

Figure 4-15 MTU length comparison for 2 consecutive days (10 trials) and MRI results (black series) for GAS M and GAS L

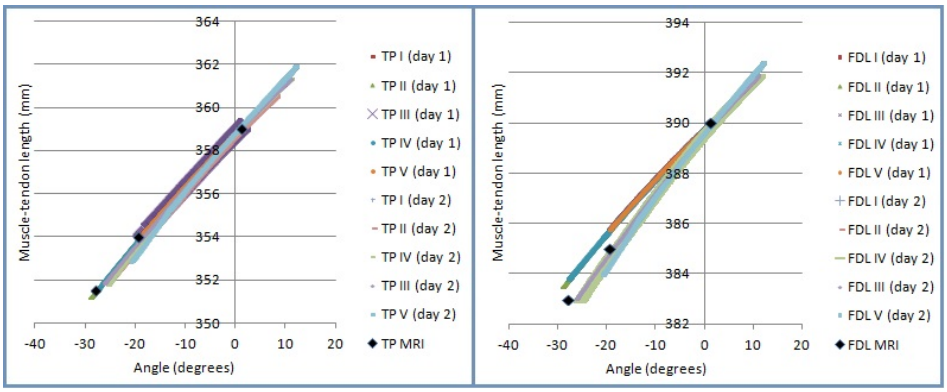

Figure 4-16 MTU length comparison for 2 consecutive days (10 trials) and MRI results (black series) for TP and FDL

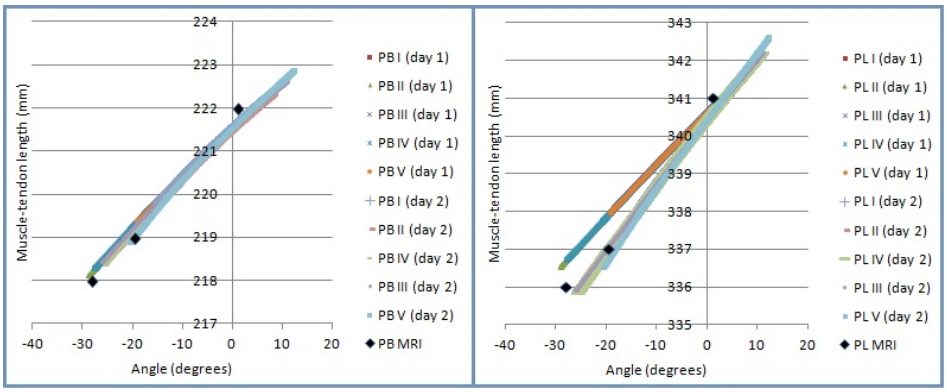

Figure 4-17 MTU length comparison for 2 consecutive days (10 trials) and MRI results (black series) for PB and PL.

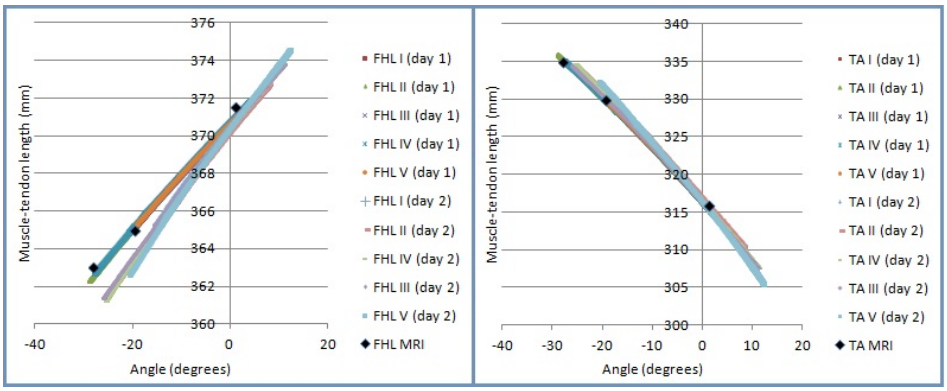

Figure 4-18 MTU length comparison for 2 consecutive days (10 trials) and MRI results (black series) for FHL and TA.

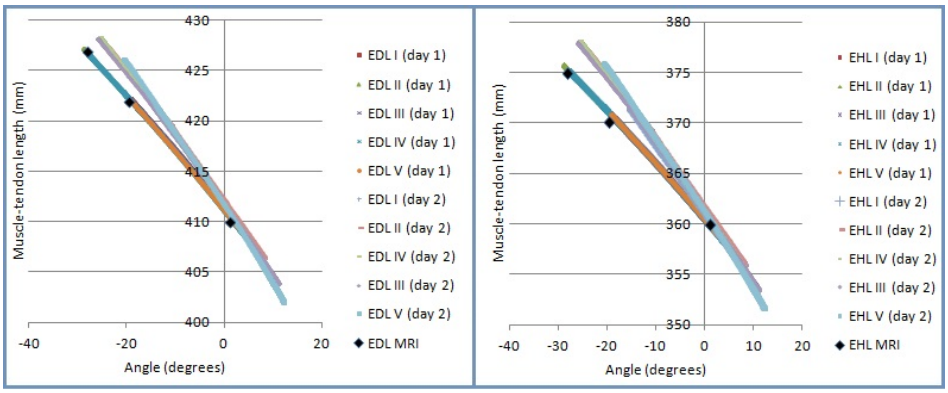

Figure 4-19 MTU length comparison for 2 consecutive days (10 trials) and MRI results (black series) for EDL and EHL.

Figure 4-20 MRI reconstruction (left) and series (right): dorsiflexion, resting, plantarflexion.

	GAS M	GAS L	FDL	FHL	PL	PB	TP	TA	EDL	EHL
R_1^2	0.989	0.987	0.978	0.974	0.965	0.998	0.998	0.997	0.984	0.969
R_2^2	0.998	0.998	0.999	0.997	0.994	0.999	0.999	0.998	0.998	0.993

R_1^2 is the correlation relating between days variability and R_2^2 compares motion capture with MRI.

Table 4-7 Correlation table for muscle-tendon length analysis

4.4.3 Moment Arm

Muscle forces can be obtained through the analysis of joint torques, if the line of action of the muscle and moment arm are known. Moment arm is defined as the

distance from the line of action to the joint of interest [Zatsiorsky and Prilutsky, 2012], and is given by:

$$M = F \times r \tag{4-2}$$

where M is the moment at the joint, F the force produced by the muscle and r the moment arm. In this study, muscle moment arm is calculated using the *principle of virtual work*. The muscle connects the origin and insertion via a pathway. According to Sherman et al. [2013], assumptions have to be made in order to be able to apply the concept of virtual work: the total muscle-tendon length (l^{MT}) is a kinematic quantity that can be calculated if the position of every segment is expressed in general coordinates (q), assuming for any given muscle:

$$l^{MT} = l^{MT}(q) \tag{4-3}$$

In the same way, the joint angle of interest will be defined by an angular quantity:

$$\theta = \theta(q) \tag{4-4}$$

Therefore, moment arm can be defined by the angle θ and muscle-tendon length l. A virtual angular displacement $d\theta$ will then produce a virtual change in muscle-tendon length dl. Moment arm can then be expressed as:

$$r_\theta \triangleq \frac{M_\theta}{F} \tag{4-5}$$

where r_θ is the moment arm and M_θ the generated moment by force F. Assuming all joints and sufaces are frictionless, according to the principle of virtual work:

$$F dl = M_\theta d\theta \tag{4-6}$$

Combining equations 4-5 and 4-6, a method for calculating the moment arm can be expressed as:

$$r_\theta = \frac{dl}{d\theta} \tag{4-7}$$

This method has been applied in this study, to calculate the moment arm for the muscles analysed in the previous section (figures 4-21 to 4-25). These results show good agreement with the MRI measurements as shown in figures 4-21 to 4-25.

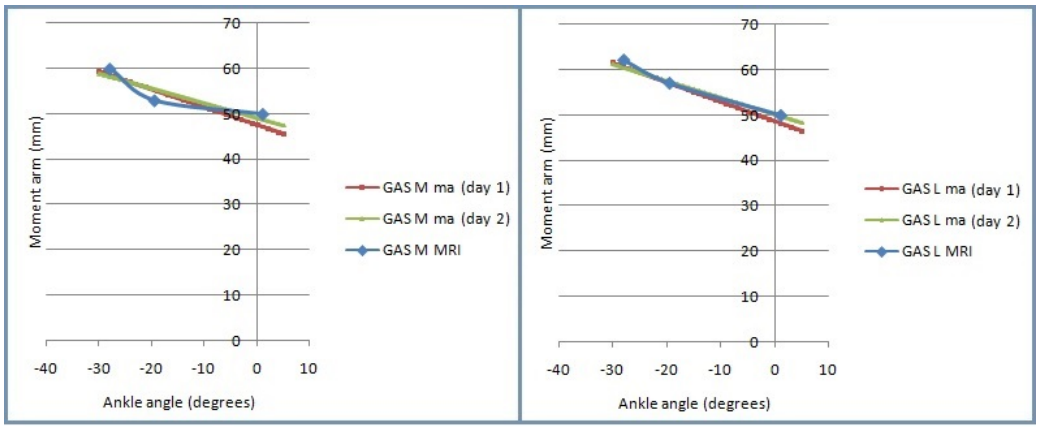

Figure 4-21 Moment arm: motion capture (trendline for day 1 and 2) and MRI results (blue series) for GAS M and GAS L.

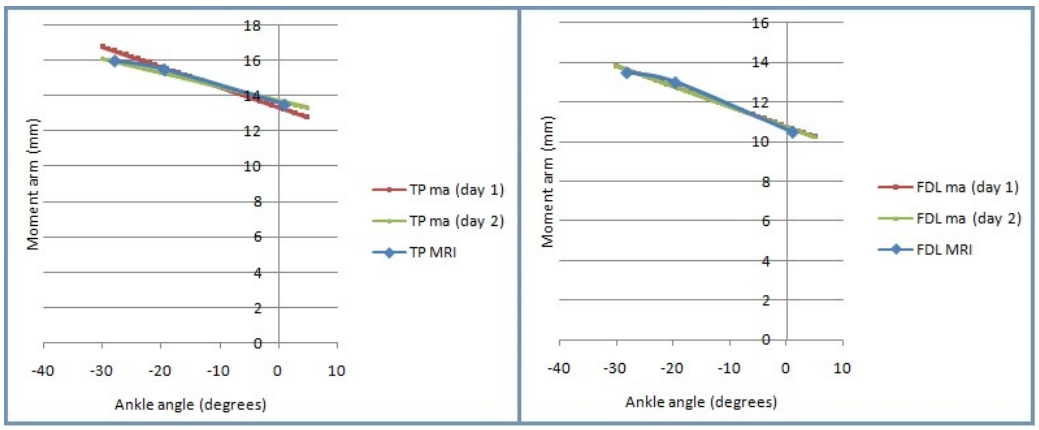

Figure 4-22 Moment arm: motion capture (trendline for day 1 and 2) and MRI results (blue series) for TP and FDL.

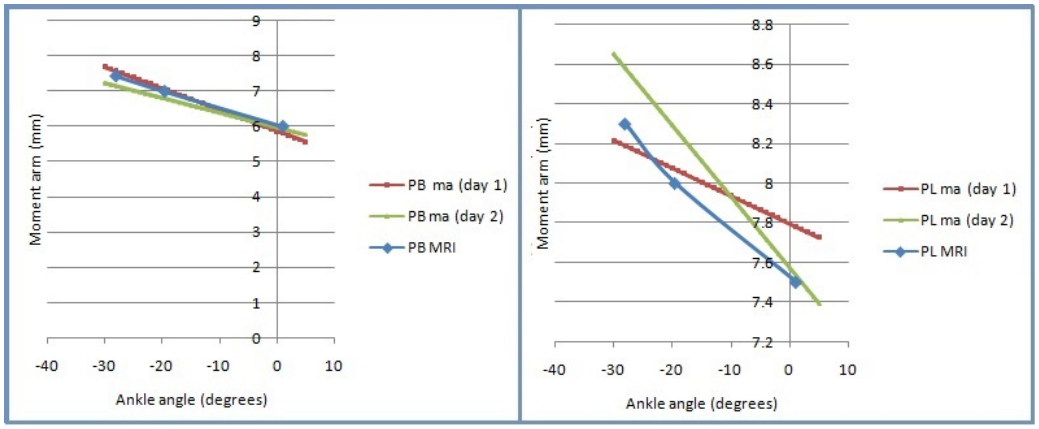

Figure 4-23 Moment arm: motion capture (trendline for day 1 and 2) and MRI results (blue series) for PB and PL.

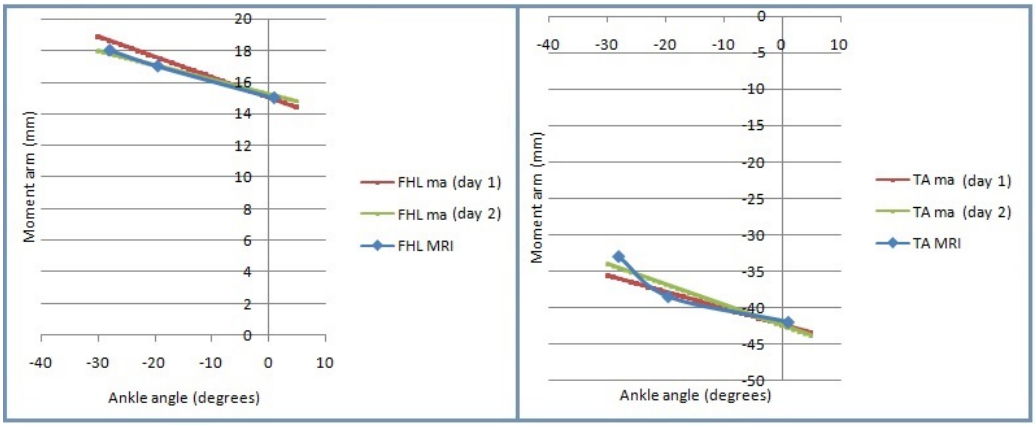

Figure 4-24 Moment arm: motion capture (trendline for day 1 and 2) and MRI results (blue series) for FHL and TA.

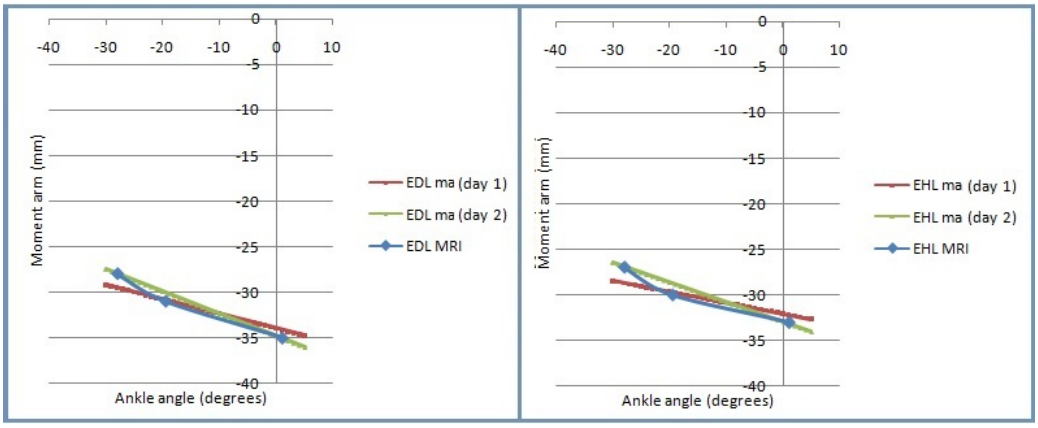

Figure 4-25 Moment arm: motion capture (trendline for day 1 and 2) and MRI results (blue series) for EDL and EHL.

4.4.4 Pennation angle

The pennation angle is the angle between muscle fibres and the aponeurosis of the tendon. As the pennation angle increases, the force transmitted to the tendon decreases. According to many authors (Olney and Winter [1985] for example), this angle can be neglected as it only has a small effect on muscle output as $F^T = F^{fibre}.\cos(\alpha)$ and α is usually less than 20 degrees, causing a maximum error of 6% in the output. Other studies use the optimal pennation angle and assume that it remains constant [Bobbert and Schenau, 1990]; and other authors agree that the model should incorporate pennation angle and its dependency on fibre length [Woittiez et al., 1984].

In this study, in order to assess pennation angle using ultrasound, each subject was

asked to lie on a bed and perform a maximum voluntary contraction test with the right leg, verified by means of a handheld dynamometer. The subject performed an isometric test in dosiflexion, the neutral position and plantarflexion. Information on fibre length and pennation angle were obtained for each of the cases. Six lower limb muscles were studied in this case: Tibialis Anterior (TA), Lateral Gastrocnemius (GAS L), Medial Gastrocemius (GAS M), Tibialis Posterior (TP), Flexor Hallucis Longus (FHL), Peroneus Longus (PL). A study analysing different pennation scenarios was performed in order to study the effect of pennation angle in terms of fibre force production. This study followed the procedure decribed by Scott and Winter [1991] where different scenarios were considered:

1. No pennation angle: all fibres are parallel to the tendon, so $\alpha = 0$

2. Constant pennation angle: optimal pennation angle (angle at the optimal fibre length) is considered to remain constant, $\alpha = \alpha_0$. This value is obtained from ultrasound measurements.

3. Variable pennation angle: assuming that the width of the muscle remains constant, $L^{fibre} \sin\alpha = L_0^{fibre} \sin\alpha_0 = w$, where L_0^{fibre} is the optimal muscle fibre length and α_0 the optimal pennation angle. Therefore, the pennation angle can be expressed as a function of the fibre length, if optimal fibre length and pennation angle are known (4-26):

$$\alpha = \sin^{-1} \frac{L_0^{fibre} \sin\alpha_0}{L^{fibre}} \tag{4-8}$$

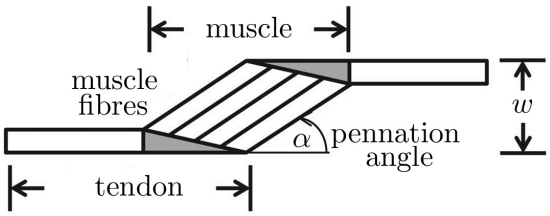

Figure 4-26 Pennated muscle diagram

4. Real pennation angle: least-squares regression on ultrasound measurements was performed to obtain the pennation angles for the 6 lower limb muscles (see figure 4-27(bottom)). The three previous models were compared to this last one.

Table 4-8 summarises optimal fibre length l_0 and optimal pennation angle α_0 used for the studied muscles.

	TA	GAS L	FHL	TP	PL	GAS M
l_0(mm)	58.82	56.56	14.74	27.483	33.207	48.73
α_0(deg)	10.29	17.40	15.60	17.81	13.15	9.5

Table 4-8 Optimal fibre length l_0 and optimal pennation angle α_0.

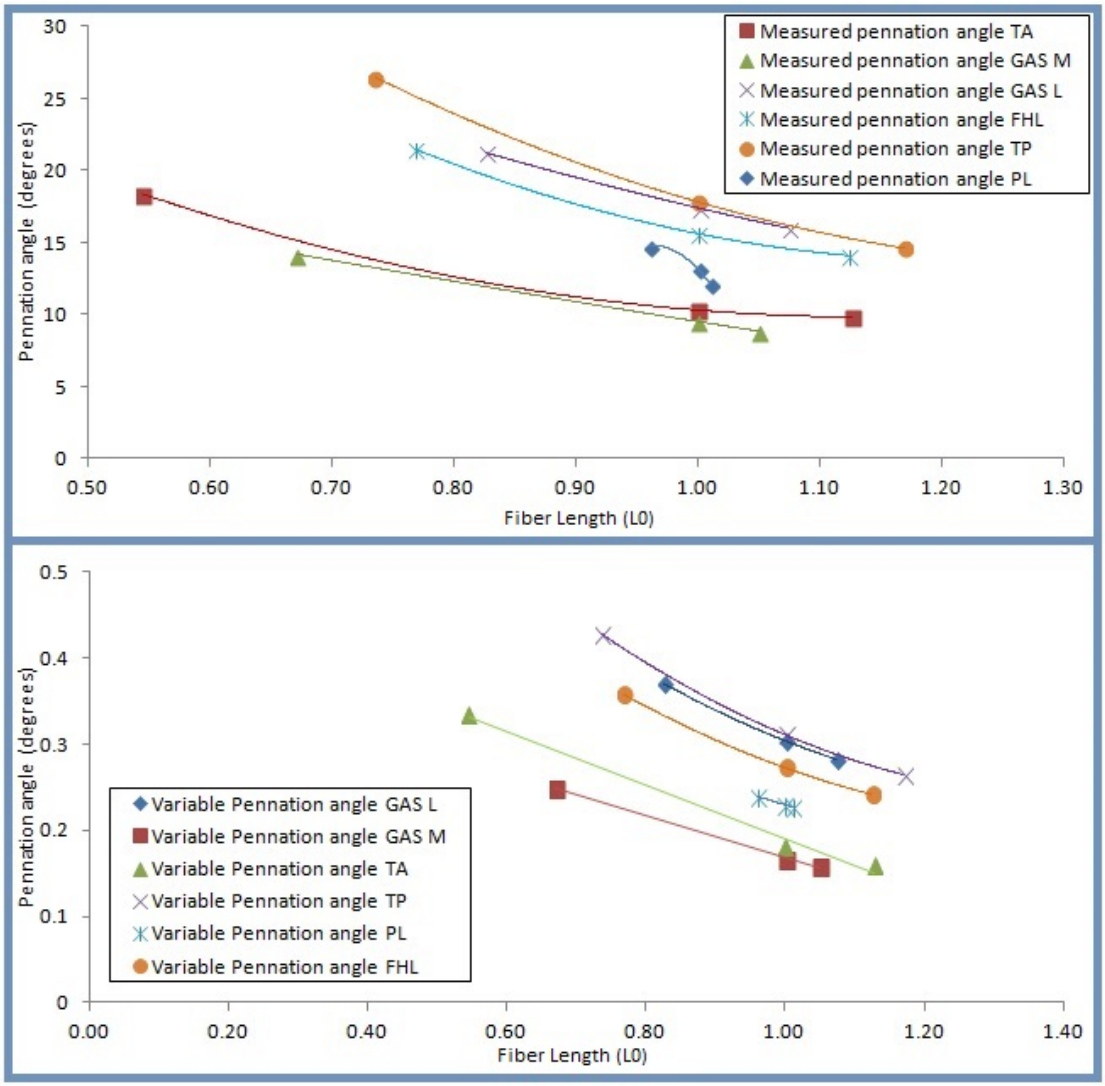

Figure 4-27 Pennation angles for both, (top) variable and (bottom) regression models

An analysis was performed on Force-Length and Force-Velocity relationships, depicted in the following figures 4-28 to 4-33. The blue series denote no pennation angle assumption, red denotes constant pennation angle, cyan variable pennation angle and dashed curves correspond to regression pennation. In all of the cases, the variable pennation angle provided the best fit to the regression data. As can

be seen from the figures, the output force until the fibre length reaches its resting length, is slightly smaller in the case of variable pennation, fixed pennation and regression pennation, in comparison with the no pennation angle assumption. However, it provides the smallest output force after 1.2 times the resting length. As in Scott and Winter [1991], substracting each model from the regression one, an estimate of the model error can be obtained. The error is always small around resting length ($l = l_0$). When analysing the Force-Velocity relationship, it can be noticed that the error is biggest for the constant pennation angle assumption. The errors tend to be small when shortening and bigger while lengthening. The variable model provides the best fit, followed by the no pennation angle model. The fixed pennation angle assumption provides the worst estimates in terms of the Force-Velocity relationship. According to this study, if there is no available information regarding the pennation regression, a good estimate of the force output can obtained by assuming no pennation angle.

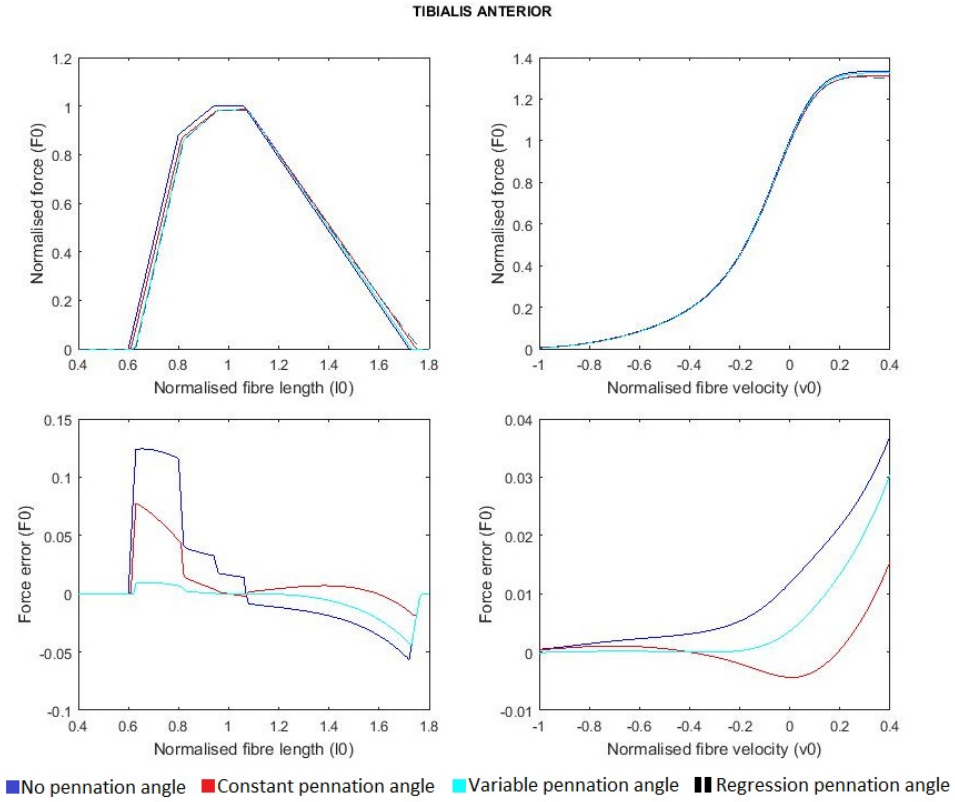

Figure 4-28 Tibialis Anterior pennation angle analysis.

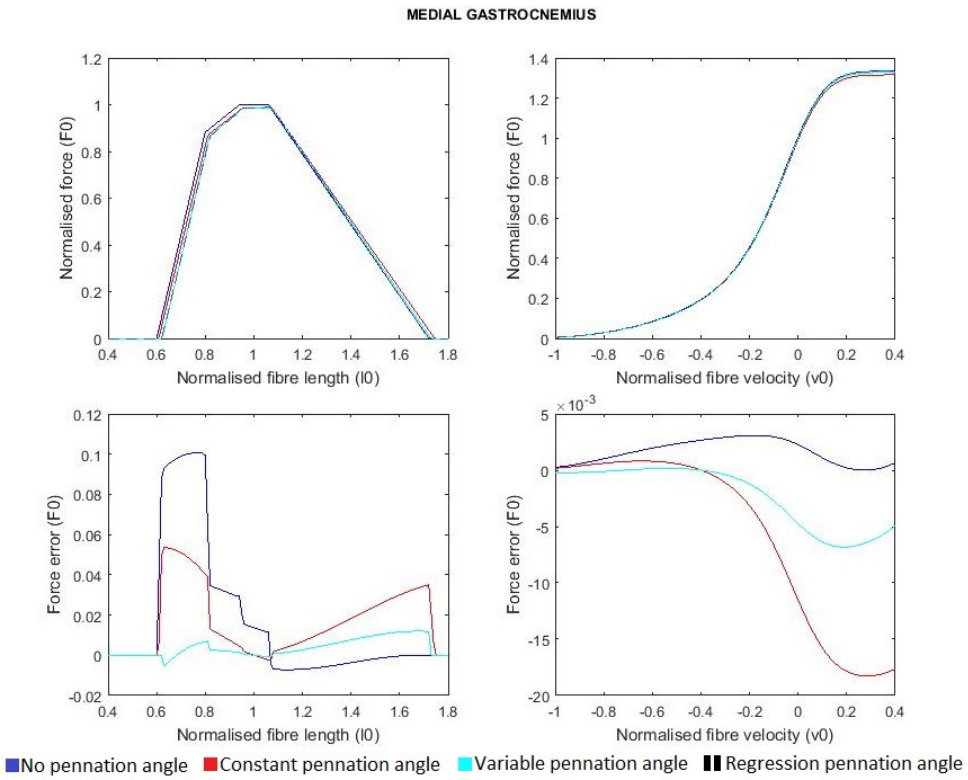

Figure 4-29 Medial Gastrocnemius pennation angle analysis.

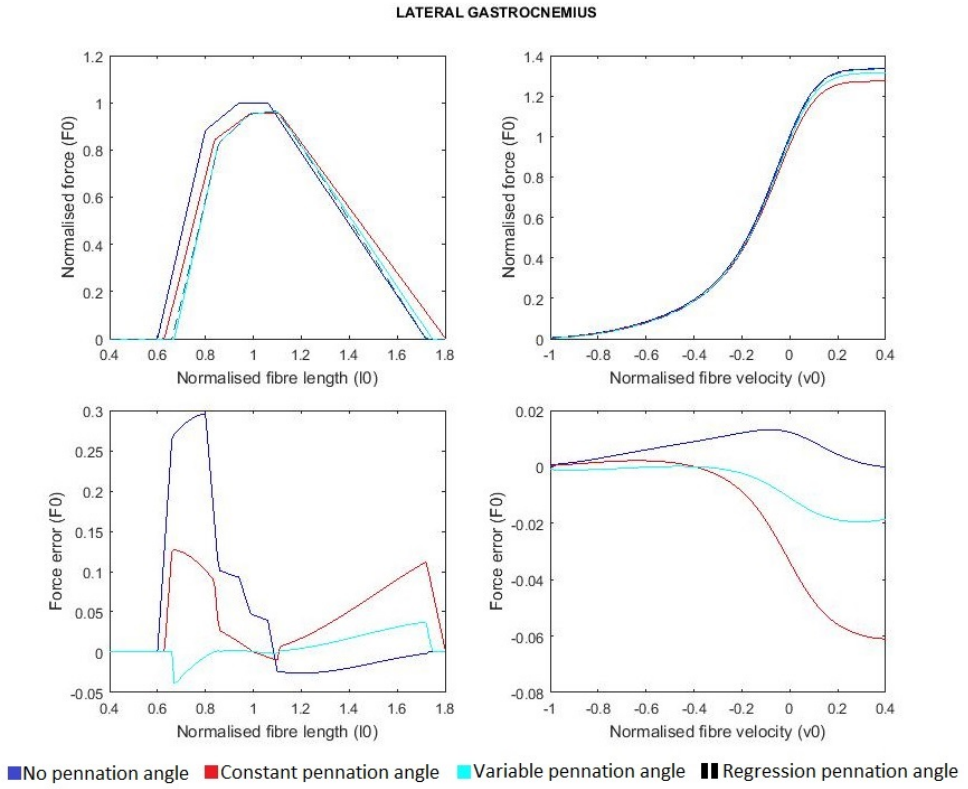

Figure 4-30 Lateral Gastrocnemius pennation angle analysis.

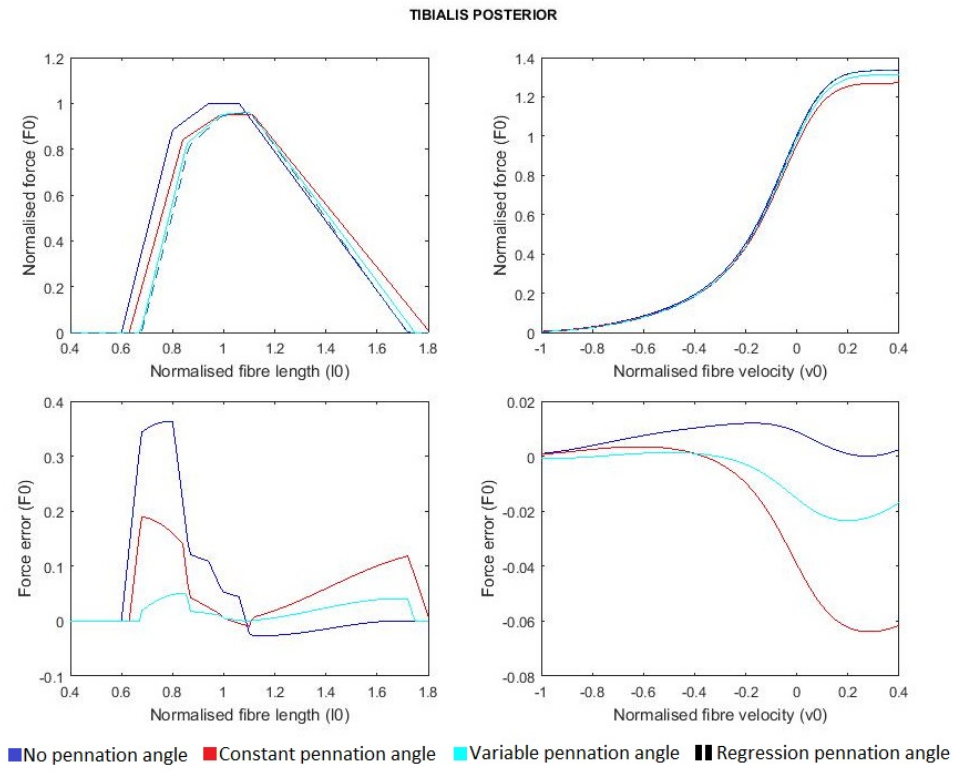

Figure 4-31 Tibialis Posterior pennation angle analysis.

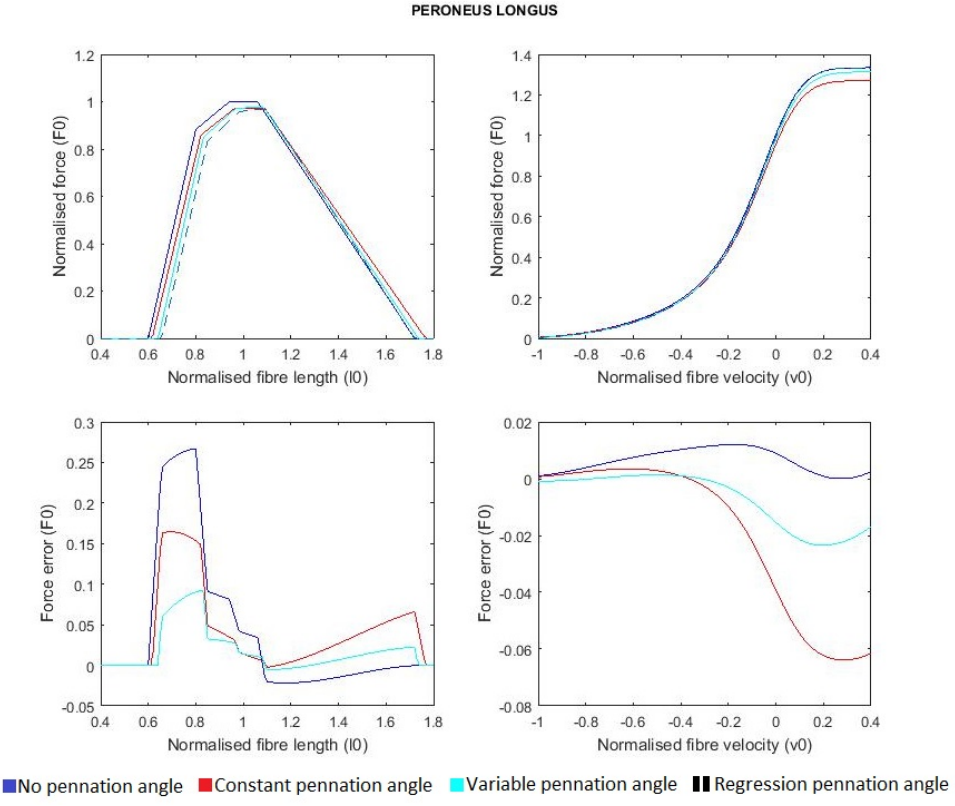

Figure 4-32 Peroneus Longus pennation angle analysis.

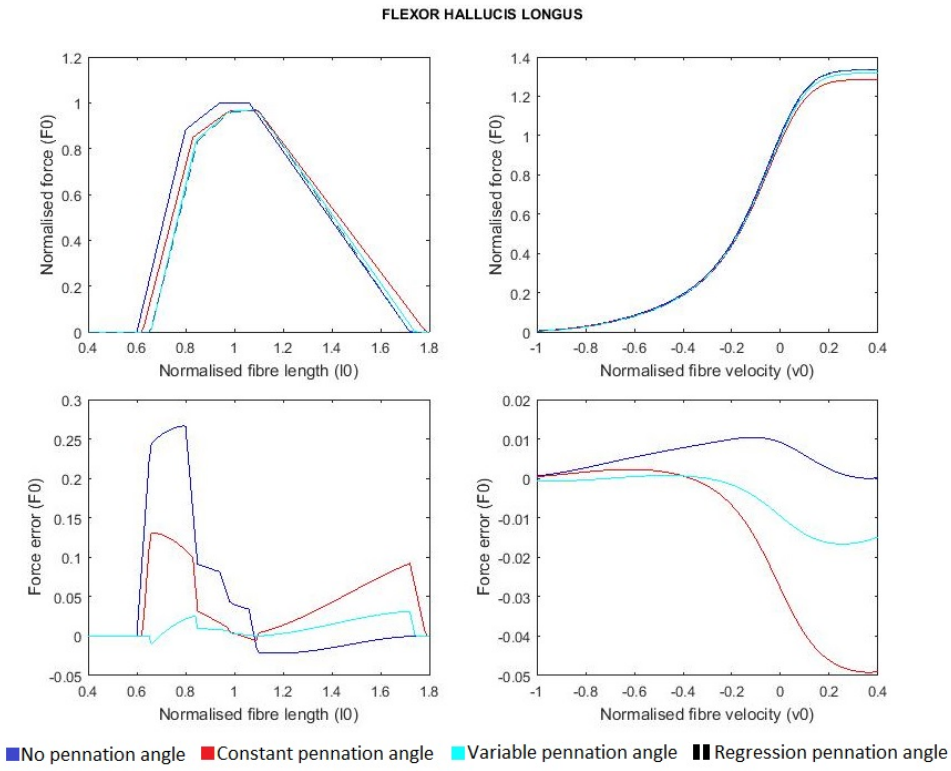

Figure 4-33 Flexor Hallucis Longus pennation angle analysis.

4.4.5 Muscle Activation

Any motor task requires the central nervous system to send an activation signal to the muscle which will contract and transmit this force to the tendon, thus moving the bones. Muscle activation is a fundamental parameter when modelling the muscle-tendon unit, and the only way we can assess fibre recruitment is by means of electromyography. This type of analysis gives qualitative information regarding which muscles are involved in motion tasks and its analysis has already been described in section 3.2. Given that the muscle has a passive and an active component, it is essential to understand which of them (if not both) are present during the gait cycle or whether one is contributing a negligible amount. In order to study muscle activation, the same subject was markered up and electrodes were placed on the skin, above the studied muscles on the right leg as shown in figure 4-34. The muscles studied were: Tibialis Anterior (TA), Extensor Digitorum Longus (EDL), Extensor Hallucis Longus (EHL), Lateral Gastrocnemius (GAS L), Medial Gastrocemius (GAS M), Tibialis Posterior (TP), Flexor Digitorum Longus (FDL), Flexor Hallucis Longus (FHL), Peroneus Longus (PL), Peroneus Brevis (PB), Ab-

ductor Hallucis (AH) and Abductor Digiti Minimi (ADM). Muscle-tendon units were first palpated according to Houglum and Bertoti [2012], Field and Hutchinson [2008], Muscolino [2009] and Palastanga and Soames [2011], and then the electrodes were placed following SENIAM [2003] recommendations. For a detailed description of muscle palpation and position of each electrode refer to appendix E.

The subject perfomed diferent movements according to the trial. The study consisted of three different experiments performed by the same subject: maximum voluntary contraction (MVC) trials, one walking trial and a passive movement trial, which will be described in the following sections.

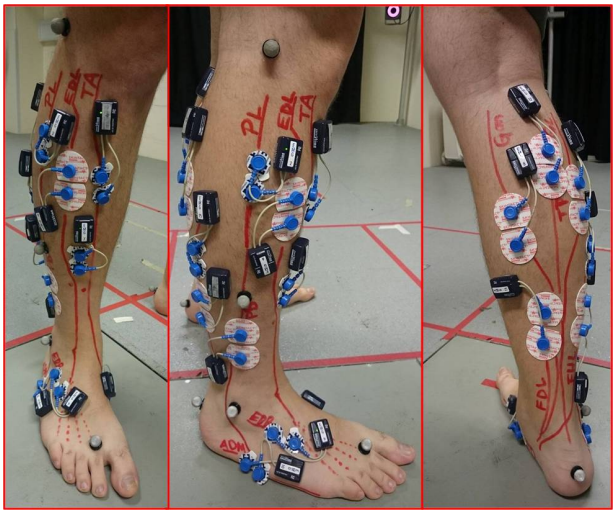

Figure 4-34 EMG electrode placement on the lower limb for the activation study

4.4.5.1 Maximum voluntary contraction

In order to normalise the electromyographic signals, it is necessary to first perform a maximum voluntary contraction (MVC) test. In this type of test, the subject produces the maximum amount of force during an isometric exercise. For this purpose, a rig was built, in which the maximum force was measured by the plantar pressure insoles as depicted in figure 4-35. The subject was first asked to perform an isometric test in plantarflexion and then dorsiflexion, to study both the flexor and extensor muscles. Two trials were recorded (5 seconds each), with a resting period of 30 seconds in between. An analysis was then performed to see if

the maximum voluntary contraction was reached (by comparing pressure maps). Values for EMG were also recorded to normalise the rest of the trials.

Figure 4-35 Isometric testing rig, dorsiflexion (left) and plantarflexion (right)

4.4.5.2 Muscle activation during walking trials

For this second experiment, the subject was asked to walk at his natural pace. Kinematic and kinetic data were collected, as well as electromyographic data. The latter were analysed using the methods described in 3.2 and the results from these experiments are shown in figures 4-36 to 4-38. These results are consistent with the ones found by Saraswat et al. [2010], which are shown in figure 4-39.

As can be inferred from the EMG patterns, not all of the muscles are active throughout the whole cycle. When inactive, muscle belly can still be moved by the surrounding connective tissue (the passive component) and also agonist and antagonist muscles. It can also be seen that, reasonably, there is not even one moment during the gait cycle when all of the muscles are inactive and therefore only produce passive force. Therefore, it is necessary to perform other types of experiments in order to estimate the parameters for the muscle-tendon passive elements first.

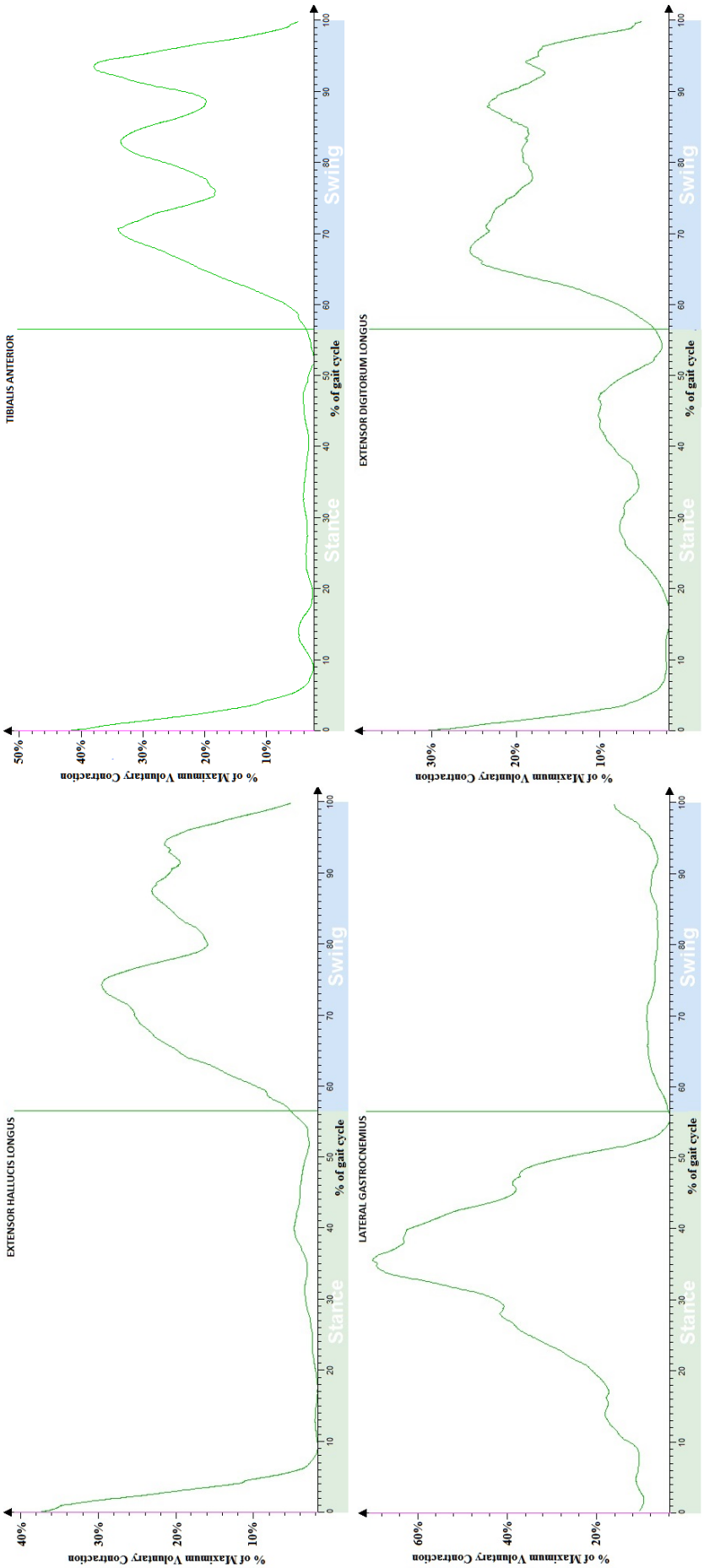

Figure 4-36 Electromyographic analysis of lower limb muscles during walking (I).

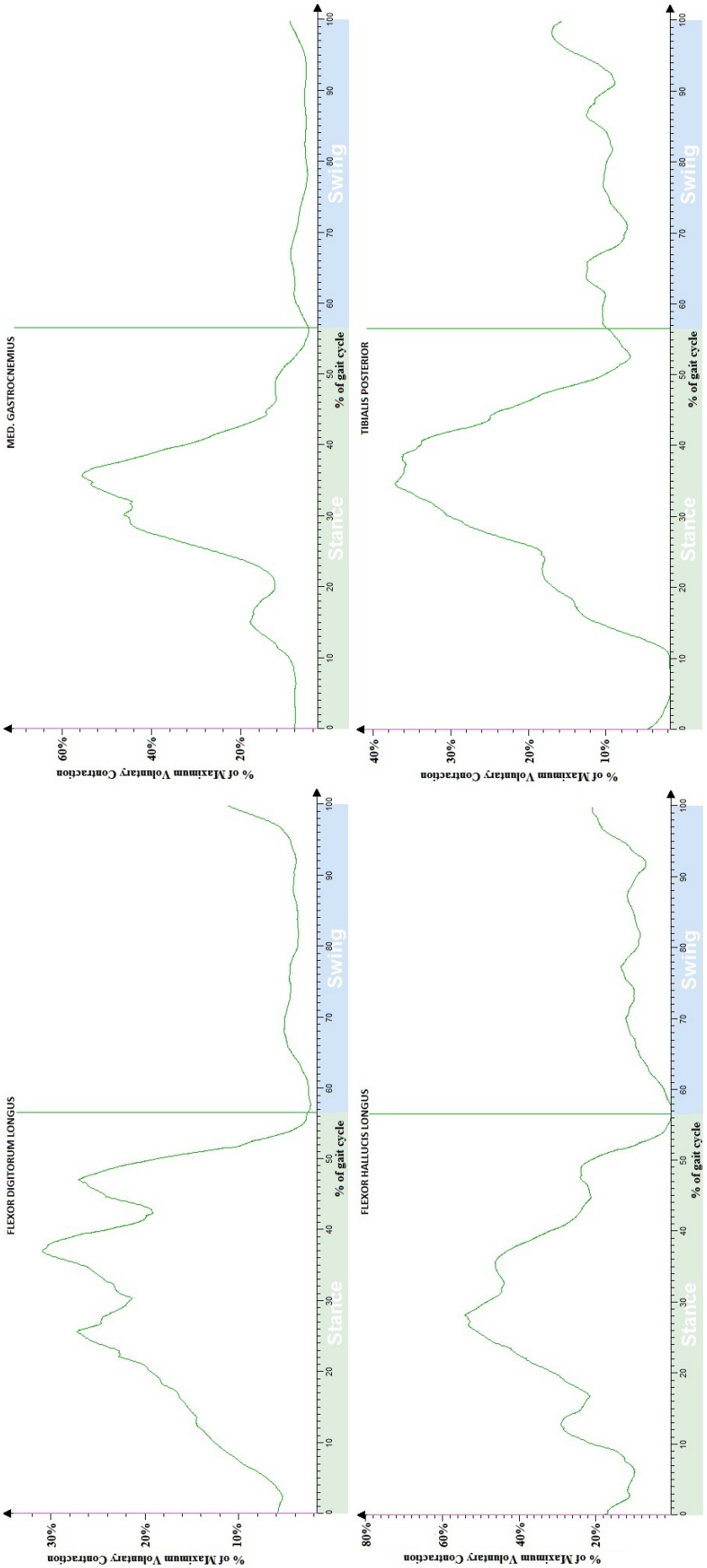

Figure 4-37 Electromyographic analysis of lower limb muscles during walking (II).

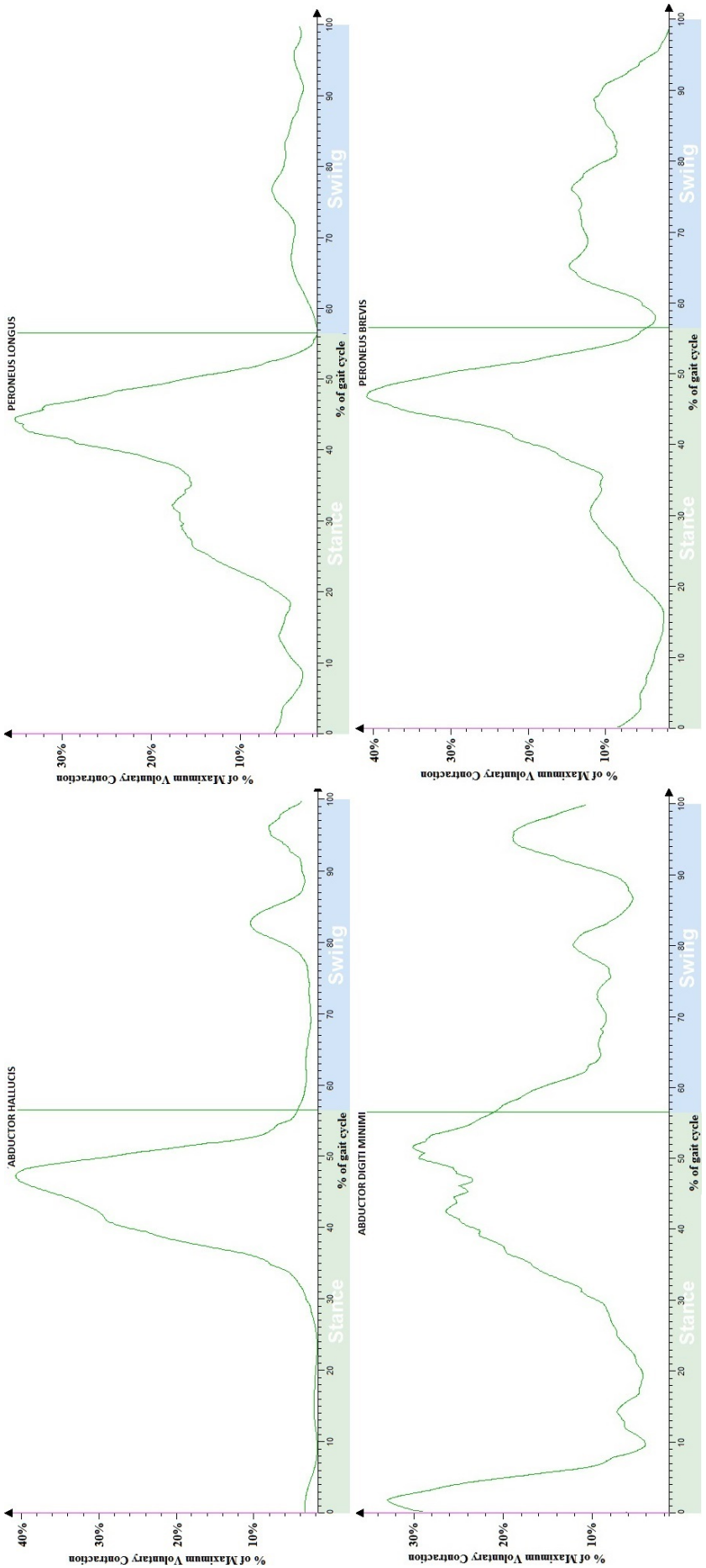

Figure 4-38 Electromyographic analysis of lower limb muscles during walking (III).

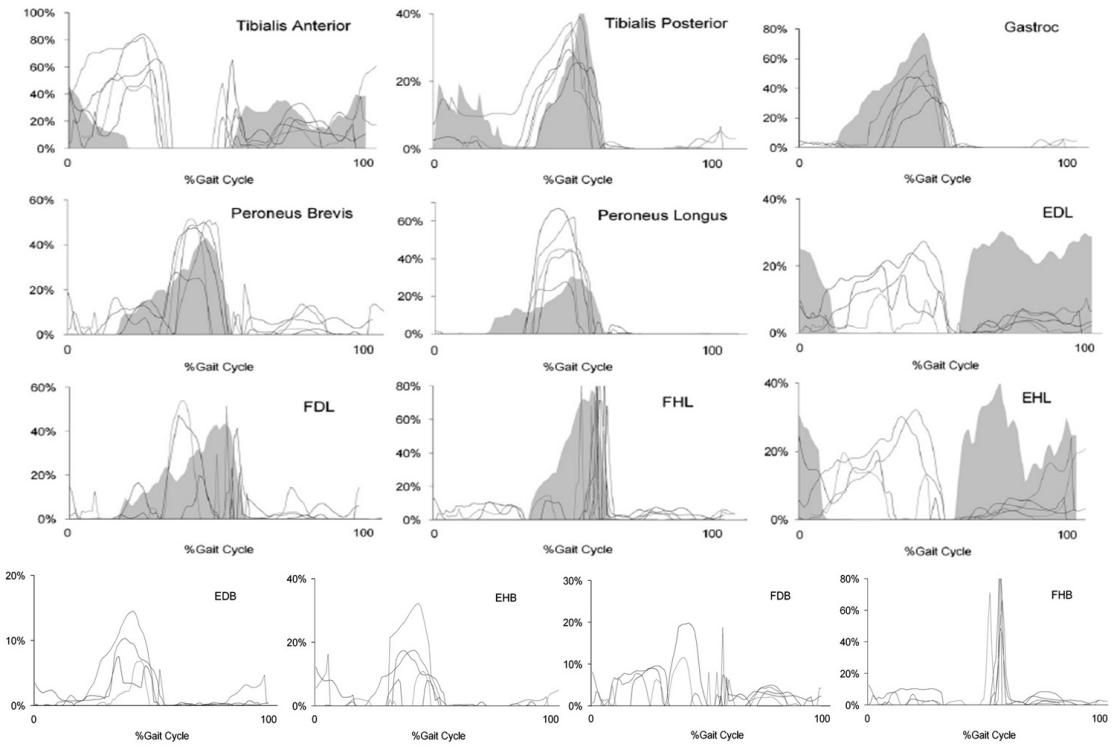

Figure 4-39 Muscle activation taken from Saraswat et al. [2010]. Muscle activation patterns corresponding to musculoskeletal model proposed by Saraswat et al. [2010] (lines) and values obtained from Perry [1992] (shaded).

4.4.5.3 Muscle activation during passive movement

The same subject was asked to lie on a bed in order to perform passive stretching. The subject was asked not to perform any voluntary movements, the ankle was passively dorsiflexed and plantarflexed manually (figure 4-40), while assessing electromyography (figure 4-41).

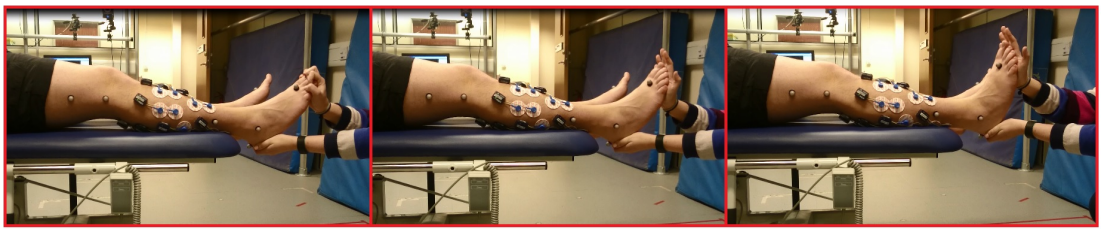

Figure 4-40 Passive ankle dorsiflexion/plantarflexion assessment.

As can be noticed from the electromyographic results, the only signal the electrodes catch is noise as it represents less than the minimum voltages considered in any other active assessment. Therefore, during the passive movement there is no

muscle activation; and this method will be used in the following chapters for assessing passive components of the muscle.

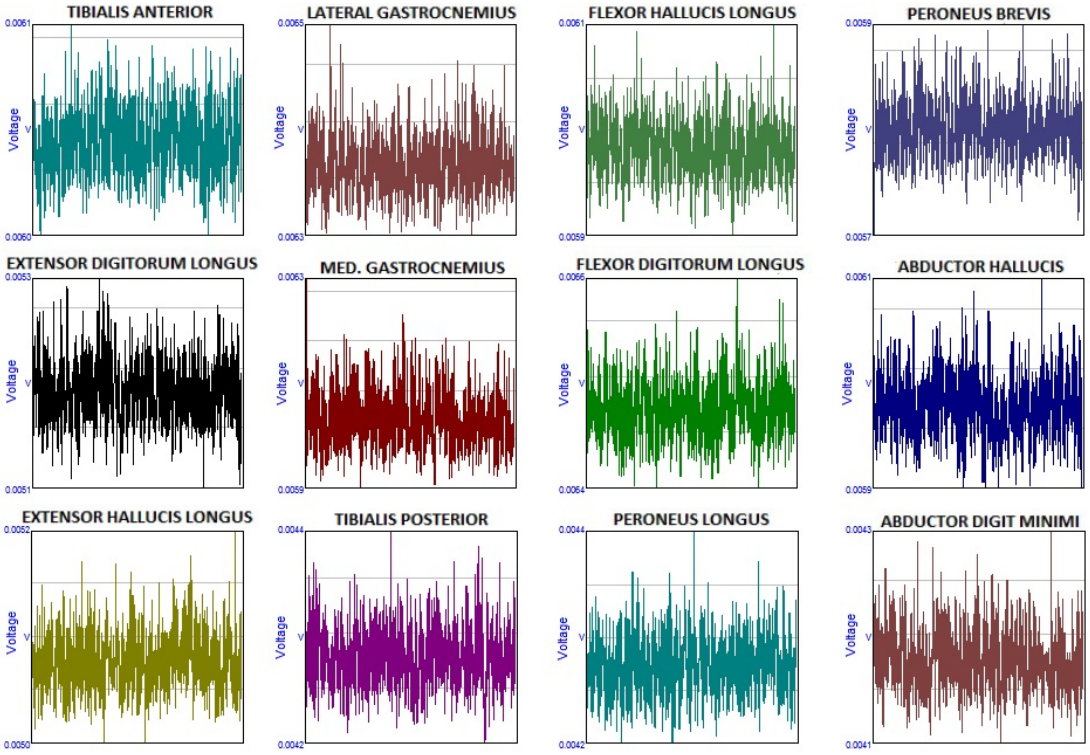

Figure 4-41 Muscle activation during passive testing: Activation patterns measured with the Aurion Zero-wire system.

5

Multi-segment foot model

The main objective of this chapter is to develop a mechanical model that can describe the behaviour of skeletal muscle. There are several models describing muscle function, of particular interest is the Hill muscle model which is analysed from a numerical and structural point of view in this chapter. A multi-segment foot model is proposed, and parameters for tendon and muscle damping and stiffness are obtained for 15 subjects through fitting techniques.

5.1 Introduction - mechanical models

There are multiple models that have been developed to explain the mechanical properties of the muscle, of particular interest is the Hill muscle model which is here analysed from a numerical and structural point of view. Hill muscle models are commonly used in biomechanics in order to predict passive and active muscle forces. This type of model is phenomenological so the behaviour of the muscle is characterised and predicted by means of differential equations and parameters that govern the model using springs, an active contractile element and a damping element [Haeufle, 2014]. This model is used to describe the relationship between input and output in muscle force production from a mechanical point of view. Figure 5-1 depicts Hill muscle model.

- Contractile Element (CE): corresponds to the active part, responding to

motor neuron units, and resulting in force production due to an activation signal.

- Parallel Damping element (b): it works in parallel with the contractile element, and represents the fluid within the muscle.
- Parallel Elastic element (PEC): represents the connective tissue surrounding the muscle and responsible for producing the elastic force that restores the muscle to its resting length. k_m denotes the elastic constant for the PEC.
- Serial Elastic element (SEC): representing tendon and aponeuroses. k_t denotes the elastic constant for the SEC.

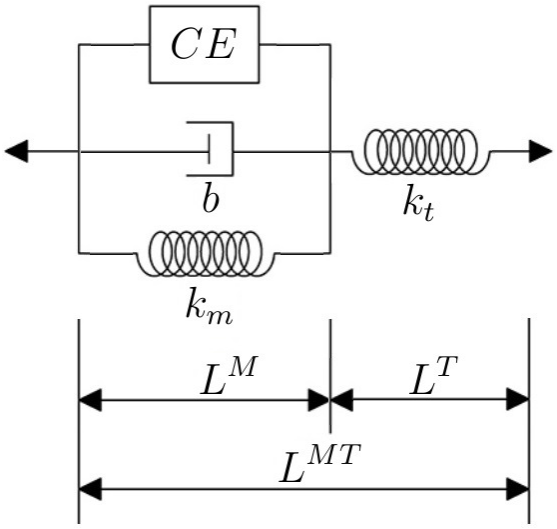

Figure 5-1 Hill muscle model

5.1.1 Model equations

As mentioned in chapter 2, muscle comprises an active component, which generates force if active and depends on the contractile element, and a passive component, which resists movement once beyond the resting length and depends on the elastic elements. Then, the force generated by the contractile element in the Hill muscle model, is given by:

$$F^M(t) = F_0^M a(t) f(v) f(l) \tag{5-1}$$

where $F^M(t)$ is the muscle force, F_0^M is the maximum isometric force, $a(t)$ refers to the activation dynamics, $f(v)$ represents the normalised relationship between fibre force and shortening velocity and $f(l)$ the normalised relationship between fibre force and its length. The musculotendon unit comprises activation and contraction dynamics (see figure 5-2). It uses as an input the muscle excitation and muscle length. The output is the muscle/tendon force.

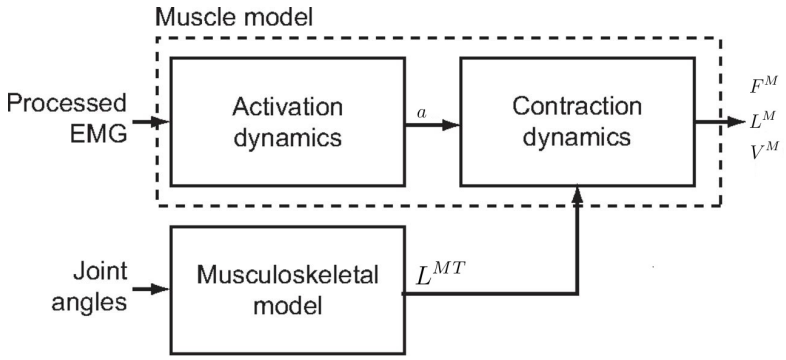

Figure 5-2 Activation and contraction dynamics

Contraction dynamics can be described through the following equations:

$$F^T(t) = k_t(L^T(t) - L_o^T) \tag{5-2}$$

$$F^M(t) = F^{CE}(t) - k_m(L^M(t) - L_o^M) - b\frac{dL^M(t)}{dt} \tag{5-3}$$

where $F^T(t)$ and $F^M(t)$ are the tendon force and muscle force respectively, L_o^M is the muscle resting length and L_o^T is the tendon slack. The force produced by the muscle must be equal to the force produced by the tendon:

$$F^{CE}(t) - k_m(L^M(t) - L_o^M) - b\frac{dL^M(t)}{dt} = k_t(L^T(t) - L_o^T) \tag{5-4}$$

5.1.2 Structural identifiability of the Hill muscle model

It is highly important to understand whether the parameters for the elements are unique with respect to the observed response, as they cannot be directly measured and need to be estimated through model fitting. In order to determine whether these parameters can be uniquely estimated, a structural identifiability analyses is performed. These methods analyse the known equations of the multiple input/output model and determine if the parameters are uniquely identifiable, meaning that

there is only one set of parameter values for the observed responses [Godfrey and DiStefano, 1987] for the given observations. The parameters can also be locally identifiable (when there is a finite or countable number of solutions) or unidentifiable (infinite number of solutions). One common approach is to use Laplace transform and transfer function analysis as follows:

Given equations 5-2 and 5-3, the displacement of the muscle and tendon and muscle-tendon unit can be expressed as:

$$\varepsilon(t) = L^M(t) - L_o^M + L^T(t) - L_o^T \tag{5-5}$$

$$\varepsilon_m(t) = L^M(t) - L_o^M \tag{5-6}$$

$$\varepsilon_t(t) = L^T(t) - L_o^T = \varepsilon(t) - \varepsilon_m(t) \tag{5-7}$$

Replacing in equations 5-2 and 5-3, we obtain:

$$F^T(t) = k_t(\varepsilon(t) - \varepsilon_m(t)) \tag{5-8}$$

$$F^M(t) = F^{CE}(t) - k_m\varepsilon_m(t) - b\frac{d\varepsilon_m(t)}{dt} \tag{5-9}$$

Applying Laplace on equations 5-8 and 5-9 on both sides:

$$F^T(s) = k_t(E(s) - E_m(s)) \tag{5-10}$$

$$F^M(s) = F^{CE}(s) - k_m E_m(s) - bsE_m(s) \tag{5-11}$$

Because $F^M(s) = F^T(s) = F(s)$, equating equations 5-10 and 5-11 result in:

$$k_t(E(s) - E_m(s)) = F^{CE}(s) - k_m E_m(s) - bsE_m(s) \tag{5-12}$$

Rearranging 5-12:

$$F^{CE}(s) = k_t(E(s) - E_m(s)) + k_m E_m(s) + bsE_m(s) \tag{5-13}$$

$$F^{CE}(s) = k_t E(s) + (k_m + bs - k_t)E_m(s) \tag{5-14}$$

Expressing equation 5-10 in terms of $E_m(s)$ yields:

$$E_m(s) = E(s) - \frac{F^T(s)}{k_t} \tag{5-15}$$

Substituting in 5-14 yields:

$$F^{CE}(s) = k_t E(s) + (k_m + bs - k_t)\left(E(s) - \frac{F^T(s)}{k_t}\right) \tag{5-16}$$

$$F^{CE}(s) = k_t E(s) + (k_m + bs - k_t)E(s) - (k_m + bs - k_t)\frac{F^T(s)}{k_t} \tag{5-17}$$

Rearranging 5-17 and replacing $F^T(s)$ for $F(s)$

$$F^{CE}(s) = (k_m + bs)E(s) - \frac{(k_m + bs - k_t)}{k_t}F(s) \tag{5-18}$$

Expressed in terms of exerted force 5-18 yields:

$$F(s) = \frac{(k_m + bs)k_t}{(k_m + bs - k_t)}E(s) - \frac{k_t}{(k_m + bs - k_t)}F^{CE}(s) \tag{5-19}$$

The second term in equation 5-19 is affected by the contractile element (i.e. active part of the model). If activation is zero, for passive moment we can define:

$$F_{pass}(s) = \frac{(k_m + bs)k_t}{(k_m + bs - k_t)}E(s) \tag{5-20}$$

Transfer function can be inferred from equation 5-21 as follows:

$$\frac{F_{pass}(s)}{E(s)} = \frac{(\frac{k_m}{b} + s)k_t}{s + \frac{(k_m - k_t)}{b}} \tag{5-21}$$

Analysing numerator and denominator coefficients of s and s^0:

Numerator s^1:

$$k_t = \bar{k}_t \tag{5-22}$$

Numerator s^0:

$$\frac{k_t k_m}{b} = \frac{\bar{k}_t \bar{k}_m}{\bar{b}} \tag{5-23}$$

From 5-22 and 5-23, can be inferred:

$$\frac{k_m}{b} = \frac{\bar{k}_m}{\bar{b}} \tag{5-24}$$

Denominator s^0:

$$\frac{k_t + k_m}{b} = \frac{\bar{k}_t + \bar{k}_m}{\bar{b}} = \frac{\bar{k}_t}{\bar{b}} + \frac{\bar{k}_m}{\bar{b}} \tag{5-25}$$

from 5-23 and 5-25, can be inferred:

$$\frac{k_t}{b} = \frac{\bar{k}_t}{\bar{b}} \tag{5-26}$$

Because $k_t = \bar{k}_t$ (from equation 5-22), $b = \bar{b}$ (replacing in equation 5-26) and therefore $k_m = \bar{k}_m$ (replacing in equation 5-23), and therefore muscle stiffness (k_m) and damping (b) and tendon stiffness (k_t) are identifiable.

5.2 Proposed Model

In order to study foot biomechanics, a multi-segment foot model is presented comprising of 13 muscles (10 extrinsic and 3 intrinsic) based in the one studied by Morlock and Nigg [1991]. Soft tissue behaviour under three loading places (heel pad, metatarsal head and hallux) is also modelled and results are presented in chapter 6. The musculoskeletal part of the model is depicted in figure 5-3, showing the path of the analysed muscles, where GAS is Gastrocnemius, EDL is Extensor Digitorum Longus, TA is Tibialis Anterior, EHL is Extensor Hallucis Longus, FHB is Flexor Hallucis Brevis, PL is Peroneus Brevis, TP is Tibialis Posterios, FDL is Flexor Digitorum Longus, FHL is Flexor Hallucis Longus and FDB+AH+ADM refers to the group of muscles Flexor Digitorum Brevis, Abductor Hallucis and Abductor Digit Minimi respectively. The muscles were selected because they are the ones that contribute the most to motion activities. Each muscle-tendon complex is modelled using a the Hill muscle model introduced in the previous section. Given that the strongest movement the foot perfoms is in the sagittal plane, this study focuses on the forces and moments produced in that direction. The plantarflexors (red, black and green in figure 5-3) are the strongest muscles, working against gravity to keep balance and also providing propulsion when needed.

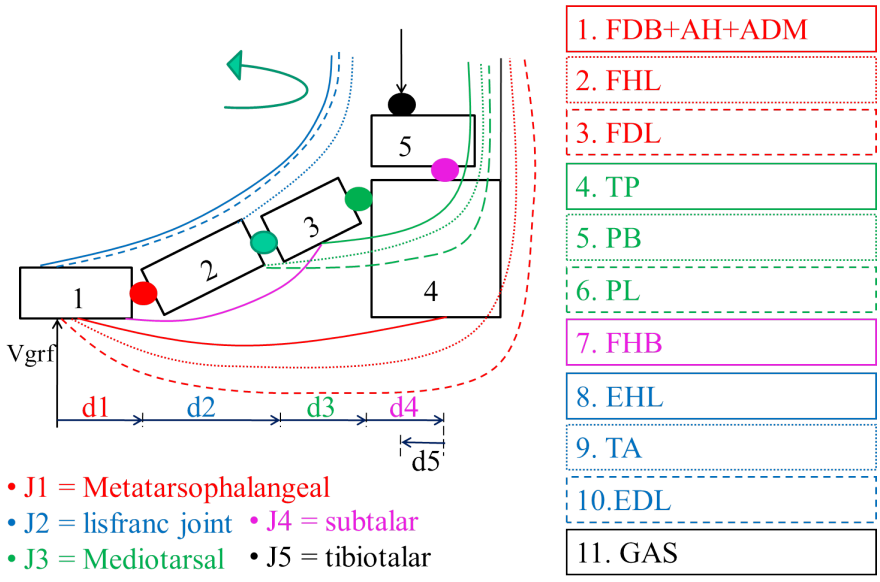

Figure 5-3 Proposed multi-segment foot model

5.2.1 Free body diagrams

A useful tool to perform this kind of study is the free-body analysis, in which we input all the forces and moments that affect the system. Note that the forces are represented by arrows that are only indicative of the line of action.

5.2.1.1 Ankle joint

In order to study the ankle joint, we have to analyse all the muscles crossing the joint of interest. A free-body diagram is presented in figure 5-4(a). As can be seen, there are ten muscles (considering Gastrocnemius as lateral and medial) crossing the ankle joint (muscles are as defined in figure 5-3).

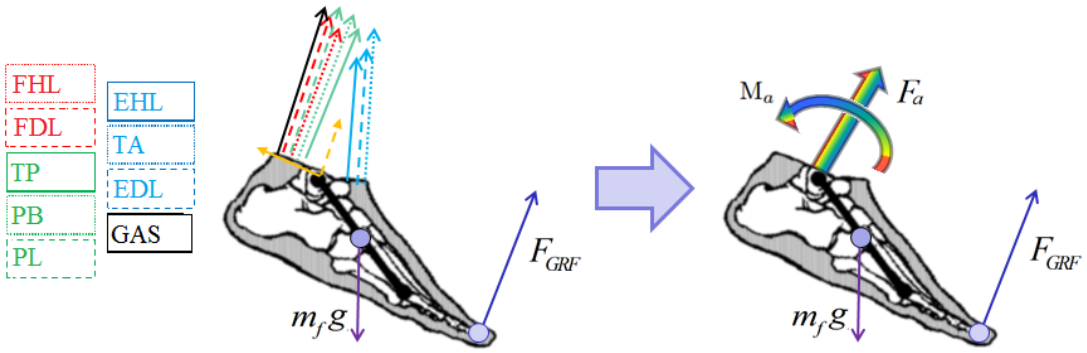

Figure 5-4 Foot free body diagram

Modified from Robertson et al. [2013]

In static situation, the equations describing the model are the following:

$$\sum F_x = 0 \Rightarrow F_{a_x} + F_{GRF_x} = 0 \tag{5-27}$$

$$\sum F_y = 0 \Rightarrow F_{a_y} + F_{GRF_y} - m_f g = 0 \tag{5-28}$$

For dynamic situations, the equations of motion that govern the model can then be derived as follow:

$$\sum F_x = m_f a_x \Rightarrow F_{a_x} + F_{GRF_x} = m_f a_x \tag{5-29}$$

$$\sum F_y = m_f a_y \Rightarrow F_{a_y} + F_{GRF_y} - m_f g = m_f a_y \tag{5-30}$$

$$\sum M_a = I_f\alpha \Rightarrow M_a + [r_{a-COM} \times F_a] + [r_{COM-GRF} \times F_{GRF}] = I_f\alpha_f \quad (5\text{-}31)$$

where F_x is the force at x direction, F_y is the force at y direction, m_f the mass of the foot, F_{a_x} is the force at the ankle in x direction, F_{a_y} is the force at the ankle in y direction, a_x is foot acceleration in x direction, a_y is foot acceleration in y direction, M_a is the moment at the ankle, I_f is the moment of inertia of the foot, α_f the angular acceleration, r_{a-COM} the distance from the ankle to the center of mass of the foot, $r_{COM-GRF}$ is the distance to the point of application of ground reaction force to the center of mass of the foot, g is gravity. Rearraging in 5-31, yields:

$$M_a = I_f\alpha_f - [r_{a-COM} \times F_a] - [r_{COM-GRF} \times F_{GRF}] \quad (5\text{-}32)$$

The moment at the ankle is the outcome of all the muscle forces applied at the ankle joint:

$$M_a = \sum_{i=1}^{nf} F_i \times r_i - \sum_{i=1}^{ne} F_i \times r_i \quad (5\text{-}33)$$

This expression refers to the extension and flexion moments generated by muscles, calculated as the force generated by the muscle (F_i) times the moment arm (r_i). For comprehension pursposes, the abbreviation of each muscle will be used as subscripts instead of numbers. Expansion of equation 5-33 is:

$$M_a = F_{GASM} \times r_{a-GASM} + F_{GASL} \times r_{a-GASL} + F_{PL} \times r_{a-PL} + F_{PB} \times r_{a-PB} + F_{TP} \times r_{a-TP} + F_{FHL} \times r_{a-FHL} + F_{FDL} \times r_{a-FDL} - F_{EDL} \times r_{a-EDL} - F_{EHL} \times r_{a-EHL} - F_{TA} \times r_{a-TA} \quad (5\text{-}34)$$

The moment at the ankle can be obtained from experiments, and therefore it is possible to, through fitting techniques, estimate the unknown parameters. Given that the force produced by the muscle must be equal to the one produced by the tendon, it is possible to first estimate tendon parameters and obtain an estimate of muscle force. This can be done by replacing the force transmitted by tendons by the tendon displacement times its stiffness (i.e. $F^T(t) = k_t(L^T(t) - L_o^T)$ from equation 5-2) in equation 5-34.

5.2.1.2 Metatarsophalangeal joint

The metatarsophalangeal joint can be analysed in the same way as the ankle joint. However, the moment at this joint is not a model output from Vicon system, and therefore needs to be calculated. In this case, the mass and inertial moments of the phalanx are neglected [Miyazaki and Yamamoto, 1993]. The free body diagram is displayed in figure 5-5. The governing equations are:

$$M_{mtp} = F_{GRF} \times r_{mtp-GRF} \tag{5-35}$$

$$M_{mtp} = \sum_{i=1}^{nf} F_i \times r_i - \sum_{i=1}^{ne} F_i \times r_i \tag{5-36}$$

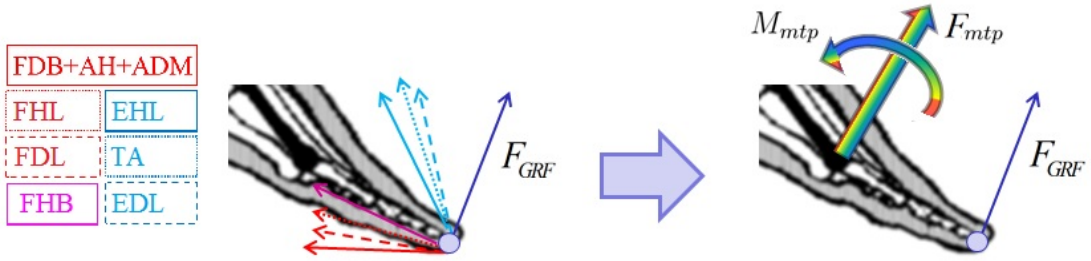

Figure 5-5 Phalanx free body diagram

Modified from Robertson et al. [2013]

Applying the same process explained in the previous section, it is possible to estimate tendon stiffness.

5.3 Parameter estimation

Due to the high number of muscles working together to perform any motor task, the determination of individual muscle forces is a very complex issue. Muscles cannot be individually measured with non invasive techniques and therefore forces (and related parameters) are usually estimated through fitting techniques from the moment at the joint of interest. Due to the complex nature of the muscles, different type of trials have to be carried out in order to estimate muscle and tendon parameters. Given that the force produced by the muscle is equal to the force produced by its tendon, it is possible to estimate first tendon stiffness from

walking trials by optimasing the moment around the joint of interest (ankle, for example, for extrinsic muscles). Unfortunately, it is not possible to estimate muscle stiffness and damping parameters from this type of trials, as it has been proven in section 4.4.5 that the active component is always present. A passive trial was then performed, allowing thus to estimate the stiffness and damping parameters for the muscle, having already calculated tendon stiffness and compliance. The procedures involved in both types of experiments have already been commented previously in chapter 4, validating muscle-tendon length assessment as well as active and passive muscle trials. For tendon parameterisation, subjects were asked to walk stepping with the right and left foot on the forceplate alternately ten times. Subjects were then asked to lie on the bed and five passive dorsi/plantarflexion trials were perfomed, where the volunteer was asked not to perform any kind of voluntary movement. In order to link this model to the diabetic foot, these same trials were carried out for the same subjects, but wearing special orthotics in order to mimic different diabetic injuries which will be discussed in chapter 7. Experiments were carried out at the University of Warwick Gait Laboratory[1] and written informed consent was obtained for the participating subjects.

5.3.1 Tendon Parameterisation

Most of the movement in the muscle-tendon unit is produced by the muscle, and therefore it is expected to find very high values for the tendon stiffness. One of the tendons that undergoes a bigger change in length is the Achilles tendon [Fukashiro et al., 1995]. However, it is very common to see in the literature the tendon considered as rigid. Data were fitted per subject basis using linear least squares regression, by optimising the moment around the ankle, using five trials for parameter estimation and one more unused trial for validation. Stiffness parameters (and its standard deviation) for 15 subjects are presented in table 5-1. Further validation is presented in figure 5-6 for eight representative subjects, where measured ankle moment (red) is compared with simulated one (blue).

[1]The experiments comply with all data protection requirements as stated in the University of Warwick BSREC ethical approval: BSREC full approval REGO-2013-582 Foot Modelling

	EDL	EHL	FDL	FHL	GAS L	GAS M
1	865.830±31.034	342.347±12.989	212.049±1.904	207.817±1.850	330.873±4.252	552.595±1.845
2	708.071±12.364	282.353±4.824	278.133±3.771	275.029±3.575	390.694±2.949	772.595±6.135
3	618.175±12.944	248.508±5.134	239.585±5.018	238.645±4.869	345.139±5.505	678.784±10.684
4	402.818±6.678	153.083±3.132	257.327±3.967	238.482±3.518	307.166±3.949	504.247±4.195
5	417.079±6.052	226.518± 3.510	294.746±2.853	271.349±2.498	455.803± 2.555	832.880±4.833
6	490.076±19.382	114.881±3.868	298.704±3.324	193.712±1.877	446.897±2.135	763.417±3.828
7	818.475±48.092	330.801±18.837	211.323± 2.308	211.981±2.128	322.911±.844	632.403±1.959
8	284.232±3.861	334.713±5.645	256.340±6.291	163.548±3.288	543.185±12.042	681.614±12.541
9	640.376±13.151	257.942±5.716	222.43±2.1782	220.2865±2.126	341.018±1.823	663.429±3.769
10	131.068±0.393	234.487±3.379	224.407±2.199	205.618±1.891	238.869±1.171	596.087±3.348
11	674.608±30.110	263.007±11.243	197.189± 2.609	184.376±2.204	398.103±2.186	761.546±4.855
12	884.165±26.081	359.404±10.556	249.711±2.704	247.719±2.624	373.972±1.505	735.742±3.372
13	1037.711±32.377	420.773±13.023	229.614±1.657	231.124±1.543	359.585±0.730	703.965±1.800
14	747.449± 14.627	300.047±5.775	277.558± 5.205	277.121±5.027	425.476±6.796	834.535± 12.885
15	642.509±15.989	330.066±8.307	283.903±4.101	282.902±3.959	394.659±3.121	616.397±4.644
	PB	PL	TA	TP	RMSE	R^2
1	4077.726±36.361	2121.311±19.242	1192.213± 45.047	1750.385±12.111	19.2	0.91
2	5269.265±71.582	2731.038±39.469	972.483±17.721	2234.556±26.567	16.3	0.91
3	4532.958±99.414	2382.803± 55.624	824.936±19.419	1942.124±39.528	0.2	0.99
4	2427.804± 37.349	1874.431±29.878	653.236±13.880	1724.444±23.289	9.8	0.96
5	5776.493±54.189	2447.043±23.497	798.956±12.431	2027.181±16.340	14.1	0.93
6	3195.985±29.710	2372.681±27.685	1328.582± 54.860	2132.418±17.385	1.6	0.88
7	4338.43±44.014	2068.685±26.073	1155.647±62.716	1829.902±12.906	0.4	0.99
8	4638.03± 126.449	3187.418±87.609	881.706±16.608	2476.323±62.376	8.8	0.95
9	863.939±9.705	5785.406±53.520	884.488±18.962	1863.151±15.578	20.8	0.93
10	2712.854±28.307	5333.935±55.284	1140.225± 18.675	1523.067±12.815	18.2	0.86
11	3599.972±50.740	2284.233±35.291	779.034±30.755	2173.43±25.086	0	0.99
12	4758.432±51.760	2415.491±28.846	1254.786±36.683	2044.864±17.884	30.6	0.71
13	4471.064±32.546	2237.432±18.280	1456.375±45.255	1896.035±10.835	0	0.99
14	5514.911±121.170	2757.77±56.584	968.089±20.056	2296.981±44.186	7.1	0.97
15	3602.469±48.655	1881.758±28.667	796.144±18.963	1947.902±23.069	0.1	0.99

Table 5-1 Tendon Stiffness Parameters (in N/mm) for muscles crossing ankle joint

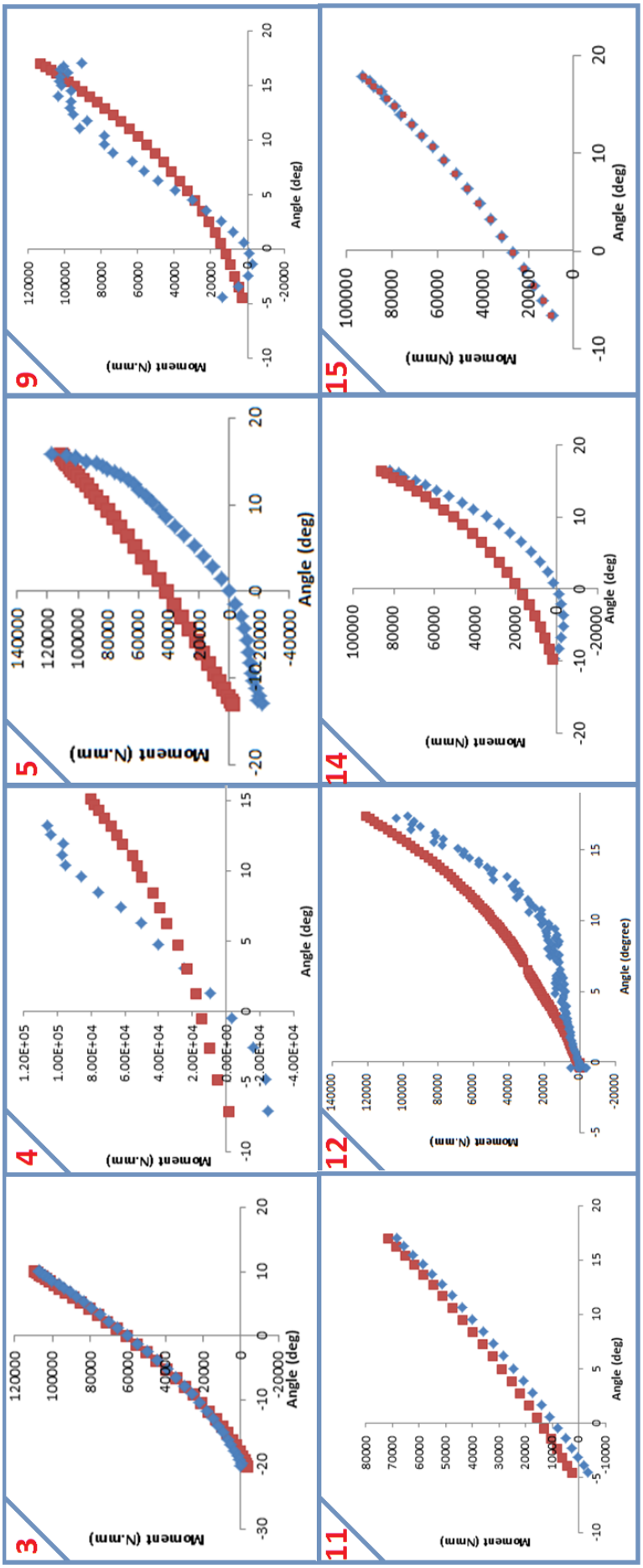

Figure 5-6 Measured and simulated ankle dorsiflexor moment

5.3.2 Muscle Parameterisation

Muscle parameters were estimated using the force obtained from tendon parameterisation. In order to obtain these parameters, passive dorsi/plantarflexion was performed as explained in chapter 4 (section 4.3). Each muscle was studied individually, parameters for fifteen subjects are displayed in table 5-2.

5.4 Discussion and conclusions

Values for tendon stiffness and muscle stiffness and damping were presented in order to model the biomechanics of the foot. The tendons proved to be very stiff and not very compliant, having a small range of movement which allows the joints to be fixed in different angles. As it can be seen from the tables, parameters do vary among subjects, but they all present very high stiffness (in comparison with muscle stiffness). For all the subjects, the tendons exhibiting higher stiffness are those corresponding to Medial Gastrocnemius, Peroneus Longus, Tibialis Anterior, Tibialis Posterior and Peroneus Brevis. The compliance is very low, and therefore similar parameters are found for all the subjects with the same structure (as the tendon stiffness is calculated as a function of the moment arm and therefore bigger subjects will have bigger moment arm). Muscles, on the other hand, presented more similar values across subjects. It was also observed that, in many cases, muscles have a low damping coefficient being this value in the order of 0.1. However, no clear trend could be found when analysing muscle's damping.

In terms of the metatarsophalangeal joints, parameters obtained through fitting were not included as they were significantly lower than the ones form the extrinsic muscle. The reason for this is that most of the moment around the metatarsophalangeal joint is produced by the extrinsic muscles, which are significantly more powerful in producing force than the intrinsic muscles.

The model presented in this chapter proved to be reliable and repeatable, providing a promising tool for musculoskeletal modelling using different types of non-invasive methodologies.

	EDL			**EHL**			**FDL**			**FHL**			**TA**		
S	k_m	b	RMSE	k_m	b	RMSE	k_m	b	RMSE	k_m	b	RMSE	k_m	b	RMSE
1	52.482	2.5	252	16.866	0.783	80.727	116.104	12.455	141.56	81.342	9.062	153.03	73.72	3.774	418.08
2	33.902	1.982	166.2	10.731	0.622	52.768	99.615	3.758	149.74	70.378	2.6059	162.06	49.816	3.075	291.29
3	40.681	7.385	41.603	12.91	2.313	13.205	127.056	9.609	57.829	89.441	7.146	62.357	58.759	11.417	71.414
4	14.297	2.546	52.769	4.185	0.748	15.097	85.866	17.277	152.88	55.591	11.41	153.81	32.612	1.123	79.831
5	28.008	1.741	86.931	11.979	0.73	37.033	83.303	0.265	74.483	53.9551	0.144	72.428	59.031	3.786	208.82
6	18.114	0.19	121.56	3.238	0.038	24.171	125.762	0.427	217.71	56.145	0.207	153.69	52.583	0.532	385.53
7	34.278	7.501	249.9	11.051	2.4	79.841	80.96	18.417	128.88	55.102	13.049	138.53	46.363	10.975	415.15
8	13.612	0.025	93.144	5.546	0.63	120.82	80.887	0.7	163.5	34.711	0.412	112.83	23.633	2.748	492.86
9	19.361	0.725	226.78	6.236	6.236	72.177	46.458	1.058	203.11	33.22	0.806	220.65	26.814	1.119	387.14
10	49.596	1.92	152.95	15.689	0.604	48.696	48.696	3.195	159.58	110.986	2.269	173.11	72.977	2.938	262.02
11	31.216	0.823	204.71	9.681	0.255	63.309	74.937	0.997	134.49	48.338	0.638	136.45	35.366	1.031	294.84
12	17.812	7.698	200.56	5.624	2.782	64.006	56.518	9.09	72.828	40.021	9.886	75.517	26.582	6.494	334.55
13	54.851	12.011	85.692	17.558	3.811	27.313	124.94	22.344	177.62	88.375	15.518	192.59	76.349	17.593	142.79
14	21.892	3.209	117.55	6.961	1.001	37.092	60.244	18.538	129.47	41.746	13.603	138.69	31.476	5.269	212.37
15	29.937	0.06	211.34	12.217	0.025	84.386	80.357	0.23	157.95	55.972	0.16	168.09	38.984	0.076	335.9
	GAS L			**GAS M**			**PL**			**PB**			**TP**		
S	k_m	b	RMSE	k_m	b	RMSE	k_m	b	RMSE	k_m	b	RMSE	k_m	b	RMSE
1	49.374	1.409	164.982	41.779	9.118	657.05	374.481	36.978	232.73	473.68	51.431	477.33	582.73	62.841	823.98
2	53.749	2.235	406.54	120.529	5.062	892.79	322.349	11.033	248.28	429.585	14.538	512.72	515.988	18.381	882.71
3	77.301	28.987	53.747	192.803	69.635	95.368	439.028	24.441	99.371	533.12	42.931	198.57	652.909	50.558	343.38
4	43.925	4.433	357.38	81.71	9.024	665.35	136.444	25.977	124.83	256.792	50.081	374.19	137.7	15.655	98.059
5	56.744	2.042	182.83	117.465	4.347	374.27	280.373	0.387	126.97	292.25	0.366	199.09	355.14	0.76	356.35
6	50.375	0.434	569.04	100.141	0.855	1100.7	223.679	0.733	200.88	428.977	1.493	606.46	525.136	1.818	1059.6
7	68.145	5.697	395.63	149.309	13.612	868.42	257.986	56.38	206.5	328.02	73.386	426.89	395.059	89.812	733.04
8	81.723	0.652	636.35	100.875	1	886.04	111.26	1.317	270.88	422.623	3.172	731.56	386.267	1.419	832.53
9	23.321	1.048	526.24	52.37	2.326	1166	165.149	3.612	328.48	198.41	4.758	683.43	245.371	5.6741	1179.4
10	95.997	2.259	420.65	214.589	5.058	923.4	504.891	9.91	270.39	676.328	13.185	559.21	809.397	16.098	956.6
11	48.12	1.065	440.05	107.657	2.372	964.46	220.862	2.707	196.37	371.146	4.386	528.52	499.76	6.078	1006.8
12	37.456	1.412	203.65	82.461	2.423	442.22	194.427	56.4247	120.11	250.544	11.259	231.27	300.647	13.89	407.08
13	57.929	13.545	449.01	128.315	31.646	990.79	399.018	67.545	292.38	529.529	88.137	607.06	641.358	26.75	993.16
14	34.889	8.378	360.19	77.064	19.475	790.51	207.039	54.606	213.14	261.762	77.881	430.05	311.943	94.563	743.27
15	37.741	0.138	391.15	66.985	0.274	694.95	173.923	0.477	171.48	229.037	0.642	357.08	337.929	0.96	757.2

Table 5-2 Muscle Stiffness Parameters (in N/mm) and Damping (in Ns/mm) for muscles crossing ankle joint

6

Plantar soft tissue model

The plantar soft tissue protects the structure of the foot and provides cushioning. It is the only interface of the body with the ground during any type of motion activity. In this chapter, a brief introduction to plantar soft tissue, its architecture and different viscoelastic models are given. Parameters for a non-Newtonian Kelvin-Voigt model are presented for 15 subjects with the purpose of characterising the properties of the soft tissue under the calcaneus (heel pad), metatarsal heads and hallux (great toe).

6.1 Introduction

The plantar soft tissue is a highly viscoelastic structure composed mainly of adipose tissue, aimed at providing cushioning to the underlying bones and shock attenuation [Cavanagh, 1999].

The heel pad is a specialised adipose tissue located on the posterior side of the calcaneus, it is a very thick tissue that is composed of small compartments filled with fat. This tissue is capable of attenuating the heel strike energy impact by up to 90% [Valiant, 1984] and undergoes loads that are higher than body weight. Its structure has been widely studied (see, for example, Aerts et al. [1995]). It acts as a shock absorber during heel strike, thus attenuating (dampening) the peak accelerations produced in movement, but it also has the capability of returning to

its original shape after weight bearing activities [Yu et al., 2014]. The force that the tissue undergoes depends on the velocity of the impact and the body mass [Giddings et al., 2000], therefore at higher velocities, it is expected to experience an increased force. The soft tissue under the metatarsal heads and toes, also provides cushioning, but does not have to attenuate such high loads.

The main techniques used to study plantar soft tissue are ultrasonography and ballistic pendulum testing, with most of these concentrated on heel pad tissue (see, for example, Cavanagh [1999] and Valiant [1984]). However, these techniques do not replicate the movement of the foot during motion activities. This chapter proposes a new method for characterising soft tissue during gait.

6.1.1 Properties of soft tissues

When studying skeletal soft tissue, a force can be applied to the tissue in order to study its deformation or vice versa [Kothonen and Saarakkala, 2011]. In any case, there are three important parameters that describe the mechanical properties of the tissue:

- **Strain (ε)**: is a unitless quantity that refers to the deformation produced when a force is applied to the soft tissue, and can be determined using the following expression:

$$\varepsilon = \frac{\Delta l}{l_0} = \frac{l(t) - l_0}{l_0} \tag{6-1}$$

  where Δl is the change in length of the tissue (when analysing shear forces) or change in thickness of the tissue (when analysing normal forces), and l_0 is the unloaded length or thickness respectively.

- **Strain rate ($\dot{\varepsilon}$)**: refers to the deformation change of the tissue over time and is given by:

$$\dot{\varepsilon} = \frac{d\varepsilon}{dt} = \frac{d}{dt}\left(\frac{l(t) - l_0}{l_0}\right) = \frac{1}{l_0}\frac{dl(t)}{dt} \tag{6-2}$$

- **Stress (σ)**: refers to the force needed to compress a material in the normal direction, and is defined as the force per unit area:

$$\sigma = \frac{F}{A_0} \tag{6-3}$$

where F is the applied force and A_0 the cross-sectional area of the application of force such that the force is normal to the its plane.

In the case of shear forces, in this study we will refer to the force per unit length (applied to the medio-lateral orientation), instead of shear stress applied over the plantar area.

6.1.2 Viscoelasticity

As the word implies, a viscoelastic material is both viscous and elastic, being the first a property of fluidic materials and the second of solid materials [Kothonen and Saarakkala, 2011]. The fluidic material will resist movement, and therefore the work required to deform the tissue will be higher. This behaviour produces an hysteresis and is depicted in stress-strain curves (see figure 6-1), where the compression and decompression paths are different. This type of material behaviour is time-dependent, and therefore the stress (σ) is defined as a function of both strain (ε) and strain rate ($\dot{\varepsilon}$): $\sigma = \sigma(\varepsilon, \dot{\varepsilon})$.

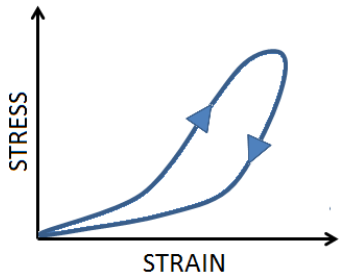

Figure 6-1 A typical Stress-Strain curve

The contact of the foot (or part of the foot) on the ground can be divided into two phases: compression and decompression (or restitution). The ascending path of the strain-stress curve reaches its highest value (both in tissue deformation and force transmitted by the tissue) when the contact velocity equals zero. From this point, decompression begins until there is no contact between the foot and the ground.

6.1.3 Soft tissue models

In order to model soft tissue, it is very common to use rheological models, which are a good approximation of viscoelastic behaviour. They typically consist of different arrangements of linear and non-linear springs and dampers. Four different variations of parallel spring-damper model were analysed in order to fit to the soft tissue deformation data generated from experiments performed. This model connects a damper in parallel to a spring, therefore the strain is the same in both components, but the stress will depend on the strain rate and there will be a contribution from both elements:

1. Linear spring and linear damper (classical Kelvin-Voigt). This model is given by:

$$\sigma = E\varepsilon + \eta\dot{\varepsilon} \tag{6-4}$$

   where σ is the stress, ε the strain, $\dot{\varepsilon}$ the strain rate, and E and η are the elastic and viscous parameters respectively.

2. Linear spring and non-linear damper (used by Gefen et al. [2001]). This model is given by:

$$\sigma = E\varepsilon + \eta\varepsilon\dot{\varepsilon} \tag{6-5}$$

   where σ is the stress, ε the strain, $\dot{\varepsilon}$ the strain rate, and E and η are the elastic and viscous parameters respectively. In Gefen et al. [2001], this heel pad model is parameterised using the transient thickness measured by a digital radiographic fluorosocpy (real time X-ray) and the contact pressure provided by a plantar pressure system, simultaneously.

3. Non-linear spring and non-linear damper (combination of non linear elements proposed by Hunt and Crossley [1975]). This model is given by:

$$\sigma = E\varepsilon^n + \eta\varepsilon^m\dot{\varepsilon} \tag{6-6}$$

   where σ is the stress, ε the strain, $\dot{\varepsilon}$ the strain rate, E and n define the elastic parameters and η and m are the viscous parameters.

4. Non-linear spring and non-linear damper (proposed by Scott and Winter

[1993]). This model is given by:

$$F = E\varepsilon^l + \eta\varepsilon^m|\dot{\varepsilon}|^n \tag{6-7}$$

where F is the force transferred by the tissue, ε the strain, $\dot{\varepsilon}$ the strain rate, E and l define the elastic parameters and η, m and n the viscous parameters. This is a more complicated model of the heel pad, where Scott and Winter [1993] used the values obtained from impact tests performed by Valiant [1984]. They assumed that the mechanical characteristics of the metatarsals and toe pads mimic those from the heel pad.

When replacing linear components by non-linear ones, a higher correlation can be found between measured stress-strain and simulation and therefore, the model will be more realistic. However, these non-linear models will require the analysis of non-linear differential equations and a more complicated parameter estimation process. The four models (equations 6-4 to 6-7) have been applied to the subject data, and an analysis was performed on the resulting correlation coefficients and root mean square error (RMSE) in order to assess the goodness of the fit of the models to the data. Figures 6-2 and 6-3 show an example of the fitting for all of the models (normal and shear respectively). Table 6-1 shows correlation coefficients (R^2) and RMSE for one subject (male, 94kg, 1910mm height), for the four analysed models regarding heel pad shear and normal stresses. Analysis on the rest of the subjects can be found in appendix F.

	Normal Stress		**Shear Force/l**	
	R^2	RMSE	R^2	RMSE
Gefen et al.	0.938	16.56	0.9152	0.111
Scott and Winter	0.9369	17.22	0.9354	0.125
Hunt and Crossley	0.9434	15.88	0.933	0.099
Kelvin Voigt	0.9084	20.13	0.8517	0.147

Table 6-1 R-squared and RMSE values for different soft tissue models. Note: units are kN/m^2 and kN/m for normal and shear force per unit length respectively.

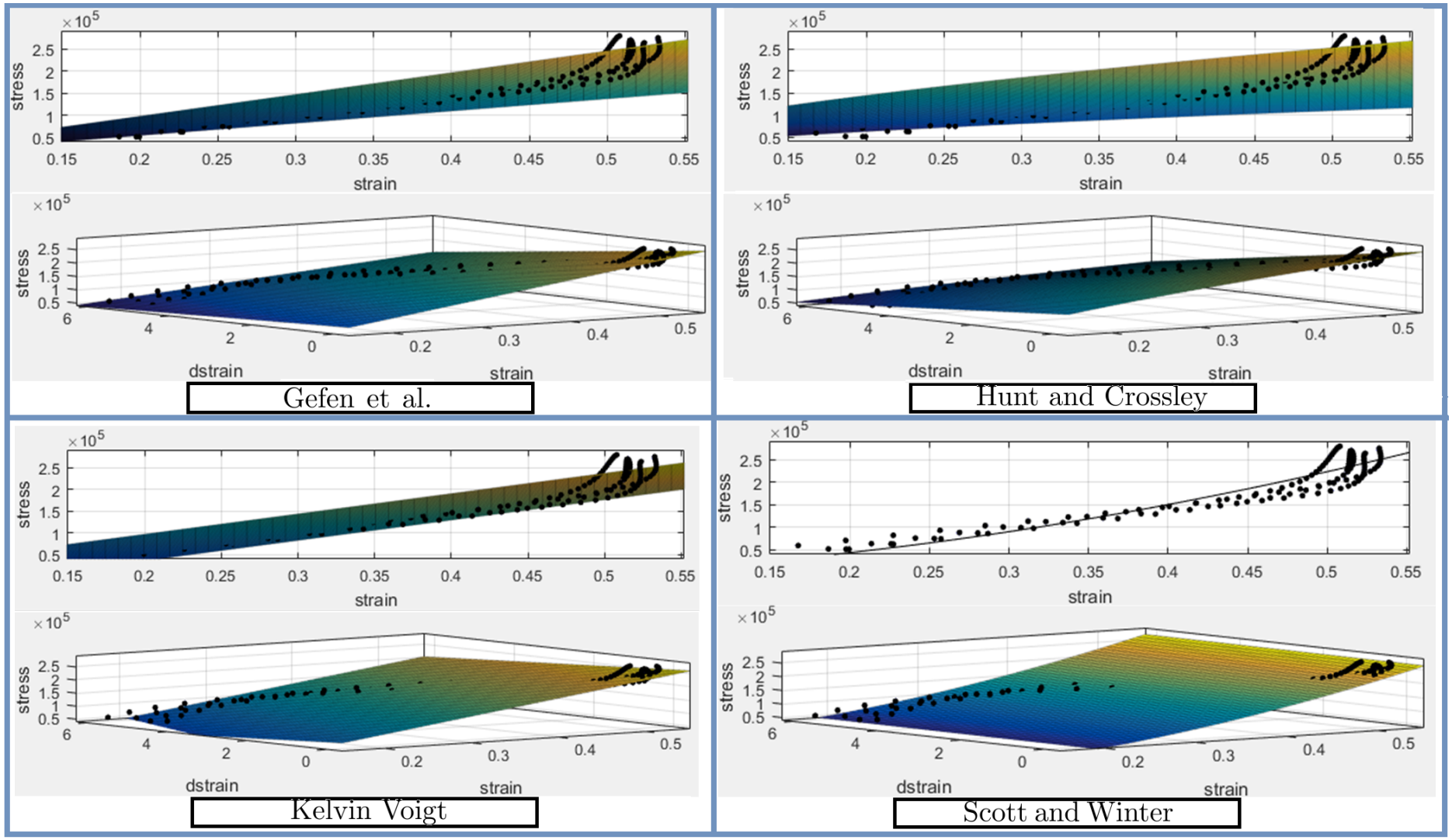

Figure 6-2 Soft tissue model fitting for normal stress (in N/m^2) using four trials

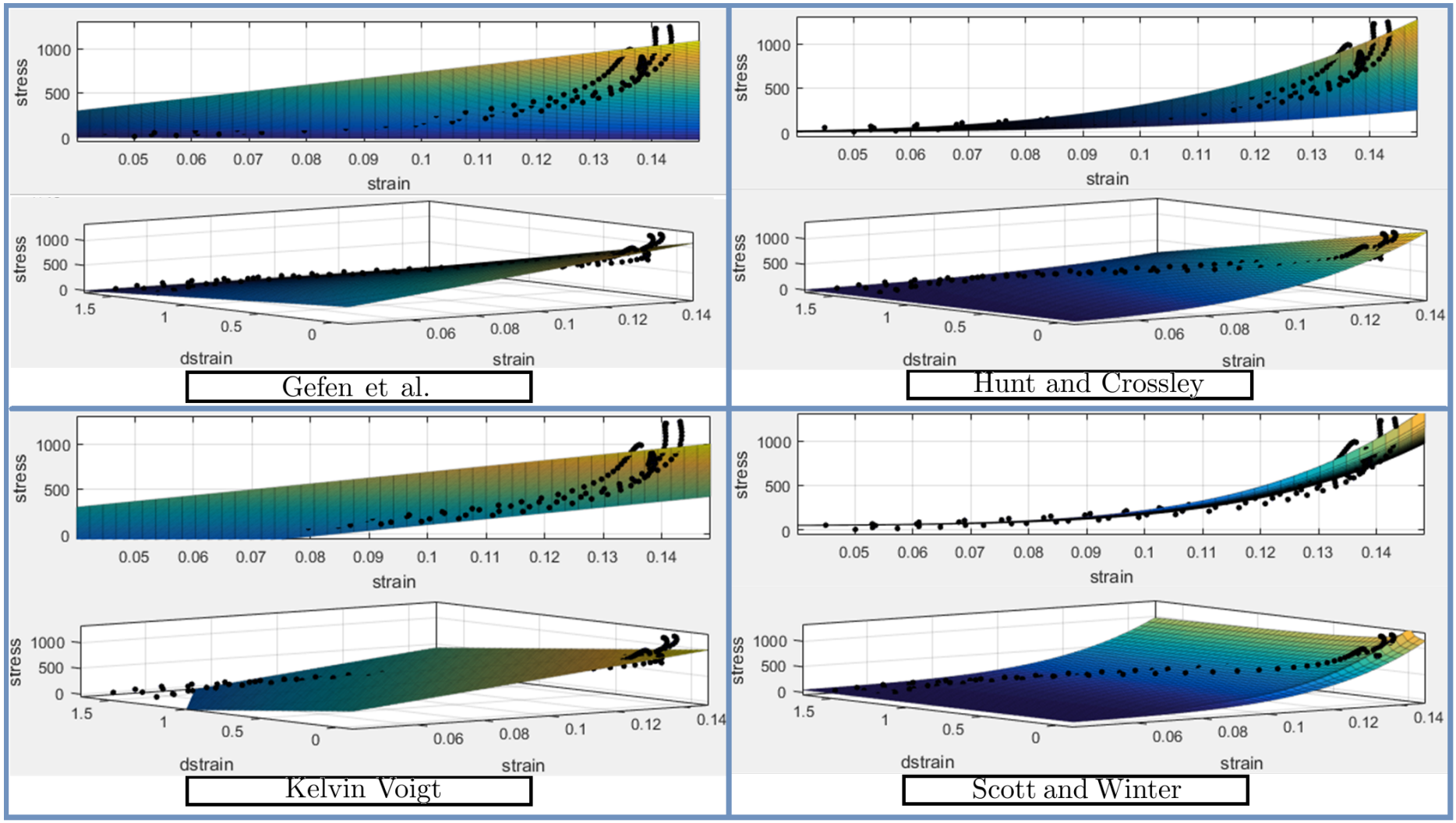

Figure 6-3 Soft tissue model fitting for shear force per unit length (in N/m) using four trials

After analysing all of the trials, the second model (used by Gefen et al. [2001], equation 6-5) was chosen. It represents a good compromise of complexity and correlation as it has only two parameters to be estimated. Good correlation coefficients and low RMSE were obtained using many trials per subject (ranging from 2 trials to 7 trials), therefore making the model more reliable. An example of model validation is provided in figure 6-4.

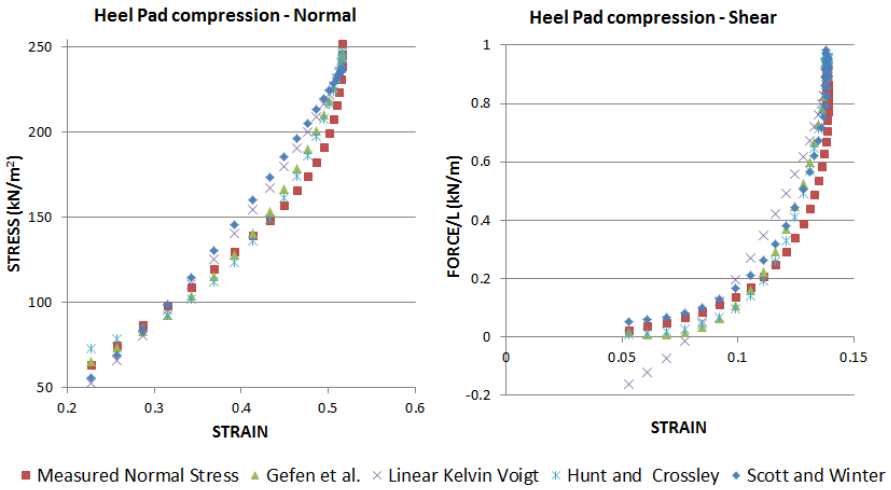

Figure 6-4 Model validation for normal stress (left) and shear (right) for the 4 models

A set of data was used for training and fitted to the four models. Another unused trial was used to compare with the estimation (obtained from taining data) for validation purposes.

6.1.3.1 Identifiability of the soft tissue model

Identifiability refers to whether it is possible to identify the unknown parameters (E and η), given known or measured variables (σ, ε and $\dot{\varepsilon}$) from the constitutive equation:

$$\sigma = E\varepsilon + \eta\varepsilon\dot{\varepsilon} \tag{6-8}$$

Analysing the model equation for two different sets of parameters (E_1, η_1) and (E_2, η_2):

$$\sigma = E_1\varepsilon + \eta_1\varepsilon\dot{\varepsilon} \tag{6-9}$$

$$\sigma = E_2\varepsilon + \eta_2\varepsilon\dot{\varepsilon} \tag{6-10}$$

Operating on both sides, we obtain:

$$0 = (E_1 - E_2)\varepsilon - (\eta_1 - \eta_2)\varepsilon\dot{\varepsilon} \tag{6-11}$$

Because both strain and strain rate are different from zero and this equation holds for all times t and ε and $\varepsilon\dot{\varepsilon}$ are linearly independent. Then the only possible outcome is that $E_1 = E_2$ and $\eta_1 = \eta_2$ and therefore the model parameters and the model are identifiable.

6.2 Experimental Design

In order to model soft tissue, motion capture experiments were carried out at the University of Warwick Gait Laboratory and written informed consent was obtained for the participating subjects[1]. Subjects were first markered according to the Plug-in-Gait lower body marker placement, previously described in chapter 3 (3.1.3) and extra markers were added to model the soft tissue. Figure 6-5 depicts the position of these markers.

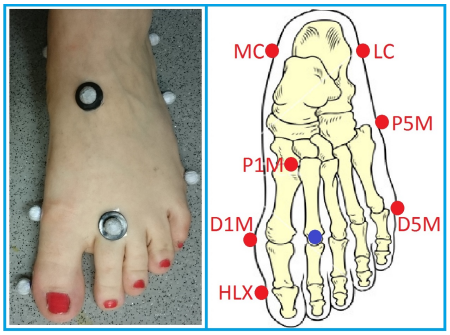

MC:	Medial side of the calcaneus
LC:	Lateral side of the calcaneus
D1M:	Distal side of 1st metatarsal
D5M:	Distal side of 5th metatarsal
P1M:	Proximal side of 1st metatarsal
P5M:	Proximal side of 5th metatarsal
HLX:	Medial side of the hallux

Figure 6-5 Marker placement for plantar soft tissue modelling. Blue marker corresponds to toe marker in Plug-in-Gait.

By calculating the distance between the calcaneus markers from heel strike to heel off, it is possible to understand the deformation of the heel pad under loading. The same procedure can be applied to the metatarsal's head. Regarding the hallux, an approximation was performed taking into consideration the displacement of

[1]The experiments comply with all data protection requirements as stated in the University of Warwick BSREC ethical approval: BSREC full approval REGO-2013-582 Foot Modelling

the hallux marker. As previously explained in chapter 3, a forceplate permits calculation of the total force applied by the foot of a subject to the ground in the three planes (F_x, F_y and F_z). Of particular interest are the normal (F_z) and shear (F_y) forces, as it has been proved in Valiant [1984] that most of the tissue movement is produced in those two planes. Subjects were instructed to walk at their own pace, and step as parallel to the forceplate as possible in order to obtain reliable shear force results. Because the forceplate provides the resultant ground reaction force, it was necessary to perform different experiments to study each particular area of the foot. The study consisted of three parts:

1. Heel Pad testing: Subjects were asked to walk at their natural pace, stepping on the forceplate only with the heel pad. This provides information regarding heel pad deformation and normal and shear force on the aforementioned area for both compression and decompression (figure 6-6).

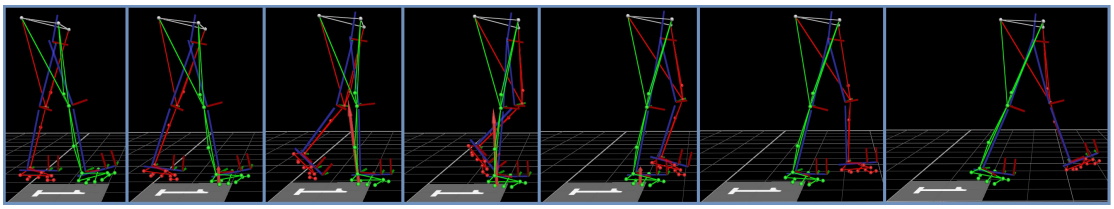

Figure 6-6 Heel pad testing

2. Metatarsal and phalanx testing - forward: Subjects were asked to walk at their natural pace, stepping on the forceplate only with the forefoot (metatarsals and phalanx). This provides information regarding metatarsal deformation and shear and normal forces during compression and phalanx deformation and shear and normal forces during decompression (figure 6-7).

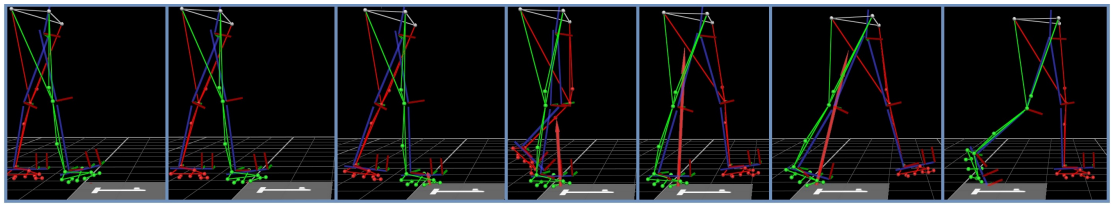

Figure 6-7 Forefoot testing: walking forwards

3. Metatarsal and phalanx testing - backwards: Subjects were asked to walk

backwards at their natural pace, stepping on the forceplate only with the forefoot (metatarsals and phalanx). This provides information regarding phalanx deformation and shear and normal forces during compression and metatarsal deformation and shear and normal forces during decompression (figure 6-8).

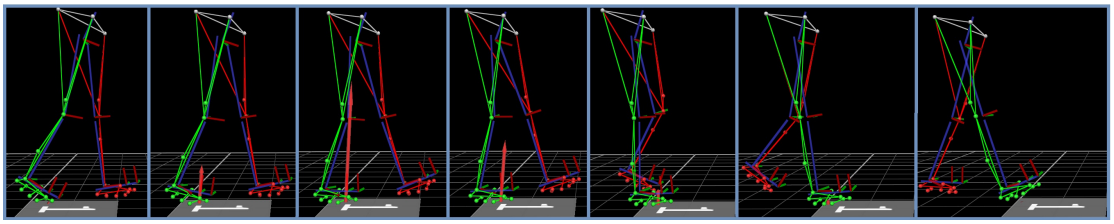

Figure 6-8 Forefoot testing: walking backwards

Subjects were able to practice before each part in order to hit the forceplate with the region of interest in every case. They were instructed to walk at their natural pace and not to look down; therefore a "natural" gait was achieved as closely as possible. A caliper was used to obtain unloaded values for heel pad, metatarsals and hallux thicknesses. The distances between the MC and LC markers and D1M and D5M markers were measured with Vicon Nexus and validated via caliper measurements. Regarding the compressed area of soft tissue, this was monitored throughout the gait cycle using Tekscan Insoles as shown in figure 6-9 where the studied areas are circled. This allowed measurement of the required area to be considered in the stress analysis. Table 6-2 presents unloaded thickness, width and area values for the heel pad, metatarsal heads and hallux for all of the subjects.

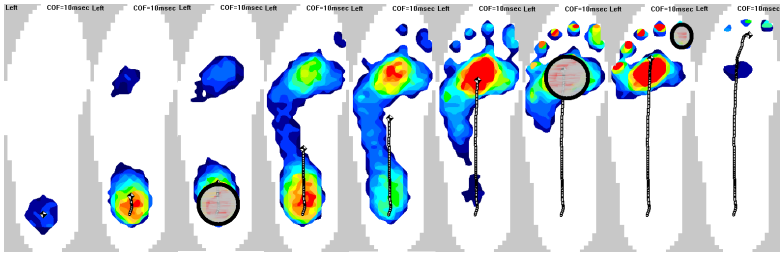

Figure 6-9 Plantar pressure: studied areas circled in grey

S	Height	Body Mass	Heel Pad			Metatarsals			Hallux		
			Thickness	Width	Area	Thickness	Width	Area	Thickness	Width	Area
1	1865	111	19.2	66.01	0.003	16.54	102.74	0.0035	10.78	23	0.0008
2	1570	47	13.24	53.18	0.0019	10.35	71.55	0.002	9.8	21	0.0005
3	1790	75	19.8	59.09	0.0028	16.7	101.67	0.0025	12.95	21	0.0006
4	1650	72	14.72	56.52	0.002	12.8	89.09	0.0027	11	20	0.0006
5	1720	61.5	15.89	53.89	0.0018	12.98	86.37	0.0025	8.1	21	0.0008
6	1780	88	16.05	58.09	0.0025	14.3	88.84	0.0026	12.148	21	0.0008
7	1690	77	16.01	60.34	0.0025	14.41	87.18	0.0025	11.19	23	0.0008
8	1625	51.5	14.56	57.31	0.002	11.32	91.04	0.0032	9.32	19	0.0007
9	1865	77	19.19	66.16	0.0023	15.9	104.4	0.004	12.7	21	0.0009
10	1670	52.5	14.7	58.74	0.0018	12.53	88.23	0.002	13.1	19	0.0005
11	1630	74.5	16.42	61.08	0.0022	13.9	89.97	0.0028	13	20	0.0008
12	1820	74.5	18.6	64.02	0.0029	15.9	93.21	0.0033	12	22.9	0.0008
13	1910	90	20.19	68.27	0.003	16.7	102.65	0.005	13.32	23	0.0009
14	1630	69.5	15.42	52.38	0.0022	12.71	88.24	0.0028	12.03	21.11	0.0006
15	1680	73.5	17.1	66.2	0.0025	14.4	99.8	0.0027	12.9	23	0.0008

Table 6-2 Soft tissue properties for 15 subjects (1-15). Body mass is in kilograms, height. thickness and width in mm and area in m^2.

The metatarsal heads, could not be studied independently, but as a whole. As can be seen in figure 6-10, the ground reaction force is distributed across the 5 metatarsals, but given the impossibility of isolating the ground reaction force from the forceplate data nor the tissue strain, the area under the metatarsals has been considered as one element.

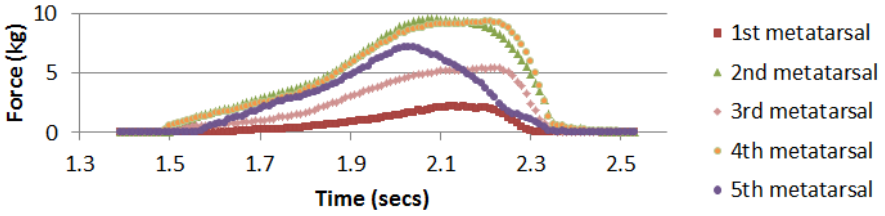

Figure 6-10 Plantar pressure: soft tissue analysis over the five metatarsal heads

All data were processed using Vicon Nexus 1.8.5, Excel and Matlab. Due to the fact that the forceplate and the cameras sample at different rates (1000Hz and 200Hz respectively), a downsampling was performed on the forceplate data. An analysis was perform to investigate the use of cubic spline interpolation for the downsampling, which can be found in appendix G.

6.2.1 Repeatability analysis

A repeatability analysis was performed in order to validate the proposed methodology for soft tissue deformation measurement. The same subject was markered on two consecutive days and was asked to perform walking trials each day: 10 corresponding to the heel pad, 10 corresponding to metatarsal and phalax testing walking forwards and 10 walking backwards. Trials were grouped by velocity of impact and the median for each day and each type of trial undertaken. An analysis was performed on the strain-stress curves, showing good correlation between days for the trials, ranging from 0.8028 to 0.9952 (see table 6-3 and figures 6-11 to 6-22).

	COMPRESSION		DECOMPRESSION	
	HEEL PAD NORMAL	HEEL PAD SHEAR	HEEL PAD NORMAL	HEEL PAD SHEAR
Right	0.9925	0.8454	0.851	0.8982
Left	0.9261	0.8852	0.9144	0.809
	METATARSAL NORMAL	METATARSAL SHEAR	METATARSAL NORMAL	METATARSAL SHEAR
Right	0.9695	0.9774	0.993	0.9725
Left	0.8559	0.8028	0.9919	0.9952
	PHALANX NORMAL	PHALANX SHEAR	PHALANX NORMAL	PHALANX SHEAR
Right	0.9861	0.793	0.9934	0.9842
Left	0.9916	0.9851	0.9868	0.9904

Table 6-3 Between days correlation for the soft tissue trials

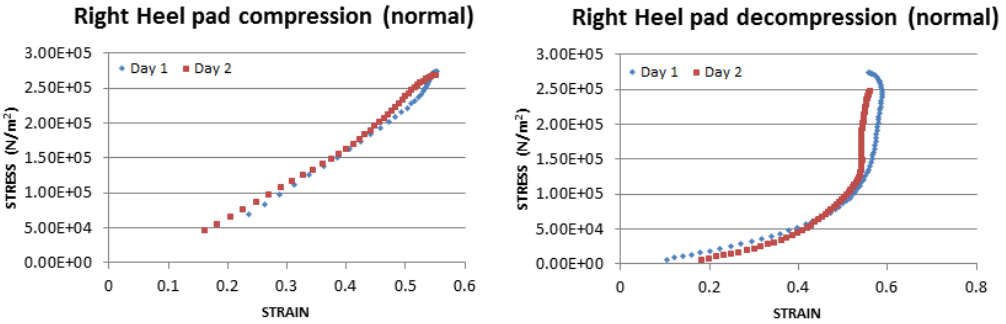

Figure 6-11 Repeatability analysis for the right heel pad (normal)

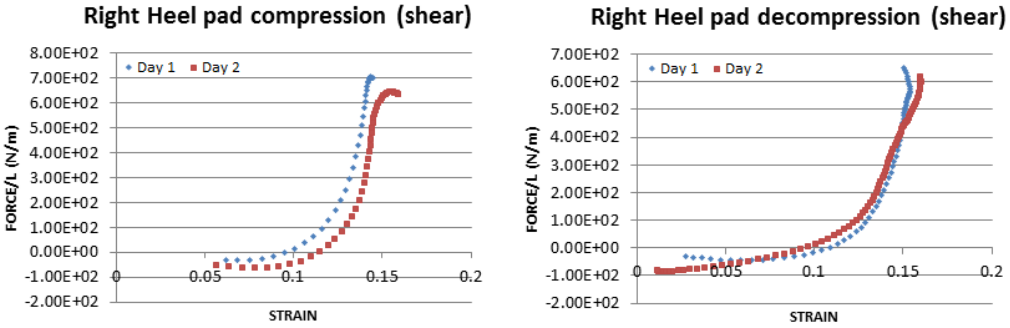

Figure 6-12 Repeatability analysis for the right heel pad (shear)

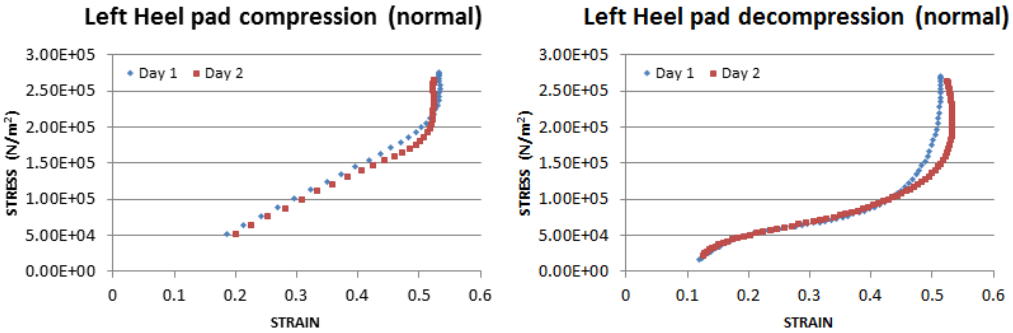

Figure 6-13 Repeatability analysis for the left heel pad (normal)

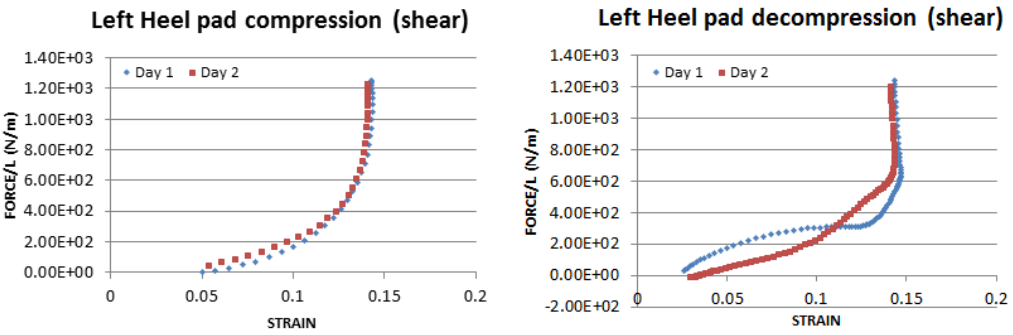

Figure 6-14 Repeatability analysis for the left heel pad (shear)

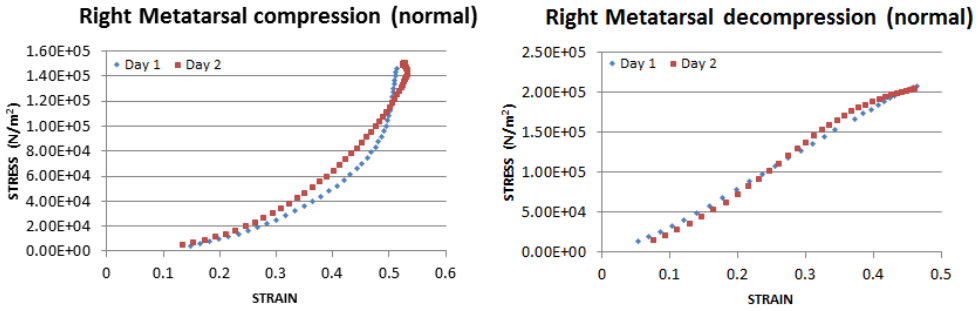

Figure 6-15 Repeatability analysis for the right metatarsal (normal)

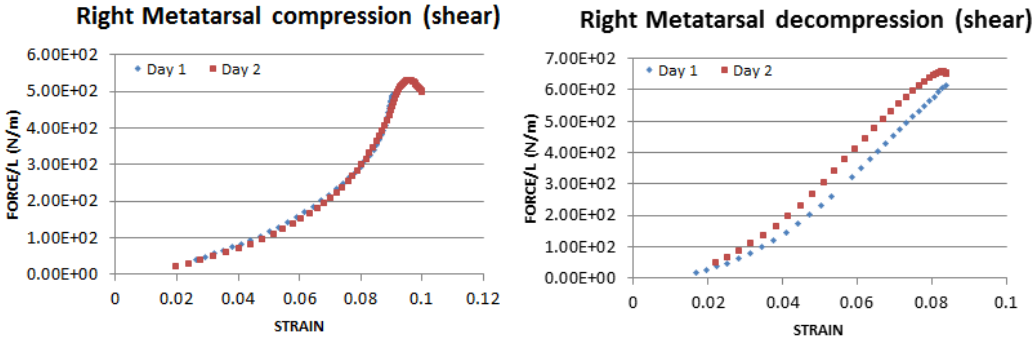

Figure 6-16 Repeatability analysis for the right metatarsal (shear)

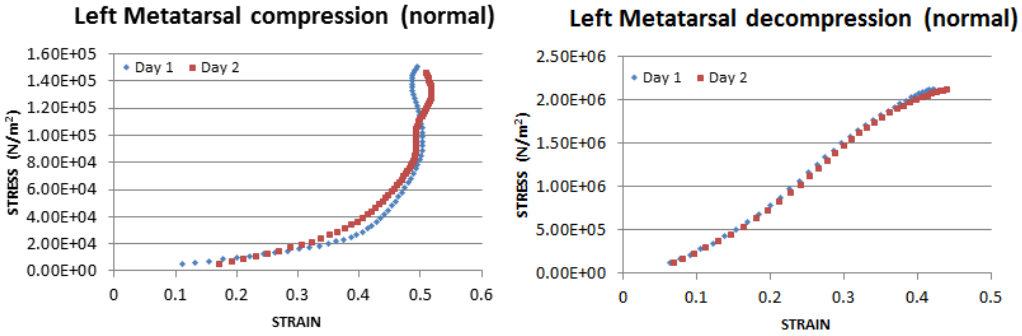

Figure 6-17 Repeatability analysis for the left metatarsal (normal)

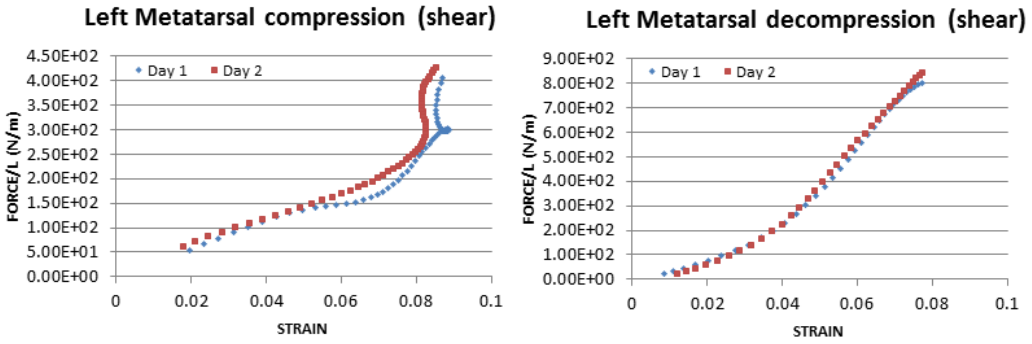

Figure 6-18 Repeatability analysis for the left metatarsal (shear)

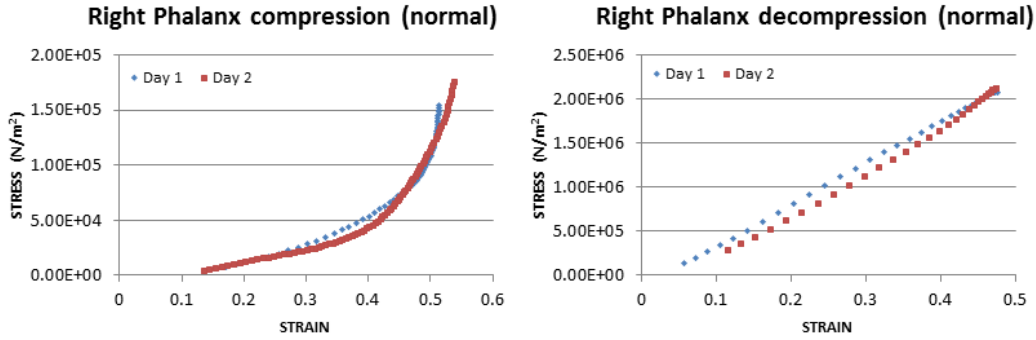

Figure 6-19 Repeatability analysis for the right phalanx (normal)

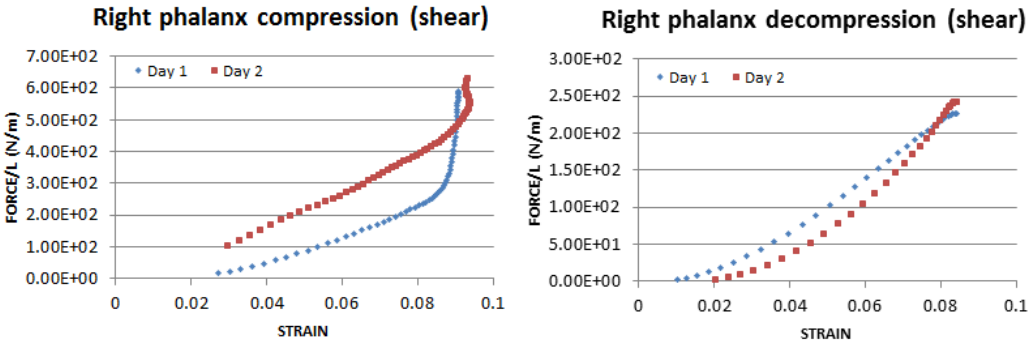

Figure 6-20 Repeatability analysis for the right phalanx (shear)

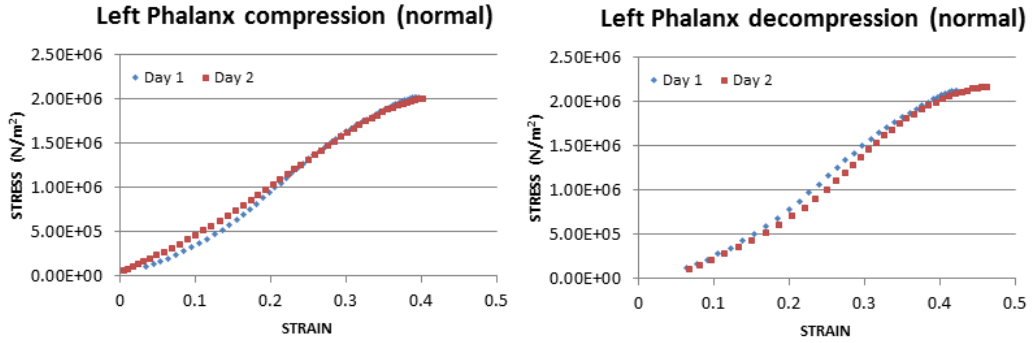

Figure 6-21 Repeatability analysis for the left phalanx (normal)

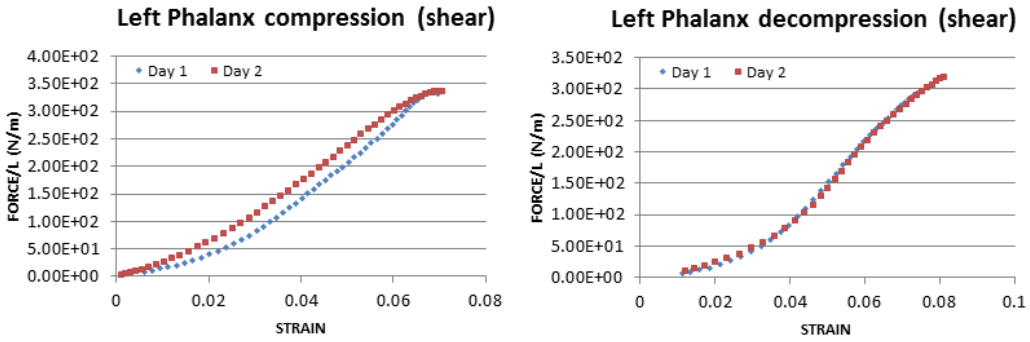

Figure 6-22 Repeatability analysis for the left phalanx (shear)

6.3 Model parameterisation and validation

The model was parameterised on a per subject basis using a least squares method. In each part of the study, ten trials were acquired. Given that the model is velocity dependant, trials with the same impact velocity were chosen for parameterisation purposes. The number of trials used varied from subject to subject, with two being the fewest and seven being the most. One more unused trial was selected, in order to compare it with the simulated data post fitting for validation purposes.

Heel pad parameters are presented in compression and decompression, whereas when analysing the rest of the trials, it was noticed that the two types of trials performed for metatarsals and hallux characterisation (walking forwards and backwards), produced very similar results. Comparable values were found for normal and shear stresses in almost all of the cases throughout the two phases, and therefore only one elastic and one viscous parameter are used for the whole cycle, which is the average of ones corresponding to the ascending and descending parts of the curve. It is important to highlight that the soft tissue was considered to be homogeneous and isotropic in the three studied areas. Parameters for the right foot are displayed in tables 6-4, 6-5 and 6-6 and graphs assessing validity between measured and simulated data are here displayed for two subjects in figures 6-23 and 6-24. Validation graphs for the rest of the subjects can be found in appendix H.

	NORMAL STRESS				SHEAR STRESS			
SUBJECT 1	E	η	R_f^2	R_v^2	E	η	R_f^2	R_v^2
Heel pad (compression)	574.8±6.326	89.06±5.188	0.9448	0.9945	6.146±0.085	11.09±0.275	0.9541	0.9702
Heel pad (decompression)	589.2±16.5306	261.7±20.459	0.8702	0.9533	6.119±0.191	21.84±1.03	0.9128	0.9202
Metatarsals	266.4±7.244	47.37±6.234	0.9154	0.9201	7.275±0.156	6.588±0.836	0.8509	0.7613
Hallux	550.8±0.156	17.18±0.836	0.9432	0.9773	0.8766±0.059	0.01±0.006	0.7703	0.902
SUBJECT 2	E	η	R_f^2	R_v^2	E	η	R_f^2	R_v^2
Heel pad (compression)	619.6±10.102	77.65±7.342	0.9172	0.9945	6.73±0.283	7.809±0.783	0.9274	0.9632
Heel pad (decompression)	600.9±9.081	261.4±17.38	0.8726	0.9003	7.139±0.305	18.3±1.897	0.829	0.8306
Metatarsals	314.9±1.53	79.68±2.316	0.9885	0.9882	1.685±0.098	14.45±0.734	0.8601	0.86
Hallux	699.2±41.938	66.3±17.397	0.9765	0.9835	5.431±0.133	10.49±0.381	0.9922	0.99
SUBJECT 3	E	η	R_f^2	R_v^2	E	η	R_f^2	R_v^2
Heel pad (compression)	513.6±6.4285	29.79±4.561	0.9139	0.9645	7.347±0.0780	7.563±0.1683	0.9826	0.9745
Heel pad (decompression)	507.5±7.806	220.2±10.102	0.8674	0.9915	7.106±0.104	8.496±0.411	0.9276	0.965
Metatarsals	369.5±8.3673	48.48±4.755	0.9001	0.8208	5.381±0.162	4.536±0.590	0.8323	0.847
Hallux	1744±95.408	145.2±22.551	0.852	0.865	2.284±0.141	0.2141±0.031	0.8293	0.988
SUBJECT 4	E	η	R_f^2	R_v^2	E	η	R_f^2	R_v^2
Heel pad (compression)	553.2±12.04	82.65±9.107	0.8315	0.8358	1.83±0.087	6.436±0.272	0.9291	0.9244
Heel pad (decompression)	531±5.714	199.3±7.448	0.9125	0.8923	3.905±0.189	23.21±0.989	0.8576	0.9322
Metatarsals	332.9±12.448	72.02±8.224	0.8795	0.9575	4.75±0.194	7.639±0.893	0.8655	0.9502
Hallux	645.5±45.612	2.865±1.22	0.9169	0.9816	0.1729±0.109	0.2726±0.053	0.8036	0.9723
SUBJECT 5	E	η	R_f^2	R_v^2	E	η	R_f^2	R_v^2
Heel pad (compression)	755.2±11.581	87.27±9.198	0.9255	0.9845	4.574±0.226	8.413±617.346	0.831	0.984
Heel pad (decompression)	464.2±8.265	196±8.112	0.9151	0.9856	2.368±0.0311	3.247±103.571	0.9505	0.9754
Metatarsals	400.1±8.469	70.08±4.857	0.9572	0.9881	4.994±0.13	5.639±496.938	0.9331	0.9882
Hallux	562.4±37.346	47.38±13.096	0.9759	0.951	2.984±0.448	0.2755±0.432	0.6712	0.9924

Table 6-4 Stiffness (E) and viscosity (η) parameters for soft tissue modelling (subjects 1 to 5)

R_f^2 and R_v^2 are fitting and validation correlations respectively. Note that for normal curves, the strain displayed is the modulus of the strain (which negative in compression). E and η are expressed in kN/m^2 for normal forces and in kN/m for shear forces.

	NORMAL STRESS				SHEAR STRESS			
SUBJECT 6	E	η	R_f^2	R_v^2	E	η	R_f^2	R_v^2
Heel pad (compression)	580.1±23.265	86.1±17.301	0.8677	0.9425	6.47±0.183	4.247±0.494	0.9253	0.9531
Heel pad (decompression)	542.6±11.122	123.2±8.673	0.9598	0.95	6.378±0.108	1.274±0.303	0.9635	0.9751
Metatarsals	225.1±5.357	27.87±2.612	0.8663	0.9057	4.029±0.173	6.051±0.56	0.8586	0.8535
Hallux	764.8±39.795	56.6±8.877	0.9624	0.9881	1.649±0.246	0.663±0.139	0.9084	0.92
SUBJECT 7	E	η	R_f^2	R_v^2	E	η	R_f^2	R_v^2
Heel pad (compression)	726.4±6.836	104.2±7.653	0.9648	0.9763	7.973±0.337	12.54±1.535	0.7898	0.8585
Heel pad (decompression)	615.5±10.510	314.9±17.193	0.8666	0.9036	6.627±0.219	30.13±1.301	0.9112	0.9116
Metatarsals	266.9±8.316	43.18±6.066	0.8099	0.9789	3.932±0.122	6.826±0.484	0.9269	0.9275
Hallux	716±36.683	76.56±17.954	0.8653	0.8346	1.876±0.107	0.7796±0.111	0.9176	0.9254
SUBJECT 8	E	η	R_f^2	R_v^2	E	η	R_f^2	R_v^2
Heel pad (compression)	562.7±10.918	90.08±8.071	0.8961	0.9482	8.973±0.046	9.649±0.136	0.9986	0.9366
Heel pad (decompression)	558.1±8.826	177.4±8.775	0.9418	0.9574	6.267±0.07	1.25±0.227	0.9838	0.9236
Metatarsals	380.7±4.489	139.8±5.765	0.9829	0.9832	4.122±0.05	24.93±0.52	0.9864	0.9865
Hallux	1117±72.448	119±31.872	0.8779	0.9086	2.156±0.201	0.3676±0.0748	0.8682	0.8327
SUBJECT 9	E	η	R_f^2	R_v^2	E	η	R_f^2	R_v^2
Heel pad (compression)	761±6.377	92.72±6.265	0.9781	0.995	7.015±0.22	15.19±0.663	0.9514	0.9515
Heel pad (decompression)	745.5±15.408	312.5±28.979	0.8696	0.854	3.999±0.12	7.389±0.553	0.8204	0.8217
Metatarsals	355.4±5.816	97.09±7.403	0.9058	0.9294	6.075±0.136	24.35±1.142	0.882	0.9129
Hallux	1199±77.04	344.5±70	0.9176	0.9258	32.35±2.596	5.643±4.287	0.7898	0.8728
SUBJECT 10	E	η	R_f^2	R_v^2	E	η	R_f^2	R_v^2
Heel pad (compression)	600.1±2.653	11.28±1.365	0.9973	0.9971	4.574±0.079	5.483±0.158	0.9909	0.9916
Heel pad (decompression)	631.5±11.071	187.8±12.908	0.9215	0.9881	7.905±0.096	1.264±0.362	0.9829	0.9928
Metatarsals	274.6±3.367	46.66±2.897	0.9498	0.973	0.227±0.057	4.339±0.305	0.794	0.7984
Hallux	2311±85.714	376.5±47.142	0.9324	0.9794	2.605±0.24	2.76±0.307	0.9198	0.9298

Table 6-5 Stiffness (E) and viscosity (η) parameters for soft tissue modelling (subjects 6 to 10)

R_f^2 and R_v^2 are fitting and validation correlations respectively. Note that for normal curves, the strain displayed is the modulus of the strain (which negative in compression). E and η are expressed in kN/m^2 for normal forces and in kN/m for shear forces.

	NORMAL STRESS				SHEAR STRESS			
SUBJECT 11	E	η	R_f^2	R_v^2	E	η	R_f^2	R_v^2
Heel pad (compression)	751.5±15	185.1±14.948	0.8995	0.9967	15.03±0.285	26.73±1.091	0.9473	0.9707
Heel pad (decompression)	613.2±10.459	193.6±14.693	0.8274	0.9989	12.71±0.229	26.17±1.311	0.9455	0.9455
Metatarsals	326±10	68.1±6.178	0.8935	0.9135	2.792±0.087	3.299±0.352	0.874	0.8805
Hallux	1060±51.530	118.8±20.571	0.9439	0.9524	2.126±0.203	0.888±0.128	0.8938	0.8944
SUBJECT 12	E	η	R_f^2	R_v^2	E	η	R_f^2	R_v^2
Heel pad (compression)	623.5±14.591	161.8±19.948	0.8613	0.9643	3.507±0.206	9.757±0.904	0.7887	0.7816
Heel pad (decompression)	536.4±9.387	180.9±8.928	0.9082	0.9884	3.267±0.069	8.238±0.268	0.929	0.9502
Metatarsals	378.8±5.357	76.46±3.688	0.9433	0.9793	3.169±0.131	5.888±0.456	0.8368	0.9073
Hallux	935.5±53.826	42.1±10.403	0.949	0.9642	2.045±0.137	0.012±0.011	0.8685	0.942
SUBJECT 13	E	η	R_f^2	R_v^2	E	η	R_f^2	R_v^2
Heel pad (compression)	552.2±5.765	27.34±2.602	0.9371	0.9617	7.942±0.143	4.475±0.227	0.915	0.9947
Heel pad (decompression)	508.5±6.938	125.4±6.53	0.9416	0.9544	6.764±0.13	9.245±0.426	0.922	0.9847
Metatarsals	273.6±3.3673	67.78±2.545	0.9763	0.973	6.227±0.217	8.187±0.654	0.9337	0.9853
Hallux	2261±55.102	171.9±19.846	0.9719	0.973	6.734±0.196	0.7468±0.0895	0.9619	0.9636
SUBJECT 14	E	η	R_f^2	R_v^2	E	η	R_f^2	R_v^2
Heel pad (compression)	590.8±6.989	31.94±3.433	0.9225	0.9229	5.077±0.097	2.701±0.164	0.9215	0.9304
Heel pad (decompression)	615.1±11.428	138.9±10.51	0.9001	0.9496	5.183±0.044	2.592±0.102	0.9698	0.9962
Metatarsals	304.6±6.479	63.12±4.551	0.8781	0.9605	2.233±0.0612	1.187±0.2915	0.8171	0.8264
Hallux	1748±63.775	457.1±52.04	0.9893	0.9478	3.624±0.245	4.896±0.352	0.9255	0.9285
SUBJECT 15	E	η	R_f^2	R_v^2	E	η	R_f^2	R_v^2
Heel pad (compression)	628.8±10.102	26.67±5.602	0.9743	0.9923	4.432±0.222	8.057±0.531	0.818	0.9811
Heel pad (decompression)	670.9±10.816	264±15.714	0.8955	0.8711	4.562±0.141	19.95±0.989	0.9303	0.9312
Metatarsals	257.8±5.51	35.97±2.627	0.8721	0.9787	3.832±0.118	0.7264±0.322	0.8542	0.8979
Hallux	1400±107.142	43.5±18.373	0.8953	0.9395	2.617±0.177	0.407±0.059	0.9402	0.9416

Table 6-6 Stiffness (E) and viscosity (η) parameters for soft tissue modelling (subjects 11 to 15)

R_f^2 and R_v^2 are fitting and validation correlations respectively. Note that for normal curves, the strain displayed is the modulus of the strain (which negative in compression). E and η are expressed in kN/m^2 for normal forces and in kN/m for shear forces.

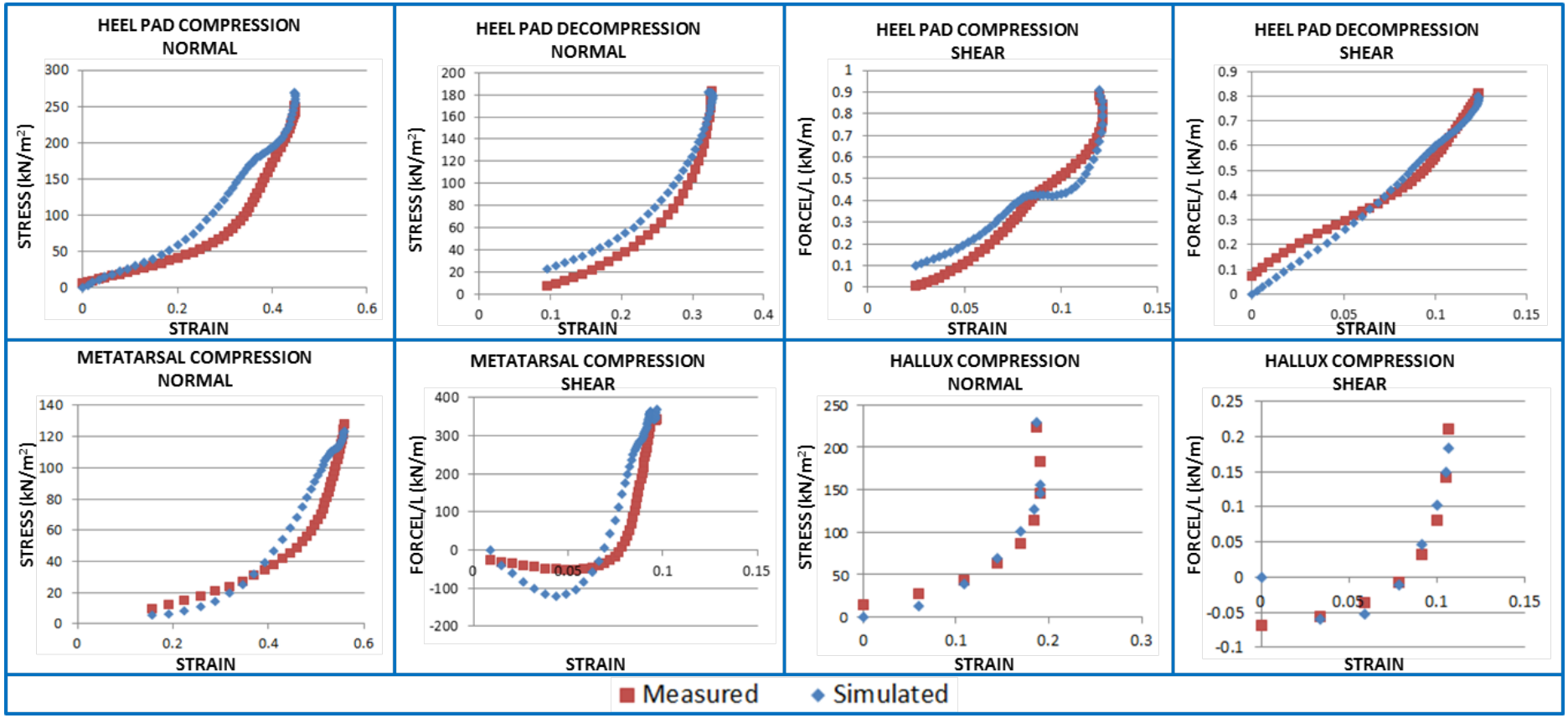

Note: For heel pad characterisation, 3 trials were used, 3 for metatarsal area and 2 for hallux.

Figure 6-23 Soft tissue model validation - subject 6: measured (red) and simulated (blue) stress-strain curves

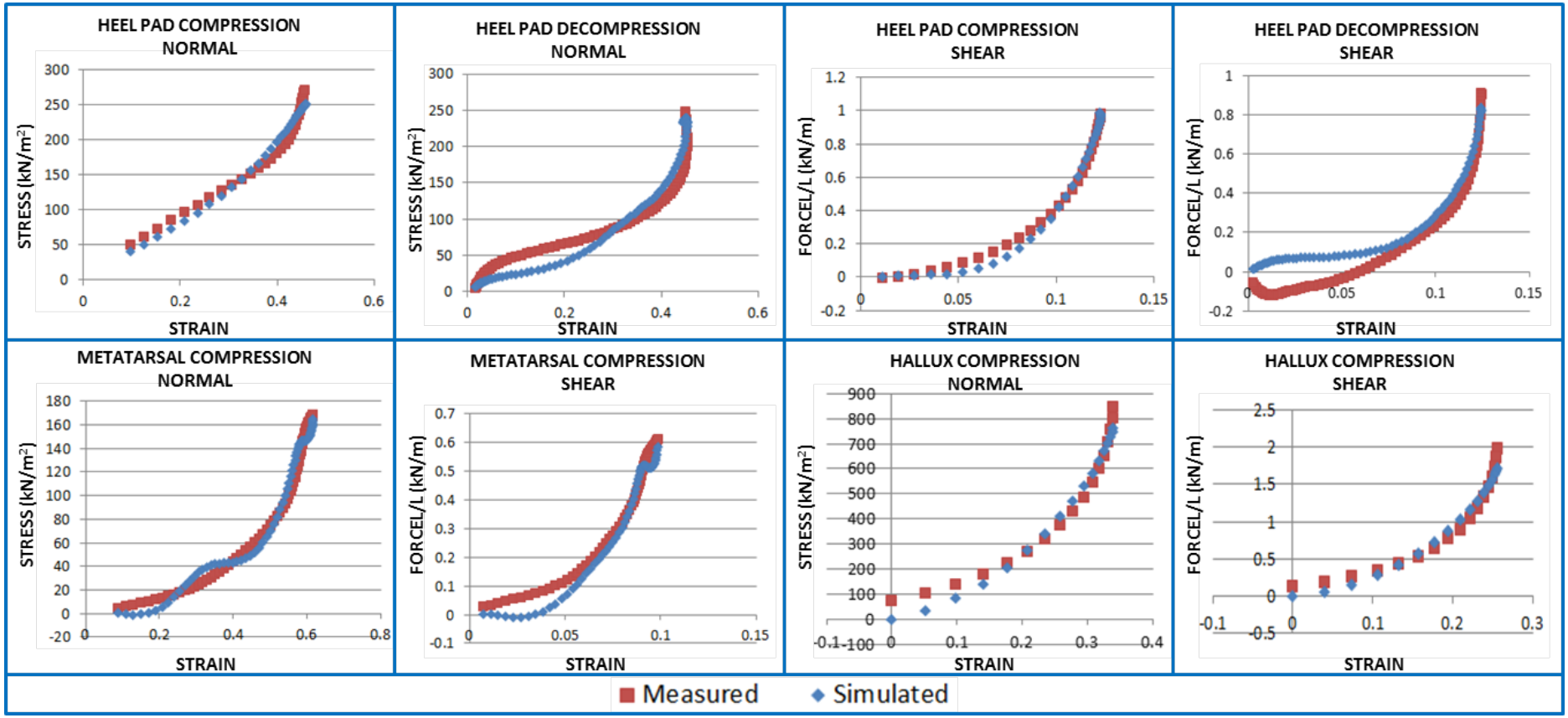

Note: For heel pad characterisation, 7 trials were used, 3 for metatarsal area and 2 for hallux.

Figure 6-24 Soft tissue model validation - subject 13: measured (red) and simulated (blue) stress-strain curves

6.4 Discussion

As can be seen from the tables 6-4, 6-5 and 6-6, the elastic modulus is very similar between compression and decompression, falling into each interval of confidence in most of the cases. This suggests the possibility of using only one elastic modulus for both compression and decompression. An appreciable difference however can be found in the viscous element. In some of the subjects, there was an increase in damping when decompressing while in other subjects this was the other way around. An inspection of the different stress-strain curves shows the reaction for each soft tissue. Characteristic curves for heel pad normal stress-strain are shown in figure 6-25, where each number corresponds to the participating subject.

Subjects with thinner soft tissue demonstrated an increased elastic modulus and a loop in the hysteresis due to the accommodation of tissue. On the other hand, subjects with thicker soft tissue exhibited two different types of behaviour, either the soft tissue restored rapidly to the original thickness (thus giving a lower damping coefficient for decompression) or the soft tissue recovered slowly, throwing a bigger damping coefficient. This last case was the clearest seen across the subjects. Moreover, in this type of stress-strain curve the area enclosed by the compression and decompression curves is the smallest, thus demonstrating lower energy dissipation.

It can be commonly found in the literature (see, for example, Alcantara et al. [2002]), that the ascending part of the curve divides into two parts. In the beginning there is a high elastic modulus allowing the strain to increase at a small strain rate. In the second part or the curve the stiffness increases rapidly until reaching maximum stress. Studies referring to this type of curve provide soft tissue models and parameters fitted from trials performed with diverse devices as explained in the introduction. This type of behaviour could be found in the submetatarsal tissue and under the hallux. However the curves corresponding to heel pad strain and exhibited in figure 6-25 differ slightly from those obtained in ballistic pendulum experiments, for example, but are in very good agreement to those obtained during normal gait (see, for example, Wearing et al. [2009]).

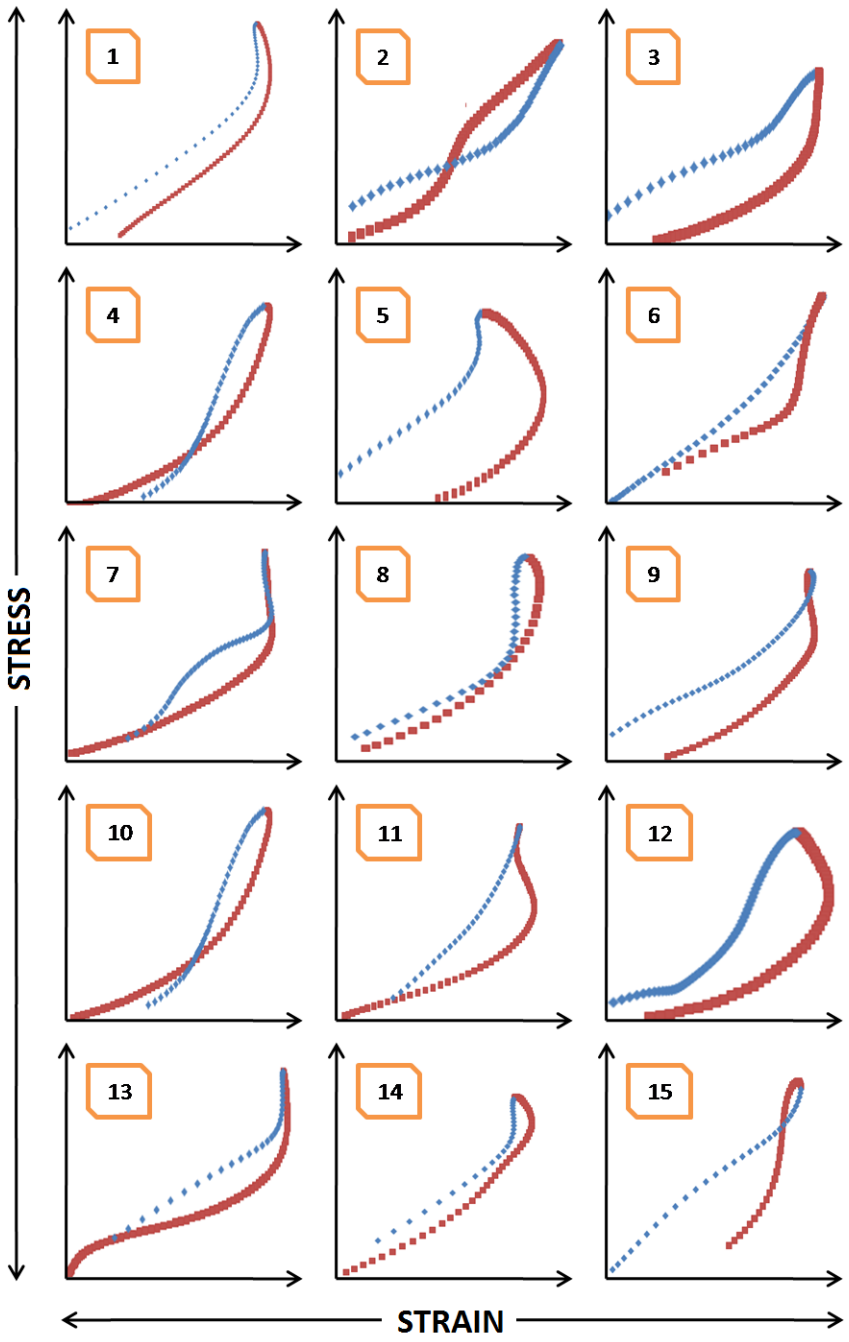

Figure 6-25 Different Stress-Strain curves to characterise tissue, per subject. Blue path corresponds to loading phase and red one to unloading phase.

Other reviewed studies adopted only one elastic modulus and viscosity for the whole cycle (see, for example Gefen et al. [2001]). In some cases, this will still provide a very good fit, but with lower stiffness and damping values. A separate analysis on compression and decompression of the tissue, however, can provide a better insight of the topic and minimise the error between simulated and measured

data. An example showing this issue is provided in figure 6-26. For the same subject and using the same trials, parameters were first found by dividing the data into compression and decompression phases (fit 2 in green) and then for the whole cycle (fit 1 in red). The set of parameters for each case can be found in table 6-7.

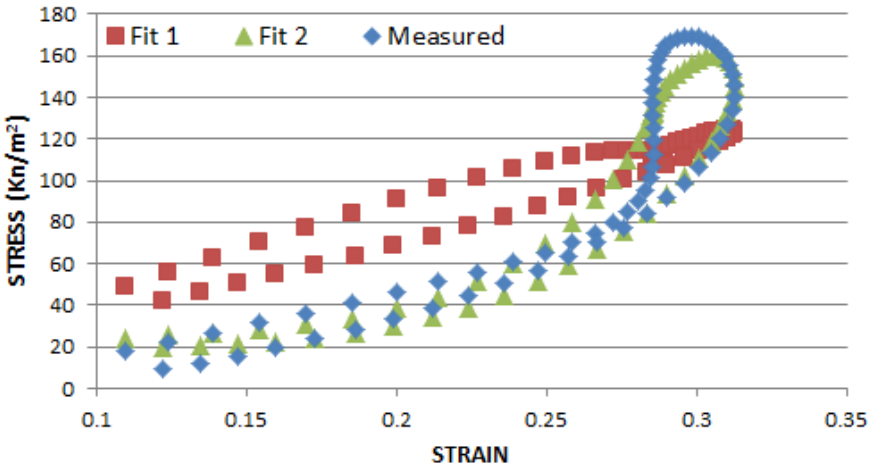

Figure 6-26 Stress-Strain curves for measured data (blue), fitting with unique values for the whole cycle (red) and fitting with different values for compression and decompression (green)

FITTING	E	η	R^2	RMSE
Fit 1	394.1±16.479	19.83±13.011	0.5805	34.03
Fit 2 (compression)	493.9±18.826	101.6±14.897	0.8289	21.06
Fit 2 (decompression)	465.2±4.489	123.7±3.52	0.9911	5.25

Table 6-7 Correlation and RMSE values for two types of fitting for the stress-strain curve: fit 1 for the whole curve and fit 2 diving the data into ascending and descending parts of the curve.

As expected, due to its shock absorption properties, the heel pad proved to be very elastic. It was also noticed that there was no significant difference in the deformation or in the stress between left and right feet for each subject. The soft tissue under the hallux, on the other hand, is the least elastic tissue. Due to the short contact time and small area of the first phalanx, the number of data points used in order to characterise its soft tissue behaviour was smaller in comparison with the rest of the foot. Small shear forces are found in subjects with very thin tissue (for example subjects 2 and 10).

Comparing the parameters obtained with those in the literature, it can be observed that those found here are slightly higher. Gefen et al. [2001] found an elastic modulus of 175kPa and a viscosity of 22kPa. However this study only analysed two subjects and one parameter for the whole strain-stress curve. Scott and Winter [1993] found parameters comparable with the ones presented in this thesis using the curves obtained from the tables in Valiant [1984].

6.5 Conclusion

The plantar soft tissue is a highly compressive tissue, capable of attenuating impact forces and restoring its shape when offloaded. In order to characterise its behaviour it is necessary first to study physical parameters and compressibility. Previous studies reported results on the heel pad when performing in vivo testing, or for different parts of the foot if using cadavers. However, there are very few studies that analyse soft tissue behaviour under gait conditions. The proposed method for soft tissue modelling proved to be repeatable and validated. It is a non-invasive protocol that provides a new approach towards plantar thickness analysis during gait, thus allowing the study of the deformation of the tissue while bearing weight which is of high interest, in particular, with regard to the diabetic foot. The model provides parameters for elasticity and viscosity of the soft tissue and allows therefore simulation of ground reaction forces (both normal and shear) on each studied area. This model, used in conjunction with an appropriate musculoskeletal model, provides a complete analysis of foot biomechanics and permits the study of both normal and altered gait.

7

Application to diabetic foot

Diabetes is a progressive disease which still represents a challenge for medical experts, and has a particularly harmful effect on the foot and ankle, producing changes in its function and structure. In this context, a clear understanding of the changes brought about by the disease in the foot biomechanics is essential to promote innovations in the orthopaedic industry and to improve the quality of life of the patients. The model in chapters 5 and 6 present a comprehensive analysis on both musculo-tendon and soft tissue parameters. This chapter presents results on model alterations in order to mimic different types of foot injuries aiming at improving the understanding of an altered gait in diabetes.

7.1 Introduction

The gait pattern is the result of the neuromuscular system and diverse structures working together. An abnormality at any part of the locomotion system will produce, inevitably, and altered gait. In chapters 5 and 6 normal gait was described by parameterising both muscle-tendon units and soft tissue. Knowledge of a normal gait is necessary in order to understand a pathological one. According to many authors (Boffeli et al. [2002], Edmonds and Watkins [1999] and Frykberg et al. [2006] for example), diabetic patients have an altered gait in terms of kinetics and kinematics thus affecting plantar pressure. These problems can be related to

peripheral neuropathy, foot deformites, foot trauma and increased plantar pressure [Van Schie et al., 2005]. Gait analysis studies for diabetic patients can vary greatly (in terms of samples, technologies used, data collection, for example), but they all agree that diabetic patients have also shown a decreased speed and an increased base of support (which is the distance between the feet measured from heel to heel) [Brach et al., 2008]. The gait pattern of diabetic patients who suffer neuropathy is modified to be more cautious, less efficient and variable. Diabetic patients also showed altered lower limb joint mechanics, with limited mobility at the ankle, subtalar and first metatarsal joints [Ledoux, 2007].

As previously explained in chapter 2, most of the injuries diabetic patients suffer in their feet are the result of a mechanical trauma that cannot be perceived due to neuropathy [Cavanagh, 1999], which reduces and can even inhibit the sensation of protection, causing changes in the foot structure and its functions [Sawacha et al., 2012]. In this context, increased plantar pressure plays an important role in the development of diabetic foot ulceration [Giacomozzi and Martelli, 2006]. There are several causes associated to high plantar pressure, such as foot deformities (e.g. charcot foot and hallux limitus), callus formation and fractures (e.g. Lisfranc joint injury).

In this chapter different types of injuries are simulated and results are obtained in terms of kinetics and kinematics. Different scenarios are also presented for soft tissue alteration, by modifying the model validated in chapter 6 and analysing what effect this modifications produces in plantar soft tissue. This experimental analysis allows an understanding of the altered foot biomechanics and gait in diabetic patients. In order to study changes brought about by diabetes, different bandages and comercially available hallux valgus supports were used to mimic different conditions (see figure 7-1). The main areas of study were the ankle and 1st metatarsophalangeal joint. Injuries on the ankle were simulated restricting its movement as shown in figure 7-1(left), one brace was placed in the medial side of the ankle and one on the lateral side. Hallux limitus was simulated by means of a hallux valgus support thus immobilising the great toe as shown in figure 7-1(right). Gait was analysed in terms of velocity, stance phase duration, joint angles, joint

moments and ground reaction force.

Figure 7-1 Orthosis used to mimic ankle (left) and metatarsophalangeal (right) joint injuries

Fifteen subjects were markered with Oxford Foot Model marker placement and instructed to walk at their own pace, stepping with the right foot on the forceplate (as orthotics were always placed on the preferred leg). Experiments were carried out at the University of Warwick Gait Laboratory[1] and written informed consent was obtained for the participating subjects. In this study, control subjects refer to the subjects walking normally (without any restriction), and ankle injury and hallux limitus to the simulated injuries in the ankle and great toe respectively. For each of the subjects, five trials consisting of at least one stance were averaged in each of the scenarios. Ankle injury and hallux limitus were not studied simultaneously, experiment was set up first as described in figure7-1(a) and then as figure 7-1(b).

7.1.1 Cadence, velocity and duration of stance phase

In the experiments performed, no difference was observed in terms of cadence, velocity and duration of stance phase in any of the three cases. Table 7-1 shows mean values and standard deviation for the whole sample.

	Velocity	**Cadence**	**Stance %**
Control Subjects	0.895±0.095	86.05±13.55	59.95±3.15
Ankle Injuries	0.92±0.12	85.45±12.95	59.55±2.75
Hallux Injuries	0.87±0.07	85.05±11.55	60.85±4.05

Table 7-1 Gait temporal space parameters for control subjects, ankle injured and hallux limitus. Velocity is in m/s, cadence in $steps/min$ and stance as a percentage of one gait cycle.

[1]The experiments comply with all data protection requirements as stated in the University of Warwick BSREC ethical approval: BSREC full approval REGO-2013-582 Foot Modelling

7.1.2 Joint mobility

The range of motion of a joint will depend on diverse intrinsic parameters of the person, such as age and sex. Diabetes can produce a decrease in this range for lower limb joints. Moreover, this reduction in joint movement has been suggested to be an important factor for increased plantar pressure, thus producing ulceration [Frykberg et al., 2006]. In this section, the effect of injuries in the ankle and hallux is studied in terms of hip, knee, ankle and 1st metatarsophalangeal joint mobility.

7.1.2.1 Ankle Injury

When ankle injury was simulated, subject demonstrated to have a lower range of dorsi-plantarflexion as expected (figure 7-2). It was also noticed that the mobility of both hip and knee were limited (figures 7-4 and 7-3). This trend was observed in all the subjects, with an average decrease of 25% in ankle dorsiflexion at peak stance (between 40%-60% of stance) and a decrease of more than 50% during swing phase. Knee extension was also reduced by 30% during swing phase, this could be the reaction of the body to maintain stability, compensating for the limited ankle joint mobility. Values for maximum and minimum angles for the participating subjects can be found in appendix I.

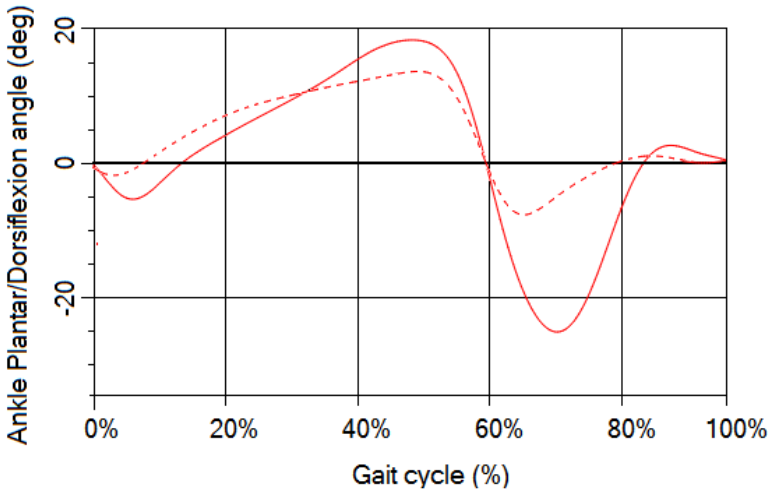

Figure 7-2 Ankle joint mobility assessment: Ankle joint motion for control subject (bold) and ankle injured (dotted)

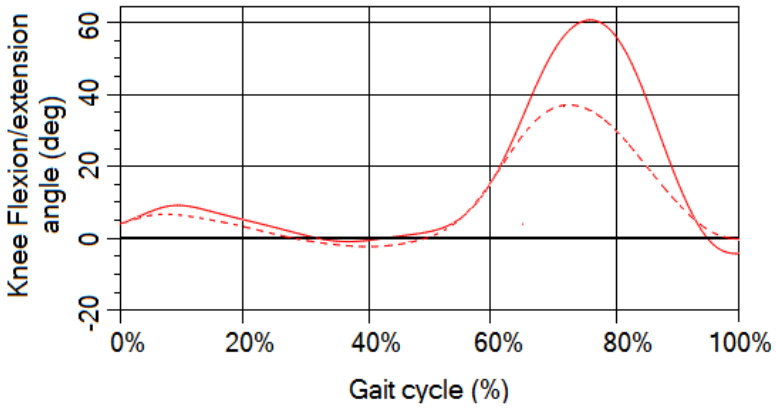

Figure 7-3 Knee joint mobility assessment: Knee joint motion for control subject (bold) and ankle injured (dotted)

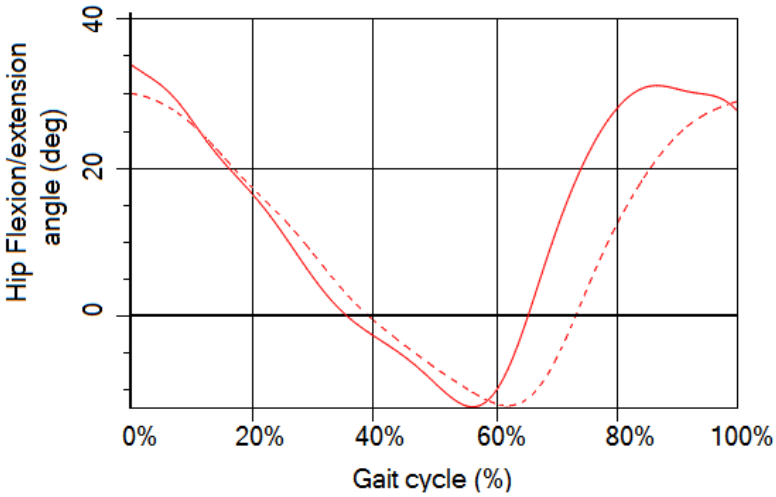

Figure 7-4 Hip joint mobility assessment: Hip joint motion for control subject (bold) and ankle injured (dotted)

7.1.2.2 Hallux Injury

Dorsiflexion and plantarflexion of the first metatarsophalangeal joint can also be affected by diabetes. This joint has an essential role during toe off, when the body weight moves forward the hallux thus dorsiflexing the joint and therefore the force acting on that joint is approximately the body weight [Van Schie et al., 2005]. If the joint movement is limited, a high peak pressure is found under the hallux during toe off [Cavanagh and Ulbretch, 2008] which can lead to ulceration. Figure 7-5 displays, the joint movement for one gait cycle, for one control subject (bold) and the hallux injury (dotted).

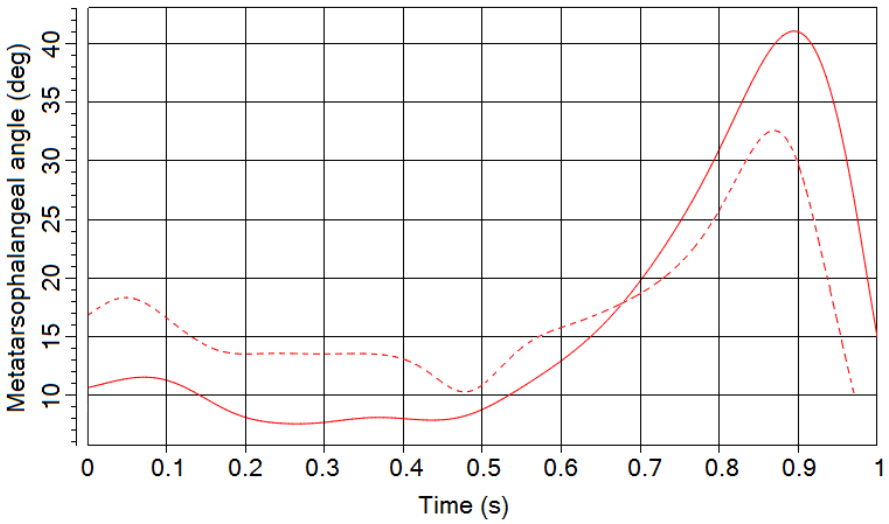

Figure 7-5 1st Metatarsophalangeal joint mobility assessment: 1st Metatarsophalangeal joint motion for control subject (bold) and ankle injured (dotted)

Further analysis can be performed if observing the plantar pressure map produced by both scenarions (see figure 7-6 and 7-7). By simple inspection of the distribution of the average values of peak forces (figure 7-6), it can be noticed how the hallux and first metatarsal heads (circled in black) are significantly more loaded for this type of injury than for control subjects. It can also be observed that the center of pressure moves forward, thus making the subject more prone to undergoing imbalance and instability issues.

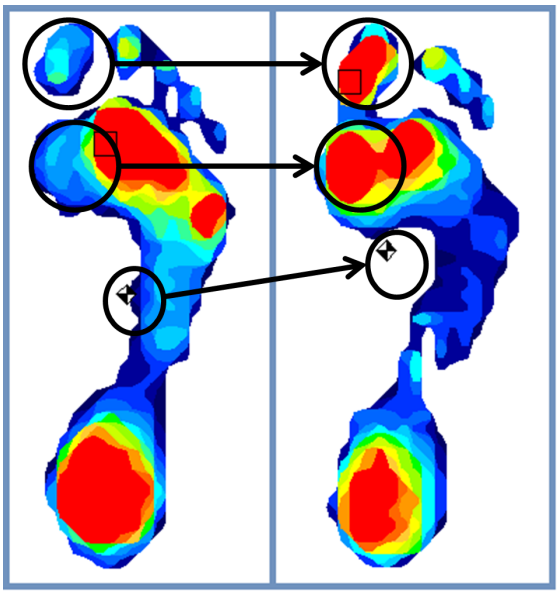

Figure 7-6 Plantar pressure assessment: Control subject (left) and Hallux injury (right) Peak/stance average map

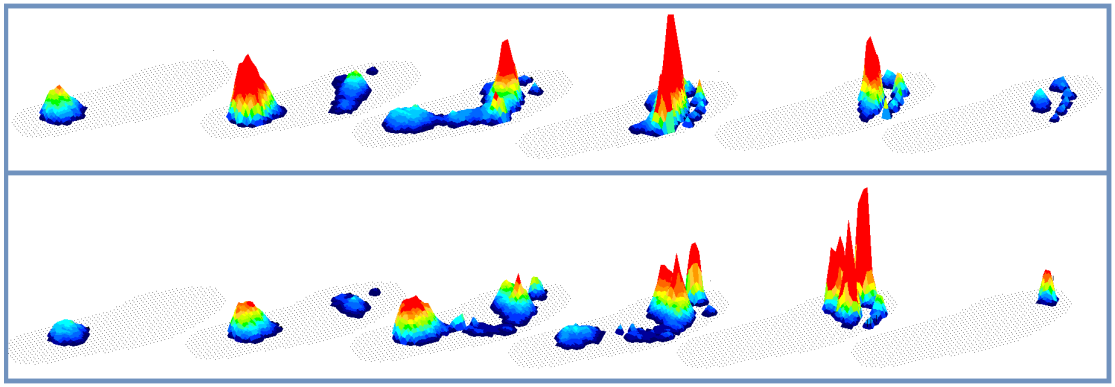

Figure 7-7 Plantar pressure assessment: Control subject (top) and Hallux injury (bottom) walking pressure maps

7.1.3 Ground Reaction force

In terms of ground reaction force, it was possible to study the forceplate results. Previous studies proved that there is a delay in the peak force and also an increased push off vertical force [Eils et al., 2004]. In their study, they simulated neuropathy by using ice immersion technique in 40 healthy subjects. They concluded that this simulation led to a more "cautious" gait, meaning that subjects walked at a lower speed than in normal conditions and therefore at a lower stride rate. In the present study, a very small difference was observed between both scenarios as can be seen from the diagram of the forceplate in figure 7-8. The magenta curve corresponds to vertical ground reaction force for the simulated injury and the yellow one for the control subject.

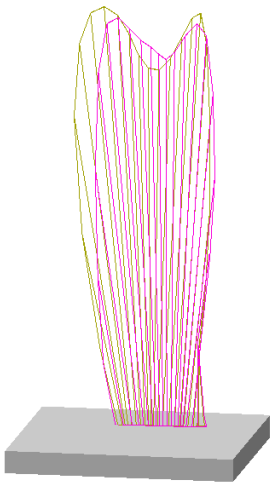

Figure 7-8 Ground reaction force assessment, magenta corresponding to ankle injury, and yellow to control subject

7.1.4 Joint Moment

Many authors have studied the effect of ankle injuries, finding a slighlty higher dorsiflexor moment (see for example, Cavanagh [1999]). Figure 7-9 depicts ankle moment for healthy subject (bold) and simulated ankle injury (dotted). Graphs are normalised to gait cycle, with the first 60% corresponding to stance phase. As it can be observed, there is a slightly incresed ankle moment in the second case. However, this was not the case for all of the subjects. While some presented an increased moment, most of them presented decreased one, in between 5% and 10%.

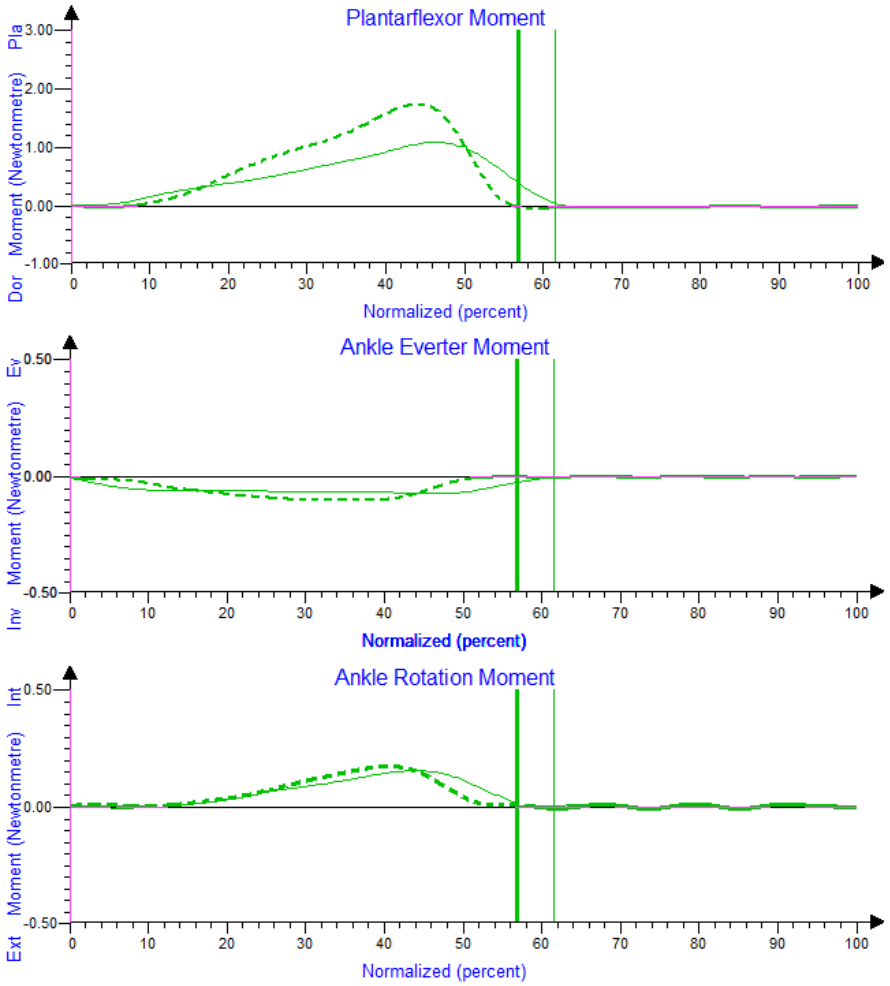

Figure 7-9 Joint moment assessment: Ankle moment in 3 planes for ankle injury (dotted) and control subject (bold). Moment normalised by bodymass.

7.2 Effect on soft tissue

It has been already reviewed from the literature, that diabetes can specifically change the mechanical behaviour of plantar soft tissue. Stiffer tissue will not be able to deal with the distribution of higher loads, and thus it is very probable to find areas of extremely high stresses (both normal and shear). This will ultimately lead to poor offloading of peak pressure areas and will produce ulcers and other biomechanical consequences. In order to study how diabetes can affect soft tissue, healthy soft tissue model (heel pad in this case) is analysed over four different scenarios. This allows a better understanding on the changes the disease can bring about and also on how foot ulcers might be prevented.

7.2.0.1 Thinner tissue

The plantar soft tissue exhibited by diabetic patients is much harder and thinner that the one of healthy subjects [Cavanagh and Ulbretch, 2008]. In order to simulate this condition, plantar thickness has been decreased by 10%, 20%, 30%, 40% and 50% (see figure 7-10). It can be observed that in the extreme scenario (50%), the tissue compresses more than 65%.

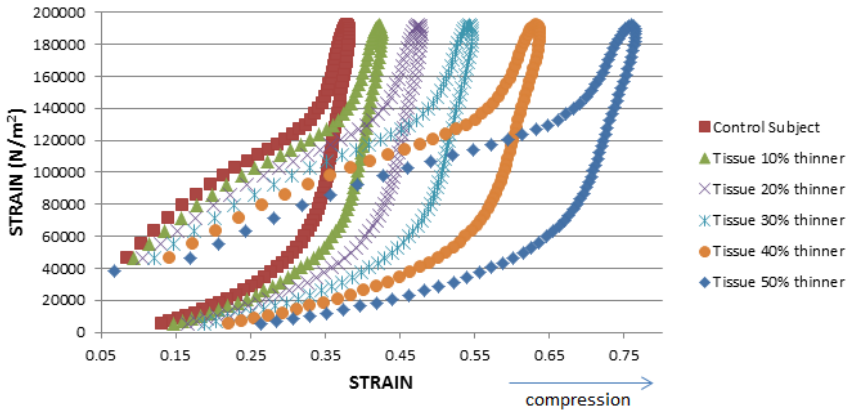

Figure 7-10 Effect of decreasing soft tissue thickness in stress-strain curves

7.2.0.2 Increased stiffness

In order to simulate this condition, stiffness values were increased by 10%, 20%, 30%, 40% and 50% (from 513.6kPa to 770.4kPa - see figure 7-11). Plantar soft tissue in diabetic patients proved to be stiffer, this is an important issue because less compliant tissue cannot distribute pressure in an appropriate way. Stiffer tissue will reach higher loads at the same strain rate, thus loading the region of interest up to 50% more.

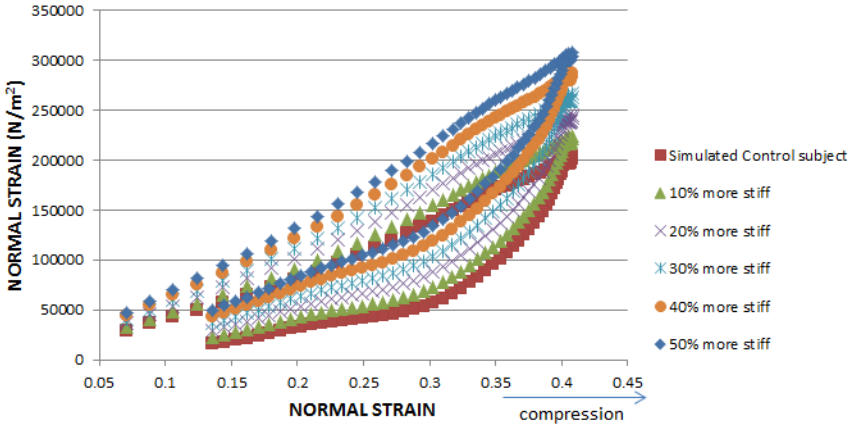

Figure 7-11 Effect of increasing soft tissue stiffness in stress-strain curves

7.2.0.3 Decreased area of force application

"Pressure is the critical quantity that determines de harm done by the force" [Brand, 1986]. The force itself does not say anything regarding how harmful it might be. It is necessary to understand that force in the area where it is applied (i.e. stress). If reducing the area, applying the same force, the pressure (stress) will rise. Stress will be here modified from normal and shear perspectives by 10%, 20%, 30%, 40% and 50% (see figures 7-12 and 7-13). The initial region of interest was a circumference of $0.0028m^2$ and a diameter of $0.059m$.

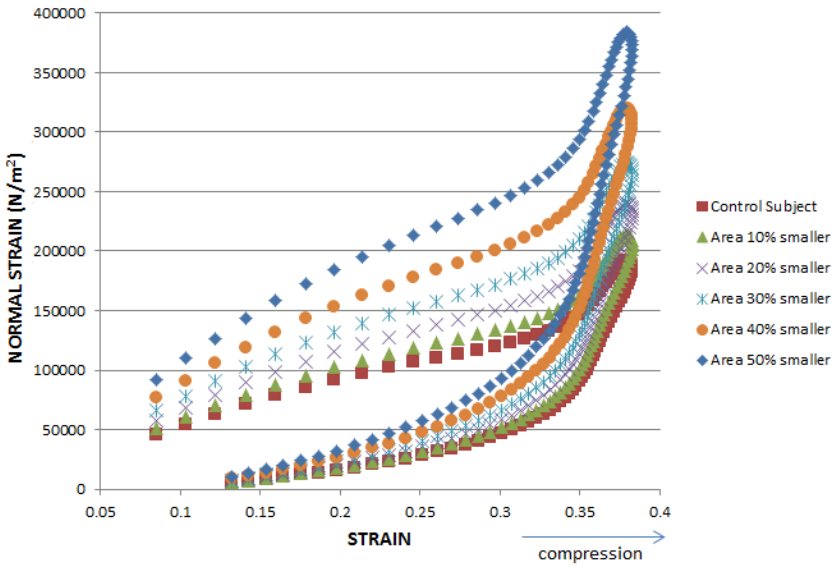

Figure 7-12 Effect of decreasing the area of application of force in normal stress-strain curves

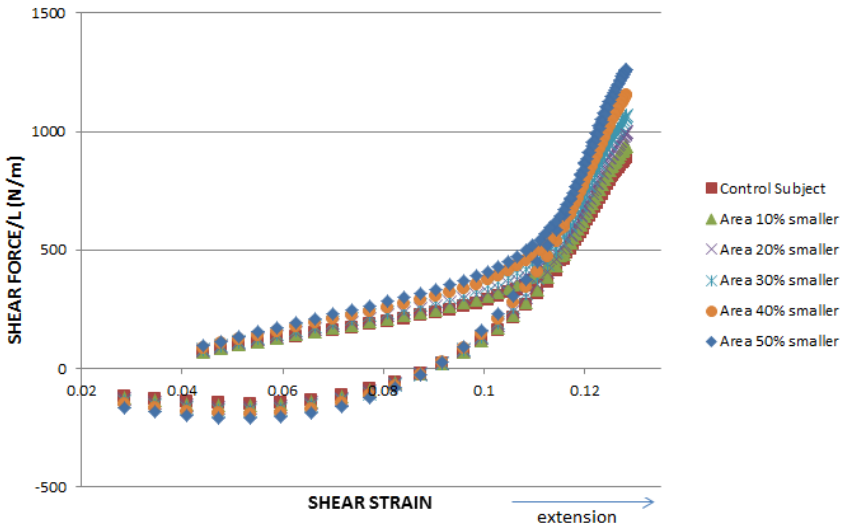

Figure 7-13 Effect of decreasing the area of application of force in shear stress-strain curves

7.2.0.4 Increased force

By increasing the force (and maintaining the area) we obtain a similar scenario as in the increased stress, given that the stress is the ration of the applied force over the area.

7.3 Discussion

Results on altered gait have already been discussed in previous sections. However it is important to highlight that a limited joint mobility implies also that the muscle-tendon units will not be stretching/lengthening efficiently. Figures 7-14 and 7-15 display muscle-tendon length (in percentage of natural length) over the gait cycle for one subject (with normal and altered gait). It can be observed that for the stance phase these values do not vary, however during swing phase, muscle-tendon units in altered gait cannot stretch nor extend in the same proportion as in a normal one. This same trend was confirmed across all the subjects.

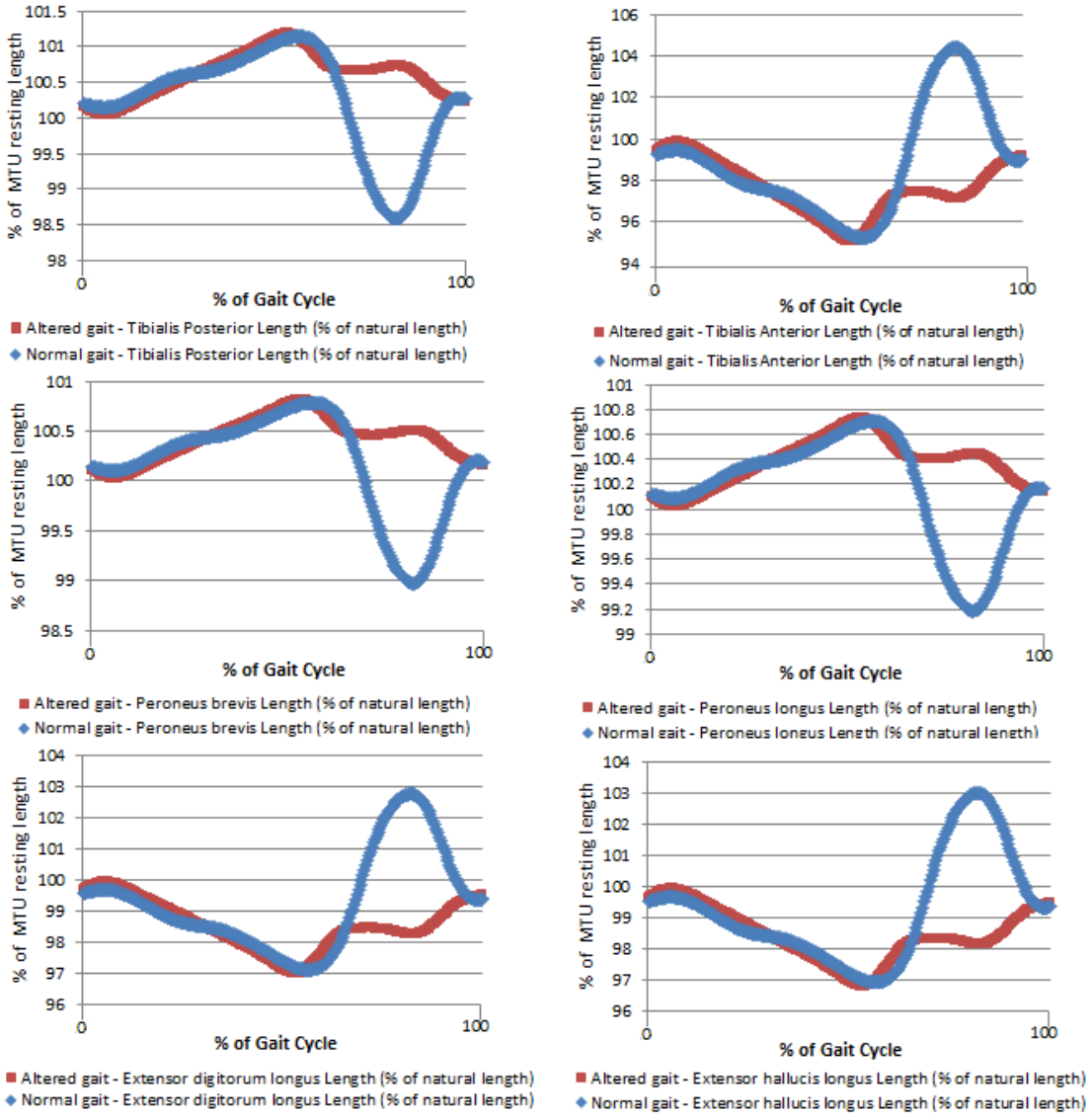

Figure 7-14 Effect of limited joint mobility on muscle-tendon length (I)

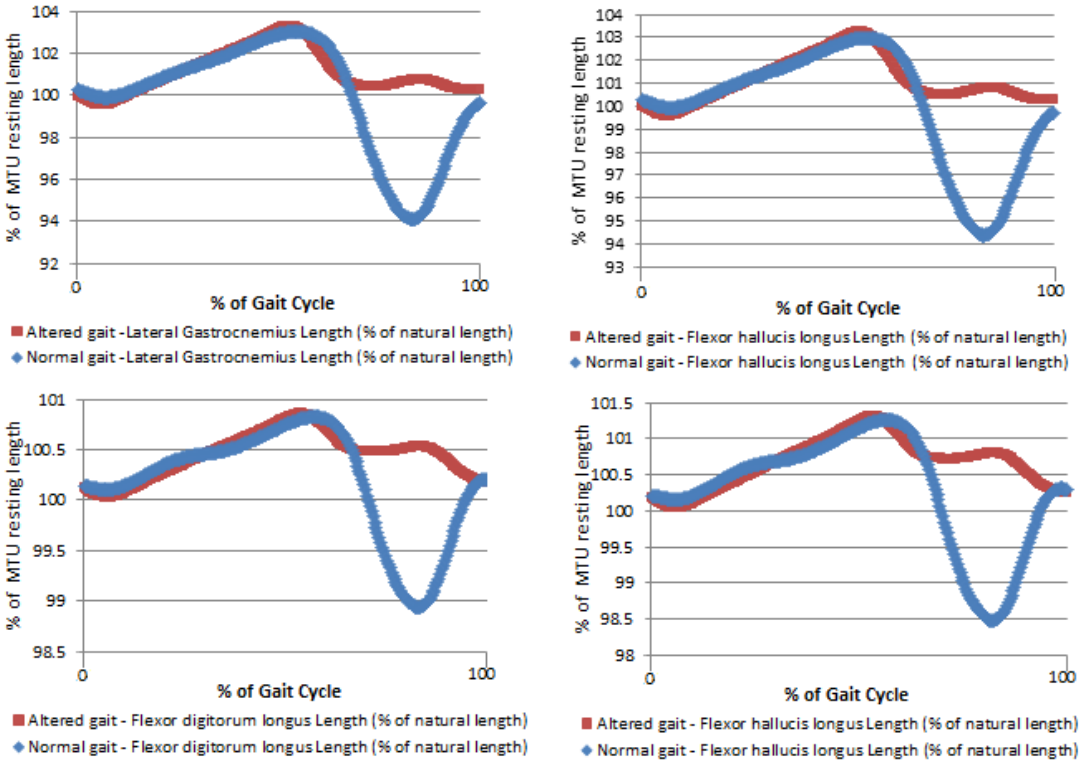

Figure 7-15 Effect of limited joint mobility on muscle-tendon length (II)

7.4 Conclusions

Knowledge of a healthy foot can improve our understanding of its biomechanical behaviour during walking. A simple alteration on the small structure that represents the foot can trigger an abnormality in any other part of the musculoskeletal system. In the previous chapters (5 and 6), a comprehensive analysis and modelling was performed on healthy foot which included muscle-tendon, joint mechanics and characterisation of the soft tissue behavoiur. In this chapter, altered gait in diabetes was studied from an experimental and modelling point of view, adapting the model to simulate different injuries that induce an altered gait. The same subjects from previous experiments (in chapters 5 and 6), participated in this study. Ankle and metatarsophalangeal joint injuries were studied in terms of gait temporal spatial parameters, joint mobility, joint moments and ground reaction force in order to obtain normative values for control subjects and subjects with

the aforementioned injuries. The fact that the same subject was tested under the three conditions made the study comparable intra-person and inter-session, which is advantageous. In general, samples for studies about diabetic foot consist of a group of control subject (non-diabetic), diabetic patients and diabetic patients who suffer neuropathy.

It was already reviewed in chapter 2 that the injuries diabetic patients suffer are commonly located in the ankle joint and 1st metatarsophalangeal joint. The experimental analysis proposed in section 7.1 potentially allows an understanding of the altered foot mechanics and gait in diabetic patients as it can mimic different conditions diabetic patients can normally suffer, by restricting movement of ankle and 1st metatarsophalangeal joints. It was possible to observe a clear pattern of decreased joint mobility across subjects; which is a crucial issue in diabetic patients given that it is associated with increased plantar pressure and an eventual ulceration. The results are consistent with previous studies with diabetic patients, which validates the methods used to simulate diabetic gait and allows for an understanding of altered gait in diabetes.

Regarding soft tissue, a modification of the model parameters can provide an insight of the degenerative process diabetes has on plantar soft tissue. It can predict plantar soft tissue behaviour under different scenarios, with data obtained from non-invasive experiments using plantar pressure measurement and motion capture. The model was modified in terms of plantar thickness, area where the force is applied and tissue stiffness. This adapted soft tissue model permits the study of different scenarios, and therefore represents a valuable tool for diabetic foot assessment.

8

Conclusions and future work

8.1 Conclusions

The main objective of the work described in this thesis is to develop musculoskeletal scaled models to enable an understanding of altered gait in diabetes. An innovative combination of gait, joint goniometry, plantar pressure analysis, and image processing with associated well validated parameterised models was presented in this thesis to overcome the constraints of past studies.

Throughout this research, different steps were taken towards the completion of a foot model that could replicate both normal and altered gait. First, a method was developed to reconcile barefoot and shod conditions for simultaneous gait and plantar pressure analysis as these two methodologies require different settings. In order to develop a meaningful musculoskeletal system, it was first necessary to obtain muscle-tendon parameters that are not directly measurable (i.e. muscle-tendon length and moment arm). Methods for measuring these intrinsic characteristics of muscles using motion capture were developed, tested and validated with magnetic resonance imaging (chapter 4). Another important parameter for muscle force production is the pennation angle, which was analysed using ultrasound. It was concluded that, for the studied muscles, this angle can be neglected as it causes a maximum error of 4% in the output force.

The Hill muscle model was used to explain the mechanical properties of the muscle

from a numerical and structural point of view (chapter 5). Thirteen muscles were included in the model, to control foot movement in the sagittal plane. Values for the stiffness and damping of the muscles and stiffness of the tendons were derived by optimising the moment around the joint of interest and estimating the parameters using least squares regression. Structural identifiability was also assessed, to test that all parameters in the model are identifiable. Tendons proved to be very stiff and not very compliant, and to have a small range of movement which allows the joints to be fixed in different angles. The estimated values fall in the range of the values found in the literature.

The second part of the model consists of the plantar soft tissue. Various models that display hysterestic curves were analysed to find the model that would best fit the viscoelastic behaviour. In chapter 6, plantar tissue was divided into the areas of peak pressure during stance and stiffness and damping parameters were found for each area, for normal and shear stresses. Through the analysis of the parameters, it was noticed that the elastic modulus is very similar during compression and decompression. However this was not the case for the viscosity. While subjects with thinner soft tissue exhibited an increased elastic modulus and reaccommodation of tissue, for subjects with thicker soft tissue either it restored rapidly to the original thickness (thus giving a lower damping coefficient for decompression) or the soft tissue recovered slowly, throwing a bigger damping coefficient.

The final aim of this research is to understand altered the gait in diabetes. In chapter 7, the healthy foot model is studied from an experimental and modelling perspective in order to mimic different injuries very common in diabetic patients. Experimental analysis was performed to study the effect of injuries in metatarsophalangeal and ankle joint, on joint's kinetics and kinematics. It was possible to observe a clear pattern of decreased joint mobility across subjects; which is a crucial issue in diabetic patients given that it is associated with increased plantar pressure and an eventual ulceration. The results are consistent with previous studies with diabetic patients, which validates the methods used to simulate diabetic gait and potentially allows an understanding of altered gait in diabetes. Subjects with injuries proved to have limited joint mobility and modified ankle moment. In

terms of soft tissue, alterations on healthy foot model can simulate the degenerative process produced by diabetes and therefore predict tissue response in different scenarios such as increased peak force and decreased area.

The models presented on this thesis proved to be reliable and to replicate the normal and altered gait. The analysis was always performed on a per-subject basis to obtain fitted parameters for each individual. Parameters for foot biomechanics, soft tissue behaviour and altered gait were obtained for the same subjects, thus making both models comparable. Previous studies on foot modelling, not only simplified the foot in terms of geometry, structure and geometry [Qiu et al., 2011], but most of them do not study the foot under gait conditions, which is of particular interest in diabetic patients. The musculoskeletal model, combined with the soft tissue model, provide a complete analysis of foot biomechanics which permits the study of both the normal and altered gait. Regarding soft tissue, a modification of the model parameters can provide an insight of the degenerative process diabetes has on plantar soft tissue. It can predict plantar soft tissue behaviour under different scenarios, with data obtained from non-invasive experiments using plantar pressure measurement and motion capture. The model was modified in terms of plantar thickness, area where the force is applied and tissue stiffness. This adapted soft tissue model allows the study of different scenarios, and therefore represents a valuable tool for diabetic foot assessment.

8.2 Future Work

In order to continue with the study of the altered gait in diabetes, the natural next step is to complete the same experiments but with diabetic population. The main issue with the current methods for clinical assessment of diabetic foot is that the increment in stress cannot be measured, but it is its consequence that will be ultimately seen (e.g. ulceration). If implementing this model to a diabetic population, through regular assessment, it would be possible to predict soft tissue failure, for example, under peak pressure areas before the ulceration appears.

Another avenue for future research is the difference in foot biomechanics across

subject with and without neuropathy. Because the sensory nerve system provides environmental information, neuropathic patients tend to have an altered gait not only because of joint or tissue alterations but also because they cannot feel the interaction with the ground. This has also great impact on muscle contraction and activation dynamics.

It would also be an important development if the proposed model could be tested in diabetic population with limb loss. This study could provide an insight on how kinematics and kinetics can be altered, given the high incidence of lower limb amputation in diabetic population.

In summary, diabetes presents a challenge for the medical community as well as for scientists and engineers. Current methods aim at finding a solution once harm is already done instead of predicting injuries. A combination of preventive strategies, patient education, and continuous assessment can contribute to an early diagnosis which is imperative in order to provide appropriate medical care, and in turn avoid amputation which is a high factor of morbidity.

References

ACFAS (2009). American College of Foot and Ankle Surgeons: Hallux Rigidus, Lisfranc injuries, Charcot foot. http://www.foothealthfacts.org/. Accessed: 25-06-2013.

Aerts, P., Ker, R., De Clercq, D., Ilsley, D., and Alexander, R. (1995). The mechanical properties of the human heel pad: A paradox resolved. *Journal of Biomechanics*, 28:1299–1308.

Alcantara, E., Forner, A., Ferrus, E., Garcia, A., and Ramiro, J. (2002). Influence of age, gender, and obesity on the mechanical properties of the heel pad under walking impact conditions. *Journal of Applied Biomechanics*, 18:345–356.

AMTI (2001). Force plates for gait analysis. http://www.amti.biz. Accessed: 15-04-2016.

Arnold, M. and Delp, S. (2011). Fibre operating lengths of human lower limb muscles during walking. *Philosophical Transactions of The Royal Society B Biological Sciences*, 366:1530–39.

Baker, R. (2011). Muscle length modelling software for Vicon users. https://wwrichard.net. Accessed: 30-09-2015.

Balint, G., Korda, J., Hangody, L., and Balint, P. (2003). Regional musculoskeletal conditions: foot and ankle disorders. *Best Practice & Research: Clinical Rheumatology*, 17:87–111.

Barlas, N., Ali, M., and Hussain, S. (2009). Lisfranc's dislocation and fracture in the Charcot Foot. *International Journal of Diabetes Mellitus*, 1:57–58.

Bartold, S. (2004). The plantar fascia as a source of pain – biomechanics, presentation and treatment. *Journal of Bodywork and Movement Therapies*, 8:214–226.

BB (2013). Boundless Biology: Types of Synovial Joints. https://www.boundless.com. Accessed: 26-04-2015.

Bishop, C., Paul, G., and Thewlis, D. (2012). Recommendations for the reporting of foot and ankle models. *Journal of Biomechanics*, 45:2185–94.

Bobbert, M. and Schenau, I. (1990). Isokinetic plantar flexion: experimental results and model calculations. *Journal of Biomechanics*, 23:105–19.

Boffeli, T., Bean, J., and Natwick, J. (2002). Biomechanical abnormalities and ulcers of the great toe in patients with diabetes. *Journal of Foot and Ankle Surgery*, 41:359–64.

Brach, J., Talkowski, J., Strotmeyer, E., and Newman, A. (2008). Diabetes mellitus and gait dysfunction: possible explanatory factors. *Physical Therapy*, 88:1365–1374.

Brand, P. (1986). *The diabetic foot, in Clinical Diabetes Mellitus: A Problem Oriented approach*. Davidson JK, New York.

Broder, J. (2010). *Chapter 14 - Imaging the Extremities, in Diagnostic Imaging for the Emergency Physician*. W.B. Saunders, Saint Louis.

Buchanan, T., Lloyd, D., Manal, K., and Besier, T. (2004). Neuromusculoskeletal Modeling: Estimation of muscle forces and joint moments and movements from measurements of neural command. *Journal of applied biomechanics*, 20:367–395.

Carson, M., Harrington, M., Thompson, N., O'Connor, J., and Theologis, T. (2001). Kinematic analysis of a multi-segment foot model for research and clinical applications: a repeatability analysis. *Journal of Biomechanics*, 34:1299–1307.

Cavanagh, P. (1999). Plantar soft tissue thickness during ground contact in walking. *Journal of Biomechanics*, 32:623–628.

Cavanagh, P., Lipsky, B., Bradbury, A., and Botek, G. (2005). Treatment for diabetic foot ulcers. *Lancet*, 366:1725–35.

Cavanagh, P. and Ulbretch, J. (2008). *Chapter 6 The biomechanics of the foot in Diabetes Mellitus, in Levin and O'Neal's The Diabetic Foot (7th Edition).* Bowker, J.H. and Pfeifer, M.A., Philadelphia.

Cheung, J. and Nigg, M. (2008). Clinical Applications of Computational Simulation of Foot and Ankle. *Sports Orthopaedics and Traumatology*, 23:264–271.

Christman, R. (2003). *Chapter 16 - Overview of Special Imaging Studies, in Foot and Ankle Radiology.* Churchill Livingstone, Saint Louis.

Cornwall, M. and McPoil, T. (1999). Three-dimensional movement of the foot during the stance phase of walking. *Journal of the American Podiatric Medical Association*, 89:56–66.

De Berardis, G., Pellegrini, F., Franciosi, M., Belfiglio, M., Di Nardo, B., Greenfield, S., Kaplan, S., Rossi, M., Sacco, M., Tognoni, G., Valentini, M., and Nicolucci, A. (2005). Are Type 2 diabetic patients offered adequate foot care? The role of physician and patient characteristics. *Journal of Diabetes and its Complications*, 19:319–27.

De Luca, C. (1997). The use of surface electromyography in biomechanics. *Journal of Applied Biomechanics*, 13:135–163.

Deschamps, K., Staes, F., Roosen, P., Nobels, F., Desloovere, K., Bruyninckx, H., and Matricali, G. (2011). Body of evidence supporting the clinical use of 3D multisegment foot models: a systematic review. *Gait & Posture*, 33:338–349.

Dixon, P., Bohm, H., and Doderlein, L. (2012). Ankle and midfoot kinetics during normal gait: a multi-segment approach. *Journal of Biomechanics*, 45:1011–6.

Edmonds, M. and Watkins, P. (1999). *Plantar neuropathic ulcer and Charcot joints: Risk factors, presentation, and management, in Diabetic Neuropathy.* Saunders, W.B., Philadelphia.

Eils, E., Behrens, S., Mers, O., Thorwesten, L., Vlker, K., and Rosenbaum, D. (2004). Reduced plantar sensation causes a cautious walking pattern. *Gait & Posture*, 20:54–60.

Field, D. and Hutchinson, J. (2008). *Lower Limb Anatomy, Palpation & Surface Markings (1st Edition).* Churchill Livingstone, London, UK.

Flavin, R., Halpin, T., O'Sullivan, R., FitzPatrick, D., Ivankovic, A., and Stephens, M. (2008). A finite-element analysis study of the metatarsophalangeal joint of the hallux rigidus. *The Journal of Bone & Joint Surgery*, 90:1334–40.

Foster, A. (2006). *Chapter 4 - Offloading the diabetic foot, in Podiatric Assessment and Management of the Diabetic Foot.* Churchill Livingstone, Edinburgh.

France, D. (2009). *Human and Nonhuman Bone Identification: A Color Atlas.* CRC Press: Taylor & Francis group, Boca Raton.

Franklin, S., Grey, M., Heneghan, N., Bowen, L., and Li, F. (2015). Barefoot vs common footwear: A systematic review of the kinematic, kinetic and muscle activity differences during walking. *Gait & Posture*, 42:230–239.

Freivalds, A. (2004). *Biomechanics of the upper limbs: Mechanics, Modeling and Musculoskeletal Injuries.* CRC Press, Boca Raton, United States.

Frykberg, R., Zgonis, T., Armstrong, D., Driver, V., Giurini, J., Kravitz, S., Landsman, A., Lavery, L., Moore, J., Schuberth, J., Wukich, D., Andersen, C., and Vanore, J. (2006). Diabetic Foot Disorders: A Clinical Practice Guideline. *The Journal of Foot and Ankle Surgery*, 45:1–66.

Fukashiro, S., Komi, P., Jrvinen, M., and Miyashita, M. (1995). In vivo Achilles tendon loading during jumping in humans. *European Journal of Applied Physiology*, 71:453–458.

Gage, J. (1997). *Clinical Gait Analysis, A focus on Interpretation*. Connecticut Childrens Medical Center, Connecticut.

Gefen, A., Megido-Ravid, M., and Itzchak, Y. (2001). In vivo biomechanical behavior of the human heel pad during the stance phase of gait. *Journal of Biomechanics*, 34:1661–5.

Giacomozzi, C. and Martelli, F. (2006). Peak pressure curve: an effective parameter for early detection of foot functional impairments in diabetic patients. *Gait & Posture*, 23:464–70.

Giddings, V., Beaupre, G., Whalen, R., and Carter, D. (2000). Calcaneal loading during walking and running. *Medicine and Science in Sports and Exercise*, 32:627–634.

Gilchrist, L. and Winter, D. (1996). A two-part, viscoelastic foot model for use in gait simulations. *Journal of Biomechanics*, 29:795–798.

Godfrey, K. and DiStefano, I. (1987). *Chapter 1 - Identifiability of model parameters, in Identifiability of Parametric Models*. Pergamon, Oxford.

Gooding, G., Stess, R., Graf, P., Moss, K., Louie, K., and Grunfeld, C. (1986). Sonography of the sole of the foot. Evidence for loss of foot pad thickness in diabetes and its relationship with ulceration of the foot. *Investigative Radiology*, 21:45–48.

Haeufle, D. (2014). Hill-type muscle model with serial damping and eccentric forcevelocity relation. *Journal of Biomechanics*, 47:1531–36.

Heintz, S. (2006). *Technical report: Muscular Forces from Static Optimization*. Royal Institute of Technology KTH Mechanics, Sweden.

Hermens, H., Freriks, D., Disselhorst-Klug, C., and Rau, G. (2000). Development of recommendations for sEMG sensors and sensor placement procedures. *Journal of Electromyography and Kinesiology*, 10:361–74.

Hockenbury, T. (2006). *Chapter 77 - Fractures and Dislocations of the Foot and Ankle, in Orthopaedic Physical Therapy Secrets (2nd Edition)*. Mosby, Saint Louis.

Holst, K., Liebgott, H., Wilhjelm, J., Nikolov, S., Torp-Pedersen, S., Delachartre, P., and Jensen, J. (2013). Internal strain estimation for quantification of human heel pad elastic modulus: A phantom study. *Ultrasonics*, 53:439–46.

Houglum, P. and Bertoti, D. (2012). *Brunnstrom's Clinical Kinesiology (6th Edition)*. F.A. Davis Company, Philadelphia, US.

Hrones, J. and Nelson, G. (1983). *Analysis of the four-bar linkage : its application to the synthesis of mechanisms*. Technology Press of the Massachusetts Institute of Technology and Wiley, New York.

Hunt, A., Smith, R., Torode, M., and Keenan, A. (2001). Inter-segment foot motion and ground reaction forces over the stance phase of walking. *Clinical biomechanics*, 16:592–600.

Hunt, K. and Crossley, F. (1975). Coefficient of restitution interpreted as Damping in vibroimpact. *Journal of Applied Mechanics*, 42:440–445.

Jaitman, A., Evans, N., and Chappell, M. (2015). Barefoot and shod conditions: how to reconcile them for plantar pressure analysis in the Oxford Foot Model. *Journal of Mechanics in Medicine and Biology*, 15:1–6.

Jenkins, S. (2005). *Sports Science Handbook: A-H*. Multi-Science, New York.

Kidder, S., Abuzzahab, F., Harris, G., and Johnson, J. (1996). A system for the analysis of foot and ankle kinematics during gait. *IEEE Trans Rehabil Eng*, 4:25–32.

Kirtley, C. (2006). *Chapter 3 - Three-dimensional gait analysis, in Clinical Gait Analysis*. Churchill Livingstone, Edinburgh.

Kothonen, R. and Saarakkala, S. (2011). *Biomechanics and Modeling of skeletal Soft Tissues in Theoretical Biomechanics*. InTech, Intechopen.

Kung, S., Fink, P., Hume, P., and Shultz, S. (2015). Kinematic and kinetic differences between barefoot and shod walking in children. *Footwear Science*, 7:95–105.

Leardini, A., Benedetti, M., Berti, L., Bettinelli, D., Nativo, R., and Giannini, S. (2007a). Rear-foot, mid-foot and fore-foot motion during the stance phase of gait. *Gait & Posture*, 25:453–462.

Leardini, A., Benedetti, M., Catani, F., Simoncini, L., and Giannini, S. (1999). An anatomically based protocol for the description of foot segment kinematics during gait. *Cinical Biomechanics*, 14:528–536.

Leardini, A., Sawacha, Z., Paolini, G., Ingrosso, S., Nativo, R., and Benedetti, M. (2007b). A new anatomically based protocol for gait analysis in children. *Gait & Posture*, 26:560–571.

Ledoux, W. (2007). *The Biomechanics of the Diabetic Foot, in Foot and Ankle Motion Analysis: Clinical treatment and technology*. CRC Press: Taylor & Francis group, Florida.

Logan, A. and Rowe, L. (1995). *The Foot and Ankle: Clinical Applications*. Aspen Publication, Gaithersburg.

MacWilliams, B.A.and Cowley, M. and Nicholson, M. (2003). Foot kinematics and kinetics during adolescent gait. *Gait & Posture*, 17:214–224.

Marks, R., Harris, G., and Smith, P. (2007). *Foot and Ankle Motion Analysis: Clinical treatment and technology*. CRC Press: Taylor & Francis group, Florida.

Marquez, A. and Oliva, M. (2010). Hallux rigidus: aetiology, diagnosis, classification and treatment. *Revista Española de Cirugía Ortopédica y Traumatología*, 54:321–328.

Mayer, D. and Kabbani, Y. (2003). *Chapter 17 -MRI/Cross-Sectional Imaging, in Foot and Ankle Radiology*. Churchill Livingstone, Saint Louis.

Miyazaki, S. and Yamamoto, S. (1993). Moment acting at the metatarsophalangeal joints during normal barefoot level walking. *Gait & Posture*, 1:133–140.

Morlock, M. and Nigg, B. (1991). Theoretical considerations and practical results on the influence of the representation of the foot for the estimation of internal forces with models. *Clinical Biomechanics*, 6:3–13.

Muscolino, J. (2009). *The Muscle and Bone Palpation Manual with Trigger Points, Referral Patterns and Stretching (1st Edition)*. Mosby, Missouri, US.

Nakamura, S., Crowninshield, R., and Cooper, R. (1981). An analysis of soft tissue loading in the foot – a preliminary report. *Bulletin of Prosthetic Research*, 10:27–34.

Nawoczenski, D., Saltzman, C., and Cook, T. (1998). The effect of foot structure on the three-dimensional kinematic coupling behavior of the leg and rear foot. *Physical Therapy*, 78:404–416.

Nordin, M. and Frankel, V. (2001). *Basic Biomechanics of the Musculoskeletal System*. Lippincott Williams & Wilkins, Philadelphia.

Olney, S. and Winter, D. (1985). Predictions of knee and ankle moments of force in walking from EMG and kinematic data. *Journal of Biomechanics*, 18:9–20.

Pai, S. and Ledoux, W. (2010). The compressive mechanical properties of diabetic and non-diabetic plantar soft tissue. *Journal of Biomechanics*, 43:1754–1760.

Palastanga, N. and Soames, R. (2011). *Anatomy and Human Movement (6th Edition)*. Churchill Livingstone, London, UK.

Palestro, C., Love, C., and Miller, T. (2006). Infection and musculoskeletal conditions: Imaging of musculoskeletal infections. *Best Practice & Research: Clinical Rheumatology*, 20:1197–218.

Patil, K., Braak, L., and Huson, A. (1996). Analysis of stresses in two-dimensional models of normal and neuropathic feet. *Medical & Biological Engineering & Computing*, 34:280–284.

Perry, J. (1992). *Gait Analysis: Normal and Pathological Function*. SLACK Incorporated, New Jersey.

Qiu, T., Teo, E., Yan, Y., and Lei, W. (2011). Finite element modeling of a 3D coupled foot-boot model. *Medical Engineering & Physics*, 33:1228–1233.

Rankine, J. (2009). Imaging of foot and ankle disorders. *Orthopaedics and Trauma*, 23:412–419.

Rao, S., Saltzman, C., and Yack, H. (2007). Segmental foot mobility in individuals with and without diabetes and neuropathy. *Clinical Biomechanics*, 22:464–71.

Razak, A., Zayegh, A., Begg, R., and Wahab, Y. (2012). Foot Plantar Pressure Measurement System: A Review. *Sensors*, 12:9884–9912.

Richards, J. (2008). *Biomechanics in clinic and research*. Churchill Livingstone Elseiver, Philadelphia.

Ritchie, D. (1997). Imaging the adult ankle and foot. *Foot and Ankle Surgery*, 3:105–120.

Roach, N. (2011). *Chapter 47 - MRI of the Foot and Ankle, in Radiology Secrets Plus (Third Edition)*. Mosby, Philadelphia.

Robertson, G., Caldwell, G., Hamill, J., Kamen, G., and Whittlesey, S. (2013). *Research Methods in Biomechanics*. Human Kinetics, United States.

Roug, I. and Pierre-Jerome, C. (2012). MRI spectrum of bone changes in the diabetic foot. *European Journal of Radiology*, 81:1625–9.

Salathe Jr, E., Arangio, G., and Salathe, E. (1986). A biomechanical model of the foot. *Journal of Biomechanics*, 19:989–1001.

Sanchis-Salesa, E., Sancho-Brub, J., Roda-Salesb, A., and Pascual-Huertac, J. (2016). Kinematics and kinetics analysis of midfoot joints of 30 normal subjects during walking. *Revista Española de Podología*, 27:6–12.

Sanders, L. and Frykberg, R. (2008). *Chapter 12 The Charcot Foot (Pied de Charcot), in Levin and O'Neal's The Diabetic Foot (Seventh Edition)*. Bowker, J.H. and Pfeifer, M.A., Philadelphia.

Saraswat, P., Andersen, M., and MacWilliams, B. (2010). A musculoskeletal foot model for clinical gait analysis. *Journal of Biomechanics*, 43:1645–52.

Sawacha, Z., Guarneri, G., Cristoferi, G., Guiotto, A., Avogaro, A., and Cobelli, C. (2012). Integrated kinematics-kinetics-plantar pressure data analysis: a useful tool for characterizing diabetic foot biomechanics. *Gait & Posture*, 36:20–26.

Scott, S. and Winter, D. (1991). A comparison of three muscle pennation assumptions and their effect on isometric and isotonic force. *Journal of Biomechanics*, 24:163–7.

Scott, S. and Winter, D. (1993). Biomechanical model of the human foot: Kinematics and kinetics during the stance phase of walking. *Journal of Biomechanics*, 26:1091–1104.

SENIAM (2003). SENIAM: Surface ElectorMyoGraphy for the Non-Invasive Assessment of Muscle. http://www.seniam.org. Accessed: 21-05-2016.

Sherman, M., Seth, A., and Delp, S. (2013). What is moment arm? Calculating muscle effectiveness in biomechanical models using generalized coordinates. *Proceedings of the ASME 2013 International Design Engineering Technical Conferences and Computers and Information in Engineering Conference IDETC CIE 2013*, 13633:1–9.

Simkin, A. (1982). *Structural Analysis of the Human Foot in Standing Posture*. PhD thesis, Tel-Aviv University.

Simon, S. (2004). Quantification of human motion: gait analysis-benefits and limitations to its application to clinical problems. *Journal of Biomechanics*, 37:1869–80.

Snell, R. (2004). *Clinical Anatomy: An Illustrated Review with Questions and Explanations*. Lippincott Williams & Wilkins, Edinburgh.

Stebbins, J., Harrington, M., Thompson, N., Zavatsky, A., and Theologis, T. (2006). Repeatability of a model for measuring multi-segment foot kinematics in children. *Gait & Posture*, 23:401–410.

Switaj, T. and O'Connor, F. (2008). *Chapter 43 - Gait Analysis, in The Sports Medicine Resource Manual*. W.B. Saunders, Philadelphia.

Tan, P. and Teh, J. (2007). MRI of the diabetic foot: differentiation of infection from neuropathic change. *The British Journal of Radiology*, 80:939–48.

Thordarson, D. (2004). *Foot and Ankle*. Lippincott Williams & Wilkins, New York.

Trigo, E. and Navarro, C. (2005). The skeletal muscle. *ADEM and AFM*, 401:1–15.

Valiant, G. (1984). *A determination of the mechanical characteristics of the human heel pad in vivo*. PhD thesis, The Pennsylvania State University, University Park, PA.

Van Schie, C., Rawat, F., and Boulton, A. (2005). Reduction of plantar pressure using a prototype pressure-relieving dressing. *Diabetes Care*, 28:2236–2247.

Vicon (2010). Vicon Plug-in-Gait Product Guide Foundation Notes 2.0 (Vicon Motion Systems Unlimited).

Vicon (2012). Oxford Foot Model 1.4 Release Notes (Vicon Motion Systems Unlimited).

Voloshin, A. and Kim, W. (1995). Role of the plantar fascia in the load bearing capacity of the human foot. *Journal of Biomechanics*, 28:1025–33.

Wang, R., Thurb, C., Gutierrez-Farewika, E., Wretenbergb, P., and Brostromc, E. (2010). One year follow-up after operative ankle fractures: A prospective gait analysis study with a multi-segment foot model. *Gait & Posture*, 31:234–240.

Wearing, S., Smeathers, J., Yates, B., Urry, S., and Dubois, P. (2009). Bulk compressive properties of the heel fat pad during walking: A pilot investigation in plantar heel pain. *Clinical Biomechanics*, 24:397–402.

Whittle, M. (2007a). *Chapter 1 - Basic sciences, in Gait Analysis*. Butterworth-Heinemann (4th Edition), Edinburgh.

Whittle, M. (2007b). *Chapter 2 Normal gait, in Gait Analysis*. Butterworth-Heinemann (Fourth Edition), Edinburgh.

WHO, W. H. O. (1998). World Health Organization: Diabetes Programme WHO. http://www.who.int/diabetes/en/. Accessed: 25-06-2013.

Winter, D. (2005). *Biomechanics and motor control of human movement*. John Wiley Sons, N.J., US.

Woittiez, R., Huijing, P., Boom, H., and Rozendal, R. (1984). A three-dimensional muscle model: a quantified relation between form and function of skeletal muscles. *Journal of Morphologyl*, 182:95–113.

Wright, C., Arnold, B., Coffey, T., and Pidcoe, P. (2011). Repeatability of the modified Oxford Foot Model during gait in healthy adults. *Gait & Posture*, 33:108–112.

Wu, G., Siegler, S., Allard, P., Kirtley, C., Leardini, A., Rosenbaum, D., Whittle, M., D'Lima, D., Cristofolini, L., Witte, H., Schmid, O., and Stokes, I. (2002). ISB recommendation on definitions of joint coordinate system of various joints for the reporting of human joint motion – part I: ankle, hip, and spine (International Society of Biomechanics). *Journal of Biomechanics*, 35:543–548.

Yu, J., Wai-Chi Wong, D., and Zhang, M. (2014). *Computational Biomechanics of the Musculoskeletal System: Dynamic Foot Model for Impact Investigation*. Zhang, M. and Fan, Y., CRC Press.

Zajac, F. (1989). Muscle and tendon: properties, models, scaling and application to biomechanics and motor control. *Clinical reviews in biomedical engineering*, 17:359–410.

Zatsiorsky, V. and Prilutsky, B. (2012). *Biomechanics of skeletal muscles*. Human Kinetics, United States.

Zhang, X., Paquette, M., and Zhang, S. (2013). A comparison of gait biomechanics of flip-flops, sandals, barefoot and shoes. *Journal of Foot and Ankle Research*, 6:45.

Appendices

A

Ethical Approval

Consent form and PIL: BSREC full approval REGO-2013-582 Foot Modelling.

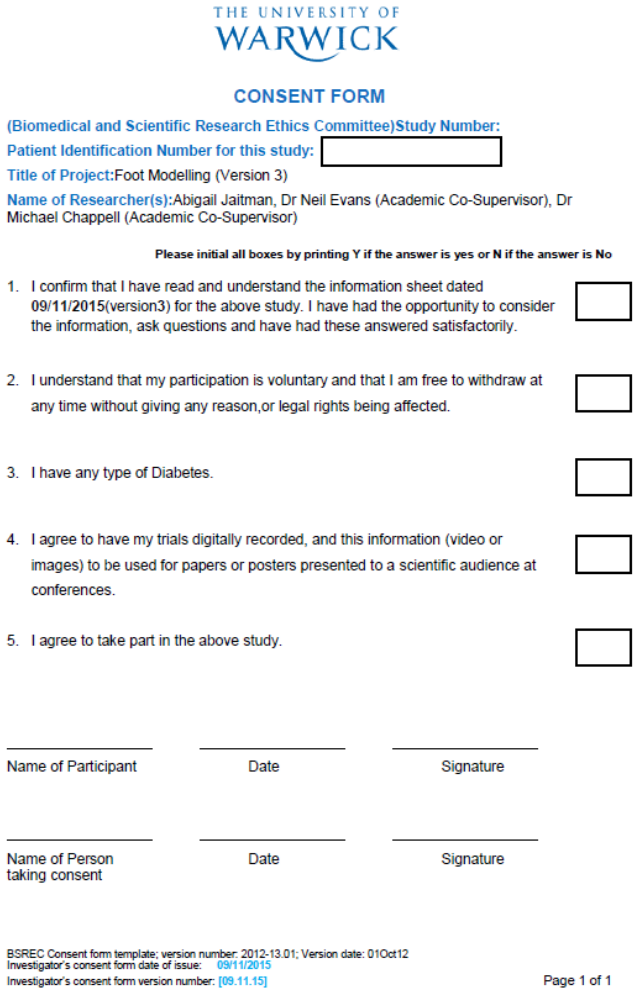

THE UNIVERSITY OF WARWICK

CONSENT FORM

(Biomedical and Scientific Research Ethics Committee)Study Number:

Patient Identification Number for this study:

Title of Project:Foot Modelling (Version 3)

Name of Researcher(s):Abigail Jaitman, Dr Neil Evans (Academic Co-Supervisor), Dr Michael Chappell (Academic Co-Supervisor)

Please initial all boxes by printing Y if the answer is yes or N if the answer is No

1. I confirm that I have read and understand the information sheet dated 09/11/2015(version3) for the above study. I have had the opportunity to consider the information, ask questions and have had these answered satisfactorily. ☐
2. I understand that my participation is voluntary and that I am free to withdraw at any time without giving any reason,or legal rights being affected. ☐
3. I have any type of Diabetes. ☐
4. I agree to have my trials digitally recorded, and this information (video or images) to be used for papers or posters presented to a scientific audience at conferences. ☐
5. I agree to take part in the above study. ☐

Name of Participant	Date	Signature
Name of Person taking consent	Date	Signature

BSREC Consent form template; version number: 2012-13.01; Version date: 01Oct12
Investigator's consent form date of issue: 09/11/2015
Investigator's consent form version number: [09.11.15]

Page 1 of 1

Figure A-1 Ethical approval: Consent Form

THE UNIVERSITY OF WARWICK

PARTICIPANT INFORMATION LEAFLET

Study Title: Foot Modelling (Version 3)

Investigator(s): Abigail Jaitman, Dr Neil Evans (Academic Co-Supervisor), Dr Michael Chappell (Academic Co-Supervisor)

Introduction

You are invited to take part in a Research study. Before you decide, you need to understand why the research is being done and what it would involve for you. Please take the time to read the following information carefully. Talk to others about the study if you wish.

(Part 1 tells you the purpose of the study and what will happen to you if you take part. Part 2 gives you more detailed information about the conduct of the study)

Please ask us if there is anything that is not clear or if you would like more information. Take time to decide whether or not you wish to take part.

PART 1

What is the study about?

My research project consists of developing a mathmatical and computational model of the human foot. In order to do this, an experimental study will be carried out in the School of Engineering's Gait Laboratory. Gait is defined as the way in which a person walks, and such an analysis allows us to measure and analyse movement patterns, together with the forces that are produced by movements and reactions with a force plate.

The ultimate aim of this study is to develop an innovative foot model, integrating different methodologies including motion capture, plantar pressure and joint measurements to provide a better understanding of the foot, its shape and the effects of changes in its structure.

We are looking for volunteers to participate in motion capture experiments. You will be asked to walk around the Gait Laboratory, and on top of a 10cm high platform, wearing reflective markers so that the infrared cameras located in the laboratory can reconstruct your trajectory and therefore track the movement of the body in motion and hence calculate the gait pattern.The markers will be placed by one of the researchers on the lower limbs, either on the skin or tight fitting clothing, using double-sided tape. The system requires specific information about the subject in order to reconstruct the foot (body mass, height, leg length, knee width and ankle width). In addition to the markers, some angle measurement sensors (electrogoniometers) will be attached across the joints. These will allow the collection of angle data in real time and therefore permit understanding of the interaction between different joints and their influence on gait patterns. Commercially available bandages will be used to study joint movement under different scenarios.

In order to study the forces applied by the foot to the ground, you may be provided with a pair of shoes with insoles that will measure the plantar pressure, which is the pressure acting between the foot and the support surface during daily activities. Parameters such as peak pressure and contact time will be the output of these experiments. Approximately thirty volunteers in total will be needed for the study.

Do I have to take part?

Figure A-2 Ethical approval: Participant Information Leaflet (page 1/4)

It is entirely up to you to decide. We will describe the study and go through this information sheet, which we will give you to keep. If you choose to participate, we will ask you to sign a consent form to confirm that you have agreed to take part (if part of this study is an online or postal questionnaire/survey, by returning a completed questionnaire/survey, you are giving your consent for the information that you have supplied to be used in this study and formal signed consent will not be collected where postal or online questionnaires/surveys are concerned). You will be free to withdraw at any time, without giving a reason and this will not affect you or your circumstances in any way.

What will happen to me if I take part?

You will be asked to walk and stand still in the Gait Laboratory wearing 41 reflective markers placed on the lower half of your body. The systems require specific information about you in order to reconstruct the foot. The physical parameters that are needed are: body mass, height, leg length, knee width and ankle width (these last three, for both legs). You will be asked to stand still on the force plate at first in order to calibrate the system and scale the model according to your parameters. You will then be asked to walk around the Gait Laboratory and on a 10cm hight platform which is connected to an ultrasound probe for plantar soft tissue thickness measurement. Commercially available bandages will be used in order to mimic different joint scenarios. An electrogoniometer will be placed on the studied lower limb joints in order to measure the interaction between the different joints and their influence on the gait patterns.

You will also be provided with a pair of insoles, used to measure the plantar pressure. You will be asked to walk around, either within the Gait Laboratory or its surroundings. We will probably keep a digital video record comprising only the lower limbs to assist on the analysis of the data. You will be asked to attend one laboratory session, but we may wish to contact you for a follow up session. It is entirely up to you to decide whether you want to continue or not (further details on withdrawal are included in part 2)

What are the possible disadvantages, side effects, risks, and/or discomforts of taking part in this study?

The study will involve everyday activities as normal walking, therefore there are no real risks for the participant. The participant should not experience any major disadvantages, side effects, risks and/or discomforts other than the one produced by the removal of the double-sided tape in the cases in which the markers are placed directly on the skin. A tape around the platform highlights the edge, thus minimizing the risk of tripping.

What are the possible benefits of taking part in this study?

Although there are no likely direct personal benefits of taking part in this study, your participation will aid in research supporting the development of a new widely accepted and validated foot model that will offer valuable input to promote innovation in orthopaedics. This general model will help the development of an adapted model to characterise diabetic patients, both will be compared in order to help patients with diabetes to gain an in-depth understanding of the effects of changes in structure and shape of the foot brought about by the disease and also to evaluate the effects of interventions and other measures to aid their long-term rehabilitation. My ultimate objective is to contribute to a better cost-benefit assessment of the treatment alternatives that diabetic patients have at different stages of the illness.

Expenses and payments

You will not receive any reimbursement as a result of taking part in the study.

What will happen when the study ends?

Once the study has ended, the collected data will be anonymised, analysed and documented. The findings will be reflected in the PhD thesis. Some findings may be also

Figure A-3 Ethical approval: Participant Information Leaflet (page 2/4)

used as inputs for other academic papers involving these experiments.

Will my taking part be kept confidential?
Yes. We will follow strict ethical and legal practice and all information about you will be handled in confidence. Further details are included in Part 2.

What if there is a problem?
Any complaint about the way you have been dealt with during the study or any possible harm that you might suffer will be addressed. Detailed information is given in Part 2.

This concludes Part 1.

If the information in Part 1 has interested you and you are considering participation, please read the additional information in Part 2 before making any decision.

PART 2

Who is organising and funding the study?
This study is a PhD research project and is not externally funded.

What will happen if I don't want to carry on being part of the study?
Participation in this study is entirely voluntary. Refusal to participate will not affect you in any way. If you decide to take part in the study, you will need to sign a consent form, which states that you have given your consent to participate.

If you agree to participate, you may nevertheless withdraw from the study at any time without affecting you in any way.

You have the right to withdraw from the study completely and decline any further contact by study staff after you withdraw.

Should you wish to withdraw from the study at any stage, or any data to be withdrawn from your data set that has not yet been processed, you are free to do so at any time. Any data collected will be erased and will not be used in any further analysis. Nevertheless, withdrawal after three months of participating in the study may mean that the data will have already been aggregated, analysed and processed; however all records will be kept anonymous and will not be identifiable. We intend to keep digital video records of the session to assist on the analysis of the collected data. However, the recorded material will be deleted immediately upon request at any time by the participant.

What if there is a problem?
This study is covered by the University of Warwick's insurance and indemnity cover. If you have an issue, please contact Jo Horsburgh (details below).

Who should I contact if I wish to make a complaint?

Figure A-4 Ethical approval: Participant Information Leaflet (page 3/4)

Any complaint about the way you have been dealt with during the study or any possible harm you might have suffered will be addressed. Please address your complaint to the person below, who is a Senior University of Warwick official entirely independent of this study:
Jo Horsburgh
Deputy Registrar
Deputy Registrar's Office
University of Warwick
Coventry, UK, CV4 8UW.
T: +00 44 (0) 2476 522 713 E: J.Horsburgh@warwick.ac.uk

Will my taking part be kept confidential?
Experiments will comply with all data protection requirements. All your information will be anonymised, and you will be allocated a Subject Identifier in order to access the anonymised data. All data will be safely and securely stored for 10 years according to University policy.

What will happen to the results of the study?
The results of the study will be used for parametrising and designing the foot model. These results will form part of a PhD thesis and therefore will be available in the Warwick Research Active Portal. Some findings may be also used as inputs for other academic papers involving these experiments.

Who has reviewed the study?
This study has been reviewed and given favourable opinion by the University of Warwick's Biomedical and Scientific Research Ethics Committee (BSREC): Insert your BSREC number here (given to you when your study is approved) and include the date on your approval letter from BSREC.

What if I want more information about the study?
If you have any questions about any aspect of the study or your participation in it not answered by this participant information leaflet, please contact:
Abigail Jaitman (PhD Student)
A.D.Jaitman@warwick.ac.uk
+44 (0) 7450274280

Thank you for taking the time to read this participant information leaflet.

Figure A-5 Ethical approval: Participant Information Leaflet (page 4/4)

B

Resolution Analysis

A resolution analysis was performed in order to understand the sensitivity of the system. The experiment depicted in figure B-1 consisted of moving, by steps of 0.01mm, the marker attached to the caliper and fixed to the floor. It consisted of thirty trials for each of the axis, each trial of 2 seconds. The value considered for each trial was the average displacement over the 2 second. The subset of trials considered for the analysis were the ones for which the displacement, measured by the caliper, was 0.01mm.

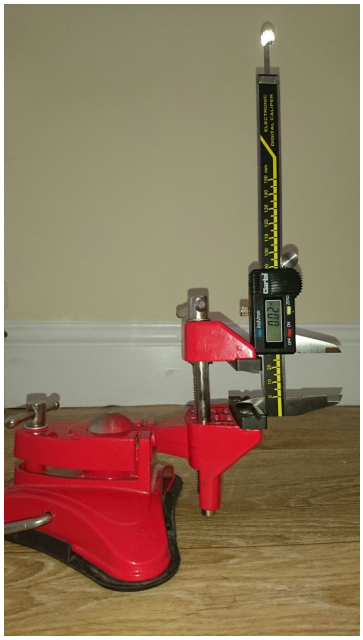

Figure B-1 Experimental setup for resolution analysis in Gait Laboratory

Figure B-2 depicts the result of this analysis: for X and Y axes, for a movement of 0.01mm, the system obtained a displacement of 0.013mm while for the Z axis the captured displacement was 0.006mm.

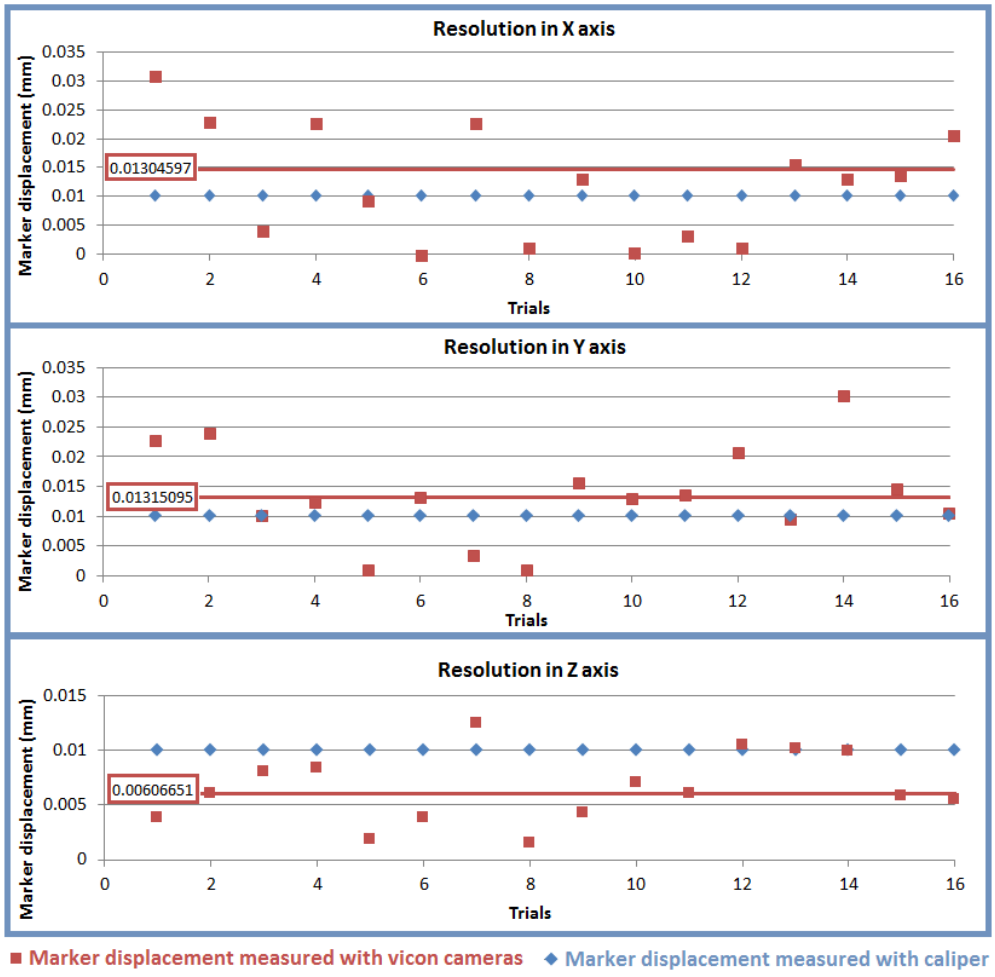

Figure B-2 Vicon Cameras resolution analysis in Gait Laboratory

C

EMG analysis

Function EMGanalysis takes as input a matrix with the already normalised raw EMG.

```
function [emgprocessed]=EMGanalysis (EMGraw)
Fs = 1000; %sampling frequency
Fcut = 5; %cutoff frequency
n = 4;%order of the filter
Wn = Fcut*2/Fs;
%raw data
figure
subplot (3,1,1)
plot(EMGraw)
title ('EMG raw data')
%now we rectify the signal
EMGrectified = abs (EMGraw)
subplot (3,1,2)
plot(EMGrectified)
title ('EMG rectified data')
%now we apply 4th order low pass filter
[B, A] = butter(n,Wn, 'low');
EMG=filter(B, A, EMGrectified);
subplot (3,1,3)
plot(EMG)
title ('EMG postprocessed')
```

D

Plantar pressure results

Figures D-1 and D-2 display results for subjects 1-14, showing total force vs. percentage of stance for plain and designed shoes. Figures D-3 and D-4 display results for subjects 1-14, showing force by foot segment for plain and designed shoes.

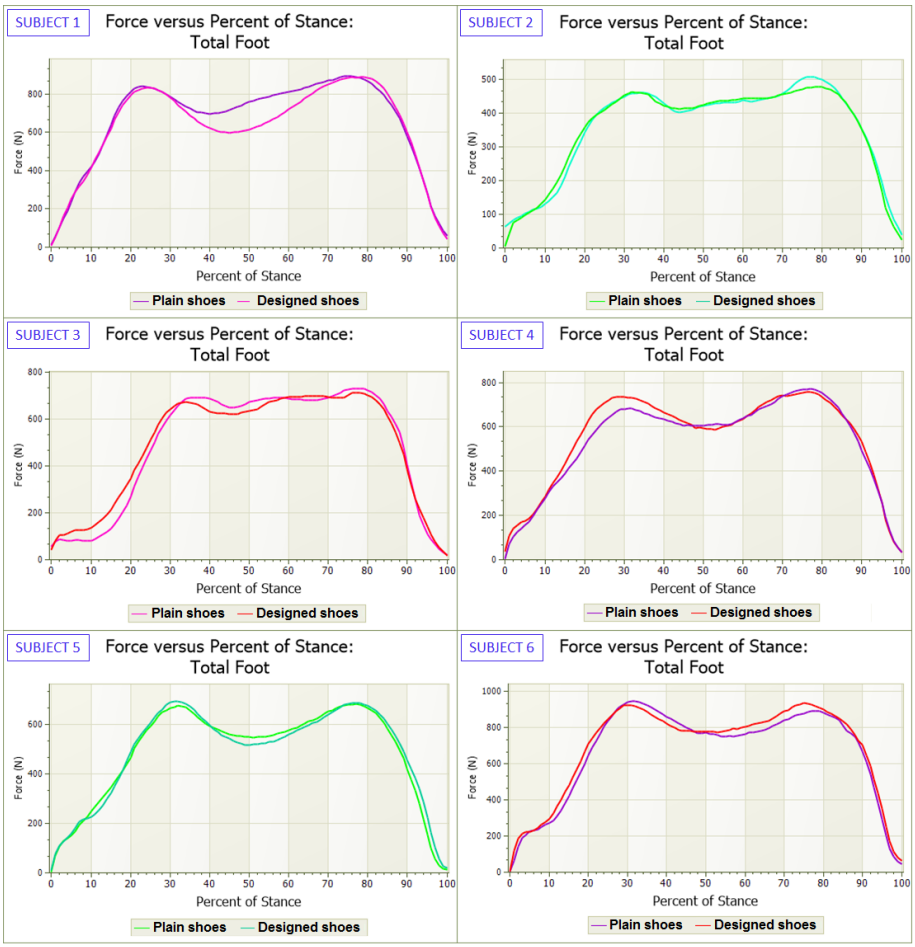

Figure D-1 Total foot force vs. Percent of Stance graph, for plain and designed shoes, subjects 1-6.

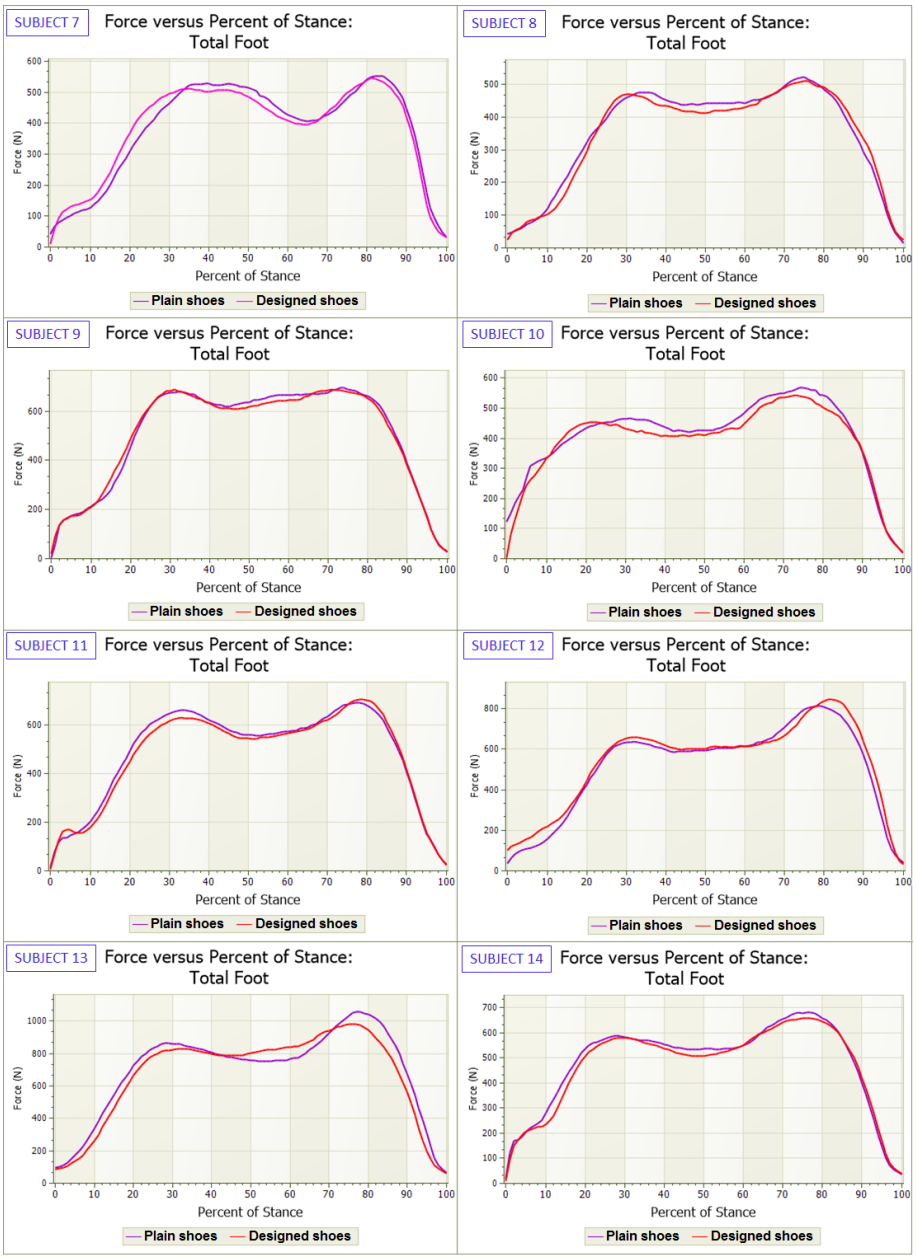

Figure D-2 Total foot force vs. Percent of Stance graph, for plain and designed shoes, subjects 7-14.

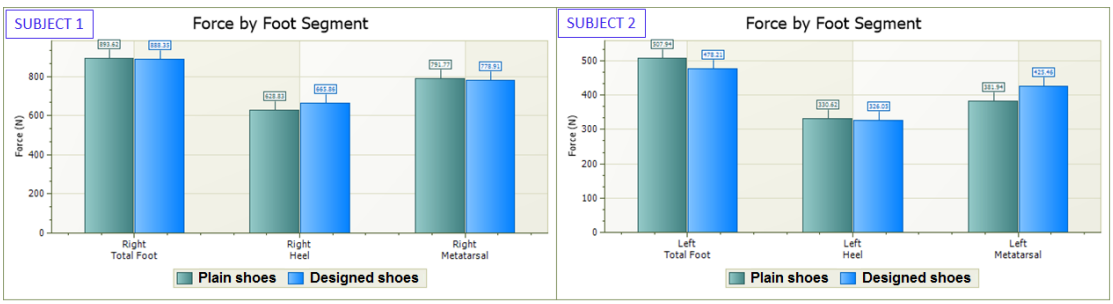

Figure D-3 Force by foot segment (plain and designed shoes), subjects 1-2.

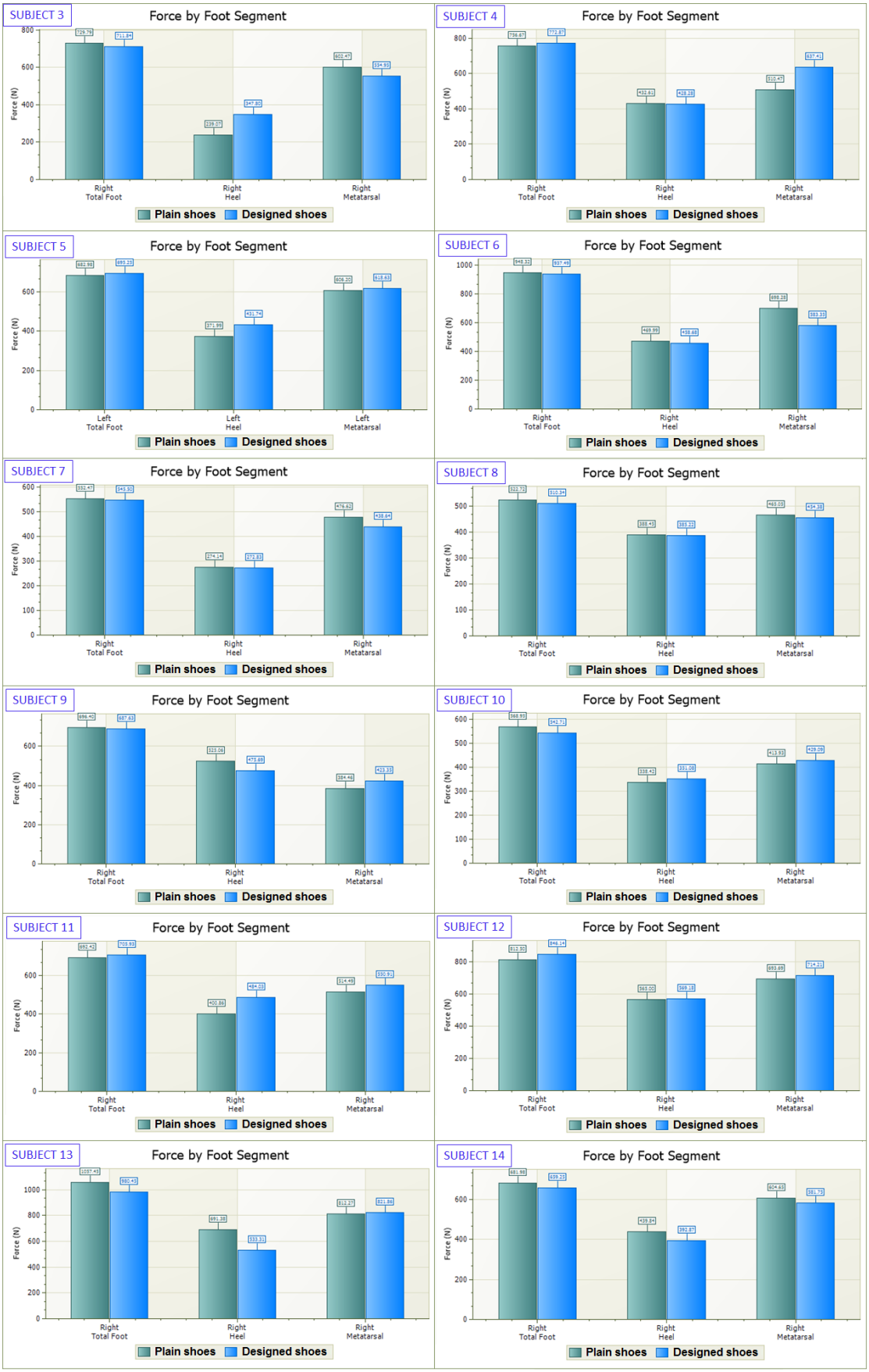

Figure D-4 Force by foot segment (plain and designed shoes), subjects 3-14.

E

MTU palpation and EMG placement

E.1 Muscle-tendon unit palpation

Inspection and palpation of muscle and tendons taken from Houglum and Bertoti [2012], Field and Hutchinson [2008], Muscolino [2009] and Palastanga and Soames [2011] as follows:

Posterior group of muscles

- Gastrocnemius: In standing position, both lateral and medial can be palpated if the subject is contracting and rising on tiptoes [Houglum and Bertoti, 2012].
- Tibialis Posterior: In sitting position, have tested limb crossed over the other one (in a relaxed and plantarflexed position), tendon will lie closest to medial malleolus. Go from plantarflexion and inversion to dorsiflexion and eversion [Houglum and Bertoti, 2012].
- Flexor Digitorum Longus: In sitting position, have tested limb crossed over the other one (in a relaxed and plantarflexed position), tendon will lie on the medial aspect of medial malleolus while flexing the toes [Houglum and Bertoti, 2012].
- Flexor Hallucis Longus: In sitting position, have tested limb crossed over the other one (in a relaxed and plantarflexed position), tendon can be easily confused with the Flexor Digitorum Longus one. For an isolated contraction, subject should flex the distal interphalangeal joints of toes [Houglum and Bertoti, 2012].

Lateral group of muscles

- Peroneus Brevis: In sitting position, subject should resist eversion. Peroneus brevis tendon stands out more than Longus one and can be followed till its attachment on the 5th metatarsal [Houglum and Bertoti, 2012].
- Peroneus Longus: In sitting position, subject should resist eversion. Above malleolus, tendon lies slightly posterior to Brevis tendon. Bellow the malleolus, the tendon lies close to the bone [Houglum and Bertoti, 2012].

Anterior group of muscles

- Tibialis Anterior: In sitting position, subject should flex the toes. It can be easily palpated when is passes over the ankle; it dorsiflexing foot and flexing and extending big toe, Extensor Hallucis Longus is noticeable as well, lying laterally [Field and Hutchinson, 2008].
- Extensor Hallucis Longus: In sitting position, subject should resist dorsiflexion of great toe. Muscle is almost entirely covered by Tibialis Anterior and Extensor Digitorum longus and cannot be easily distinguished [Houglum and Bertoti, 2012].
- Extensor Digitorum Longus: In sitting position, subject should lift toes off the floor, maintaining sole of the foot on the floor. Tendon stands out better if resistance is given to the four lesser toes. The tendons can be seen as they pass the ankle and insert in the lesser toes, as the examiner resists dorsiflexion of the foot on the dorsum of the toes [Houglum and Bertoti, 2012].

Muscles originating below ankle joint

- Extensor Digitorum Brevis: In sitting position, examiner should place one hand on the proximal phalanges (2nd, 3rd and 4th toes) and resist subject from extending the aforementioned toes. Contraction of the Extensor Digitorum Brevis can be then visualised and muscle can be palpated [Muscolino, 2009].
- Flexor Digitorum Brevis: In sitting position, examiner should place one hand on 2nd, 3rd, 4th and 5th toes while the subject flexes those digits. Muscle will contract and can be palpated through the calcaneus [Palastanga and Soames, 2011].
- Abductor Hallucis: Belly of the muscle can be palpated under the longitudinal arch while subject flexes the toes [Palastanga and Soames, 2011].
- Abductor Digiti Minimi: Muscle can be palpated only if the subject can abduct the 5th toe [Field and Hutchinson, 2008].
- Flexor Hallucis Brevis: This muscle cannot be palpated as it is in the deep plantar surface [Field and Hutchinson, 2008].

E.2 Electrodes placement

Electrodes were attached according to SENIAM [2003] recommendations as follows:

- Lateral Gastrocnemius: Lying with the face down, the knee extended and the foot projecting over the end of the table, electrodes should be placed at 1/3 of the line between the head of the fibula and the heel, laterally [SENIAM, 2003].
- Medial Gastrocnemius: Lying with the face down, the knee extended and the foot projecting over the end of the table, electrodes should be placed placed on the most prominent bulge of the muscle [SENIAM, 2003].
- Peroneus Brevis: In sitting position with extremity medially rotated, electrodes should be placed anterior to the tendon of the muscle Peroneus Longus at 25% of the line from the tip of the lateral malleolus to the fibula-head [SENIAM, 2003].
- Peroneus Longus: In sitting position with extremity medially rotated, electrodes should be placed at 25% on the line between the tip of the head of the fibula to the tip of the lateral malleolus [SENIAM, 2003].
- Tibialis Anterior: In supine position, electrodes should be placed at 1/3 on the line between the tip of the fibula and the tip of the medial malleolus [SENIAM, 2003].

Where no placement specification could be found in SENIAM project site [SENIAM, 2003], electrodes were placed following the general recommendations in Hermens et al. [2000]. Surface electrodes were attached in the middle region of the muscle thus avoiding both the innervation area and the attachment to tendon; and were oriented always parallel to muscle fibres.

F

Model Selection

In order to select the appropriate soft tissue model, four models were analysed in terms of R-squared values and RMSE. Table F-1 displays results for all the subjects for heel pad normal stress analysis. The Akaike criterion (AIC) was used for model selection.

		Gefen et al.	Scott and Winter	Hunt and Crossley	Kelvin Voigt
1	R^2	0.9939	0.8432	0.9591	0.9625
	RMSE	4.59E+03	2.41E+04	1.22E+04	1.14E+04
2	R^2	0.9881	0.9772	0.7283	0.9765
	RMSE	6.39E+03	9.17E+03	3.13E+04	8.97E+03
3	R^2	0.9558	0.9765	0.9953	0.9466
	RMSE	1.07E+04	7.91E+03	3.57E+03	1.17E+04
4	R^2	0.8373	0.8813	0.9252	0.8063
	RMSE	2.46E+04	2.16E+04	1.71E+04	2.68E+04
5	R^2	0.984	0.8613	0.9842	0.9592
	RMSE	8.68E+03	2.26E+04	8.77E+03	1.39E+04
6	R^2	0.8677	0.857	0.8392	0.843277
	RMSE	1.69E+05	1.89E+04	2.10E+04	1.98E+05
7	R^2	0.9789	0.9658	0.9064	0.9545
	RMSE	9.14E+03	1.19E+04	1.96E+04	1.34E+04
8	R^2	0.9674	0.8951	0.8799	0.8378
	RMSE	9.81E+03	1.78E+04	1.93E+04	2.19E+04
9	R^2	0.9948	0.9896	0.9809	0.983
	RMSE	4.93E+03	7.03E+03	9.63E+03	8.87E+03
10	R^2	0.997	0.9985	0.9999	0.9927
	RMSE	2.67E+03	1.90E+03	3.75E+02	4.13E+03
11	R^2	0.9944	0.9598	0.9968	0.9817
	RMSE	5.20E+03	1.45E+04	4.01E+03	9.41E+03
12	R^2	0.9266	0.8957	0.9957	0.9561
	RMSE	1.54E+04	1.88E+04	3.79E+03	1.19E+04
13	R^2	0.9341	0.9231	0.9558	0.9184
	RMSE	1.58E+04	1.71E+04	1.87E+04	1.99E+04
14	R^2	0.9278	0.9112	0.9318	0.9042
	RMSE	1.45E+04	1.67E+04	1.44E+04	1.67E+04
15	R^2	0.996	0.9982	0.9961	0.9953
	RMSE	3.00E+03	2.06E+03	3.05E+03	3.24E+03

Table F-1 Soft tissue model fitting for four models, analysing heel pad normal stress for fifteen subjects.

G

Interpolation analysis

An analysis was performed over different sampling frequencies (400Hz, 600Hz, 800Hz and 1000Hz) in application of cubic spline interpolation and comparison of this method with downsampling (taking both stress and strain to 200Hz which is the strain sampling rate). Figure G-1 displays stress-strain curves for the analysed frequencies. Table G-1 specifies R-squared values and root mean square errors for soft tissue model fitting using different sampling frequencies.

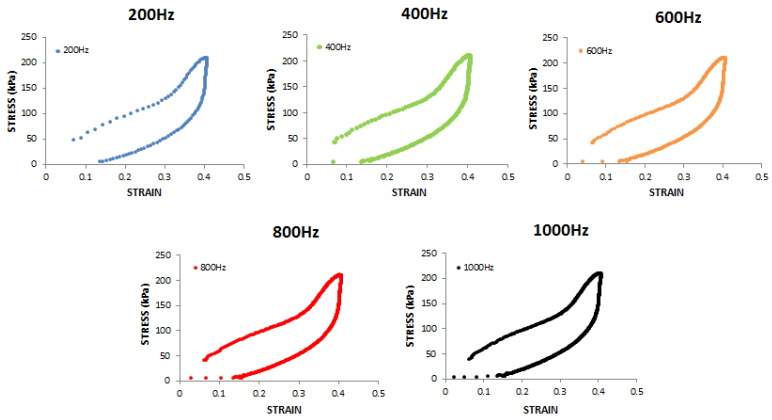

Figure G-1 Stress-strain curves for interpolation and downsampling analysis

Freq.	COMPRESSION		DECOMPRESSION	
	R^2	RMSE	R^2	RMSE
200Hz	0.9558	1.07E+04	0.9627	1.32E+04
400Hz	0.9551	1.07E+04	0.7573	3.37E+04
600Hz	0.9547	1.07E+04	0.7385	3.50E+04
800Hz	0.9545	1.07E+04	0.7305	3.56E+04
1000Hz	0.9474	1.16E+04	0.5741	4.46E+04

Table G-1 R^2 and RMSE for five different sampling frequencies

H

Soft tissue validation

Graphs H-1 to H-13 display measured (red) and simulated (blue) stress-strain curves for the remaining 13 subjects. Note that, in the case of normal stress, the strain is displayed in the graph with its absolute value (strain in this case is negative as represents compression).

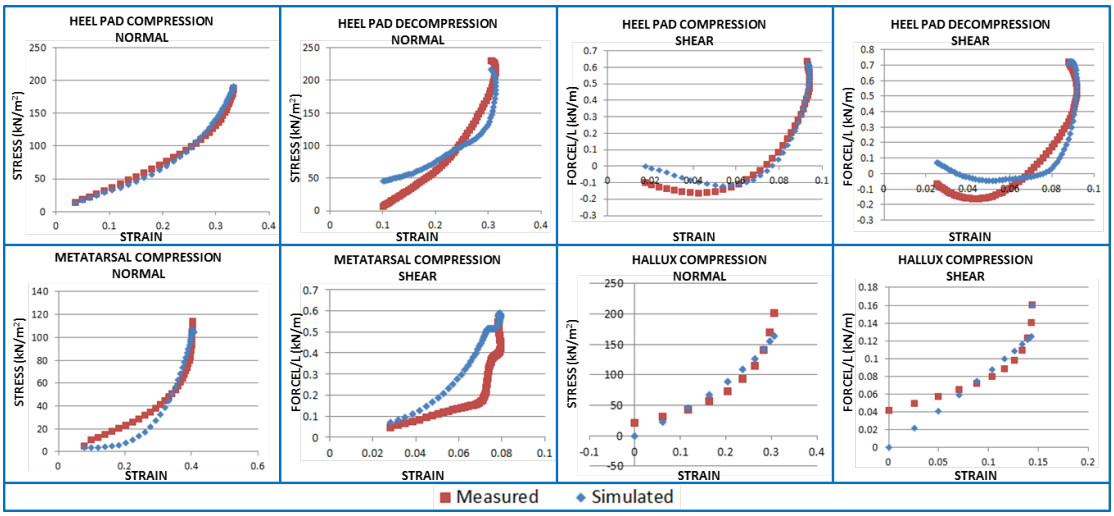

Note: For heel pad characterisation, 3 trials were used, 3 for metatarsal area and 2 for hallux.

Figure H-1 Soft tissue model validation - subject 1: measured (red) and simulated (blue) stress-strain curves

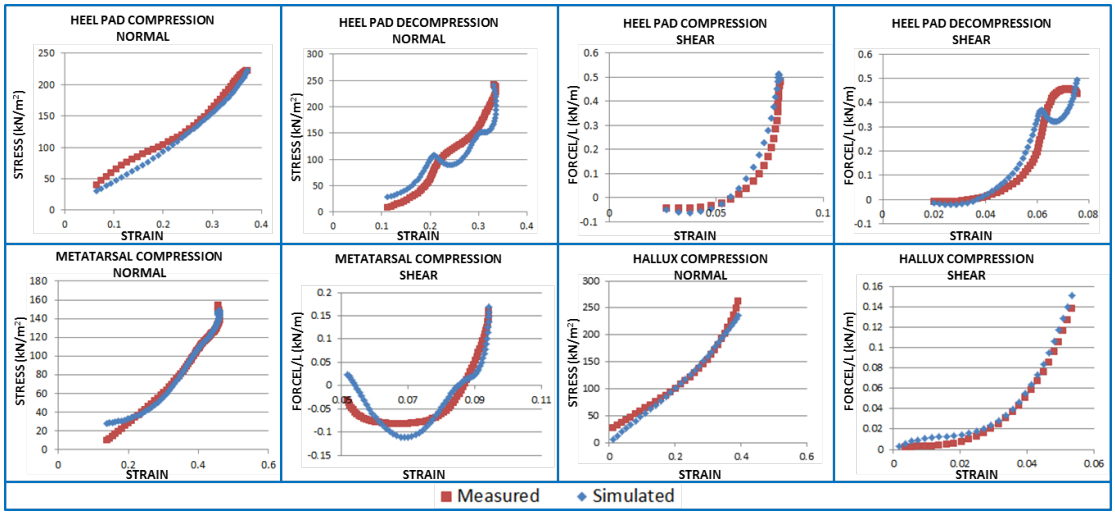

Note: For heel pad characterisation, 4 trials were used, 2 for metatarsal area and 2 for hallux.

Figure H-2 Soft tissue model validation - subject 2: measured (red) and simulated (blue) stress-strain curves

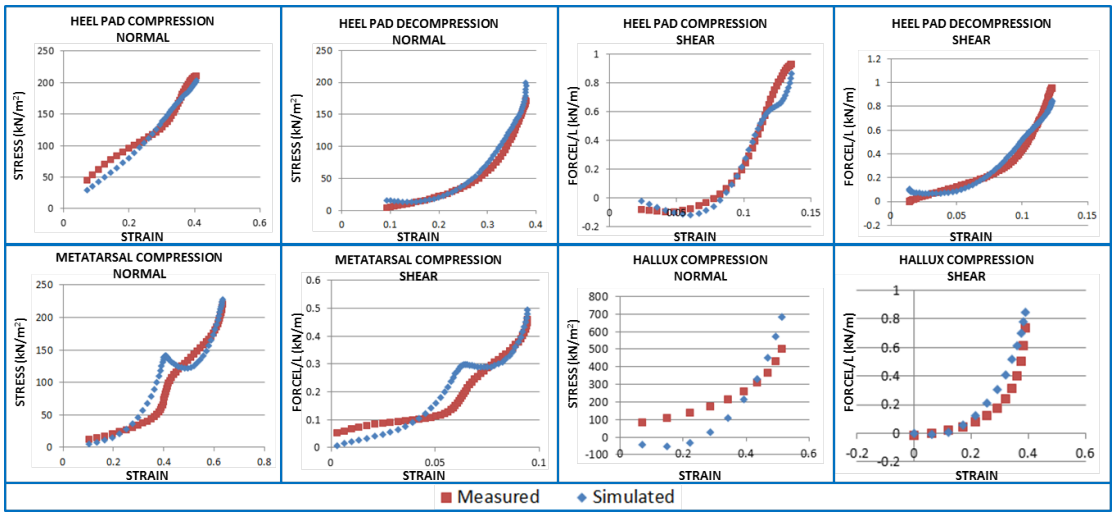

Note: For heel pad characterisation, 4 trials were used, 3 for metatarsal area and 2 for hallux.

Figure H-3 Soft tissue model validation - subject 3: measured (red) and simulated (blue) stress-strain curves

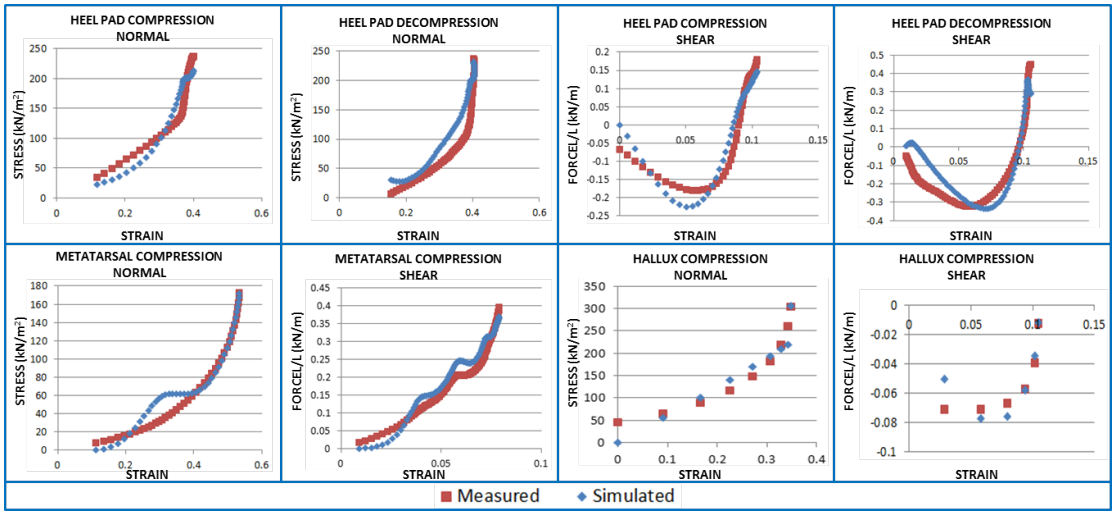

Note: For heel pad characterisation, 3 trials were used, 3 for metatarsal area and 2 for hallux.

Figure H-4 Soft tissue model validation - subject 4: measured (red) and simulated (blue) stress-strain curves

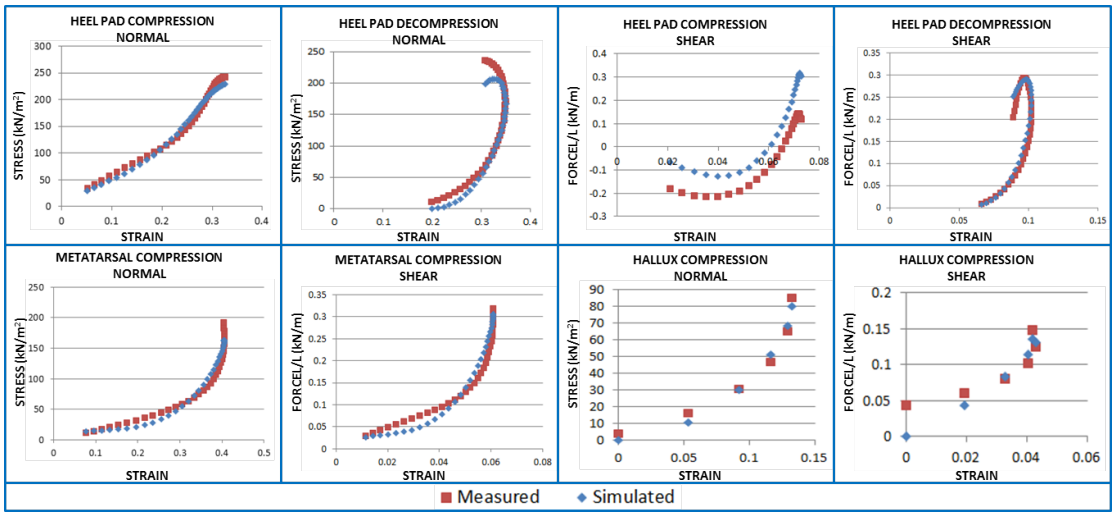

Note: For heel pad characterisation, 5 trials were used, 3 for metatarsal area and 2 for hallux.

Figure H-5 Soft tissue model validation - subject 5: measured (red) and simulated (blue) stress-strain curves

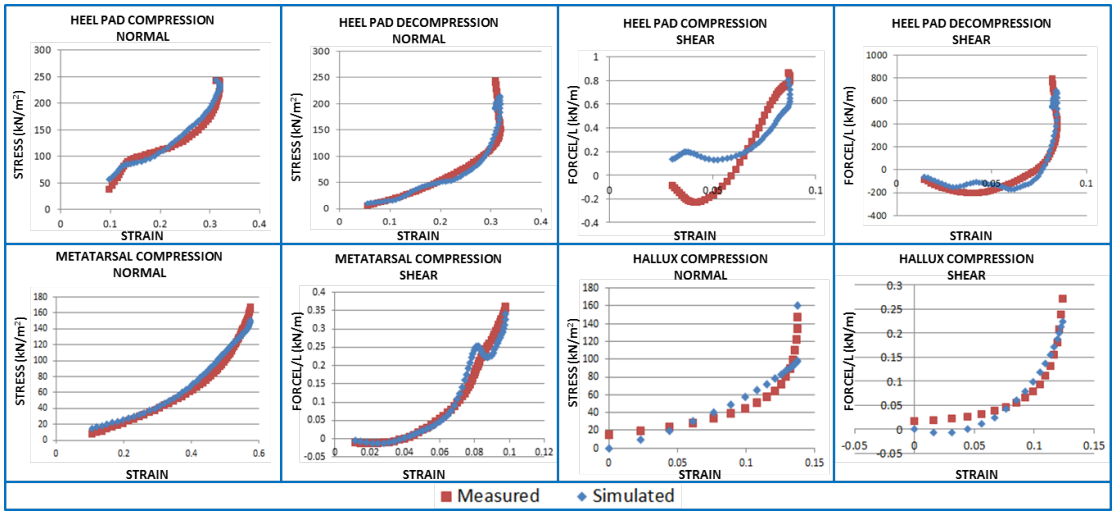

Note: For heel pad characterisation, 3 trials were used, 3 for metatarsal area and 2 for hallux.

Figure H-6 Soft tissue model validation - subject 7: measured (red) and simulated (blue) stress-strain curves

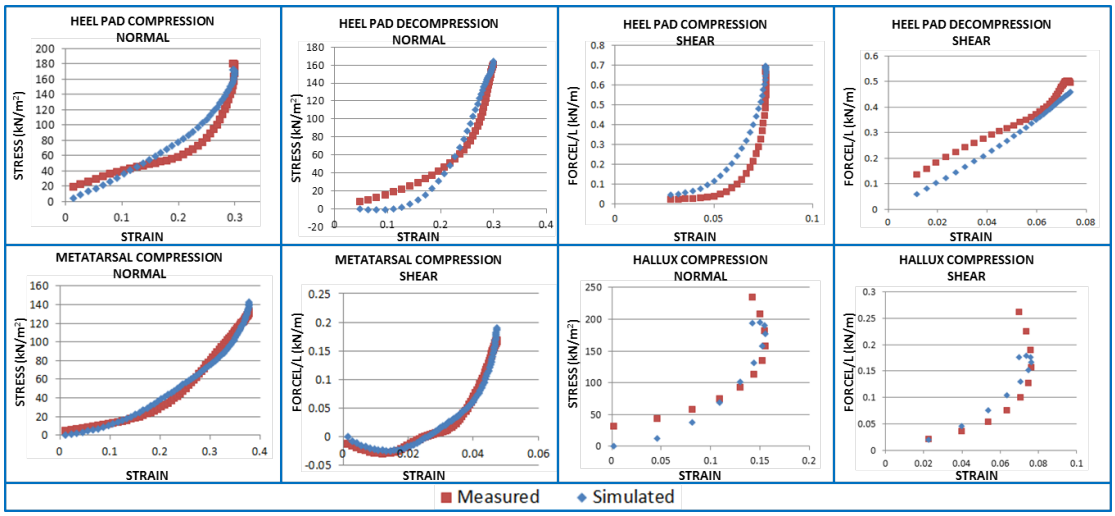

Note: For heel pad characterisation, 3 trials were used, 3 for metatarsal area and 2 for hallux.

Figure H-7 Soft tissue model validation - subject 8: measured (red) and simulated (blue) stress-strain curves

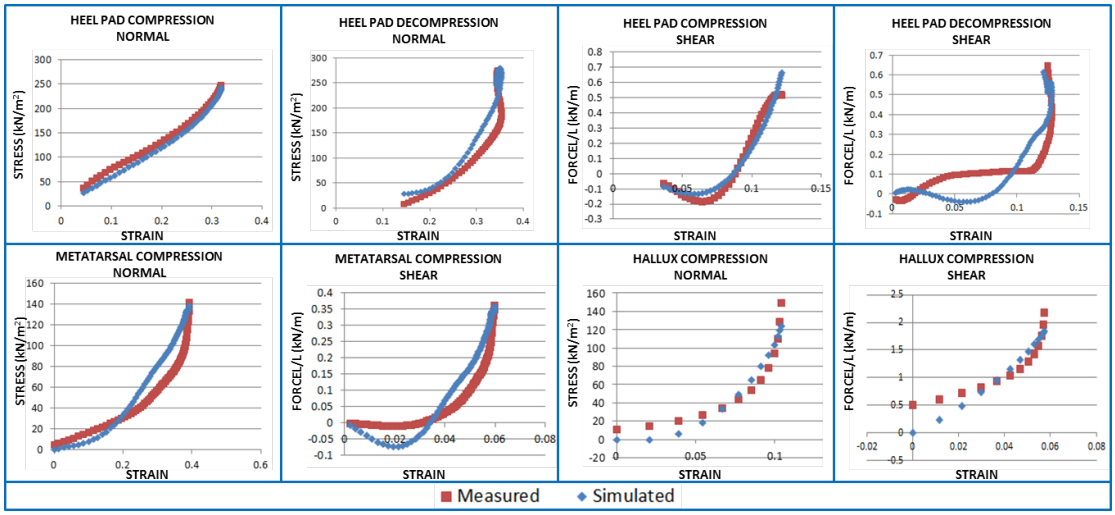

Note: For heel pad characterisation, 4 trials were used, 3 for metatarsal area and 2 for hallux.

Figure H-8 Soft tissue model validation - subject 9: measured (red) and simulated (blue) stress-strain curves

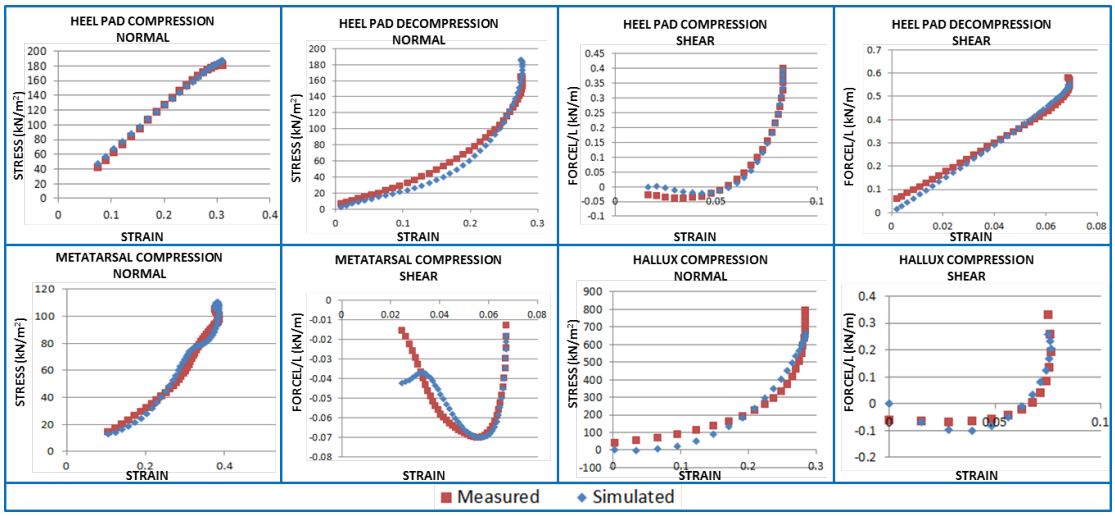

Note: For heel pad characterisation, 4 trials were used, 3 for metatarsal area and 2 for hallux.

Figure H-9 Soft tissue model validation - subject 10: measured (red) and simulated (blue) stress-strain curves

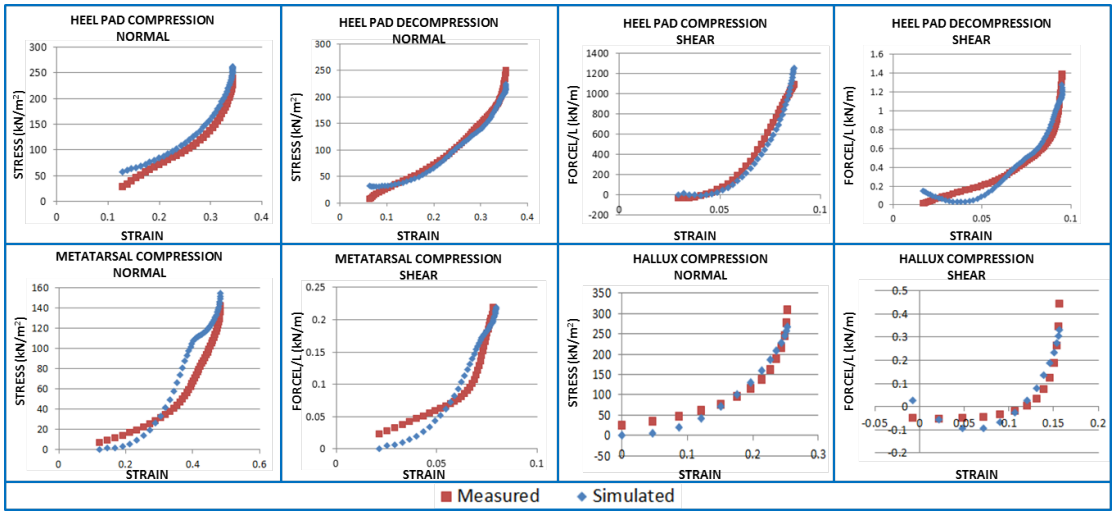

Note: For heel pad characterisation, 5 trials were used, 3 for metatarsal area and 2 for hallux.

Figure H-10 Soft tissue model validation - subject 11: measured (red) and simulated (blue) stress-strain curves

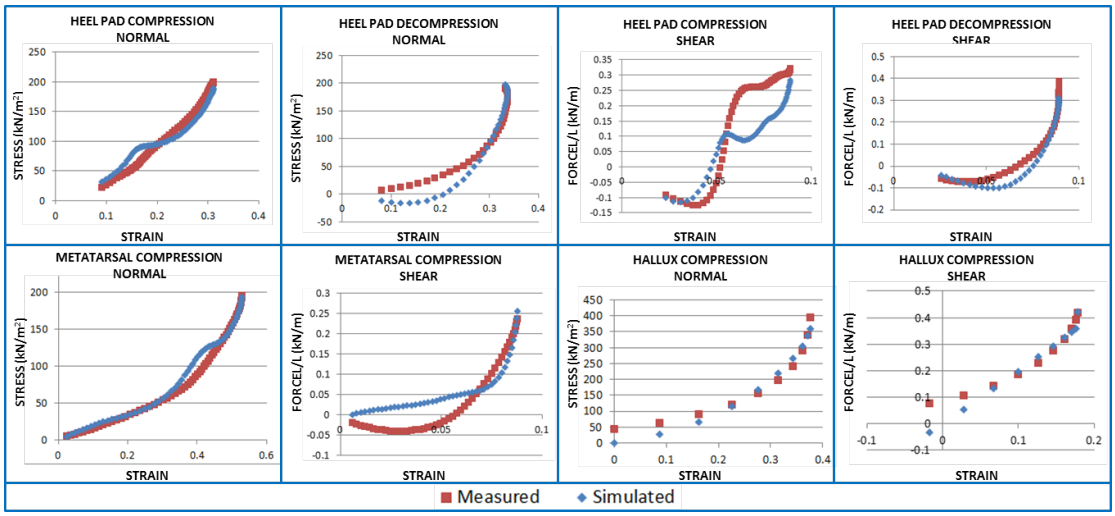

Note: For heel pad characterisation, 7 trials were used, 4 for metatarsal area and 2 for hallux.

Figure H-11 Soft tissue model validation - subject 12: measured (red) and simulated (blue) stress-strain curves

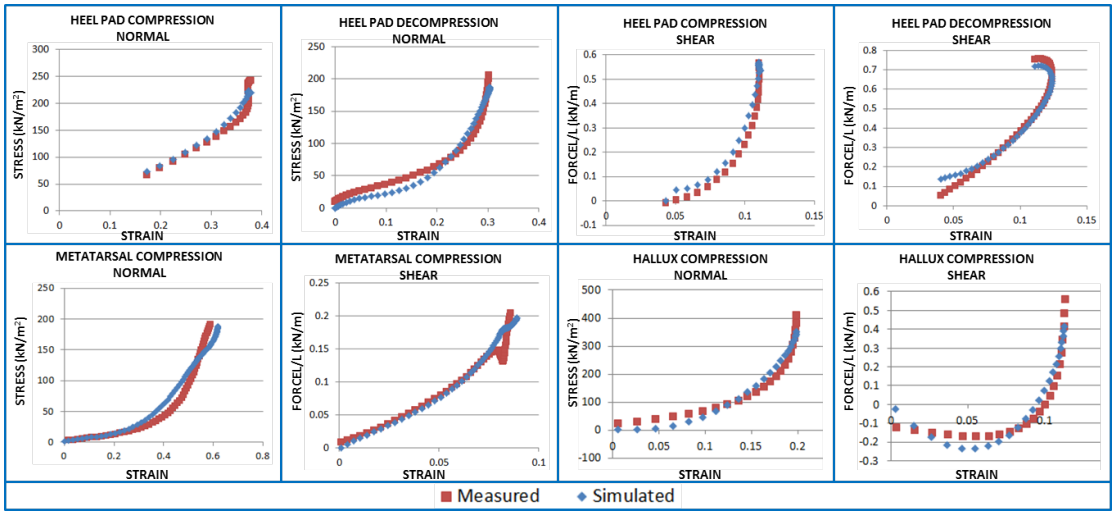

Note: For heel pad characterisation, 4 trials were used, 3 for metatarsal area and 2 for hallux.

Figure H-12 Soft tissue model validation - subject 14: measured (red) and simulated (blue) stress-strain curves

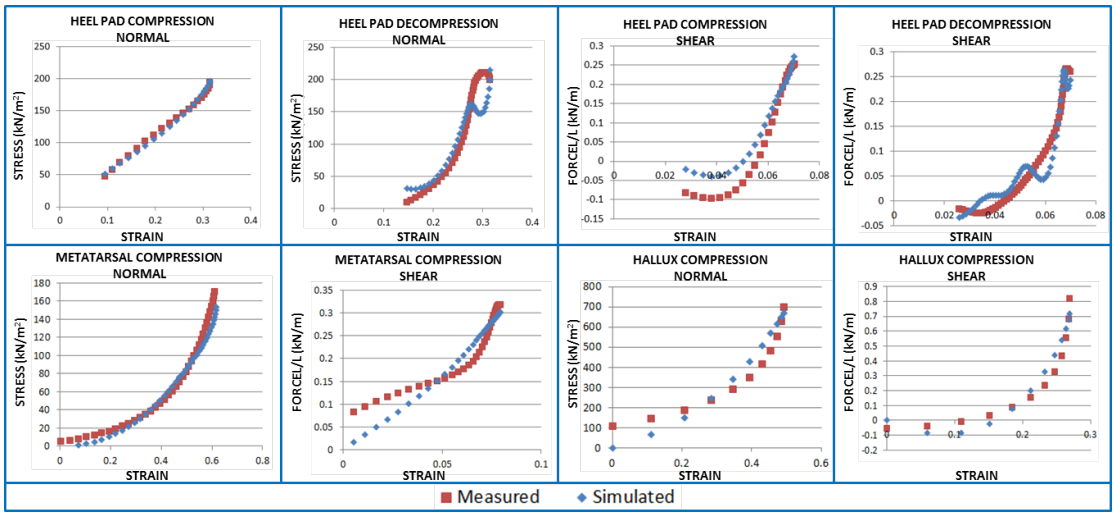

Note: For heel pad characterisation, 4 trials were used, 4 for metatarsal area and 2 for hallux.

Figure H-13 Soft tissue model validation - subject 15: measured (red) and simulated (blue) stress-strain curves

I

Joint assessment in altered gait

Kinematic and kinetic data for normal and pathological gait for eight representative subjects, displaying maximum and minimum joint angles (ankle, knee and hip) for control subjects (CS), ankle injured (AI) and hallux injured (HI).

		Ankle angle (deg)			Knee angle (deg)			Hip angle (deg)		
S		CS	AI	HI	CS	AI	HI	CS	AI	HI
8	Min	-22.4	-3.3	-13	-3.6	-1.3	-2.4	-9.7	-6.5	-9.8
	Max	11.1	12.1	13.9	41.9	48.3	42.8	23.2	27.8	29..8
9	Min	-4.3	-4	-7.6	-4.3	-4.4	-3	-13.5	-17.3	-15.4
	Max	18.3	20.7	18.4	25	27.8	30	27	26.7	23.4
10	Min	-10.2	-12.9	-12.4	-2.9	-3.5	-4.2	-19.2	-16.8	-15.2
	Max	16.8	10	13.4	27.8	25.2	26.3	26.1	20.5	24.7
11	Min	-6.7	-7.5	-8.2	-0.4	-3.5	-3.9	-13.8	-13.9	-13.12
	Max	23.3	17.5	18.9	30.8	30.2	30.3	27.5	23.5	19.9
12	Min	-3.6	-0.3	0.8	-4.5	-7.3	-3.2	-19.4	-19	-18.2
	Max	20.4	18.4	19.6	36.1	26.9	32	19.2	20.4	17.7
13	Min	-16.5	-1.1	-1.9	0.8	0.2	-1.2	-15.5	-12.3	-18
	Max	20.5	20.6	19.6	28.3	19.4	27.3	23.5	23.2	23.4
14	Min	-25	-7.9	-13.6	-0.7	-3.7	-2	-12.6	-12.5	-11
	Max	16.6	12.2	16.1	52.2	35	59.8	31.9	29.9	32.6
15	Min	-13.4	-11.5	-5.9	0.09	-0.9	1.2	-24	-24	-24.2
	Max	21.3	17.3	16.3	31.4	34.9	36.6	18.9	14.3	18.8

Table I-1 Joint angles for control subjects (CS), ankle injured (AI) and hallux injury (HI)